RUSSIAN ACADEMY OF SCIENCE
FEDERAL AGENCY ON EDUCATION OF RUSSIAN FEDERATION
RUSSIAN NATIONAL COMMISSION FOR UNESCO
COMMITTEE ON SCIENCE AND HIGHER EDUCATION OF THE GOVERNMENT OF SAINT-PETERSBURG
COUNCIL OF RECTORS OF SAINT-PETERSBURG HIGHER EDUCATION ESTABLISHMENTS
SAINT-PETERSBURG STATE UNIVERSITY OF AEROSPACE INSTRUMENTATION (SUAI)
UNESCO CHAIR "DISTANCE EDUCATION IN ENGINEERING" OF SUAI
RUSSIAN SECTION OF THE INTERNATIONAL SOCIETY OF AUTOMATION

ИЗВЕСТИЯ КАФЕДРЫ UNESCO ГУАП «ДИСТАНЦИОННОЕ ИНЖЕНЕРНОЕ ОБРАЗОВАНИЕ»

Сборник статей

Выпуск 6

BULLETIN OF THE UNESCO DEPARTMENT "DISTANCE EDUCATION IN ENGINEERING" OF THE SUAI

Collection of the papers

Issue 6

РОССИЯ, САНКТ-ПЕТЕРБУРГ 2021 SAINT-PETERSBURG, RUSSIA

ББК 378.1
УДК 74.58
И33

И33 Bulletin of the UNESCO department “Distance education in engineering” of the SUAI: Collection of the papers. St. Petersburg, Issue 6.- SPb.:SUAI,2021. - 161 p.
ISBN 978-5-8088-1571-1

ISA District 12 (The International Society of Automation) and SUAI (Saint-Petersburg State University of Aerospace Instrumentation) have organized the Seventeenth ISA European student paper competition (ESPC-2021) dedicated to the 80th anniversary of the SUAI. Papers of professors and the best students were included into this issue of the Bulletin of the UNESCO department “Distance education in engineering” of the SUAI. Papers can be interesting for students, post-graduate students, professors and specialists.

ISBN 978-5-8088-1571-1

On behalf of ISA, I would like to congratulate the ISA Russia Section and the St. Petersburg State University of Aerospace Instrumentation (SUAI) on successfully completing the XVII ISA European Student Paper Competition.

I commend the students who contributed their time, knowledge and expertise to prepare a paper for this competition. I also want to acknowledge the review committee, including ISA District 12 student volunteers, who selected the papers for publication and awards.

The students of today are the engineers of tomorrow. Our society welcomes their future contributions in helping us achieve our vision of "creating a better world through automation", and our mission of "advancing technical competence by connecting the automation community to achieve operational excellence." Educators provide an essential role by helping prepare students for their future careers.

Whichever career path these students choose, I hope ISA will continue to play an important role in their continuing education and professional development.

I extend my best wishes to all students, lecturers, and committee members in the XVII ISA European Student Paper Competition.

Sincerely,

Steve Mustard
2021 ISA Society President

International Society of Automation
67 Alexander Drive
P.O. Box 12277
Research Triangle Park, NC 27709
PHONE (919) 549-8411
FAX (919) 549-8288
E-MAIL info@isa.org
www.isa.org

I would like to extend congratulations to the ISA Russia Section, District 12 and St. Petersburg State University of Aerospace Instrumentation (SUAI) for successfully organizing the Seventeenth ISA European Student Paper Competition. This is a special year dedicated to the 80th Anniversary of the SUAI. A monumental achievement.

The papers published in this volume, selected by the advisory committee, represent the best contributions from among an excellent group of papers. The students who committed their time to prepare a paper should be very proud to be selected for this publication.

To the lecturers and professors, you are also playing an important part in shaping the future and you should feel very proud of the standard that is visible in this publication. Thank you for your continued development of today's students.

Congratulations to all students and attendees in this year's ESPC-2021 and hope ISA will continue to play an important role in your and other student's education and professional development.

Sincerely,

Brian J. Curtis
ISA Society President 2018

International Society of Automation
67 Alexander Drive
P.O. Box 12277
Research Triangle Park, NC 27709
PHONE (919) 549-8411
FAX (919) 549-8288
E-MAIL info@isa.org
www.isa.org

Setting the Standard for Automation™

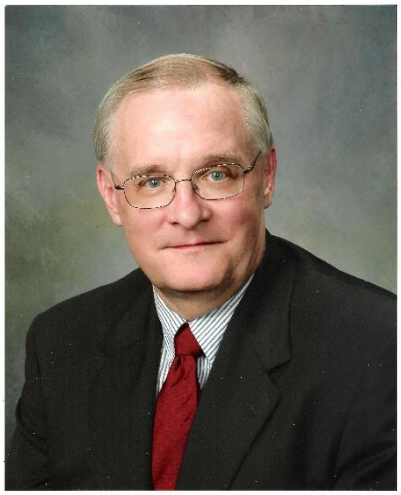

I would like to extend congratulations to the ISA Russia Section, ISA District 12, and The Saint Petersburg State University of Aerospace Instrumentation (SUAI) for successfully organizing the Seventeenth ISA International Student Paper Competition.

As an educator and a member of ISA for over 40 years, I never tire of the opportunity to share with students the amazing challenges and personal rewards that a career in automation can bring. ISA is proud to have the opportunity to nurture the next generation of automation professionals.

We look forward to continuing the close relationship we have established between ISA, the Russia Section, District 12, and the SUAI. Through distance learning classes on project management and ongoing international online forums, we are developing new understandings in the technical, cultural, and personal arenas.

Congratulations to those who developed papers for this volume and to the advisory committee who had the difficult task of making paper selections.

Sincerely,

Gerald W. Cockrell

Gerald W. Cockrell
ISA Former President

Standards
Certification
Education & Training
Publishing
Conferences & Exhibits

International Society of Automation
67 Alexander Drive
P.O. Box 12277
Research Triangle Park, NC 27709
PHONE (919) 549-8411
FAX (919) 549-8288
E-MAIL info@isa.org
www.isa.org

STRUCTURAL DIFFERENCES OF SIGNALS FORMED IN THE BASIS FINITE FUNCTIONS

Aleksandr Fedotovich Kriachko

SUAI
Saint-Petersburg, Russia
e-mail: alex_k34.ru@mail.ru

Abstract
The results of the study are proposed, showing the structural differences of the double phase shift keying signals formed on the basis of fragments of harmonics and wavelets in the frequency and time domain. An approach to the synthesis of wavelet signals is presented, their advantages and disadvantages are analyzed. An analytical expression for evaluating the noise immunity of wavelet signals is obtained. Recommendations for their application are formulated.
Keywords: wavelet signals, noise immunity, formation of phase-shift keyed signals.

Introduction

A summary of fundamental work on wavelet analysis presented by Chui C.K. in [1], opened up wide opportunities for researchers for its practical implementation in various branches of science. Traditionally, wavelet transform methods are actively used in solving problems of stochastic and fractal analysis, as evidenced by fairly recent publications [2-4], in approximation problems [5], as well as in pattern recognition and filtering [6, 7].

At the same time, the uniqueness of the properties of wavelets for energy localization in time-frequency space opens up wide opportunities for the synthesis of manipulated signals on their basis in the interests of various radio engineering applications [8, 9], including information transmission [10, 11].

This direction is quite interesting, since it opens up new opportunities for using multiple-scale analysis. In particular, the structural differences between wavelets and harmonics used as carrier oscillations endows the signals formed on their basis with unique properties that make it possible to increase the noise immunity of reception [12]. But these issues require further study.

Taking these circumstances into account, this paper presents the results of studying the structural differences between wavelets and harmonics, which are essential for noise immunity. In addition, the article presents an approach to the formation of phase-shift keyed signals based on fragments of the first-order Gaussian wavelet.

Theoretical substantiation of the possibility of using wavelets for the synthesis of signal structures based on them

According to [1], wavelets $\psi(t)$ are basic functions of some space $L^2(\mathbf{R})$ formed by integer scaling of the original mother wavelet. In [1], it is substantiated that the analogue of frequency for wavelets is the scale parameter *k*, which determines the form of representation of the resulting structures $\psi(2^k t-\tau)$ of the form, here *k*, τ – are integers.

Then, by means of scale transformations $(1/2^k)$ and time shifts $(\tau/2^k)$ of the original basic mother wavelet $\psi(t)$, it is possible to describe all the time-frequency space used for the synthesis of signal structures.

Since the norm of the wavelet basis, according to [1], is represented as

$$\| \psi(2^k t-\tau) \|_2 = 2^{-k/2} \| \psi(t) \|_2 , \quad (1)$$

then, provided that the parent wavelet $\psi(t) \in L^2(\mathbf{R})$ has a unit norm, all subsequent synthesized functions of the basis $\{\psi_{\tau k}\}$ can be described by the following expression:

$$\psi_{\tau k}(t) = 2^{k/2} \psi(2^k t-\tau), \quad \tau, k \in \mathbf{I} , \quad (2)$$

are also normalized to unity, i.e. $\| \psi_{\tau k} \|_2 = \| \psi \|_2 = 1$.

An important feature of wavelets is that any synthesized structure from space $\psi \in L^2(\mathbf{R})$ will be orthogonal with respect to others if the family $\{\psi_{\tau k}\}$ defined by relation (1) is an orthonormal basis, i.e.

$$\left\langle \psi_{\tau k}, \psi_{l m} \right\rangle = \delta_{\tau k}\delta_{l m}. \tag{3}$$

That is, any function *x* of the indicated space, i.e. $\psi \in L^2(\mathbf{R})$, can be represented as a series

$$x(t) = \sum_{k,\tau=-\infty}^{\infty} c_{k\tau}\, \psi_{k\tau}(t). \tag{4}$$

Here $c_{k\tau}$ – are the coefficients of the basis functions $\psi_{k\tau}(t)$.

However, according to [1], conditions (3) and (4) are insufficient to define a wavelet as a basis function. The strictness of this condition presupposes the existence of inverse transformations. But it was shown in [10] that for the applications under consideration it is sufficient to satisfy the properties of stability and "approximate" orthogonally.

From the indicated positions for the basis (2), such a condition is the properties of the adequacy of the expansion (scaling) and shift of the initial wavelet $(1/2^k, \tau/2^k)$, $k, \tau \in \mathbf{I}$, as well as the possibility of reverse reconstruction up to a constant factor that limits the class of possible basis functions.

In particular, the Fourier transform for basic wavelets should be equal to zero at the origin [2]. In addition, the wavelet used for reconstructions must satisfy the conditions of the Riesz basis, i.e. there are always two constants *A* and *B*, where $0 < A \le B < \infty$, which satisfy the relation [1]:

$$A \| \{c_{k\tau}\} \|_2^2 \le \left\| \sum_{k=-\infty}^{\infty} \sum_{\tau=-\infty}^{\infty} c_{k\tau}\, \psi_{k\tau} \right\|_2^2 \le B \| \{c_{k\tau}\} \|_2^2$$

carried out for any bounded and twice square-summable sequence of coefficients of the basis functions $\{c_{k\tau}\}$:

$$\| \{c_{k\tau}\} \|_2^2 = \sum_{k=-\infty}^{\infty} \sum_{\tau=-\infty}^{\infty} |c_{k\tau}\, \psi_{k\tau}|^2 < \infty. \tag{5}$$

In most practical applications, it is sufficient to satisfy the semi-orthogonally properties for the wavelet, which provides for the equality of condition (3). In the general case, the conditions for the existence of a wavelet correspond to derivatives of high orders of the Gaussian function [10]

$$\psi_m(t) = (-1)^m \partial_t^m \left\lfloor \exp(-t^2/2) \right\rfloor. \tag{6}$$

Here $\partial_t^m = \partial^m[...]/\partial t^m, \quad m \ge 1$.

Thus, the functions synthesized on the basis of expression (5), being wavelets, satisfy the conditions for the formation of bases on their basis, and, therefore, can be used as a basis for the synthesis of signal structures.

Wavelet-based signal construction model

The principle of information transmission by means of signals is based on physical differences in their parameters, the gradations of which correspond to various components of the information alphabet [10]. For signal structures synthesized in the basis of Fourier functions, these are the amplitude, frequency and phase of the carrier waves, as well as their combinations.

Since wavelets are formed by time shifts and frequency scaling, then as their modulation parameters, one can consider the initial phase, amplitude and time shift (duration), as well as their combinations. The choice of the considered parameters of wavelets for their modulation is justified in [10].

Considering that wavelets are localized functions, their use is justified only in manipulation formats with discrete parameter changes. And from the standpoint of ensuring the best noise immunity of reception in [10], it was proposed to form signal structures of phase shift keying on the basis of wavelets. In this case, it is advisable to use the binary phase-shift keying (*BPSK*) signal model [11] as the basic one.

$$s_{BPSK}(t) = A_s \cos(2\pi f_0 t + \varphi_0 + \varphi_m). \quad (7)$$

In (7) A_s - amplitude value; f_0 - carrier frequency; φ_0 - the initial value of the phase; φ_m - a variable phase value determined by the content, for example $\varphi_m = \begin{cases} 0 & if\ "1" \\ \pi & if\ "0" \end{cases}$.

In fig. 1 is a timing diagram of a square wave-keyed BPSK signal.

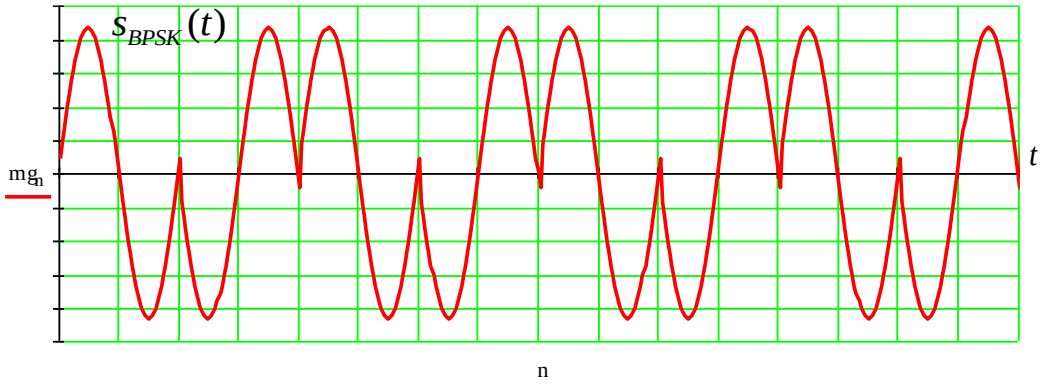

Fig. 1. BPSK test signal time base

Analysis of the signal structure $s_{BPSK}(t)$ shows that it is a set of repeating radio pulses, the phase values of which depend on the information modulating symbols, in this case they are opposite. Therefore, such a signal can be synthesized by sequential concatenation of radio pulses with different phases, the values of which will be determined by the size of the information messages [11].

In accordance with the considered approach, the synthesis of the *BPSK* signal model can be represented in the form of the circuit shown in Fig. 2, in which the bit sequence of information symbols controls the delivery of radio pulses to the channel.

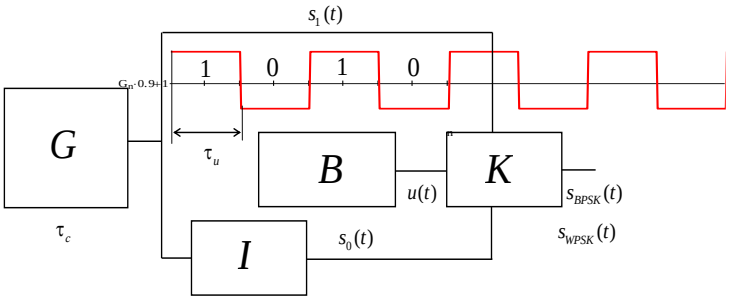

Fig. 2. Structural model of the synthesis of BPSK signals based on sequential switching of radio pulses

Here *G* - is a radio pulse generator; *I* - phase inverter; *B* - block for forming a bit pulse sequence; *K* - is the key device.

The *BPSK* signals are generated as follows.

At the first stage, the transmission rate is determined by matching the radio pulse duration and the bit sequence.

At the second stage, radio pulses are formed corresponding to the values of logical zeros and ones of the information bit sequence $u(t)$, the direct form of the radio pulse of the forming sequence $s_1(t)$ is assigned to the information value "1", and the inverse (inverse) form $s_0(t)$ to the value - "0". Or vice versa.

At the third stage, the resulting *BPSK* signal $s_{BPSK}(t)$ is generated by concatenating radio pulse elements.

Note that the resulting signal generated in the above way will not differ in its properties from the signal, the synthesis of which is reduced to the direct inversion of the high-frequency oscillation phase depending on the "1" and "0" information sequence $u(t)$.

The approach considered opens up the possibility of synthesizing *BPSK* signals, the shaping pulses of which are synthesized in any basis, including the wavelet basis.

If we define $s_1(t)$ and $s_0(t)$ the corresponding types of wavelets as elements, then the result is a phase-shift keyed wavelet signal (*WPSK*).

Then, following the principle of analogy in accordance with the approach presented in Fig. 2, it is proposed to use a first-order Gaussian wavelet $\psi(t)$, representing the first derivative of the Gaussian function, as a forming radio pulse (see formula 7). The validity of this choice is presented in [10]. Analytically, the first-order Gaussian wavelet is determined by the expression:

$$\psi(t) = -t\exp(-t^2/2). \tag{8}$$

Analysis of expression (8) indicates the localized nature of the function $\psi(t)$. Therefore, the synthesis of continuous vibration based on expression (8) is impossible. However, the direct and inverse forms of the Gaussian wavelet can be used as shaping radio pulses, from the fragments of which it is possible to synthesize the resulting *WPSK* signal [10].

Note that the localization properties of the wavelet and its two-sided temporal structure fully correspond to the properties of the forming oscillations in accordance with the approach considered above.

The transition to the synthesis of *WPSK* signals is associated with a replacement in the structural model, see Fig. 2, a generator of forming radio pulses.

In fig. 3 shows fragments of the *BPSK* and *WPSK* signals formed on the basis of the block diagram shown in Fig. 2.

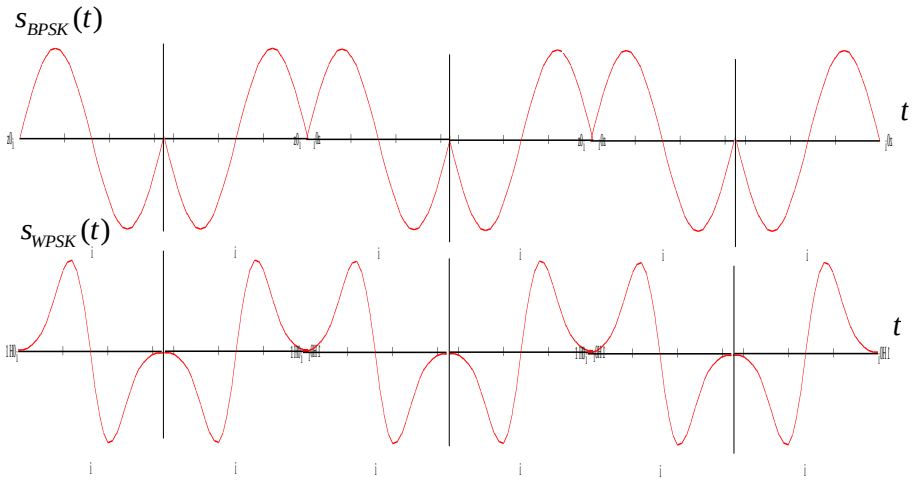

Fig. 3. BPSK signal at the top, WPSK signal at the bottom

We represent the analytical model of the WPSK signal in the following form:

$$s_{WPSK}(t) = (-1)^n t\exp(-t^2/2), \quad n = \begin{cases} 1 \ if \ \text{"1"}; \\ 0 \ if \ \text{"0"}. \end{cases} \tag{9}$$

Thus, the proposed block diagram, see Fig. 2 allows the synthesis of both BPSK and WPSK signals, depending on the type of shaping pulse generator used.

Structural differences of signal structures formed in the basis of wavelets and Fourier functions

In [10, 12], the results of a study of the noise immunity properties of WPSK signals are presented. However, their assessment was obtained on the basis of the data of the conducted modeling. In order to obtain a strict analytical dependence, it is advisable to consider in more detail the structural differences between the BPSK and WPSK signals.

So, in fig. 4 shows the fragments of the BPSK and WPSK signals for the duration of one period. Note that for equal average power, the peak WPSK outperforms BPSK by a ratio of 1.212 / 1.0, which indicates a higher crest factor [13] for the function $\psi(t)$.

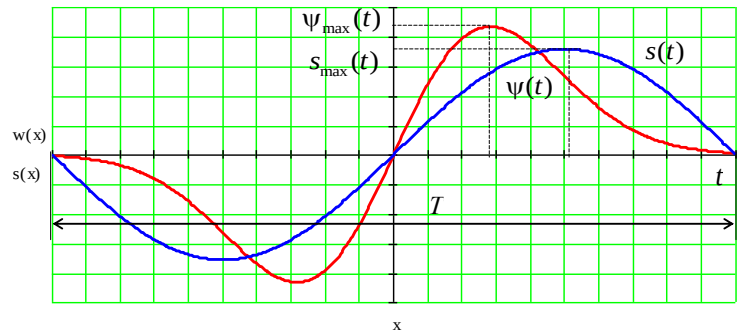

Fig. 4. Fragments of BPSK and WPSK signals

At the same time, the *BPSK* and *WPSK* signals have different rates of energy rise over the duration of the period, as indicated in [11].

$$E_x(t) = \frac{1}{T}\int_0^t x^2(t)\,\mathrm{d}t\,, \quad t \in [0;\ T]\,. \tag{10}$$

In formula (10), either a wavelet or sinusoids will act as a function. In fig. 5 shows the dependences of the energy distribution functions for the wavelet $E_\psi(t)$ and sinusoid $E_s(t)$.

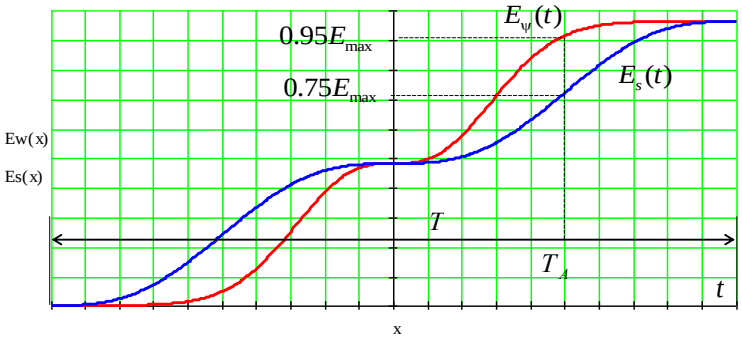

Fig. 5. Wavelet and sinusoidal energy distribution functions

At the moment indicated on the graph as a point T_A, the function $E_\psi(t)$ reaches 95% of its maximum value, while the function $E_s(t)$ gains only 75% of its maximum value.

In the course of the study, the dependence of the functions and was built with a uniform narrowing of the interval T on both sides, see Fig. 6.

$$E_x(\tau) = \frac{1}{T}\int_{(-T/2)+\tau}^{(T/2)-\tau} x^2(t)\,\mathrm{d}t\,. \tag{11}$$

This allowed us to identify the value T_E at which the difference between the functions $E_\psi(t)$ and $E_s(t)$ will be maximum $\Delta E \to \max\limits_{E_s(t)-E_s(t)}$.

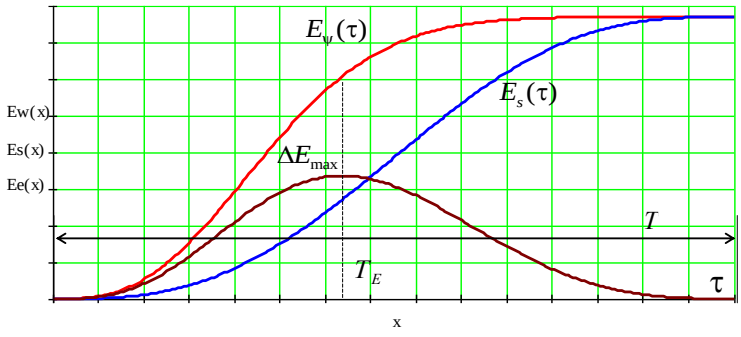

Fig. 6. Truncated functions of wavelet and sinusoid energy distributions

An analysis of the results obtained shows that narrowing the reception interval of signals built on the basis of the considered functions $\psi(t)$ and $s(t)$, by a factor of 2.29, will lead to a loss in energy for $\psi(t)$ only 19%, while the loss for $s(t)$ will reach more than 62%. This allows us to draw the following conclusion. Despite the visual similarity of the wavelet and sinusoidal shapes, their structural differences are significant.

In this regard, the possibility of receiving *WPSK* signals by paths configured to receive *BPSK* signals seems interesting.

So, in [14], an analytical expression was obtained for assessing the noise immunity of signals during their correlation reception, the interpretation of which in relation to the situation under consideration can be represented in the following form

$$p_{BPSK} = Q\left\lfloor \frac{M\lfloor \bar{\Lambda}) \rfloor}{\sqrt{\rho(N_0)}} \right\rfloor, \tag{12}$$

where $M\lfloor \bar{\Lambda} \rfloor$ is the average value of the likelihood ratio based on the results of processing N realizations; $\rho(N_0)$ - the variance of the signal difference function, which characterizes the opposite information symbols, due to the power spectral density of the noise in the channel N_0.

Then, in accordance with [14, 15], we have

$$M\left[\bar{\Lambda}\right] = \int_0^T s_{1(0)} r(t)\,\mathrm{d}t = \int_0^T s_{1(0)}(t)[\bar{s}_1(t) - \bar{s}_0(t)]\mathrm{d}t, \tag{13}$$

where $r(t) = \bar{s}_1(t) - \bar{s}_0(t)$ is the function of differences between the averaged values of the signals corresponding to the information "1" - $\bar{s}_1(t)$ and the information "0" - $\bar{s}_0(t)$.

That is, the likelihood ratio is the result of correlating the received signal corresponding to the information "0" or "1" $s_{1(0)}(t)$ with the difference function.

In turn, the variance of the signal difference function in [14] was proposed to be calculated as

$$\rho(N_0) = \frac{N_0}{2}\int_0^T [\bar{s}_1(t) - \bar{s}_0(t)]^2\,\mathrm{d}t. \tag{14}$$

For calculation $M\lfloor \bar{\Lambda} \rfloor$ under conditions of receiving a *WPSK* signal in the *BPSK* processing path, in (13) should be replaced $s_{1(0)}(t)$ with $\psi_{1(0)}(t)$. Obviously, the structural differences between wavelets and sinusoids will be reflected in the behavior of the generated difference functions. So, in fig. 7 shows the dependences of the moduli of the difference functions between opposite signals of sinusoids $r_{ss}(t)$, as well as sinusoids and wavelets $r_{ws}(t)$.

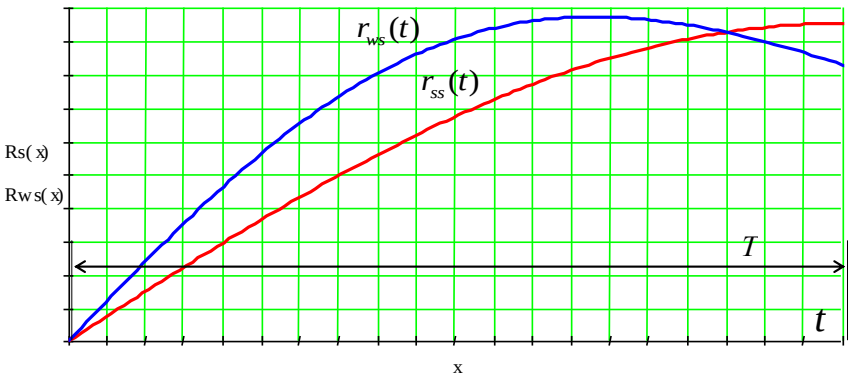

Fig. 7. Opposite signal difference functions

Analysis of the results presented in Fig. 7 is interesting in that the nature of the function $r_{ws}(t)$ has an extreme, i.e. in the conditions of a priori knowledge about the reception of the WPSK signal in the BPSK path,

it is possible to select a correlation interval that excludes a decrease in the resulting noise immunity. Since in the situation under consideration $r_{ws}(t)$, the value will be only 85% of the value $r_{ss}(t)$.

In fig. 8 shows the results of evaluating the noise immunity of reception in terms of the probability of a bit error p_{ws} and p_{ss}, accordingly, when receiving signals $s_{WPSK}(t)$ and $s_{BPSK}(t)$ in the *BPSK* processing path.

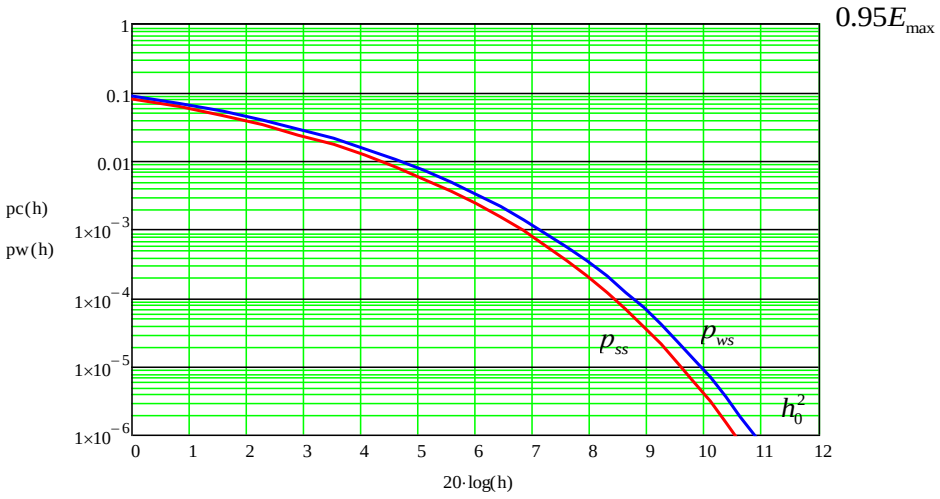

Fig. 8. The dependence of the coefficient of variation of the field amplitude at the aperture of the antenna from the efficiency

In fig. 8 h_0^2 - the ratio of the signal power to the spectral density of the noise power, expressed in dB.

It should be noted that the resulting reduction in noise immunity in terms of the bit error probability $p_{ss} = 10^{-6}$ for p_{ws} will be within 0.5 dB.

CONCLUSIONS

The results of the study of the structural differences between wavelets and sinusoids showed that the practical application of *WPSK* signals for information transmission has both its advantages and disadvantages.

The disadvantages include an increase in the reception bandwidth and an increase in the transmit crest factor. Consequently, in channels with additive white Gaussian noise, such signals will lose in reception noise immunity to BPSK signals.

However, the differences in the distribution of energy over the duration of the sinusoid and the wavelet allow, in the presence of noise, due to filtering, while reducing the processing interval, 95% of the energy for *WPSK* signals will be saved, while for *BPSK* signals only 75% will be saved. A further reduction of 2.3 times will lead to differences in energy conservation by more than 2.1 times.

The differences in the noise immunity of *WPSK* and BPSK signals will reach about 7 dB.

The authors associate further research with the synthesis of multiposition signal structures based on wavelets.

References

1. Chui C.K. An introduction to wavelets Academic Press (1992) ISBN 0-12-174584-8.

2. Ayache A., Esmili Y. Wavelet-type expansion of the generalized rosenblatt process and its rate of convergence. Journal of Fourier Analysis and Applica-tions. 2020. T. 26. № 3. C. 51..

3. Čoupek P., Duncan T.E., Pasik-Duncan B. A stochastic calculus for rosenblatt processes. Stochastic Processes and their Applications. 2020.

4. Saravanakumar S., Balasubramaniam P. On impulsive hilfer fractional stochastic differential system driven by rosenblatt process. Stochastic Analysis and Applications. 2019. T. 37. № 6. C. 955-976.

5. Shen G., Yu Q. An optimal approximation of rosenblatt sheet by multiple wiener integrals. Mediterranean Journal of Mathematics. 2017. T. 14. № 2. C. 36.

6. Muqeet M.A., Holambe R.S. Enhancing face recognition performance using tri-plet half band wavelet filter bank. International Journal of Image, Graphics and Signal Processing. 2016. T. 8. № 12. C. 62-70.

7. Srivastava R., Khare A. Threshold based image fusion in dual tree complex wavelet domain. International Journal of Image, Graphics and Signal Pro-cessing. 2016. T. 8. № 10. C. 64-74.

8. Akhtar N., Ullah H., Saif F., al Omari A. Wavelet signal processing for resolution enhancement in a recurrence tracking microscope. Journal of Russian Laser Research. 2017. T. 38. № 5. C. 399-407.

9. Gonçalves M.A., da Cunha E.F.F., Ramalho T.C., Santos L.S., Prata D.M., Peixoto F.C. Optimal wavelet signal compression as an efficient alternative to investigate molecular dynamics simulations: application to thermal and solvent effects of mri probes. Theoretical Chemistry Accounts: Theory, Computation, and Modeling (Theoretica Chimica Acta). 2017. T. 136. № 1. C. 15.

10.Dvornikov S.V., Manaenko S.S., Dvornikov S.S., Pogorelov A.A. Synthesis of phase-shift keyed wavelet signals // Information technologies. 2015.Vol. 21. No. 2. P. 140-143. (Russ. ed.: Dvornikov S.V., Manayenko S.S., Dvornikov S.S., Pogorelov A.A. Sintez fazomanipulirovannykh veyvlet-signalov // Informatsionnyye tekhnologii. 2015. T. 21. № 2. S. 140-143).

11.Dvornikov S.V. Digital synthesis of spectrally efficient television signals. Radio electronics issues. Series: Television technology. 2015. No. 6. P. 168-173. (Russ. ed.: Dvornikov S.V. Tsifrovoy sintez spektral'no-effektivnykh signalov televideniya. Voprosy radioelektroniki. Seriya: Tekhnika televideniya. 2015. № 6. S. 168-173).

12.Dvornikov S.V., Dvornikov S.S. Wavelet Signal Detection // Information and Space. 2020. No. 4. P. 11-17. (Russ. ed.: Dvornikov S.V., Dvornikov S.S. Obnaruzheniye veyvlet-signalov // Informatsiya i kosmos. 2020. № 4. S. 11-17).

13.Wu H., Song J., Liu W., Xu J., Zhang H., Wu J., Zhou P. High power high signal-to-noise ratio multiwavelength raman fiber laser based on random dis-tributed feedback. Japanese Journal of Applied Physics. 2017. T. 56. № 11. C. 110304.

14.Dvornikov S.V., Dvornikov S.S. An empirical approach to the evaluation of noise immunity of phase modulation signals // Informatics and Automation. 2020.Vol. 19, No. 6. P. 1280-1306. DOI 10.15622 / ia.2020.19.6.6 (Russ. ed.: Dvornikov S.V., Dvornikov S.S.. Empiricheskiy podkhod k otsenke pomekhoustoychivosti signalov fazovoy modulyatsii // Informatika i avtomatizatsiya. 2020. Tom 19, № 6. S. 1280-1306. DOI 10.15622/ia.2020.19.6.6).

15.R. Yuan and J. Cheng, "Free-Space Optical Quantum BPSK Communications in Turbulent Channels," 2018 IEEE Globecom Workshops (GC Wkshps), Abu Dhabi, United Arab Emirates, 2018, pp. 1-6.

16.A.A. Gavrishev, A.N. Gavrishev On the issue of calculating the peak-factor values of signals generated by common covert communication systems. Vestnik NTsBZhD. 2020. No. 3 (45). S. 149-157. (Russ. ed.: Gavrishev A.A., Gavrishev A.N. K voprosu o raschete znacheniy pik-faktora signalov, generiruyemykh rasprostranennymi skrytnymi sistemami svyazi // Vestnik NTSBZHD. 2020. № 3 (45). P. 149-157.)

AUTOMATION OF ASSESSMENT OF GENERALIZED STRESS AND SAFETY FACTOR OF PRODUCTS MADE USING ADDITIVE TECHNOLOGIES

Alexandr Chabanenko

Saint-Petersburg State University of Aerospace Instrumentation,
Saint-Petersburg, Russia
E-mail: Chabalexandr@gmail.com

Annotation
The term hardness means the ability of a polymer material to resist the pressure of other bodies into it. It is affected by the temperature, magnitude and speed of the effort, and other external factors. Soft and elastic polymer materials with low hardness can be used as sealants, sealing and padding materials. In contrast to elasts, solid polymer materials are used to make structural parts, namely, braking systems, gear wheels and bearings, parts of threaded compounds.

Solid measurements are used to optimize the plasticizer content, quantity and type of filler, processing conditions in products. In addition, the most hardness is judged by the following characteristics:

- elastic modulus,
- Poisson's ratio,
- plasticity,
- elasticity.

To determine hardness, methods are used that differ in the geometry of the indenter: Brinell, Rockwell, Vickers figure 1.

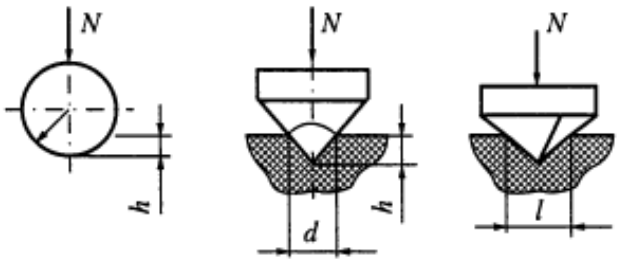

Figure 1. Inentors Schemes: 1 - Steel Ball (Brinell Method); 2 - Metal Cone (Rockwell Method); 3 - Diamond Pyramid (Vickers Method)

During the tests, either the indentation depth of the indenter h or the dimensions of the resulting indentation l are measured. By the way, GOST 4670-70 prescribes to use the Brinell method with measuring the indenter depth h to determine the hardness of a polymer material. The Brinell hardness value (HB) is calculated using the formula in table 1.

Table 1

Registration of quality levels of control effects on polymers

Symbol	Impact manager's name	Value for level		
		1	2	3
ASA-plastic	Polymer temperature	160oC	200oC	240oC
ABS EG-plastic	Polymer temperature	210oC	225oC	250oC
ABS HG-plastic	Polymer temperature	220oC	212oC	260oC
ABS MP-plastic	Polymer temperature	200oC	210oC	220oC
ABS 2020-plastic	Polymer temperature	190oC	200oC	260oC

The tension is described by the size, direction and plane on which it acts. The tension state at some point is fully described by the following components:

SX
Stress in the X direction acting perpendicular to the YZ plane.
SY
Stress in the Y direction, acting perpendicular to the XZ plane.
SZ
Stress in the Z direction acting perpendicular to the XY plane.
TXY
Stress in the Y direction acting on a plane perpendicular to the X direction (YZ plane).
TYX
Stress in the X direction acting on a plane perpendicular to the Y direction (XZ plane).
TXZ
Stress in the Z direction acting on a plane perpendicular to the X direction (YZ plane).
TZX
Stress in the X direction acting on a plane perpendicular to the Z direction (XY plane).
TYZ
Stress in the Z direction acting on a plane perpendicular to the Y direction (XZ plane).
TZY
Stress in the Y direction acting on a plane perpendicular to the Z direction (XY plane).

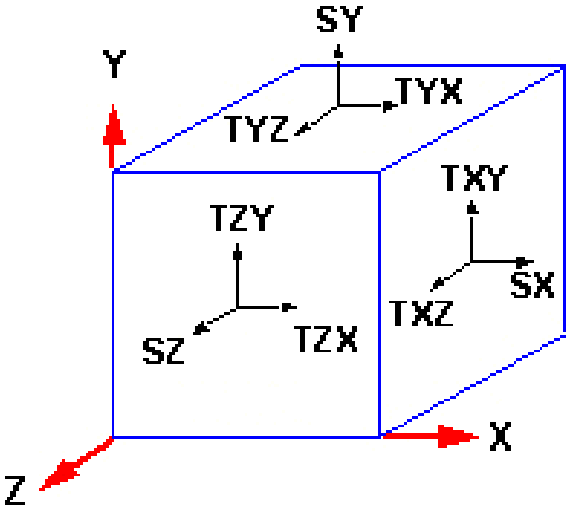

Figure 2. SX, SY and SZ normal tension

SX, SY and SZ are called normal tensions. TXY, ..., TZY are called shear stresses. Shear stresses satisfy the following equations: TXY = TYX, TXZ = TZX, and TYZ = TZY. Thus, the state of stress at some point is completely determined by six components:

Major stresses

For each point there is a plane for which there are no tangents. The state of stresses relative to this plane is completely determined by normal stresses.

P1
Normal tension in the first main direction (the biggest).
P2
Normal tension in the second main direction (intermediate).
P3
Normal tension in the third main direction (the smallest).
Below are the types of forces that affect polymers figure 3.

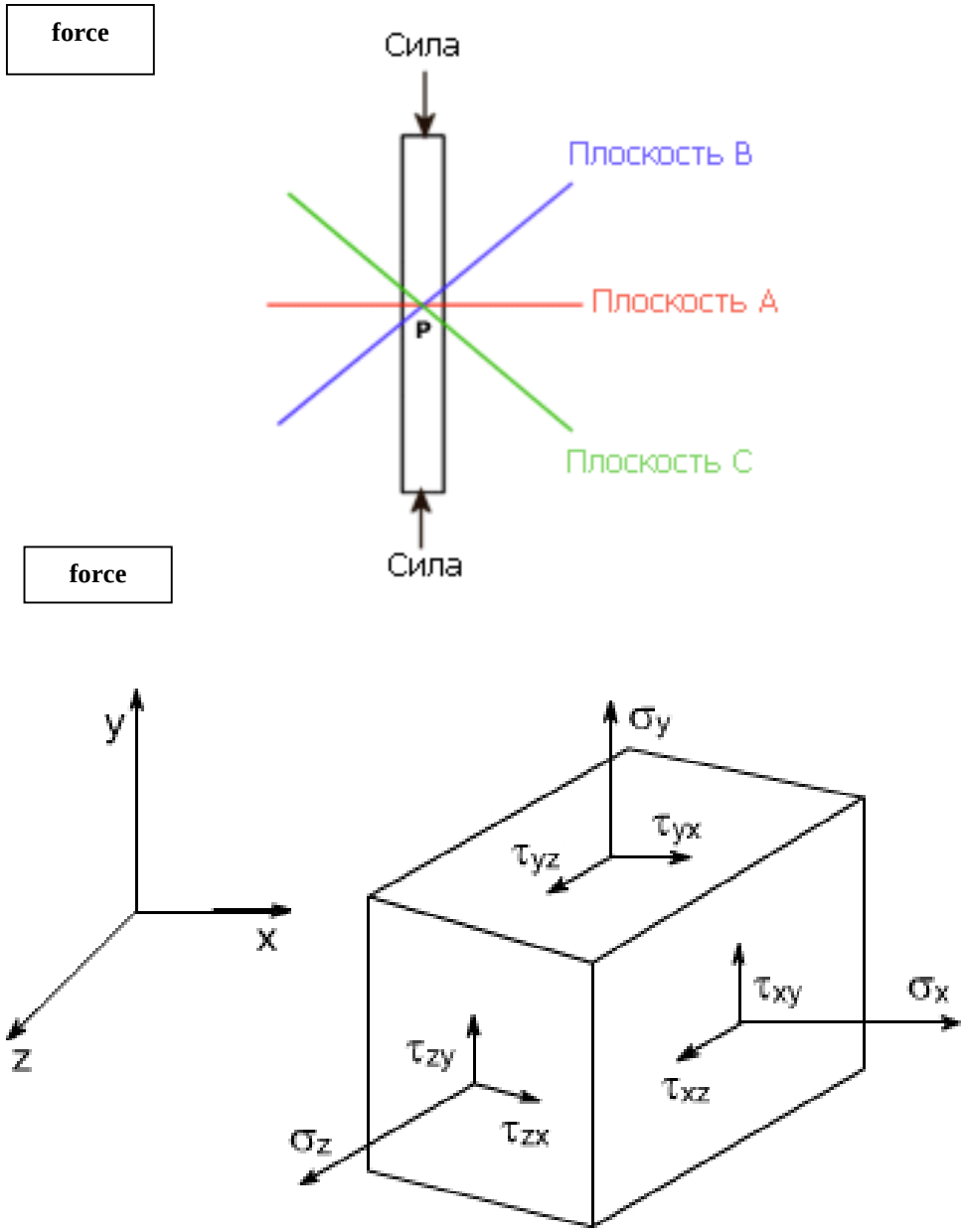

Figure 3. Direction of forces in the deformation of polymer from composite materials

σx tension to the side (on the shift of the polymer layer).

σy tension on top (on the break).

txy tension in the plane xy (tension on the kink).

σ yield nfluidity - the tension level of high-plastic materials in which significant deformations occur without further increase in tension.

Figure 4. Finished element and prototyped component base

A model was used to indicate the values of plane stresses and the yield strength of the material. Input parameters must have uniformity of units. The green dot represents the state of the main stresses figure 4.

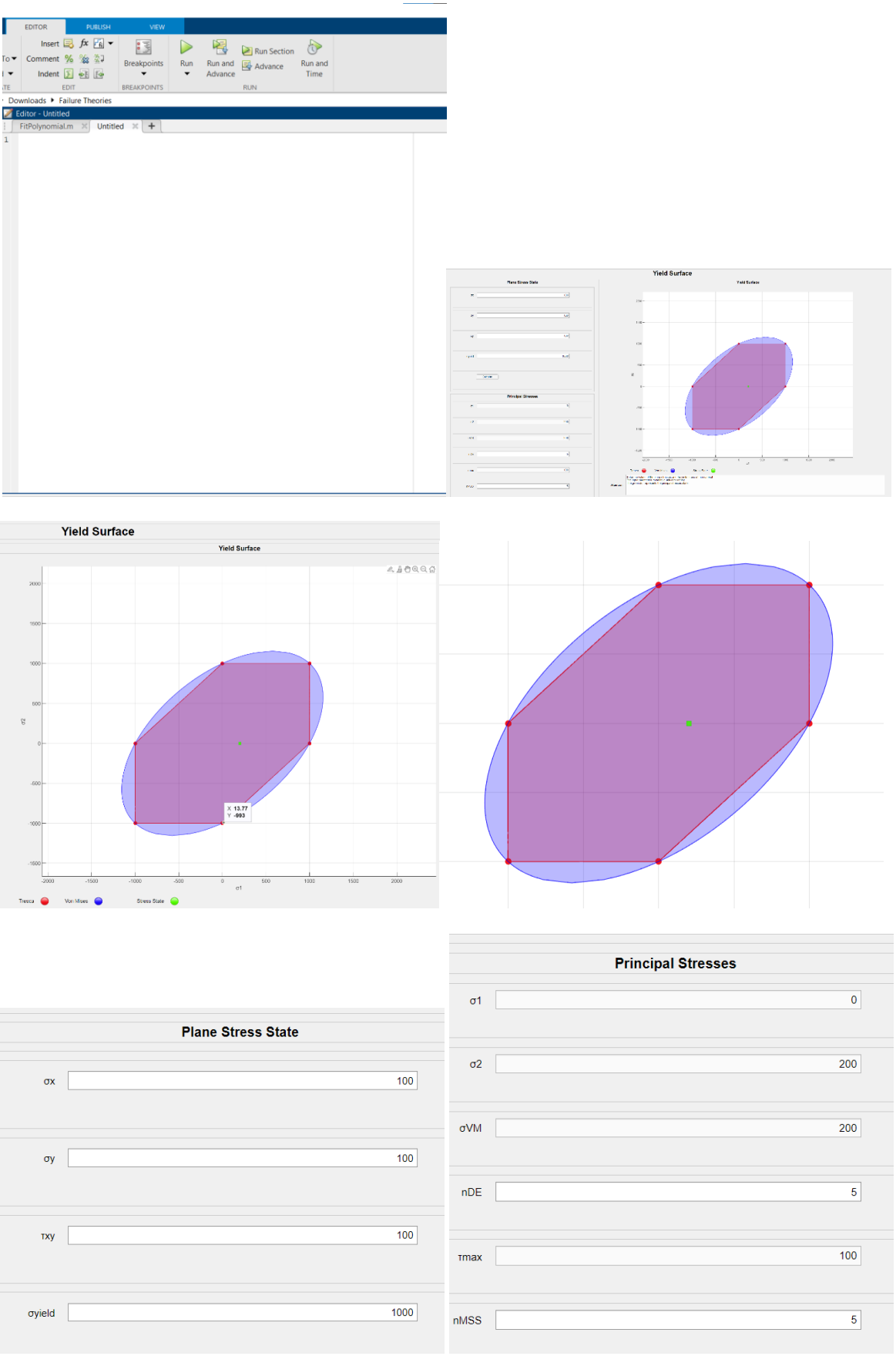

Figure 4. Simulation of polymer tensions

Indicators of polymers

Revealed indicators of ABS-type polymers special

Table 2

Polymers

№	The name of the poly-mer	Mechanical properties			
		Strength at Mpa stretching		Temperature softening on Vic at 5 kg/cm^2 in C	Density at 23 C per g/cm^3
26	ABS-OM-2020-30	at least 38 MP.		108 S.	
27	ABS-plastic 0809-30	at least 41.6 MPA		106 S.	
28	ABS-plastic 0809M	at least 40 MP.		110	
29	ABS-plastic 2020-30 of the highest grade	38,2		97	
30	ABS-plastic 2020-31 of the highest grade	49		109	
31	ABS/PC Diskar-L	at least 50 MP.		at least 120 C.	
32	ABS/PC Disair-SL	at least 50 MP.		at least 120 C.	
33	ABS/PC Disair-E	at least 50 MP.		not below 115 C.	
34	ABS-plastic 1030-30	at least 35.3 MPAs (360 kgs/cm$^{2)}$.		not below 90 C.	
35	ABS-plastic 1030-31	at least 35.3 MPAs (360 kgs/cm$^{2)}$.		not below 88 C.	
36	ABS-plastic 1106M-30	at least 38.2 MPAs (390 kgs/cm$^{2)}$.		not below 95 C.	
37	ABS-plastic 1106M-31	at least 38.2 MPAs (390 kgs/cm$^{2)}$.	not below 95 C.		
38	ABS-plastic 1106-30 of the highest grade	at least 38.2 MPAs (390 kgs/cm$^{2)}$.	not below 96 S.		
39	ABS-plastic 1530-30	at least 34.3 MPAs (350 kgs/cm$^{2)}$.	not below 90 C		
40	ABS-plastic 2020-32	at least 38.2 MPAs (390 kgs/cm$^{2)}$.	not below 97 S.		
41	ABS-plastic 2020-60	29,4	80	1,03	
42	ABS-plastic 2802-30 of the highest grade	at least 36.3 MPA (370 kgs/cm$^{2)}$.	not below 95 C.		
43	ABS-plastic ABS-C	at least 30.0 MPA (306 kps/cm$^{2)}$.	not below 95 C.		

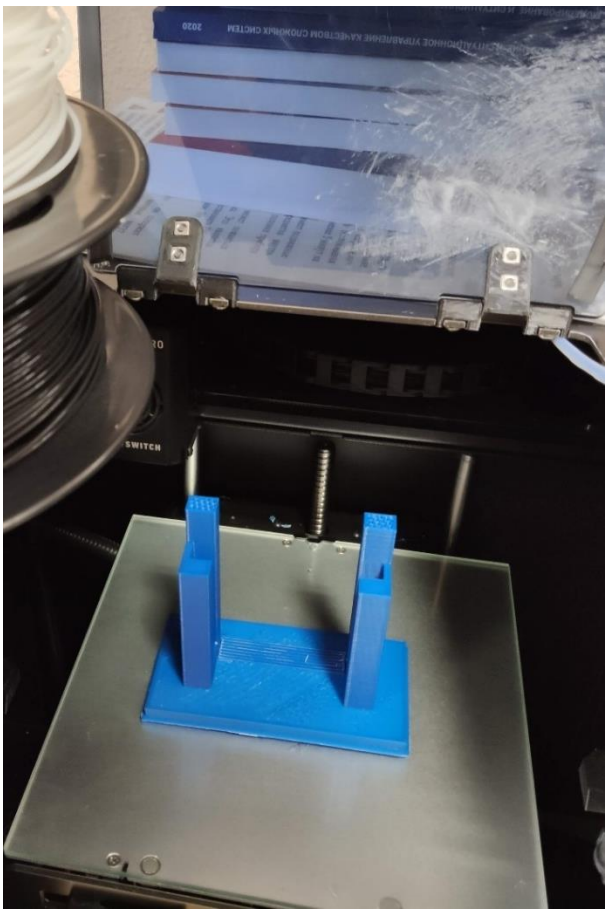

Figure 5. Ready element and prototyped component base

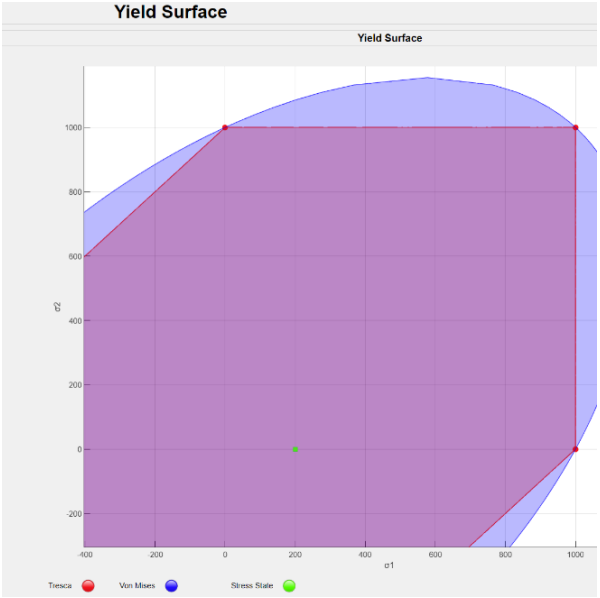

Figure 6. Drawing the load on the polymer and determining the boundaries of deformation

Among large-scale polymeric materials, the first place is occupied by

production of polyolefins. The industry produces polyethylene of different density. So, low density polyethylene (high pressure) is used for the manufacture of parts of high-frequency devices, insulation of high-frequency and ultra-high-frequency cables and wires, pressure pipes, tanks and containers for storing aggressive liquids, gear wheels operating with low load in the temperature range from - 60 to + 80 ºC, anti-corrosion coatings for metal parts, films, sheets.

High density polyethylene (low pressure) is used for the manufacture of pipes, hoses, films, parts of high-frequency installations and radio equipment, cranes, silent gears.

High density polyethylene (medium pressure) is used for pipes, hoses, films, fittings, containers for transporting and storing corrosive liquids, parts of high-frequency equipment and radio equipment, valves, silent gears, medical products, etc.

Another polyolefin is polypropylene, which is used to make pipes, gears, chemical equipment, fittings, wire insulation, bumpers for cars, etc.

Polyvinyl chloride is used as a gasket and sealing, chemically resistant material for operation at temperatures ranging from -15 to + 40 ºC. Basically, this polymer is used for the manufacture of films, hoses, insulation.

Viniplast sheet based on PVC is intended for the manufacture of parts operating in aggressive environments at temperatures from 0 ºC to + 40 ºC (parts of pumps for pumping acids and pumps, for chemical equipment, pipes, accumulator plate molding tanks, etc.).

Emulsion polystyrene is used for the manufacture of storage tanks, refrigerator parts, coil frames, capacitor parts, panels and insulators.

In turn, block polystyrene is recommended for electrical parts, refrigerator parts, capacitors. Suspension polystyrene and its copolymers are used for the manufacture of technical parts, as well as consumer goods.

Impact-resistant polystyrene is a material for large-sized parts for technical and household purposes.

Polymethylmethacrylate powder is suitable for forming parts that do not bear loads and are not exposed to heat - various caps, instrument scales, etc.

Plexiglas is used for aircraft glazing, for the manufacture of glasses for various devices, including watches.

Fluoroplast-4 is used as a sealing material in equipment (gaskets, stuffing box packing, cuffs), for fluorinated media. Electrical and radio engineering parts are made of it: plates, rings, rings, cylinders, as well as plain bearings.

Fluoroplastic-3 is consumed for sealing parts operating at high pressure, gaskets operating in aggressive media at pressures up to 3.2 MPa and operating temperatures from -70 to + 50 ºC, as well as for parts for valves of oxygen devices operating at pressures from 15 ÷ 20 MPa, membranes. In addition, this polymer material can be used as an anti-corrosion coating.

Polyamides are used for the manufacture of gaskets in machines, films, adhesives, ship fittings, protective coatings against microorganisms and fungi, as well as for hardware, various bushings, bearing shells, gears, screws and other parts. The temperature range for the operation of polyamide products is from -

70 to + 220 ºC. By the way, polyamide gears absorb shock loads well, are durable and work in conditions of little lubrication.

Polyacrylonitrile is widely used in technology and everyday life. Most of the polyacrylonitrile is used for the production of fibers for household and technical purposes, for example, technical fabrics, fishing nets, transport belts, etc.

Polyvinyl acetate is widely used in the production of varnishes, paints, and adhesives, as well as for the surface treatment of leather, paper, fabric, in the production of artificial leather, as an additive to cement, etc.

Polyvinylcarbazole is used in the chemical industry for the production of parts of chemical equipment that are resistant to aggressive media and high temperatures. Polyvinylcarbazole films are widely used in electrical engineering in the production of capacitors, parts for television, radar installations, as well as in electrophotography, as photosensitive layers.

Polyformaldehyde is widely used to replace non-ferrous metals and alloys in the automotive industry, instrument making, electronics and communications, and other industries. Bushings, gear wheels, gears, handles, instrument cases, switch parts, taps, oil and gas lines, rollers, valves are made of it by injection molding.

In the automotive industry, polyformaldehyde is used to make parts for carburetor clutches, brake systems, and in the textile industry, equipment for textile machines.

Polyurethanes are used as flexible, aging-resistant fibers and films. The main application of polyurethanes is found in the production of gas-filled plastics (foams). Closed-cell flexible foams are used for the manufacture of float products, mechanical insulation supports for work at low (liquid nitrogen) and relatively high (up to 120 ºC) temperatures. Open cell foams are used to make sponges, cushions, seats, soundproofing materials, etc. Rigid polyurethane foams are used in aircraft, auto and shipbuilding, etc.

Urea-formaldehyde resins (UFR) are widely used for the manufacture of adhesives, varnishes, and enamels. In addition, slabs for floors, backs and seats for chairs, door and window frames and other products are made from wood waste processed by FSC.

Phenol-formaldehyde resins (PFS) are available in two types: novolac and resole resins. So, novolak resins are used for the production of press powders with fibrous and sheet fillers. In turn, resole resins are used for the production of laminated plastics (textolites, electrical insulating press powders, etc.), impact-resistant materials (fiber-reinforced concrete), as well as for the manufacture of special molding masses (faolite) putty, adhesives combined with epoxy resins.

Polycarbonate is used in many areas where such qualities as high transparency, resistance to loads and impacts, heat resistance, temperature stability are required. The main areas of application of polycarbonate are construction, medicine, communication systems and electrical engineering, and the automotive industry.

Polyethylene terephthalate is widely used for the manufacture of fiber - lavsan, which is used for the manufacture of knitwear, decorative fabrics, as well as filter and cushion fabrics.

Epoxy is widely used in the production of adhesives and cements, potting compounds, laminates and other materials.

Polyorganosiloxanes are used for the production of varnishes and enamels, fiberglass, fiberglass, etc.

Rubbers are widely used for their vehicle rubber base, cushioning material, etc.

Various polymeric materials need to automate the assessment of the generalized stress and safety factor of products made using additive technologies for a comprehensive assessment of product quality.

Conclusion

In technology, many polymeric materials are used that have a whole range of useful properties. The practical use of polymeric materials is not limited to the field of structural materials. What is available for modeling the processes of loads on these materials.

The list of literature used:

1. Семенова Е. Г., Чабаненко А. В., Назаревич С. А. Выявление ключевых показателей качества технологиического процесса производства корпуса РЭА на основе FDM Радиопромышленность Вопросы радиоэлектроники. М. № 4. 2017. С. 53-59.

2. Quality Assurance of Hull Elements of Radio-Electronic Equipment by Means of Control System / Chabanenko, A.V., Anatoly P.Y. IEEE International Conference. 2018.

3. Electrodynamic analysis of materials for the antenna elements Chabanenko, A., Frolova, E., Balashov, V., Smirnova, M. 2018 IOP Conference Series: Materials Science and Engineering

4. Construction of mathematical model of training and professional development of personnel support of additive production of rea Chabanenko A.V., Kurlov A.V. В сборнике: IOP Conference Series: Materials Science and Engineering International Workshop "Advanced Technologies in Material Science, Mechanical and Automation Engineering – MIP: Engineering – 2019". Krasnoyarsk Science and Technology City Hall of the Russian Union of Scientific and Engineering Associations. 2019. С. 32041.

5. Developing intelligent decision support systems in multi-criteria problems of administrative-territorial formations infrastructure projects assessment Batkovskiy, A.M., Nesterov, V.A., Semenova, E.G., Sudakov, V.A., Fomina, A.V. 2017 Journal of Applied Economic Sciences

6. Обеспечение качества аддитивного производства посредством системы контроля послойного синтеза / А.В. Чабаненко, Е.Г. Семенова, В.О. Смирнова, А.О. Смирнов, Н.Н. Рожков // Вопросы радиоэлектроники. 2018. №10. С. 75-79.

7. Управление качеством аддитивных изделий / А. В. Чабаненко // РИА: Журнал.: «Стандарты и качество». 2018. №2. С. 90-94.

8. Процедуры преобразования 3d-модели в исполняемый файл stl для послойного синтеза Чабаненко А.В., Курлов В.В. В сборнике: МОДЕЛИРОВАНИЕ И СИТУАЦИОННОЕ УПРАВЛЕНИЕ КАЧЕСТВОМ СЛОЖНЫХ СИСТЕМ. Сборник докладов Первой Всероссийской научной конференции. Санкт-Петербург, 2020. С. 190-192.

9. Управление качеством 3d печати посредством моделирования компонентной базы аддитивной установки Чабаненко А.В. В сборнике: Избранные научные труды восемнадцатой Международной научно-практической конференции "Управление качеством". ИЗБРАННЫЕ НАУЧНЫЕ ТРУДЫ Восемнадцатой Международной научно-практической конференции. 2019. С. 362-368.

10.Создание корпусных элементов рэа на установке послойного синтеза материалов в рамках проектной работы студентов ГУАП Чабаненко А.В. В сборнике: XXIII Международный Биос-форум и Молодежная Биос-олимпиада 2018. Сборник материалов . 2019. С. 133-137.

CLASSIFICATION OF THE OBSERVED ZONES ON THE GENERATED IMAGES OF THE VIDEO FRAME FLOW IN THE ON-BOARD MONITORING SYSTEMS OF THE EARTH'S SURFACE

Victoria Afanaseva

Saint-Petersburg State University of Aerospace Instrumentation,
Saint-Petersburg, Russia
E-mail: victoria_afanaseva@mail.ru

Abstract
In this paper, we implement a method for classifying the observed zones of the earth's surface based on the captured frames of the video stream formed by the optoelectronic surveillance system of the aircraft. Deep learning methods, digital image processing methods, and semantic segmentation methods are used. The result of this work is classified frames of the video stream, segmented into the following classes: sky, vegetation, and building.
Keywords: object detection, neural network, image segmentation, computer vision.

INTRODUCTION

Classification of the observed zones by the frames taken by the aircraft equipment has recently become one of the most important tasks of scene analysis in applications of automated monitoring of the earth's surface [1].

Processing video stream frames using semantic segmentation allows you to divide the processed scene of the earth's surface into classes. The expediency of such an interpretation of the frame lies in the fact that an increasing number of applications translate computer data into a graphical form that is more understandable to humans [2].

This type of segmentation is used in various fields. These areas include: autonomous air vehicle control systems, including unmanned vehicles, as well as advanced ways of human-computer interaction, virtual reality, navigation of onboard unmanned systems, etc.

Based on this, we can conclude about the relevance of the topic of this work.

The objective of this study is to develop a method for automated identification of various zones with their subsequent classification based on the use of an appropriate neural network.

FEATURES OF IMAGE CLASSIFICATION AND SEGMENTATION

There are several types of segmentation, such as instance segmentation and semantic image segmentation.

Instance segmentation is the division of an image into separate areas or classes corresponding to a specific object or zone. For example, selecting the sky, road, vegetation, buildings, etc. Image segmentation is used in systems to assist the operator of autonomous aerial unmanned vehicles. Semantic image segmentation is the division of an image into separate groups of pixels, areas corresponding to a single object, while simultaneously determining the object type of each area, that is, its classification [3].

Semantic segmentation of images generated on board unmanned vehicles to classify different attributes is quite a difficult task, since the differences are very large, the terrain is not always the same and homogeneous, which makes it difficult to classify it. Thus, there is a need to implement such systems that automatically implement this segmentation process in quasi-real time.

Semantic segmentation differs from instance segmentation in that different objects of the same class will have different labels, for example, different houses will be marked with the same color and, accordingly, with the same «Building» label. Figure 1 shows the difference between these types of segmentation.

Semantic segmentation of video frames obtained from aircrafts to classify different attributes is quite a difficult task, since the differences are very large, you cannot expect that the earth's surface will be uniform. Segmenting these images for use in different applications is a complex task, and the process never ends. Thus, there is a need to automate a system that performs this process using a convolutional neural network.

Convolutional neural network is a concept of deep learning, which in this case is used to work with video frames (figure 2).

a) Object detection

b) Semantic segmentation

c) Instance segmentation

d) Classification

Figure 1 – Example of different types of segmentation

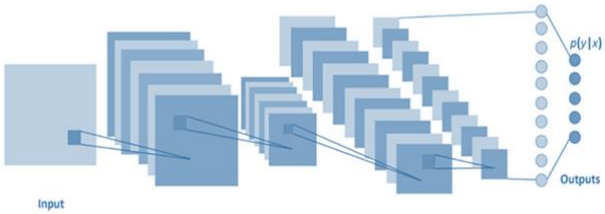

Figure 2 – Convolutional neural Network structure

At the initial stage, the neural network is untrained. In a general sense, training is understood as the sequential presentation of an image to the input of a neural network, from the training set, then the received response is compared with the desired output, the resulting difference between the expected response and the received one is the result of the error function (error delta). This error delta must then be extended to all connected neurons in the network (figure 3) [4-6].

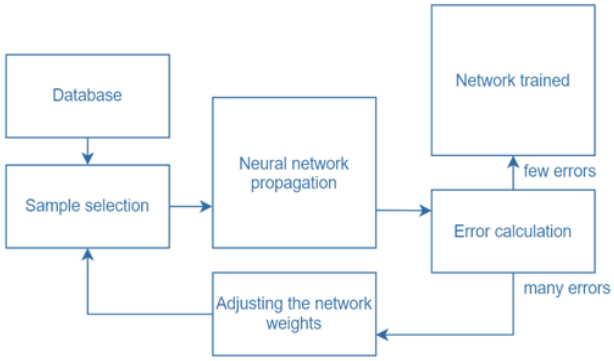

Figure 3 – Algorithm for learning neural networks

In most cases, the data sets for network training consist of no more than thousands of frames. The network is trained from scratch starting with randomly initialized weights. In the same way, a pre-trained network can be trained on its own data set [7].

Thus, it is possible to distinguish the features of this method, namely: efficiency and ease of obtaining the result, high accuracy, ease of implementation.

EXPERIMENTS ON THE CLASSIFICATION OF ZONES IN FRAMES TAKEN FROM AIRCRAFT

Figure 4 shows a frame of the video stream and the same frame, after segmenting it and selecting two classes on it. Namely: heaven and earth. The classification of this frame was obtained using MATLAB and the resnet18 neural network, specially trained on a set of video data recorded during field tests. The neural network has well separated the sky and vegetation in figure 4 (b).

(a) Source frame of video stream (b) *Segmented frame of video stream*

Figure 4 – A frame of a video stream with two classes: sky and vegetation

The video stream frames were also segmented (figure 5 and 6), where there is a more saturated landscape of the earth's surface. So in figure 4, two classes were allocated: in the other figures, three classes.

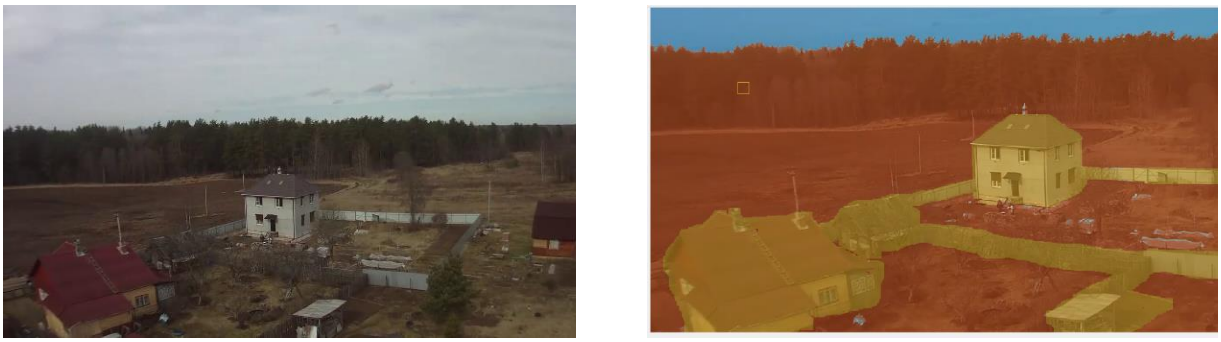

(a) Source frame of video stream (b) *Segmented frame of video stream*

Figure 5 – A frame of a video stream with two classes: sky, vegetation and building

(b) Source frame of video stream (b) *Segmented frame of video stream*

Figure 6 – A frame of a video stream with two classes: sky, vegetation and building

Thus, experiments were conducted on segmentation of video stream frames with subsequent classification of the selected zones. The sky is highlighted in blue, trees and vegetation are highlighted in orange, and various buildings are highlighted in yellow.

CONCLUSIONS

As a result of this study, a method of semantic segmentation with subsequent classification of the zones of the earth's surface allocated to separate classes based on the captured frames of the video stream formed by the aircraft equipment is implemented and considered.

At the same time, a neural network was trained that classifies several specified classes. As part of this experiment, real video data obtained from the aircraft equipment was used. Thus, it was shown that it is possible to classify the zones of the frame based on the use of semantic segmentation and neural network training.

REFERENCE

1. M. G. Vattimena, V. A. Nenashev, A. A. Sentsov and A. P. Shepeta, "On-board unlimited aviation complex of environmental monitoring", 2018 Wave electronics and its application in Information and Telecommunications systems(WECONF), St. Petersburg, 2018, pp. 1-5. doi: 10.1109/WECONF.2018.8604382

2. Podoplekin Yu. F., Shepeta D. A., Nenashev V. A. Modeling of on-board radar input signals caused by reflections of the sounding signal from the underlying surfaces of the earth and the sea // The Sea Messenger. 2016. No. 4. pp. 69-71.

3. Rybkin S. V., Nesterov A. Yu. Approaches in the recognition of road signs // In the collection: Problems of the formation of a unified scientific space. Collection of articles of the International Scientific and Practical Conference. In 4 parts. 2017. p. 16-19

4. Convolutional neural network, part 2: learning by error back propagation algorithm / / URL: https://habr.com/ru/post/348028/

5. Nenashev V. A., Sentsov A. A., Kuyumchev G. V. Modeling of the process of forming a high-resolution radar image in an on-board radar. 2013. Vol. 2. no. 3. pp. 48-56.

6. Nenashev, V. A., Kryachko, A. F., A. P. Shepeta, Burylev D. A. Features of information processing in the on-Board dip small radar on the basis of the UAV, SPIE Future Sensing Technologies, Tokyo, Japan, 2019, pp. 111970X-1-111970X-7.

7. Kapranov, E. A. Nenashev, V. A., Sergeev A. M., Burylev D. A., S. A. Nenashev Distributed matrix compression techniques, masking and error-correcting coding of images in high-speed network of information exchange, data processing and information aggregation, SPIE Future Sensing Technologies, Tokyo, Japan, 2019, pp. 111

DEVELOPMENT AND RESEARCH OF AUTOMATED ARRHYTHMIC EPISODES DETECTION ALGORITHMS BY ELECTROCARDIOGRAPHIC SIGNAL

Bella Akopyan

Saint-Petersburg State University of Aerospace Instrumentation,
Saint-Petersburg, Russia
E-mail: akopyan.bella@yandex.ru

Abstract
The objects of the research are the models of *ECG* processing and arrhythmia detection algorithms, which are based on the *QRS* complexes detection methods and could be used in the development of automatic diagnostic systems.
In the course of the research, arrhythmia detection algorithms based on the *QRS*-complexes detection methods were developed and modeled. The quality indicators of the developed algorithms were obtained, and the best of them was determined by the criterion of the minimum probability of a false decision.
Keywords: electrocardiosignal, electrocardiogram, arrhythmia, QRS-complex, signal processing, arrhythmia detection, detection algorithm, simulation model, computer model, MathCAD.

INTRODUCTION

Modern electrocardiography is characterized by a wide use of digital electrocardiographs and heart monitors with built-in algorithms for automatic processing, analysis and interpretation of electrocardiograms (ECG). In particular, such devices are widely used to diagnose heart rhythm disorders, such as different types of arrhythmia.

The methods of heart rhythm analysis are similar to the methods of heart rate variability analysis [1]. However, for reliable ECG diagnostics using variability methods, it is necessary to resort to long-term signal recording and delayed analysis of previously recorded ECG fragments, while the duration of arrhythmia diagnostics should not exceed several seconds [2]. In this regard, there is a need of real time algorithms of arrhythmia detection. The algorithms should also be insensitive to low noise levels in order to avoid false positives in real conditions and setup period should not exceed several seconds [2].

The generalized principle of automated arrhythmia detection algorithms operation can be depicted as a block diagram shown in Figure 1. After receiving and processing the received signal, it is necessary to establish the presence of the cardiac cycle in the analyzed ECG segment, and then it is required to determine whether the rhythm is normal or pathological.

To improve the reliability of automatic diagnosis of arrhythmias, it is necessary to solve two tasks. The first one is the choice of the *QRS*-complex detection method, which provides the minimum total probability of detection error, and the second one is the investigation of various heart rhythm decision-making rules and the development of rule that provides the minimum total probability of decision error.

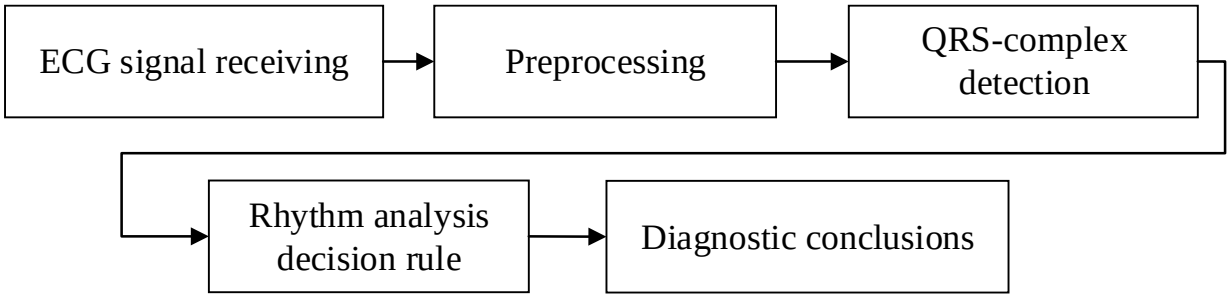

Fig.1 – The generalized principle of automated arrhythmia detection algorithms operation

BASIC QRS-COMPLEX DETECTION ALGORITHMS

The correlation-extreme detection method [3-4] and the digital filtration method [5] were chosen as methods for basic *QRS*-complex detection algorithms, since they could be used in real time mode and they are resistant to interference various additive interference signals [5-6].

As a *QRS*-complex digital filtration algorithm, an algorithm based on the one described in [5] was chosen, since it is recommended as one of the most accurate and insensitive to low noise levels. The block diagram of the algorithm is shown on Figure 2. First, the ECG signal is passed through a differentiator with a 62.5 Hz notch filter (DU), the mathematical model of which is described by the formula (1):

$$Y0_n = X_n - X_{n-4},\ n = 4,5\ldots N-1, \tag{1}$$

where *Y*0 is the output signal of the differentiator, *X* is the initial *ECG* signal, and *N* is the sample size. The differentiated data is then passed through a digital low-pass filter described as (2):

$$\begin{aligned} Y1_n &= Y0_n + 4Y0_{n-1} + 6Y0_{n-2} + \\ &+4Y0_{n-3} + Y0_{n-4},\ n = 4,5\ldots N-1, \end{aligned} \tag{2}$$

where *Y*1 is the output signal of the low-pass filter.

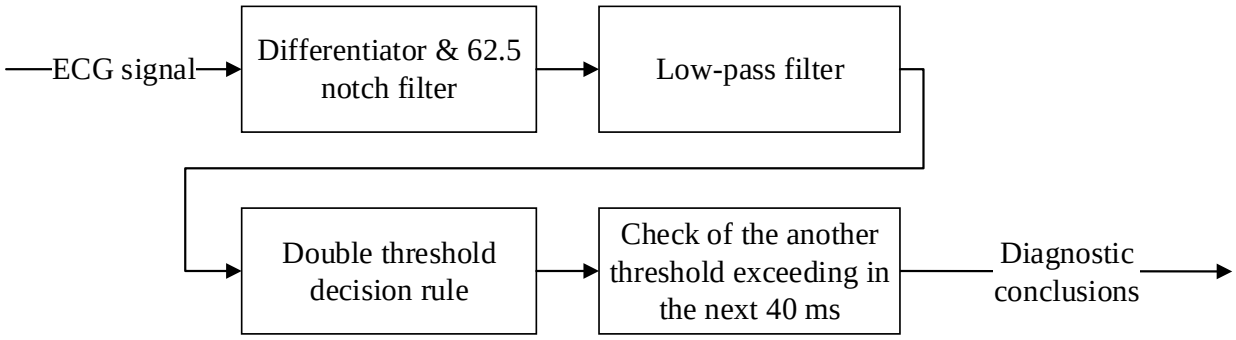

Fig.2 – The block diagram of the chosen QRS-complex digital filtration algorithm

As in [5] the two thresholds are used, which are equal in amplitude (C=3,75 mV) but opposite in polarity. As it is The output of the low-pass filter is scanned until a point with amplitude greater than the positive threshold is reached. This point is the onset of a search region (40 ms in the research). Since it is not necessary at this stage to classify the discovered *QRS*-candidate, the number of conditions used in [5] can be reduced. If no other threshold crossings occur within the search region, the occurrence is classified as a noise sample. Otherwise, the following two conditions (instead of three in [5]) are tested (3):

$$\begin{aligned} &Y1_{n+j} < -C,\ Y1_{n+k} > C, \\ &0 < j < 40,\ j < k < 40. \end{aligned} \tag{3}$$

If the conditions (3) apply, the occurrence is classified as a *QRS*-candidate.

On the other hand, the principle of the correlation-based algorithm [4] is the calculation of the correlation coefficients between the values of the *ECG* reference complex array, containing *N* discrete samples, and *ECG* samples containing N_{ECG} discrete counts (N_{ECG}>>N), which is necessary to determine the location of *QRS*-complexes by using a sliding window (4) for all samples of ECG:

$$r[k] = \frac{\sum_{n=0}^{N-1}\left(x_i[n]-m_i\right)\left(x_j[n+k]-m_j[k]\right)}{\sqrt{\left[\sum_{n=0}^{N-1}\left(x_i[n]-m_i\right)\right]^2\left[\sum_{n=0}^{N-1}\left(x_j[n+k]-m_j[k]\right)\right]^2}}, k = 0,1..N_{ECG}-N-1,$$
$$\text{where } m_i = \frac{1}{N}\sum_{n=0}^{N-1} x_i[n],\ m_j[k] = \frac{1}{N}\sum_{n=0}^{N-1} x_j[n+k], \tag{4}$$

where x_i is the samples of the reference *QRS*-complex, x_j is the input ECG array.

The *QRS*-complex detection rule could be described as formula (5):

$$k_R = \arg\max\left\{\forall k : r[k] > C\right\} + \frac{N}{2}, \tag{5}$$

where k is the sample number of *QRS*-candidate, C is the threshold value [4].

DEVELOPMENT OF THE RHYTHM ANALYZING RULES

The methods of arrhythmia detection are similar to the methods heart rate variability analysis (HRV) [1]. However, methods of arrhythmia detection must work in real time. Obviously, the results of decision-making about the heart rhythm disorders depend on the results of *QRS*-complexes detection. It should be noted that since the position of the *R*-wave peak can be estimated with some deviation from the true one, it is necessary to minimize the influence of this deviation at the stage of arrhythmia detection. In this regard, it is advisable to use the relative indicators based on *RR*-intervals. In particular, the variability of the heart rate can be judged by fluctuations in the duration of *RR*-intervals over a short period of time [1].

During this stage of the heart rate analysis the value of the current *RR*-interval is estimated, defined relative performance parameter based on the magnitude of the interval and compared against a threshold value. If the value of the parameter exceeds the threshold value, an arrhythmic episode is detected.

The simplest relative performance parameter that can be used to estimate heart rate variability is the absolute value Rd_n of the difference between adjacent *RR*-intervals. If the absolute value of the difference is less than the threshold value C, then the rhythm is normal, otherwise an arrhythmic episode is detected. Since the heart rate variability normally does not exceed 10% [1], and the minimum value of the normal heart rate F_{HR} is 60 beats/min, the threshold value can be taken as

$$C_2 = 10\% \cdot t_{RR} = 10\% \cdot \frac{60}{F_{HR}} = 10\% \cdot \frac{60}{60}[\text{s}] = 0{,}1 \text{ s}. \tag{6}$$

To develop an alternative algorithm, it is advisable to turn to standard time methods for estimating heart rate variability and upgrade them. The most common statistical time characteristics of variability in the practice of analysis, which fully reflect the nature of the heart rate, are the *SDNN* and *SDANN* [1-2]. *SDNN* is the standard deviation of *RR*-intervals over the entire period of heart rate monitoring under consideration and *SDANN* is the standard deviation of *RR*-intervals over short segments of multi-hour recordings [1]. With regard to the problem of arrhythmia detection in real time, the calculation of standard deviation could be also resorted to, but based on the fact that the arrhythmic episode corresponds to a sharp change in the duration of the *RR*-interval.

The chosen parameter is based on the principle of *SDANN* and uses the value of the standard deviation of *RR*-intervals over short segments. The proposed information parameter S is equal:

$$S_m = \sigma_m - \sigma_{m-1}, \tag{7}$$

where σ is equal the measure of standard deviation over the sliding window with a duration of several *RR*-intervals and m is the number of current window position. Based on the condition that the algorithm setup period should not exceed several seconds and the minimum normal heart rate of 60 beats/min, a duration of the sliding window was chosen equal to 5 *RR*-intervals. At the same time, the structure of the decision rule itself remains the same as for the Rd_n: if the checked parameter is less than the threshold value C_2, then the rhythm is normal, otherwise, an episode of arrhythmia is recorded. The threshold value C_2 used in this decision rule is equal $sqrt(0.1) \leq\approx 0.3$.

Thus, four algorithms for arrhythmia detection were developed:

1. Based on the correlation-based method and the difference of adjacent *RR*-intervals;
2. Based on the correlation-extremal method and the difference of the *RR*-intervals' standard deviations;
3. Based on digital filtering and the difference of adjacent *RR*-intervals;
4. Based on digital filtering and the difference of the *RR*-intervals' standard deviations.

RESULTS OF THE RESEARCH

The study uses ECG recordings created using a simulated model of a signal with interference [7] based on the parameters of real ECG recordings presented in the MIT-BIH Normal Sinus Rhythm Database and MIT-BIH Arrhythmia Database. The created ECG database contains 1200 ECG recordings lasting 120 seconds with a sampling frequency 1000 Hz, divided into three categories:

1) Normal Sinus Rhythm ECG based on the records of the MIT-BIH Normal Sinus Rhythm Database with the HRV parameter ±5%;

2) ECG of normal form based on the records of the MIT-BIH Normal Sinus Rhythm Database with simulation of single extrasystolic arrhythmic episodes (atrial and ventricular), which make up less than 10% of the total number of ECG cardiocycles;

3) ECG with atrial fibrillation based on the parameters of the records from the MIT-BIH Arrhythmia Database.

During the research, a Type I error, or false positive, is the wrong decision about the rhythm state, and Type II error, or false negative, is a mistaken decision about normal heart rate. The criterion for choosing the best of the developed algorithms is the minimum summary error probability.

Using the statistical modeling in MathCAD computer algebra system (Table 1), it was found that the minimum total probability of Type I and Type II errors corresponds to the detection algorithm based on digital filtering and the difference of the *RR*-intervals standard deviations. The examples of the best algorithm's performance are shown on Fig. 3-5.

Table 1

The estimates of the errors probability

Error probability	Algorithm based on the correlation-based method, C=0,95		Algorithm based on digital filtering, C=3,75	
	the difference of adjacent *RR*-intervals, C_2=0.1	the difference of the *RR*-intervals standard deviations, C_2=sqrt(0.1)	the difference of adjacent *RR*-intervals, C_2=0.1	the difference of the *RR*-intervals standard deviations, C_2=sqrt(0.1)
Type I	0.0042	0,0015	0,0093	0,0005
Type II	0.0098	0,0056	0,0015	0,0059
Summary	0.014	0,0071	0,0108	***0,0064***

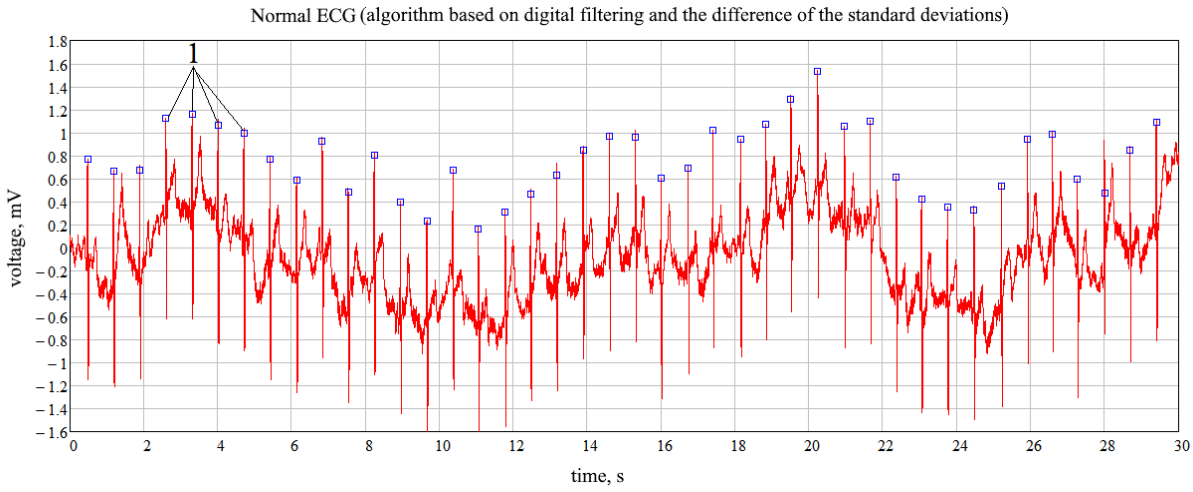

1 – Results of *QRS*-complex detection

Fig. 3 – Results of arrhythmic episode detection (Normal Sinus Rhythm ECG) by the algorithm based on the digital filtering and the difference of the standard deviations with a threshold value of C_2=sqrt(0.1)

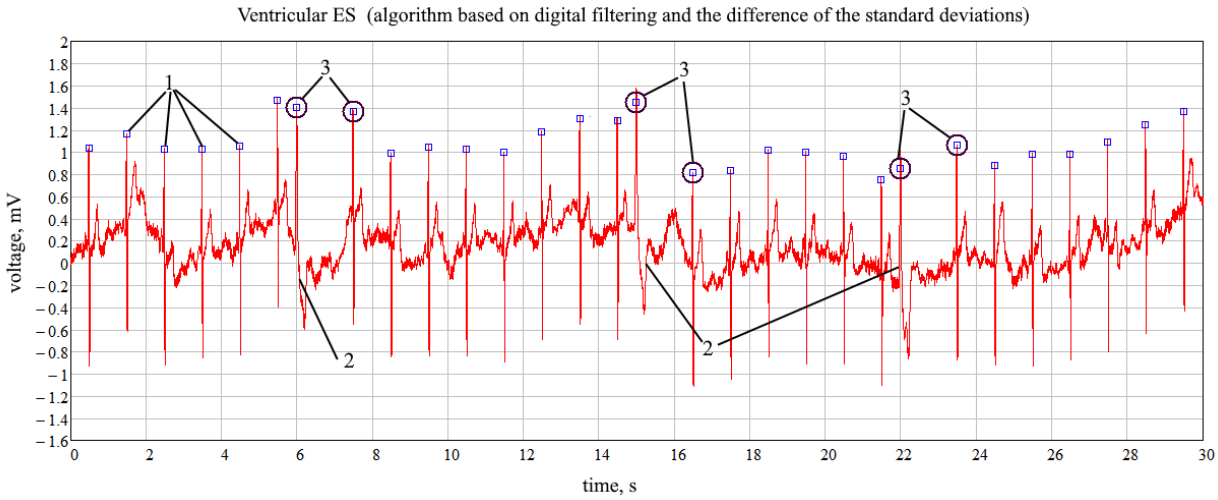

1 – Results of *QRS*-complex detection, 2 – *QRS*-complexes, defined as an arrhythmic episode

Fig. 4 – Results of arrhythmic episode detection (ECG with ventricular extrasystoles) by the algorithm based on the digital filtering and the difference of the standard deviations with a threshold value of C_2=sqrt(0.1)

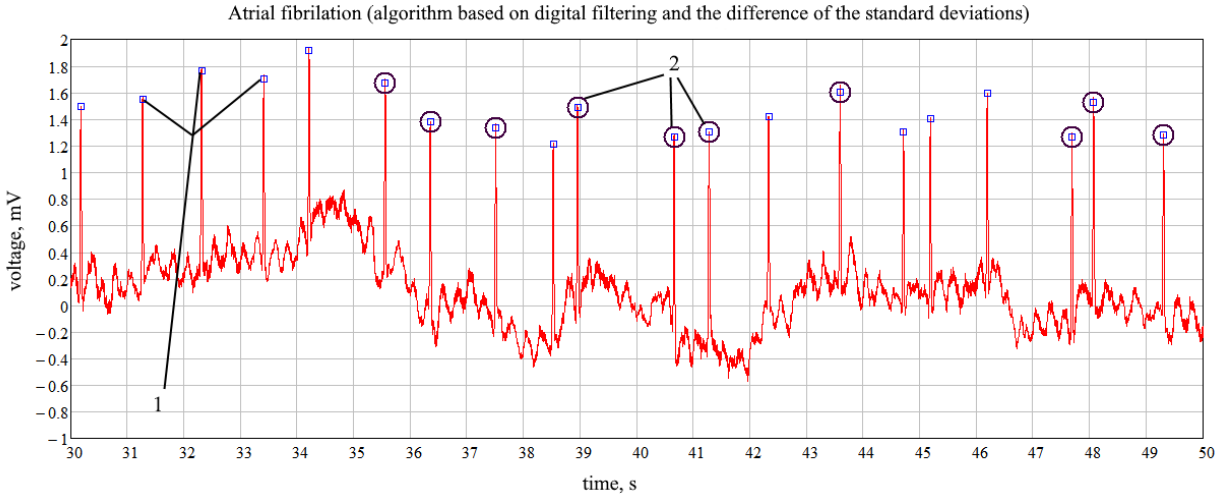

1 – Results of *QRS*-complex detection, 2 – *QRS*-complexes, defined as an arrhythmic episode

Fig. 5 – Results of arrhythmic episode detection (ECG with atrial fibrillation) by the algorithm based on the digital filtering and the difference of the standard deviations with a threshold value of C_2=sqrt(0.1)

CONCLUSION

The algorithms described above could be used as the basis for the program or software for arrhythmia detection. The algorithms based on digital filtering and the difference of the standard deviations has shown the best quality indicators it is recommended to use in heart rate monitoring systems. In the future, it is planned to develop an arrhythmic episodes classification algorithm based on the selected one.

REFERENCES

1. Heart rate variability: standards of measurement, physiological interpretation, and clinical use – Bulletin of Arrhythmology [in Russian]. URL: http://www.vestar.ru/atts/10480/HRV%20standards.pdf (accessed 30.01.2021)

2. The duration of the diagnosis of arrhythmias for emergency care should not exceed several of seconds – Medvestnik [in Russian]. URL: https://medvestnik.ru/content/interviews/Prodoljitelnost-diagnostiki-aritmii-dlya-okazaniya-ekstrennoi-pomoshi-ne-doljna-prevyshat-neskolkih-desyatkov-sekund.html (accessed 30.01.2021)

3. A robust open-source algorithm to detect onset and duration of QRS-complexes /W. Zong, G.B. Moody, D. Jiang// Computers in Cardiology №30. 2003. P. 737-740.

4. Zharinov, O. O. Application of the correlation-extreme method for solving problems of detecting and evaluating the positions of reference points of QRS complexes in an electrocardiogram/ O. O. Zharinov, I. O. Zharinov/ Scientific and Technical Bulletin of Information Technologies, Mechanics and Optics. Issue 5 St. Petersburg: ITMO, 2011. pp. 85-90. URL: https://cyberleninka.ru/article/n/primenenie-korrelyatsionno-ekstremalnogo-metoda-dlya-resheniya-zadach-obnaruzheniya-i-otsenivaniya-polozheniy-opornyh-tochek-qrs (accessed 30.01.2021)

5. Friesen, G.M. A comparison of the noise sensitivity of nine QRS-detection algorithms/ G.M. Friesen, T.C Jannett, M.A. Jadallah et al.// IEEE Transactions on biomedical engineering, vol. 37. №1. 1990. P. 85-97.

6. Köhler, B.-U. The principles of software QRS-detection/ B.-U. Köhler, C. Hennig, R. Orglmeister// IEEE Engineering in medicine and biology, №2. 2002. P. 42-57.Zong, W.

7. Akopyan, B. Development of a simulation model of an electrocardiosignal in computer algebra system//Bulletin of the UNESCO department “Distance education in engineering” of the SUAI: Collection of the papers. St. Petersburg, Issue 5.– SPb.:SUAI, 2020.

AUTOMATION OF THE ASSEMBLY PROCESS OF DESIGNING COMPLEX PRODUCTS USING ADDITIVE MANUFACTURING

Maria Belova

Saint Petersburg State University of Aerospace Instrumentation
E-mail: marebel13@mail.ru

Annotation
Automation of the assembly process of designing complex products in modern life is an important and relevant direction of development in production. To solve this multifaceted problem, various methods and models of informatics, as well as discrete mathematics, for example, graph theory, artificial intelligence, robotization, combinatorial geometry, are used.

Previously, to create complex combinatorial products in industry, various methods were used by which the degree of load, pressure and other physical, dimensional and kinematic properties of the finished product were calculated on its individual components, or using large-scale and complex calculations. But with the development of human society comes the development of industry, where Industry 4.0, based on the automation of production using cyber-physical systems, is increasingly being introduced. In this regard, the introduction of computer-aided design is applicable, which makes it possible to consider a complex product immediately as a set of elements (parts, surfaces, geometric primitives, etc.), on which relations of various physical nature (geometric, mechanical, etc. properties) are already predefined.

To solve this problem, in 1970, the production was confident that the design was theoretically computerized. The scope of the machine was small, mainly the emphasis was on the possibility of automatic drawing. So, with the development of this topic, a **computer-aided design (CAD) system appeared**, based on the use of computer systems, as well as telecommunication technologies.

As a kind of information systems, CAD is referred to as multilevel structures, which include computer technology, various types of software and service personnel.

The CAD structure is regulated by GOST 23501.101-87 and includes two classes of subsystems: design and maintenance. The main purpose of the design modules is to solve specific design tasks, and the functions of information exchange between them are assigned to the service subsystems (Figure 1).

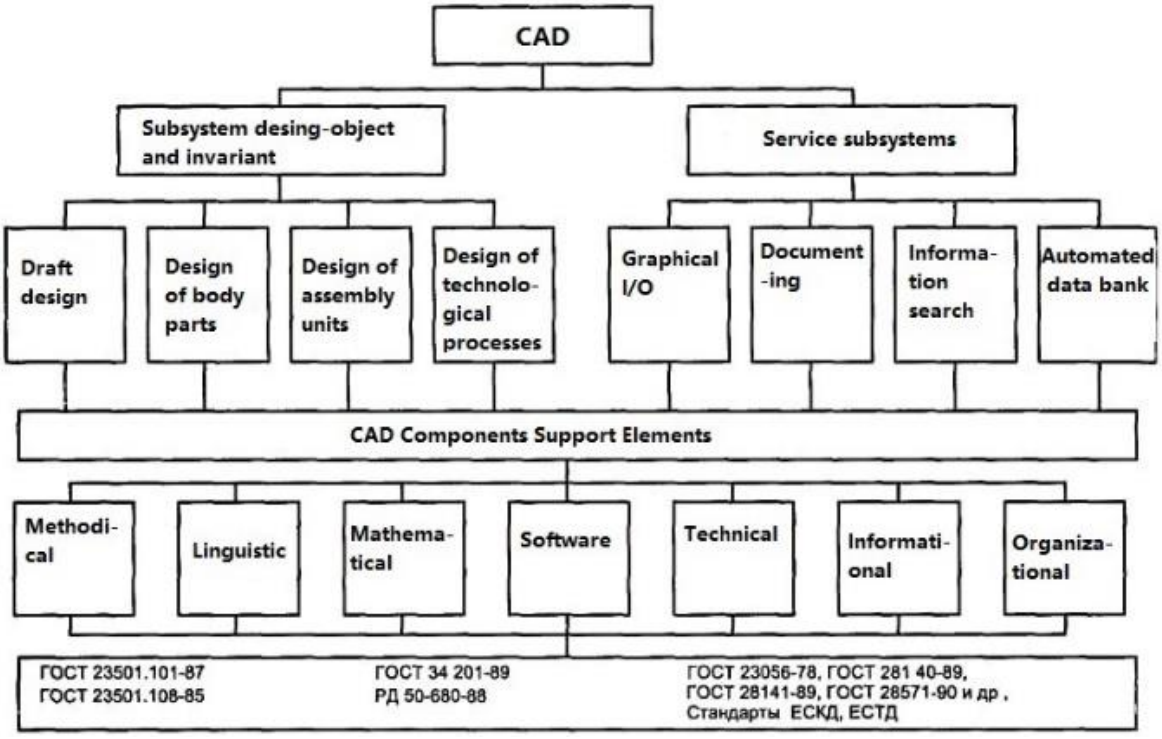

Figure 1 - CAD subsystems and components

The main goal of the computer-aided design system is to improve the quality of finished products and to instantly respond to emerging defects in these products. With the help of computers, CAD has advantages over old design methods, one of them is a fast and affordable process of designing a structure and product model, shortening project lead times, minimizing testing of finished products, reducing material waste, etc.

In general, the design process in CAD can be simplified by the diagram shown in Fig. 2. This diagram shows the elementary cell of the design and development process, from the chain that the real automated process consists of. All design systems created with the help of modern computer technology are automated. The most important role in these systems is played by a human engineer who develops the design of new technical means. A person in CAD solves all non-formalized design tasks and work planning tasks. Modern CAD is a tool of a highly qualified design engineer, therefore close interaction between a person and a computer in the design process is one of the most important principles of building and operating CAD.

The main block in the scheme of the computer-aided design process (Fig. 2) is the block of design solutions. Depending on the completeness of the formalization of our knowledge in a specific subject area, the design decision can be performed automatically or in an interactive mode. Based on the input data and constraints (independent design parameters), the block changes the variable parameters (decision factors) to obtain acceptable design solutions (dependent variables).

The design results should be presented in a form that is convenient for human perception, and contain information on the basis of which the engineer could make judgments about the design results.

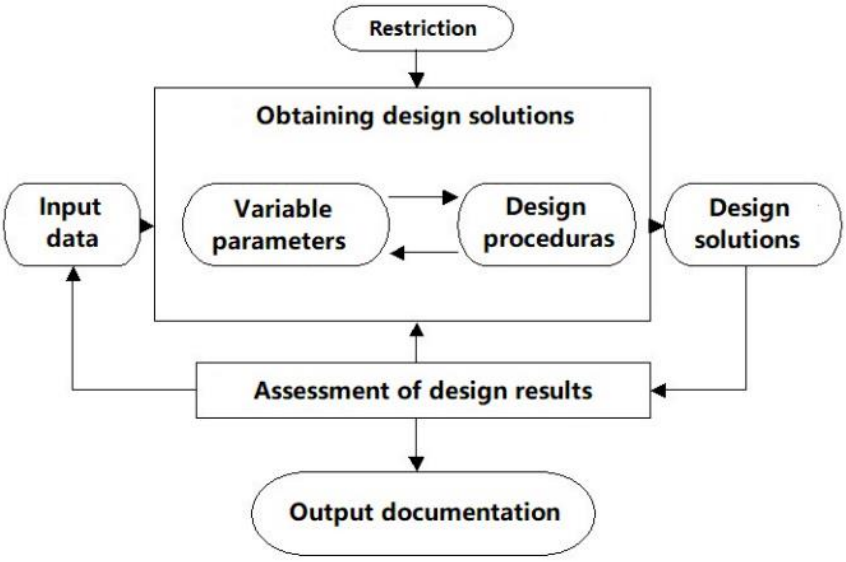

Figure 2 - Diagram of the CAD process

Consideration of even such a simplified design process diagram allows clarifying the division of function between the engineer and the computer in CAD. Obtaining options for design solutions and their presentation in a form convenient for human perception can be assigned to a computer to the extent that the mathematical support of design procedures will allow it. But even with the automatic receipt of design options, the engineer retains the most important functions - input of initial data for design, final assessment and approval of design solutions. In the interactive design mode, the engineer is directly involved in solving problems, influencing the choice of decision factors and refining the independent variables. Obtaining output documentation in accordance with existing requirements is a routine operation and should be performed automatically.

Based on the above, the software model of the automated design procedure can be represented by the diagram shown in Fig. 3.

Automation of the assembly design process in production is achieved with the help of special programs that allow you to assess all the risks and impacts on an already finished product at the initial stages of its development. The most common programs are NX, CATIA, Mastercam, AutoCad, etc., which are universal software products that offer the possibility of multivariate solutions in different operating modes. All these advantages are achieved with the help of the main CAD module - compilation of 2D models and geometric 3D modeling.

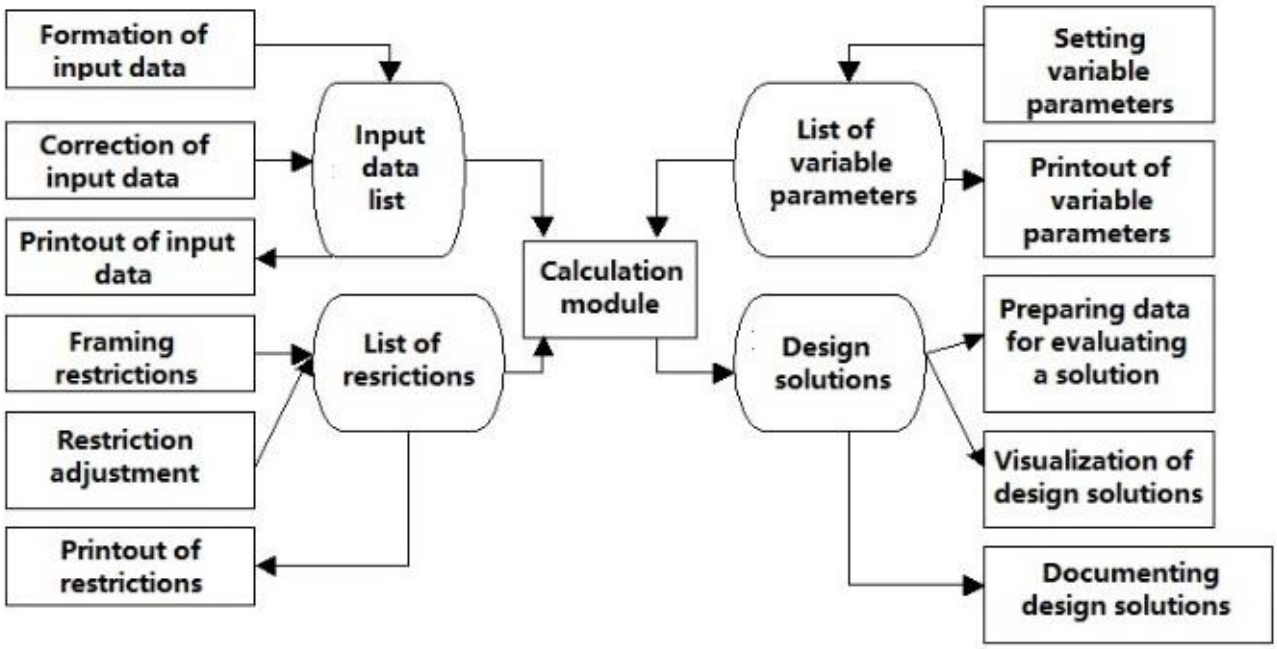

Figure 3 - Software model of the design procedure in CAD

A powerful mathematical apparatus simplifies engineering calculations, allowing in real time visually using 3D models to assess the controlled value and its dependence on changes in the designed structure. Thus, the use of CAD with the addition of additive manufacturing will several times increase the advantages of design automation, because in the manufacture of complex products it will be possible to carry out all the experiments at the initial stages, minimizing the risks of a large number of defects in finished products, as well as conducting various kinds of tests on 3D models. only on electronic computers, but also on printed prototypes made using additive technologies with a minimum amount of consumable material.

With the constant development of the industry and the introduction of robotization, computer technology and other components of Industry 4.0, each production wants to reduce the production time in the product life cycle, while maintaining its quality. That is why the use of additive technologies at the design stage will help make this process automated, because any cycle of additive manufacturing includes quality and property control. In the process of additive manufacturing, building is carried out with constant control of the main parameters of the process: monitoring the excess oxygen level in the chamber, maintaining the required laser power, controlling the temperature in the building zone, etc.

Computer-aided design systems include one of the stages of creating geometric models for a reason, because the very principle of operation of additive installations is based on the construction of thin horizontal layers from 3D models created using computer-aided design (CAD) systems.

Prospects for the development of design automation are determined by the needs of industrial production and the state of development of science and technology. Even in economically developed countries, out of 100% of the production time during which the product is in the workshop, 95% of it is in transportation and waiting, and only 5% is directly in production, and of the production time, only 30% falls directly on processing, while the rest time is spent on loading, installing, securing.

Thus, the main task of using CAD is to increase the efficiency of industrial production, increase its productivity and efficiency, and reduce the cost of products. Automation of the design of complex products will help in the future to sufficiently reduce the production time, increase the quality and complexity of finished products, ensure the optimality of technological developments by choosing them from a variety of possible solutions created on a computer.

Experts interviewed by CNews note that standardization and automation of integrated design will become the trend of the near future on the CAD systems market. This means that the exchange of information between different systems, as well as within CAD systems, will become critically important; a transition will be made to a closer integration of various modeling, design and engineering analysis tools into a single work environment for design and technological departments.

A literature:

1. Управление качеством аддитивных изделий / А. В. Чабаненко // РИА: Журнал.: «Стандарты и качество». 2018. №2. С. 90-94.

2. Комбинаторные модели для сборки и декомпозиции изделий / Божко А. Н. // Наука и образование МГТУ имени Н. Э. Баумана. Электрон. журн. 2015. № 10. DOI: 10.7463/1015.0817524

3. Virtual reality for assembly methods prototyping: a review / Seth A., Vance J., Oliver J. // Virtual Reality. 2011. Vol. 15. Issue 1. Pp. 5-20. DOI: 10.1007/s10055-009-0153-y.

4. Методы искусственного интеллекта в автоматизированном проектировании процессов сборки / Божко А. Н., Родионов С. В. // Наука и образование МГТУ имени Н. Э. Баумана. Электрон. журн. 2016. № 8. DOI: 10.7463/0816.0844719

5. Аддитивные технологии и аддитивное производство/ https://extxe.com/ (дата обращения 19.02.2021)

6. Индустрия 4.0: Big Data, цифровизация и рост экономики https://habr.com/ru/post/507822/

FULL CYCLE AUTOMATED ADDITIVE MANUFACTURING

Daniele Casadio

Saint-Petersburg State University of Aerospace Instrumentation,
Saint-Petersburg, Russia
E-mail: kazdanila@gmail. com

Annotation
Full automation of the3D printing process will minimize the possibility of marriage due to the human factor. 3D printing will be able to occur around the clock. Closed full cycle will allow to get on the output of finished products of the proper quality and appropriate regulatory sizes and evaluated by metrological equipment.

3D printing technology was introduced in 1986, when 3D Systems developed the first special printer, a stereolithography machine, which was used in the defense industry. Laser stereolithography is one of the technologies of rapid prototyping. The stereolithography device was first patented by Chuck Hull in 1986. Laser stereolithography technology is based on photo-initiated laser radiation or mercury lamp-measurement of photopolymerizing composition (FPC). Using this technology, the computer-designed 3D object is grown from liquid FPC in successive thin (0.1 -0.2mm) layers formed under the influence of laser radiation on a mobile platform immersed in a bath with FPC. 13 Laser stereolithography allows you to go from a design or design idea to a finished part model in no time (from a few hours to a few days). The first devices were extremely expensive, and the choice of material to create models was limited. The rapid development of 3D printing began with the development of design technologies (CAD), calculations and modeling (CAE), and mechanical processing (CAM). They are used to produce parts of aircraft, spacecraft, submarines, tools, prostheses and implants, jewelry and others. The first additive production systems worked mainly with polymeric materials. Today, 3D printers, embodying additive manufacturing, are able to work not only with them, but also with engineering plastics, composite powders, various types of metals, ceramics, sand.

FDM (FDM - Fused Deposition Modeling) is a process of layered overlay of molten polymer fila and thread. The FDM system will transform the concept of the product into a real copy, check it for the conformity of form and size, and even simulate the health of the product, without resorting to unnecessary time and material costs. Traditional ways of forming parts, such as cutting, casting, forging, stamping, are now known. Each method has its pros and cons depending on the scale of replication. The development of modern additive technologies in recent years has accelerated the time of design and manufacture of the part. But there are questions about the strength and reliability of parts created with additive technologies. They appear due to the fact that the change in the properties of the materials used in the process of product formation are studied to this day, thus revealing previously unknown problems of working with materials.

Additive production in action

Additive technologies have found widespread applications in industries such as automotive and aircraft, electronics, medicine, where complex machines and equipment are created, many experimental models and models of parts are made, requiring a lot of time for construction and manufacture. With the help of a 3D printer, you can create a variety of things: from shoes to jewelry, from plastic phone cases to spinal implants, which are created from medical titanium from food to human tissues and organs.

Cuttings are processed on metal-processing machines to ensure that surfaces and sizes are of the required quality in accordance with their tolerances. The formation of parts surfaces is carried out by sharpening, drilling, milling, stretching, grinding, finishing, electrophysical and other processing methods. Processing methods determine the accuracy of the manufacture, roughness of the surface and the physical and mechanical properties of the surface layer of parts, which are important for achieving high performance of products that determine the reliability of machines. However, this most common process of surface forming of a part is complicated by the attendant phenomena. These include deformations of the blank, tool, machine and equipment during processing. The deformations of individual parts of the technological system affect the accuracy of processing. The accuracy of the processing is also affected by the wear of tools. The accuracy of the processing is directly related to the accuracy of the cutting tool, the geometric inaccuracy of the machine, the inaccuracy of measurements in the processing and adjustment process for size and other factors.

Figure 1. Robotic additive maintenance complex

Manufacturers of 3D printers compete in obtaining high-quality results at the highest speed, try to simplify the software interface, automate the greatest number of functions, so that to print the model to the user was enough just to "press the button." However, 3D printers, like any other technological equipment, may, over time, produce results that do not meet our expectations, or even fail. Staff need to be trained regularly and specialists given a continuous flow of tasks, which in turn leads to high costs. The penetration of robots into all areas of human life is inevitable and their replacement of human specialists is only a matter of time. This shift is predetermined by the second wave of automation, which concentrates on artificial cognition, cheap sensors, machine learning and distributed intelligence. Future use of 3D printing could include the creation of open-source scientific equipment for use in open laboratories and other scientific applications - the reconstruction of fossils in paleontology, the creation of duplicates of priceless archaeological artifacts, the reconstruction of bones and body parts for forensic examination, the reconstruction of highly damaged evidence collected from crime scenes.

3D printing requirements

Simple geometry, a minimum number of "overhanging" elements.

The size of the single model is no more than 20 x20 x20 cm - larger models need to be cut and printed piece by piece.

The thickness of the walls is at least 1 mm. The model does not contain errors.

Ununited elements of the model are stored in separate files in the STL format. Multiple models in one file are not allowed.

Now let's take a closer look at each of the above points.

The essence of FDM technology is layered (starting with the bottom layer) melting of the molten plastic filament.

Molten plastic takes time to harden, so each next layer needs support - on the first layers of such support is the working surface of the printer, and then, as the model is built, the supporting structure is the previous layers. Abs-printer can not print objects hanging in the air - plastic does not have time to freeze and just melted without keeping the shape. Therefore, when printing under all "hanging" elements, supporting structures are built.

Another important requirement for ABS-plastic printing is that the walls in the model should be at least 1 mm thick, otherwise the printer software may simply not see the elements thinner and not seal them. The

standard thickness of the ABS-plastic printing layer is 0.2 mm, the more layers of plastic are connected to each other, the stronger and better the product is.

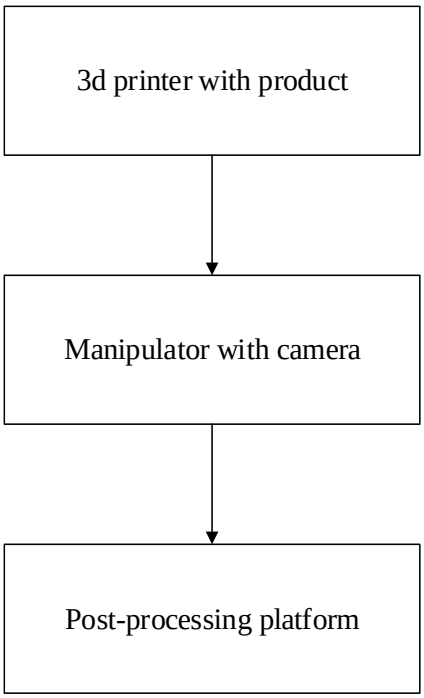

Figure 2. A larger sequence of operations in the maintenance of layered synthesis

Production of 3D parts requires constant control over the process. In this method, the product is made by extrusion of thin strands of molten material layer by layer.

The attractiveness of additive technologies is caused by a number of factors, first of all, they allow:

1. Reduce the ratio of the mass of material needed to release the part to the mass of the part itself from 20:1 (for traditional "subtraction" technologies) to 1:1 (for additive technologies). This factor contributes to a significant increase in the competitiveness of production, as it reduces the demand for raw materials.

2. Save money when you start production because the data you need to run can be stored digitally and reproduced at no additional material cost.

3. To quickly amend at any stage of the production process, to adapt production to the ever-changing demands of the market, to change the size of the batch at any time depending on the increase or decrease in demand.

The main parameter of products in additive manufacturing is strength.

Thus, the theoretical strength of the polymer material zm is the strength of the body with an ideal structure, without damage and defects at the temperature of absolute zero, i.e. in the absence of thermal movement, with a homogeneous static deformation of stretching, providing equal tension of all ties and their simultaneous rupture on the surface of destruction.

The theoretical strength is determined by the formula

$$\sigma_m = N \times F_m,$$

where N is the number of atoms or connections per unit of the section, Fm is the strength of communication (the force of interaction) of two neighboring atoms. Increased orientation leads to an increase in the density of macromolecules packaging and, consequently, to an increase in the number of chemical bonds at the polymer body's destruction area, as well as to an increase in the number of physical nodes. When a sample of a polymeric material is stretched, theoretical strength is defined as

$$\sigma_m = K \times E,$$

where E is a elasticity module and K is a constant equal to 0.08 ÷ 0.16.

It has been established that in polymers of low molecular mass destruction occurs not so much due to the rupture of chemical bonds, but by the sliding of segments, i.e. overcoming the forces of intermolecular interaction.

Products made by additive technologies need to be evaluated on the roughness of the surface and deviations from nominal sizes.

Figure 3. The rough meter

This technology is very flexible and allows you to make products of complex geometry, but in some cases the structure of the part is broken due to surface defects. The problem is solved by video control over the 3D parting production process. This control will be carried out by the developed robotic complex of continuous control of the geometric parameters of additive production, consisting of a video camera mounted on a robotic arm. This feature will allow you to shoot parts from all sides.

However, the lack of development of mechanisms and tools aimed at ensuring the quality of products made with additive technologies, monitoring the operation of additive installation and properties of polymers used in layering, leads to low efficiency of printing processes, increased consumption of materials used in the operation of the installation, inhibiting the introduction of new, production mechanisms based on the use of a digital prototype.

Conclusion

The application of this system will allow to produce products around the clock, without human intervention and to create more complex products by combining previously created spare parts. And the control of metrological equipment will ensure the required level of quality of products.

The list of literature used

1. Совершенствование процессов управления наукоемким производством и оценки его потенциала Печ. РАДИОПРОМЫШЛЕННОСТЬ Издательство: Центральный научно-исследовательский институт экономики, систем управления и информации «Электроника (Москва) ISSN: 2413-9599 Номер: 4 Год: 2016 38-43 Семенова Е.Г., Чабаненко А.В.

2. Управление качеством аддитивных изделий / А. В. Чабаненко // РИА: Журнал.: «Стандарты и качество». 2018. №2. С. 90-94.

3. Процедуры преобразования 3d-модели в исполняемый файл stl для послойного синтеза Чабаненко А.В., Курлов В.В. В сборнике: МОДЕЛИРОВАНИЕ И СИТУАЦИОННОЕ УПРАВЛЕНИЕ КАЧЕСТВОМ СЛОЖНЫХ СИСТЕМ. Сборник докладов Первой Всероссийской научной конференции. Санкт-Петербург, 2020. С. 190-192.

4. Управление качеством 3d печати посредством моделирования компонентной базы аддитивной установки Чабаненко А.В. В сборнике: Избранные научные труды восемнадцатой Международной научно-практической конференции "Управление качеством". ИЗБРАННЫЕ НАУЧНЫЕ ТРУДЫ Восемнадцатой Международной научно-практической конференции. 2019. С. 362-368.

5. Создание корпусных элементов рэа на установке послойного синтеза материалов в рамках проектной работы студентов ГУАП Чабаненко А.В. В сборнике: XXIII Международный Биос-форум и Молодежная Биос-олимпиада 2018. Сборник материалов . 2019. С. 133-137.

6. Quality Assurance of Hull Elements of Radio-Electronic Equipment by Means of Control System / Chabanenko, A.V., Anatoly P.Y. IEEE International Conference. 2018.

MODERNIZATION OF EXISTING SUPPLY CHAINS IN ANYLOGISTIX

Angelina Dobrovolskaya

Saint-Petersburg State University of Aerospace Instrumentation,
Saint-Petersburg, Russia
E-mail: angd999@gmail.com

Abstract

The modern world is developing at a tremendous speed, and logistics is no exception, which is closely interrelated not only with the work of large enterprises, but also with each individual consumer. Supply chain design is an urgent and important task, since companies often deal with a huge number of customers and with a different product range, which requires taking into account many factors, as well as random phenomena. That is why it is necessary to study and apply modern software tools that allow you to effectively design and manage supply chains from the manufacturer to the end user.

Introduction

The supply chain is the process of moving information, material and financial flows between different participants in the chain, aimed at meeting the need for goods or services (Figure 1). When designing supply chains, there is a need to choose the optimal procurement, supply, and logistics strategy.

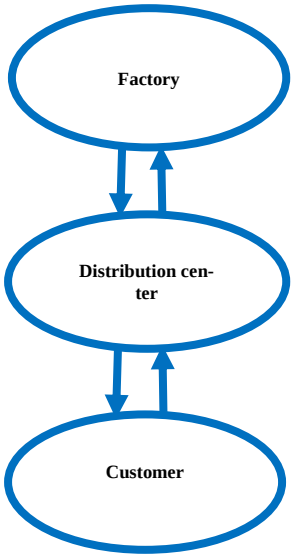

Figure 1-Supply chain structure

Supply chain design involves finding the optimal location of supply chain objects: manufacturers, distribution centers, as well as the distribution of flows between supply chain objects[4]. The cost of finished products depends largely on the cost of transportation, so the entire supply chain should be a well-established and interconnected mechanism that allows you to properly plan inventory and distribute products. Large companies often deal with a variety of customers and with a variety of product ranges, which requires taking into account many factors and working with big data.

Typical tasks of supply chain design[2]:

- Selection of the best order batch;
- Vehicle selection;
- Evaluation of the efficiency of the distribution center;
- Assessment of the efficiency of warehouse space.

In addition, the design of supply chains is a constant and continuous process, since it is largely associated with the occurrence of random processes and phenomena. For the system to work effectively, it is necessary to take into account a large number of factors and quickly respond to emerging changes in the chain.

Modern supply chains require the use of huge amounts of information for analysis, design and optimization at all parts of the chain, which requires more powerful software tools.

Methods for solving supply chain problems[1]:

- Analytical optimization

Assumes a description of the chain by linear equations. When solving the problem, the analytical model used will be optimal, but there is a problem of taking into account new factors, and as the supply chain becomes more complex, the mathematical model will also become more complex.

- Dynamic modeling

The dynamic model reflects the behavior of the supply chain over time, taking into account a large number of factors in all its sections. This model has an advantage for large supply chains, because it has a high level of detail of the chain features.

Consider ways to modernize the existing supply chain using gravity analysis. This method is based on the fact that the costs are directly proportional to the number of goods transported and inversely proportional to the distance of transportation. The optimal location is achieved by minimizing the weighted distance between the distribution center and the consumers.

Gravity analysis is used in the early stages of supply chain design, because it allows you to determine the optimal number and location of chain objects. For gravity analysis in AnyLogistix[3], a minimum amount of input data is required: the number and location of customers, the type of products produced, and the distance of customer service. The result of the analysis is to determine the optimal places for placing objects, when choosing which transport costs are minimized.

Consider the supply chain of some products to consumers in Russia, which has 3 distribution centers and a factory for the production of goods, but the supply chain is inefficient. First, you need to build this supply chain using anyLogistix simulation tools(Figure 2).

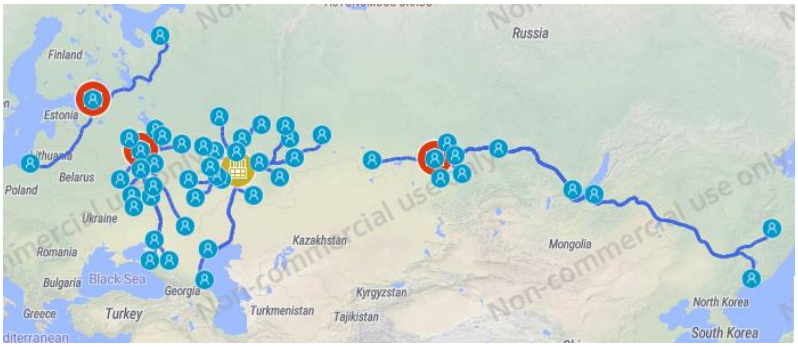

Figure 2-Supply chain

To speed up the delivery of finished products to customers, we will set a limit on the delivery distance of 1000 km(Figure 3):

Figure 3-Optimal location of warehouses

Thus, to meet the existing needs of customers with this distance restriction, 7 warehouses of finished products are needed. After that, using gravity analysis, we will find the optimal location of the factory(Figure 4).

Figure 4-Supply chain with factory

Create an inventory management policy for the factory - the required volume of products is ordered when the order is received. When producing goods in batches, the monetary and time costs for the production of one commodity unit are reduced. We set the size of the order batch; the production time of one batch; the cost of production of one batch. In addition, we add a rule for placing orders that will correspond to the size of the factory's production batch(Figure 5).

#	Source	Product	Type	Batch Size	Step Size
1	Factory	Product	Starts From	5,000	1,000

#	Site	Product	Type	Parameters
1	Factory	Product	Simple make pol.	Time = 3.0 (day)

#	Destination	Product	Rule	Limit, units
1	(All sites)	Product	Can Increase	500
2	(All sites)	Product	Can Decrease	500

Figure 5-Adding experiment data

After starting the experiment, it is necessary to evaluate the statistics of interest and the work of the supply chain(Figure 6).

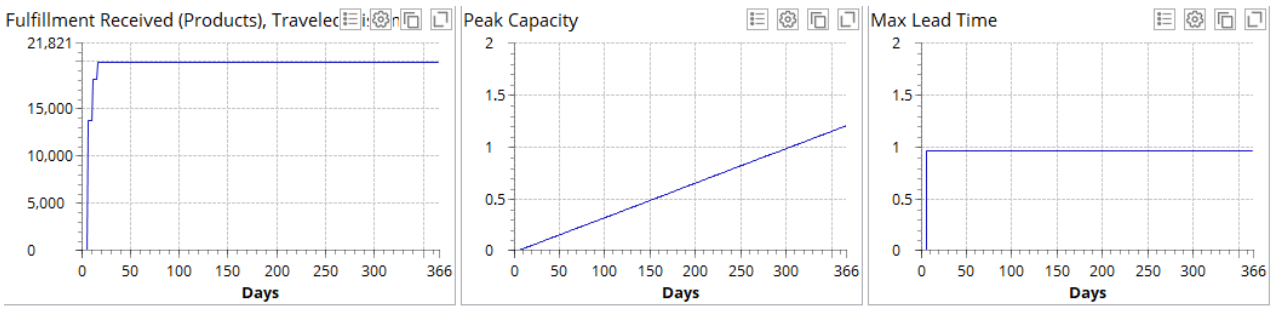

Figure 6-Experiment statistics

Conclusion

The main advantage of AnyLogistix is the combination of analytical optimization tools and dynamic modeling, which allows you to create the most realistic models of supply chains. AnyLogistix allows you to analyze a large amount of data for the efficient functioning of the supply chain. In this case, using gravity analysis, it was revealed that the number and location of warehouses and production of the existing chain is not optimal to meet the existing demand. As a result of the design, a supply chain was created, consisting of 7 warehouses and a factory for the production of finished products. However, the supply chain needs to be refined, as the production and order execution policies are not optimal. It is necessary to have more data so that the chain is as close to reality as possible and allows you to extract the maximum profit of the company.

List of used literature:

1. AnyLogistix supply chain modeling [Electronic resource] Url: https://www.anylogistix.ru/supply-chain-simulation/ (09/03/2021);

2. Supply chain modeling and design[Electronic resource] Url: http://supplychains.ru/2013/11/25/supply-chain-design/ (09/03/2021);

3. Gravity analysis in the AnyLogistix environment [Electronic resource] Url: https://www.anylogistix.ru/solving-facility-location-problem-with-greenfield-analysis/ (09/03/2021);

4. AnyLogistix supply chain design [Electronic resource] Url: https://www.anylogistix.ru/supply-chain-network-design-software/ (09/03/2021).

BELIEF PROPAGATION DECODING WITH CHANNEL ESTIMATION STEP OVER GILBERT-ELLIOTT CHANNEL

Anna Fominykh

Saint-Petersburg State University of Aerospace Instrumentation,
St. Petersburg, Russia
E-mail: aawat@ya.ru

Abstract

The paper studies the effects of channel estimation step when applied to low-density parity-check (LDPC) codes under belief propagation decoding on bit error probability.

Keywords: LDPC, Gilbert-Elliott channel, belief propagation decoding.

INTRODUCTION

Nowadays, information processing and transmission systems are widespread. Due to the properties of such systems the information that is transmitted is a subject to errors, therefore, the task of information integrity appears. For this purpose, coding theory uses methods of error-correcting coding, namely, theory of coding proposes to intentionally introduce redundancy to the information that may be exploited after the transmission in order to correct errors. The redundancy is introduced by means of error-correcting codes. One of the most common types of codes that are used in many modern standards are low-density parity-check codes (LDPC codes).

Low-density parity-check codes (LDPC codes) were firstly proposed by Robert G. Gallager in 1962 [1], but due to the limitation in computational effort in implementing the coder and decoder for such codes, LDPC codes were ignored for almost 30 years. LDPC codes were rediscovered by David Mackay in the 1990s and subsequent development of computers arose a new wave of interest to LDPC codes, which deserve attention due to the near-Shannon-Limit error-correcting capability, low error-floor [2], and easy design with parallel decoding.

When considering mathematical models of channels, it is often assumed that the errors that occur in channels are independent, but in real communication channels, errors that appear are not independent. The question arises whether it is possible to take into account the information about the channel properties during decoding in a case of not independent errors. This issue was discussed in a number of papers [3, 4]. In this work we study the operation of the decoding algorithm for low-density codes, which takes into account information about the properties of the channel. We present the simulation results obtained for specific parameters of the Gilbert-Elliott channel [5].

LDPC codes

A binary (n, k) linear code is a k-dimensional subspace of an n-dimensional vector space over $\mathbb{F}_2$. If a parity-check matrix of a code is sparse, then the corresponding code is called a low-density parity-check (LDPC) code [1]. The sparse nature of LDPC codes means that decoding processes have a fast run-time, as there are fewer operations to compute when compared to a non-sparse parity-check matrix. LDPC decoding algorithms are iterative in nature since decoding proceeds until the codeword has zero syndrome or a predefined number of iterations is reached. The most common decoding algorithm is the belief propagation algorithm. LDPC codes can be specified by a matrix **H**. The parity check matrix is usually visualized as a bipartite graph (Tanner graph) between check nodes and variable nodes, as shown in Fig. 1. Every variable node of the graph corresponds to a column of **H**, while every check node corresponds to a row. The example of parity-check matrix

$$\mathbf{H} = \begin{vmatrix} 1 & 1 & 1 & 0 & 1 & 0 \\ 1 & 0 & 1 & 1 & 0 & 1 \\ 0 & 1 & 0 & 1 & 1 & 1 \end{vmatrix}$$

and its corresponding Tanner graph

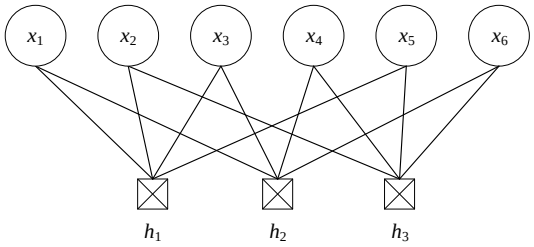

Figure 1 – Tanner graph

Gilbert-Elliott Channel Model

The Gilbert-Elliott model that is depicted in Figure 2 is one of the earliest memory channel models, which is still relevant and widely used in describing real systems. The model was proposed by G. Elliot in 1963 [5] and is a general case of the Gilbert model presented in 1960.

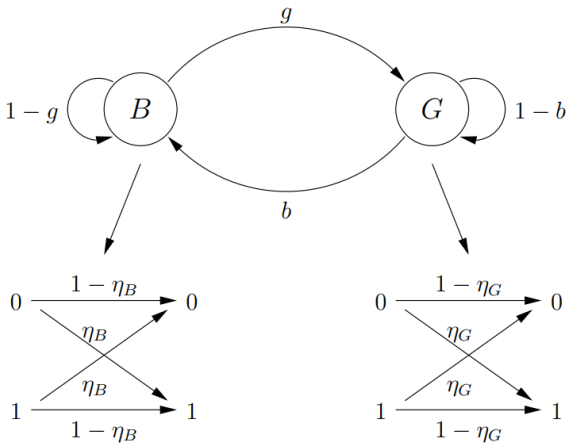

Figure 2 – Gilbert-Elliott channel model

The Gilbert-Elliott model describes a discrete memory channel in which the state of the channel depends on the previous state. The channel is described by two states = {*B*, *G*}, «good» – *G* and «bad» *B*. In a «good» state, the bit error probability in the channel is η_G, in a «bad» state – η_B.

The channel can go from one state to another at any moment. The transition probabilities in «bad» and «good» state may differ. Let us introduce simplified notations that will be used further in this work: the probability of transition from a «good» state to a «bad» one is *b*, and the probability of a transition from a «bad» state to a «good» one is *g*. The transition matrix **P** corresponding to these probabilities has the form

$$\mathbf{P} = \begin{bmatrix} 1-b & b \\ g & 1-g \end{bmatrix}$$

The channel may be described by the set of the following parameters (b, g, η_B, η_G), where $0 < (b, g) < 1$ and $0 < \eta_G < \eta_B < 1$.

Channel states estimation

To assess the channel states, we use channel state estimation algorithm described in [6]. In which the channel state estimation is made based on the channel parameters and the word received from the channel. Channel estimation step is applied before belief propagation decoding algorithm. The result of the estimation step is then fed as an input to the belief propagation algorithm, which performs a certain number of iterations. If the stopping conditions are not met, that is, the code word is not found or a fixed number of iterations is not reached, then the algorithm proceeds from the evaluation step.

Simulation results

The simulation is performed for (576, 288) low-density parity-check code from WiMAX standard [7] and progressive-edge-growth (PEG) [8] code of length 100 and rate 1/2. We consider comparison of three decoding algorithms and compare their performance in Gilbert-Elliott (GE) channel and binary-symmetric channel

(BCS). The first algorithm is the belief propagation decoding algorithm (GE BP). The second algorithm is the same – belief propagation, but with an additional channel state estimation step (GE BP+Estim). The third algorithm is the bit flipping algorithm (GE BF). All algorithms are compared by the probability of error in the information word, i.e., bit error rate (BER). Additionally, the results of the belief propagation algorithm (BSC BP) and the bit flipping algorithm (BSC BF) for a binary symmetric channel (BSC) with varying error probability p_e are presented.

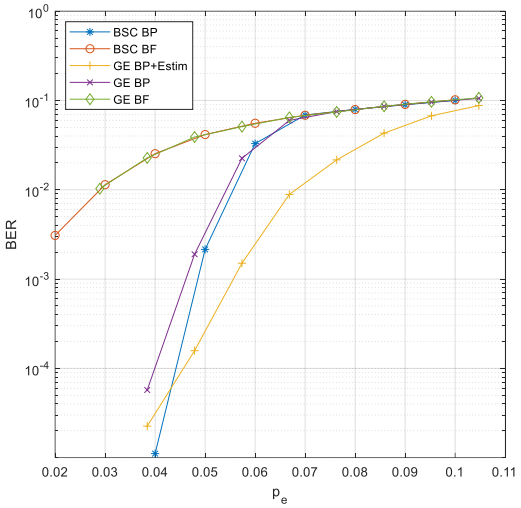

Figure 3 – BER for WiMAX code

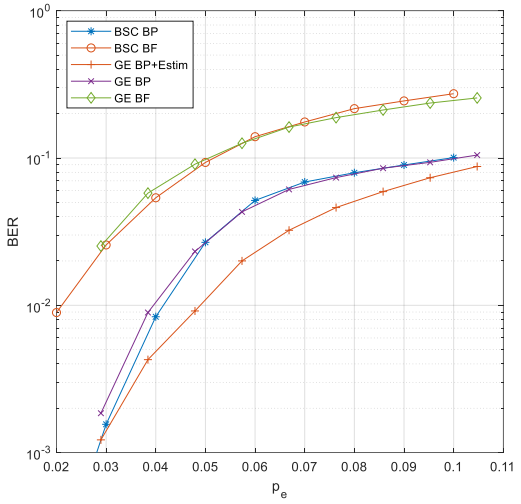

Figure 4 – BER for PEG code

CONCLUSION

The paper examined the effects of channel estimation step when applied to low-density parity-check codes under belief propagation decoding on bit error probability over Gilbert-Elliott channel. From a simulation results it may be concluded that the belief propagation algorithm with an additional channel state estimation step outperforms the standard belief propagation algorithm without estimation step as well as bit flipping algorithm over Gilbert-Elliot channel for considered codes.

REFERENCES

1. Gallager R. Low-density parity-check codes //IRE Transactions on information theory. – 1962. – Т. 8. – №. 1. – С. 21-28.

2. Richardson T. Error floors of LDPC codes //Proceedings of the annual Allerton conference on communication control and computing. – The University; 1998, 2003. – Т. 41. – №. 3. – С. 1426-1435.

3. Eckford A. W., Kschischang F. R., Pasupathy S. Designing very good low-density parity-check codes for the Gilbert-Elliott channel //Proc. 8th Canadian Workshop on Information Theory. – 2003.

4. Eckford A. W., Kschischang F. R., Pasupathy S. On designing good LDPC codes for Markov channels //IEEE Transactions on Information Theory. – 2006. – Т. 53. – №. 1. – С. 5-21.

5. Gilbert E. N. Capacity of a burst-noise channel //Bell system technical journal. – 1960. – Т. 39. – №. 5. – С. 1253-1265.

6. Eckford A. W., Kschischang F. R., Pasupathy S. Analysis of low-density parity-check codes for the Gilbert-Elliott channel //IEEE Transactions on Information Theory. – 2005. – Т. 51. – №. 11. – С. 3872-3889.

7. IEEE Standard for Air Interface for Broadband Wireless Access Systems. //IEEE Std 802.16-2017 (Revision of IEEE Std 802.16-2012). – 2 March 2018. – P. 1–2726

8. MacKay D. J. C. Good error-correcting codes based on very sparse matrices //IEEE transactions on Information Theory. – 1999. – Т. 45. – №. 2. – С. 399-431.

OVERVIEW OF APPROXIMATION METHODS

Viktoria Goncharova

St. Petersburg State University of Aerospace Instrumentation
Saint - Petersburg, Russia
goncarovav344@yandex.ru

Keywords: Polynomial approximation, piecewise linear approximation, approximation by transcendental functions.

Polynomial approximation

This approximation method is convenient to use when considering the principles of operation of many nonlinear converters: modulators, demodulators, generators, and others when they are exposed to one or more harmonic oscillations. The power approximation consists in writing the current-voltage characteristic *i = f (u)* in the form of a polynomial (polynomial) of the *n*-th degree.

Using such a polynomial, you can make an approximation with any degree of accuracy. In this case, the accuracy will be higher if we use high-order polynomials. However, this is inconvenient for analysis.

In practice, the following polynomials are used

first degree (*k = 1*) (fig.1)

$$i = \sum_{k=0}^{n} a_k U^k = a_0 + a_1 U + a_2 U^2 + ... + a_n U^n$$

second degree *(k = 2)*

$$i = a_0 + a_1 u;$$

a shortened third-degree polynomial *(k = 3, a2 = 0)*

$$i = a_0 + a_1 u + a_2 u^2;$$

a shortened polynomial of the fifth degree *(k = 5, a2 = a4 = 0)*

$$i = a_0 + a_1 u + a_3 u^3 + a_5 u^5$$

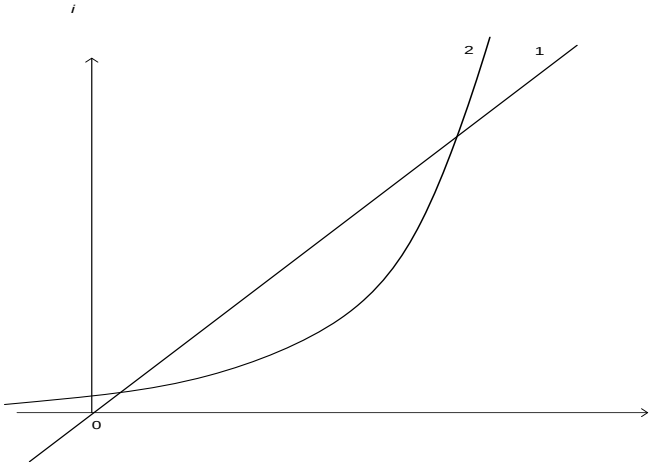

Fig.1- Approximation of the current-voltage characteristic of a nonlinear converter by a straight line (1) and a parabola (2)

Note that the approximation by a polynomial of the first degree, which leads to a straight line 1 (see Fig.1), does not allow us to study nonlinear transformations, for example, the transfer of the signal spectrum to another frequency. This type of approximation is used only in the study of linear processes, such as amplification. The

second-degree polynomial (quadratic parabola 2) already allows us to study nonlinear processes, but only when exposed to weak signals. In general, to use a power approximation, you need to know the coefficients of the polynomial, which are usually determined using the "method of selected points". In other words, the coefficients are found from the condition of equality of the values of the ordinates of the approximated and real characteristics at the selected points.

Piecewise linear approximation

This method is based on the approximate replacement of the real smoothly changing current-voltage characteristic $i = f(u)$ by straight line segments with different slopes.

Fig. 2 shows an approximated characteristic containing two linear sections.

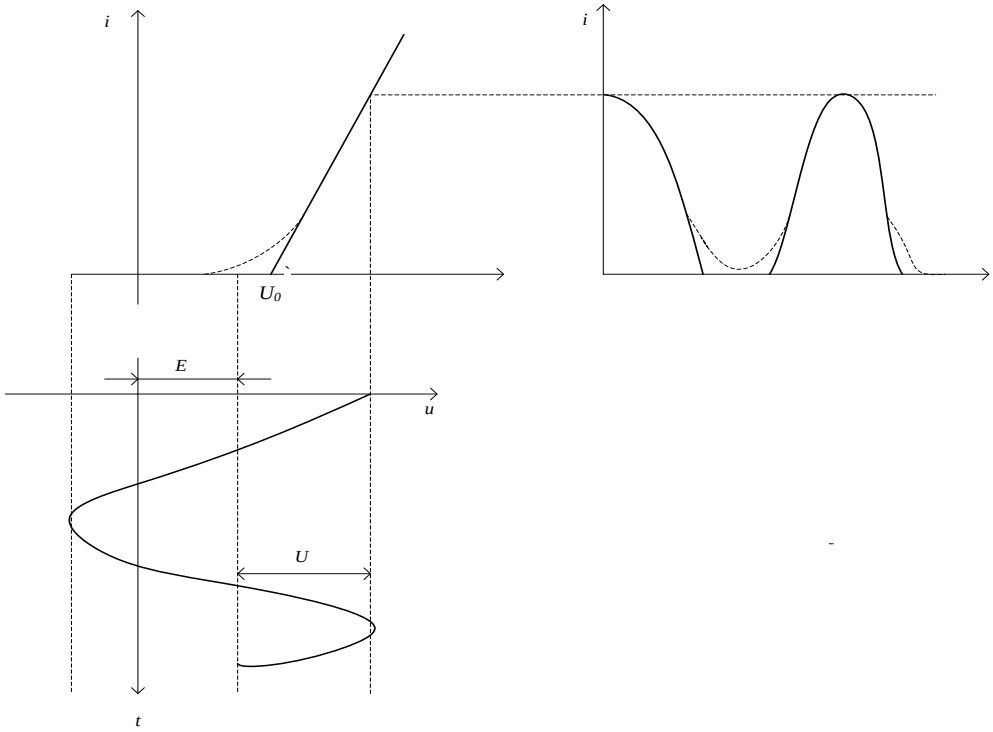

Fig.2 - Approximation of the current-voltage characteristic of a nonlinear converter by straight line segments

Mathematically, this approximated characteristic can be written as, where U_0 is the cut-off voltage; S is the steepness of the characteristic, which has the dimension of conductivity *(Cm or A / B)*. In Fig. 2, the current pulses obtained under the influence of a harmonic oscillation with a large amplitude are constructed by the projection method. When the pulses are decomposed into a Fourier series, the constant component and the amplitudes of the first few harmonics are also close to each other. In other words, for large signals, piecewise linear approximation gives sufficient accuracy of calculations. With small signals, the accuracy drops, and the results may be incorrect. Thus, the piecewise linear approximation method is usually used in the analysis of nonlinear transformation processes in the case of large input signal amplitudes. [1]

Approximation by transcendental functions

In this method, exponents or their sums (but no more than two terms), hyperbolic, trigonometric, and some other functions are used as approximating functions. Most often, the exponential approximation is used. So, in particular, the characteristic of a semiconductor diode can be approximated by an exponent:

$$i(U) = \begin{cases} 0, & U < U_0 \\ S(U - U_0), & U \geq U_0, \end{cases}$$

where *i(U)* is the reverse saturation current; α is the constant that characterizes the temperature potential. This expression defines the initial part of the characteristic well. In other words, the exponential approximation is quite accurate at small amplitudes of the input signals. Otherwise, the calculation error is significant. To determine the suitability of this approximation method for the calculation, the so-called linear reduction is used, the essence of which is as follows. First, the previously presented expression for the current *i* is logarithmed:

$$i = I_0(e^{\alpha U} - 1),$$

Further, the dependence is built on the real current-voltage characteristic

$$\alpha U = \ln(i / I_0 + 1).$$

Then, in the voltage range ΔU, the degree of difference between this characteristic and a straight line is checked. If this difference is small, then the initial characteristic of a nonlinear element (a semiconductor diode) can be approximated by an exponent.

Nonlinear dependencies of a more complex form can be approximated by the sum of two transcendental functions. For example, the characteristic of a tunnel diode is described by the expression

$$\ln(i / I_0 + 1) = f(u)$$

in which the first term determines the tunnel current, and the second — the diffusion current.

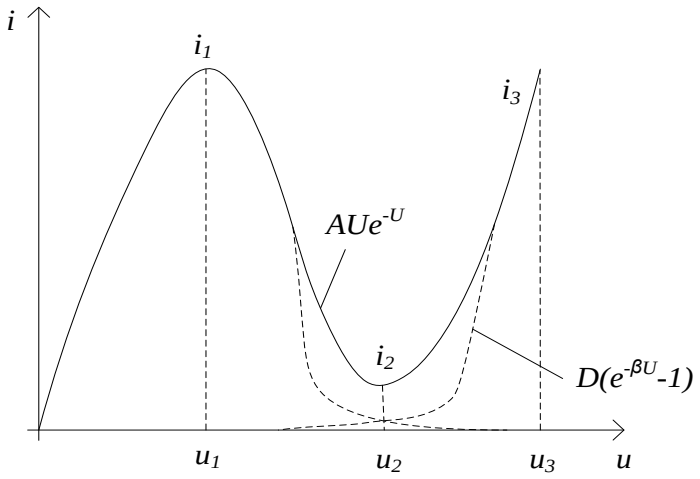

Fig.3 - Example of approximation of the tunnel diode characteristic by transcendental functions

A graphic representation of this characteristic is shown in Figure 3, where the total current is shown as a solid line, and its components are shown as a dashed line.

Fractional-rational approximation (Pade approximation)

Fractional-rational approximation (Pade approximation). Using information about the analytical properties of elementary and special functions can significantly reduce the amount of calculations. The possibility of representing the calculated functions by convergent power series of the form is significantly used

$$\sum_{k=0}^{\infty} c_k z^k$$

Here is $z = x - x_0$; x_0 - the point where the function is decomposed into a series. Note, however, that contrary to popular belief, such series are almost never directly used to calculate functions. The currently widely used method of representing functions is to approximate them by rational fractions of the form

$$R(z) = \frac{a_0 + a_1 z + ... + a_n z^n}{b_0 + b_1 z + ... + b_m z^m} \quad (1)$$

There are various ways to arrive at fractional-rational approximations. In some cases, rational interpolation is used — the interpolation of a function with a rational fraction (1). Then the coefficients $a_j (j = 0,1,...,n)$, $b_k (k = 0,1,...,m)$ are found from the set of relations $R(z_i) = y_i (0 \le i < N, N = n + m + 1)$, which can be written in the following form:approximations come in different ways. In some cases, rational interpolation is used — the interpolation of a function with a rational fraction (1). Then the coefficients are found from the set of relations which can be written in the following form:

$$\sum_{j=0}^{n} a_j x_i^j = y_i \sum_{k=0}^{m} b_k x_i^k$$

These relations form a system of *N* linear algebraic equations with respect to *N + 1* unknowns. Such systems always have non-trivial solutions. We can also write *R(z)* explicitly if we use the apparatus of inverse divided differences. One possible way is to use the theory of continued (or continuous) fractions. For example, the function *tg x* is represented by a continued fraction

$$tg\ x = \cfrac{x}{1 - \cfrac{x^2}{3 - \cfrac{x^2}{5 - ...}}} \quad (2)$$

By breaking off such an infinite fraction, one obtains some finite fraction approximating the function.

More and more popular in recent years, the method of approximating analytical functions is the Pade approximation — such a fractional-rational approximation (1), for which

$$\sum_{k=0}^{\infty} c_k z^k = \frac{a_0 + a_1 z + ... + a_n z^n}{b_0 + b_1 z + ... + b_m z^m} + O(z^{n+m+1}). \quad (3)$$

Equality (3) means that the coefficients of the fraction (1) are selected so that in its expansion into the Taylor series, the first terms exactly coincide with the corresponding terms of the series (2).

As an example, we give two approximations of the Pade function in the cases

$$e^x \approx \frac{12+6x+x^2}{12-6x+x^2},$$

$$e^x \approx \frac{12(x^2+10)+x(x^2+60)}{12(x^2+10)-x(x^2+60)}.$$

Note that $|x| \le 0.5 \ln 2$ the approximation (3) provides the accuracy of $9 \cdot 10^{-9}$

Parabolic approximation

If the linear polynomial fails exactly to approximate the experimental data, a nonlinear approximation is used – an approximation of the second and higher orders. The second-order approximation (parabolic) is described by the polynomial [2-6]

$$P_2(x) = a_0 + a_1 \cdot x + a_2 \cdot x^2.$$

The coefficients a_i are determined by the least squares method

$$F \sum_{i=1}^{n} (y_i - a_0 - a_1 \cdot x_i - a_2 \cdot x_i^2)^2 \to \min_x$$

We make a system of equations, equating the partial derivatives to zero:

$$\begin{cases} \dfrac{dF}{da_0} = -2\sum_{i=1}^{n}(y_i - a_0 - a_1 \cdot x_i - a_2 \cdot x_i^2) \cdot 1 = 0; \\ \dfrac{dF}{da_0} = -2\sum_{i=1}^{n}(y_i - a_0 - a_1 \cdot x_i - a_2 \cdot x_i^2) \cdot x_i = 0; \\ \dfrac{dF}{da_0} = -2\sum_{i=1}^{n}(y_i - a_0 - a_1 \cdot x_i - a_2 \cdot x_i^2) \cdot x_i^2 = 0. \end{cases}$$

After the transformations, we get a system of linear equations with three unknowns *(a_0, a_1, a_2):*

$$\begin{cases} a_0 \cdot n + a_1 \cdot \sum_{i=1}^{n} x_i + a_2 \cdot \sum_{i=1}^{n} x_i^2 = \sum_{i=1}^{n} y_i, \\ a_0 \cdot \sum_{i=1}^{n} x_i + a_1 \cdot \sum_{i=1}^{n} x_i^2 + a_2 \cdot \sum_{i=1}^{n} x_i^3 = \sum_{i=1}^{n} (x_i \cdot y_i), \\ a_0 \cdot \sum_{i=1}^{n} x_i^2 + a_1 \cdot \sum_{i=1}^{n} x_i^3 + a_2 \cdot \sum_{i=1}^{n} x_i^4 = \sum_{i=1}^{n} (x_i^2 \cdot y_i), \end{cases}$$

Let's introduce the notation:

$$\begin{aligned} &S_1 = \sum_{i=1}^{n} x_i;\ S_2 = \sum_{i=1}^{n} x_i^2;\ S_3 = \sum_{i=1}^{n} x_i^3;\ S_4 = \sum_{i=1}^{n} x_i^4 \\ &S_5 = \sum_{i=1}^{n} y_i;\ S_6 = \sum_{i=1}^{n} (x_i \cdot y_i);\ S_7 = \sum_{i=1}^{n} (x_i^2 \cdot y_i). \end{aligned} \tag{4}$$

Taking into account the accepted designations, the system (4) will take the form:

$$\begin{cases} a_0 \cdot n + a_1 \cdot S_1 + a_2 \cdot S_2 = S_5, \\ a_0 \cdot S_1 + a_1 \cdot S_2 + a_2 \cdot S_3 = S_6, \\ a_0 \cdot S_2 + a_1 \cdot S_3 + a_2 \cdot S_4 = S_7. \end{cases}$$

The coefficients a_0, a_1, a_2 are found by the Kramer method, according to which:

$$a_0 = \frac{\Delta_0}{\Delta},\ a_1 = \frac{\Delta_1}{\Delta},\ a_2 = \frac{\Delta_2}{\Delta}.$$

Where

$$\Delta = \begin{vmatrix} n & S_1 & S_2 \\ S_1 & S_2 & S_3 \\ S_2 & S_3 & S_4 \end{vmatrix};\ \Delta_0 = \begin{vmatrix} S_5 & S_1 & S_2 \\ S_6 & S_2 & S_3 \\ S_7 & S_3 & S_4 \end{vmatrix},\ \Delta_1 = \begin{vmatrix} n & S_5 & S_2 \\ S_1 & S_6 & S_3 \\ S_2 & S_7 & S_4 \end{vmatrix},\ \Delta_2 = \begin{vmatrix} n & S_1 & S_5 \\ S_1 & S_2 & S_6 \\ S_2 & S_3 & S_7 \end{vmatrix}.$$

Approximation in the form of a power (exponential) function

The power function has the form

$$y = b \cdot x^a$$

Logarithmizing the last equation, we get

$$\lg(y) = \lg(b) + a \cdot \lg(x)$$

Let's introduce the notation:

$$Y = \lg(y),\ B = \lg(b);\ A = a;\ X = \lg(x)$$

Using the least squares method, we find the unknown coefficients *B* and *A*:

$$F = \sum_{i=1}^{n} (Y_i - (B + A \cdot x_i))^2 \to \min_x$$

The formulas for calculating the coefficients *A* and *B* are similar as for the case of linear approximation (5,6):

$$A = \frac{n \cdot \sum_{i=1}^{n} (x_i \cdot Y_i) - \sum_{i=1}^{n} x_i \cdot \sum_{i=1}^{n} Y_i}{n \cdot \sum_{i=1}^{n} x_i^2 - \left(\sum_{i=1}^{n} x_i \right)^2}, \; B = \frac{\sum_{i=1}^{n} Y_i - A \sum_{i=1}^{n} x_i}{n} \tag{5,6}$$

After determining the coefficients, we will return to the previously accepted notation

$$b = 10^B, \; a = A, \; y_i = 10^{Y_i}, \; x_i = 10^{X_i}$$

References:

1. Andreev V. S. Theory of nonlinear electrical circuits: A textbook for universities. - M.: Radio and Communication, 1982. - 280 p.

2. Bessonov L. A. Theoretical foundations of electrical engineering: Electrical circuits. For students of electrical engineering, energy and instrument-making specialties of universities. - 7th ed., reprint. and additional-M.: Higher School, 1978. -528 p.

3. Theoretical foundations of electrical engineering. Studies for universities. In three volumes. Under the general editorship of K. M. Polivanov. T. 2. Zhukhovitsky B. Ya., Negnevitsky I. B. Linear electric circuits (continued). Nonlinear circuits. - M.: Energiya - 1972. -200 p.

4. A. A. Bazarov, Synthesis of an automatic control system for objects with distributed parameters containing delay links, (2011)

5. Moore C. F., Smith C. L., Murrill P. W. Instruments and Control Systems, 43(1), 70(1970).

6. Besekersky V. A., Popov E. P., Theory of automatic control: Ed. 4-e pererab. and additional-SPb, publishing house "Profession", 2003-752 p. – (Series: Specialist)

ABOUT BIT-ORIENTED CALCULATION METHODS IN SIGN-DIGIT SYSTEM

Mikhail Gordeev

Saint-Petersburg State University of Aerospace Instrumentation,
Saint-Petersburg, Russia
E-mail: gordeevm2019@internet.ru

Abstract
The work focuses on bit-oriented calculation methods implemented in an excessive digit number system. The ambiguity of the representation of numbers in the redundant number system is shown and the possibility of selecting the representation of numerical data according to the weight of the number is discussed. The advantages that enable their effective use in software implementations are analized.
Keywords: bit-oriented calculations, digit number system, optimal binary representation, binary number weight.

Introduction

With the increase in performance of modern embedded computers, the number and dimension of tasks solved on them increases, various requirements for accuracy and time of calculations are imposed. In a number of real-time applications of diagnostic and management systems face the challenge of minimizing computational time. These are, for example, tasks of evaluating and predicting the development of fast-flowing processes, for which it is important to determine the trend of changing process parameters, and not their exact value.

Traditional computer calculations are carried out in floating point arithmetic with a rigidly fixed mantissa. For these tasks, with small requirements for the accuracy of the result, this leads to a significant redundancy in calculation time.

An alternative to traditional computing is computing based on processing bits of data. However, the scope of such calculations is limited by the possibilities of bitwise decomposition of binary numbers. However, here you can use sign-bit (sign-digit) encoding, which allows you to vary the data representation.

Problem statement

In the present work, for a number of computational tasks, conditions are determined and the use of bit calculation methods is proposed, which are implemented during sign-digit (redundant) data encoding. This includes organizing pipeline calculations with an additional pipeline layer implementing a conversion from binary code to redundant sign-digit code.

The focus is on the advantages of such a pipeline, which allows efficient use of methods in both hardware and software implementation with adjustable computational accuracy.

Data for processing

Data in diagnostic and monitoring systems are usually values obtained from the conversion of physical quantities by analog-to-digital converters (ADC). It is important to note that most methods of converting physical quantities give a numerical binary code by method "digit by digit", starting with the highest. For example, the analog-to-digital conversion SAR (Successful Approximation Register) is implemented by algorithm of binary "weighting". It is like solving Fibonacci's "problem of choosing the best system of weights," discussed in the book «Liber Abaci» (1202 г.) [1]. The ADC measures the value of the input signal by performing a number of successive "weights" comparisons of the input voltage value with a number of values - generated according to the principle of dichatomy. Sigma-delta ADC also generates the result sequentially "digit by digit" (bit by bit).

To organize calculations with numbers, on-line arithmetic [2] is known - pipeline processing using the representation of operands in the form of a decomposition of digits [3, 4]. Obviously, when processing binary digits at the rate of their appearance on the ADC, starting with the highest digit, using such arithmetic, it is possible to significantly reduce the calculation time when solving some problems. However, such a pipeline of calculations without converting binary code to redundant sign-digit code is not possible [4].

Sign-digit coding

Redundant sign-digit (sign-bit) coding has a number of advantages [5-7], which were used in the last century in a number of digital signal processing processors. Today, these advantages are used in the structures of modern universal processors with hardware implementation of the multiplication operation, and also in programmable logic and VLSI [8 - 10].

The processing of operands, starting with their higher digits at sign-digit coding, firstly, ensures that there are no global transfers when performing arithmetic operations. Secondly, it is possible to flexibly reduce (increase) the number of digits in the number and, accordingly, adjust the accuracy of the results (calculation time) within the accuracy of processor or the presentation of data in the programming language. Third, numbers are represented by many options and you can choose the best of them for a particular task.

Article [11] shows that the transition from the alphabet {0, 1} to the alphabet {0, + 1, -1} gives for data a different number of views depending on the bit size selected. So, for natural numbers from 1 to 4096 on a 12-bit processor, the number of accurate representations of most of them exceeds 100 and even 200 variants. At the same time, it is possible to flexibly influence the structure of the number code and its weight - the number of units in the code [2, 7].

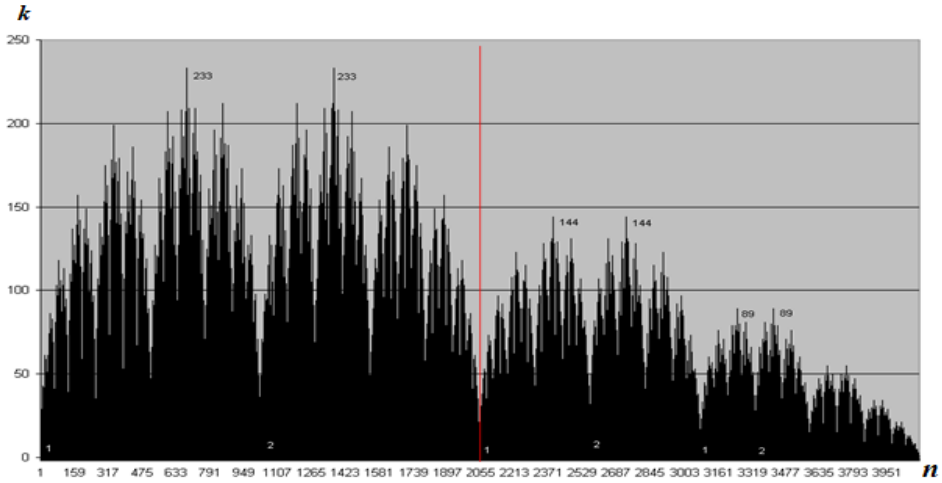

Fig. 1. Distribution of the number of representations of numbers in sign-digit encoding with a bit depth of 12

Fig. 1 shows the distribution of the number of representations k for 4096 numbers in 12-bit processor (r = 12).

Real-time converting binary code of number to sign-digit binary code

Multiple representations of the number in sign-digit code allows you to choose the best transcoding option implemented in real time and the best value of the weight of the number - an important parameter of processing complexity.

The simplest method of conversion is to "smear" the sign into all significant digits in the number, for example, as shown below:

binary code of number -0.0101101001000111_2 (8),

binary sign-digit (2sd) code of number 0.0101101001000111_{2sd} (8).

Here -1 is represented as 1, and in parentheses the value of the weight of the number.

Another simple method [4] – for each consecutive digit b_i ($i = p-1, p-2,\ldots,0$) received from the ADC, a transformation to d_i is performed in the form:

if $b_i < b_{i-1}$ (01), then $d_i = 1$;

if $b_i > b_{i-1}$ (10), then $d_i = -1$;

if $b_i = b_{i-1}$ (00 or 11), then $d_i = 0$.

The conversion delay is 1 clock cycle. The implementation of the transformation is performed by a simple comparison scheme shown in Fig.2.

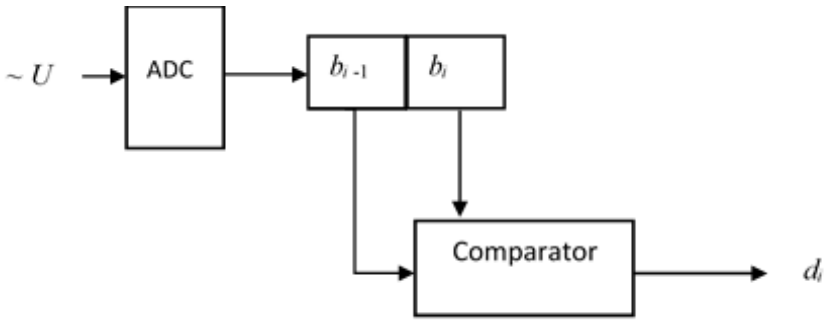

Fig. 2. Scheme of transformation

Other possible methods [4] for the same number give the following sign-bit codes:

0.0101101001001001_{2sd} (7),

0.0111111111001111_{2sd} (13),

0.1111111111111111_{2sd} (16).

They are also executed in real time and are based on a comparison of bits (groups of bits) of the converted binary code, starting with the highest bits.

Bit-oriented computing and its advantages

Bit-oriented computing methods, being an alternative to traditional ones, attract attention by the simplicity of their implementation and the presence of a number of useful properties [2].

Theory of on-line bit-oriented computing, which was created at the end of the XX century by such scientists as prof. M. Ercegovac, V. Baikov, S. Ashby, G. Pukhov, is now being improved through the use of sign-discharge and other non-traditional number systems [11, 12]. Although 30-40 years ago, the development of such computing methods was associated with the creation of specialized processors, today their use is becoming interesting and effective in software implementation.

In the absence of experimental data and proven recommendations for the representation of numbers for a specific on-line method, the use of sign-digit encoding is not very attractive. When switching to calculations with bits of numbers, the programmer needs to be sure that along with the benefits obtained, other parameters of the computing process will not be degraded. For example, for iterative computing processes, such as many bit-oriented computations, it is the accuracy of the results and the number of iterations required to achieve them.

The results of the extended computational experiment [11] showed that in sign-digit arithmetic, many time-consuming problems are solved faster using bit methods of computation, and in integer arithmetic, it is possible to achieve results with absolute accuracy when solving Diophantine equations and systems of equations [13].

Examples of calculations in sign-digit encoding

Here are some examples that demonstrate end-to-end pipelining of bits-level (digit-level) calculations.

Example 1. Solution of a system of linear algebraic equations of the form **A**X = B, where

$$\mathrm{B} = \begin{vmatrix} 0,90625 \\ 0,46875 \end{vmatrix},$$

in which the free terms in binary form are represented exactly:

$$b_1 = 0.11101_2,$$

$$b_2 = 0.01111_2.$$

The vector of solution is formed by the method described in detail in book [4], by calculating a binary digit at each step of the method. The exact solution is obtained in the form:

$$x_1 = 1.1010101_{2sd} = 1,3515625_{10},$$

$$x_2 = 0.1000101_{2sd} = 0,4765625_{10}.$$

With a bitwise representation of the free members of the system and entering them into the computational process sequentially, the solution is obtained in the form:

$$x_1 = 1.1010111_{2sd},$$

$$x_2 = 0.1000111_{2sd}.$$

This fully corresponds to the exact solution of the system of equations. The solution of such systems of equations with a predominant diagonal in the matrix A is typical for performing discrete convolution in signal processing, autoregressive analysis, forecasting of fast-flowing processes in nuclear power, etc. If the system is Diophantine, which is typical for most of the listed tasks, then you can use scaling before calculations with reverse scaling after receiving the results.

Example 2. Calculating the value of a polynomial of the form

$$P(x) = a_0 x^0 + a_1 x^1 + a_2 x^2$$

with $a_0 = a_1 = a_2 = 0{,}5$ and $x = 0{,}2$ after 8 steps is obtained in the form of

$$P(x) = 0.10011111\ldots_{2sd}.$$

Continuing the calculation process allows you to get a solution with greater accuracy.

In diagnostic and control systems, the calculation of polynomials is the basis for obtaining the values of elementary functions, approximating of trajectories, etc. with configurable result accuracy (solution time).

In the examples given, the multiplication operations are degenerate: one of the operands when calculating the sums of paired products has the value +1, -1, or 0. This determines the efficiency of the proposed calculation scheme in redundant on-line arithmetic.

In general, apart from the above examples, the following operations can be performed bitwise using only comparison and addition/subtraction in on-line arithmetic with sign-bit coding of data:

- Boolean transactions;
- addition (subtraction);
- comparison;
- shift to the right;
- multiplication (division);
- calculation of the square root from the number;
- calculation of polynomials (elementary functions);
- calculation of fractional rational functions (elementary functions, approximation problems);
- solution of linear algebraic equation systems.

Conclusion. Currently known bit-oriented methods allow the use of sign-digit coding and corresponding arithmetic for unique software implementations. This is especially important in diagnostic and control tasks, where the accuracy of the result required for decision making is significantly less than the accuracy provided by the presentation of data in the programming language, and the requirements for decision speed are maximum.

For the conscious programmatic use of bit-oriented methods in sign-digit operand coding, one must first obtain an answer to the question about the optimal representation of data from a plurality of possible ones by selecting a method for converting codes and the resulting number weight. This will determine the associated method of transcoding data from a traditional binary system in which it is represented in a computer, and will also optimize calculation methods.

References

1. Fibonacci's Liber Abaci: A Translation into Modern English of Leonardo Pisano's Book of Calculation, *Springer*, 2003. 646 p.

2. Ercegovac M. D. On-line arithmetic: on overview, *Proc. SPIE*. 1984. Vol. 495. P. 86-93.

3. Baikov V. D., Vashkevich S. N., Sergeev M. B. Applied tasks of microprocessor diagnostic and control systems, *Saint-Petersburg: Politechnika publ*., 1992. 223 p.

4. Sergeev M. B., Kasem K. M. Bitwise computation algorithms for microprocessor systems, *Saint-Petersburg: Politechnika publ*., 1997. 96 p.

5. H. Frougny, E. Pelantov´a, and M. Svobodov´a, Parallel addition in non-standard numeration systems, *Theor. Comput. Sci*. 412(2011). P. 5714–5727.

6. Nielsen A. M. and Kornerup P. Redundant Radix Representation of Rings, *IEEE Transactions on Computers* 48(1999). P. 1153–1165. DOI:10.1109/12.811100

7. Hartley R. I., Parhi K. K. Digit-serial computation, *Springer*. 1995. 306 p. https://doi.org/10.1007/978-1-4615-2327-7

8. Ercegovac M. D. and Lang T. Digital Arithmetic, *Morgan Kaufmann*, 2004. 709 p.

9. Parhi K. K. VLSI Digital Signal Processing Systems: Design and Implementation. *John Willey & Sons, Inc*. 1999. 791 p. (Chapter Redundant Arithmetic)

10.Redundant Ashish Manoharrao Ingale, Ameed Mustafa Shah Radix-4 Arithmetic Coprocessor Design Using VHDL, *International Journal of Scentific & Technology Research*, Vol. 5, Issue 4, 2016. P. 359 – 364.

11.Sergeev A. M. On the signed-digit representation of numbers and a related computational experiment, *Informatsionno-upravliaiushchie sistemy* [Information and Control Systems]. 2006. № 3, p. 56-58.

12.Marta Brzicova, Christiane Frougny, Edita Pelantova, and Milena Svobodova On-line algorithms for multiplication and division in real and complex numeration systems, *arXiv*:1610.08309v2 [cs.DS]. 11 Jun 2019

13.Sergeev M. B. Hybrid bitwise method for solving systems of equations in integer arithmetic, *Informatsionno-upravliaiushchie sistemy* [Information and Control Systems]. 2003. № 2-3, p. 16-18.

ANALYSIS OF CORRELATION CHARACTERISTICS OF DISCRETE CODE SEQUENCES BASED ON PERSYMMETRIC CYCLIC QUASI-ORTOGONAL MATRICES

Evgeniy Grigoriev

Saint-Petersburg State University of Aerospace Instrumentation,
190000, St. Petersburg, st. B. Morskaya, 67
E-mail: ev.grig95@gmail.com

Abstract
The article presents an analysis of new discrete code sequences obtained from rows of persymmetric cyclic quasi-orthogonal matrices. A comparative analysis of the characteristics of the new code sequences obtained is given. The advantages of the sequences obtained in this work are discussed in the aspects of improving the correlation characteristics, their detection and noise immunity in radio channels of distributed systems. The use of new code sequences obtained from rows of quasi-orthogonal matrices is aimed at improving the characteristics of compression, detection, accuracy, resolution, and noise immunity. The results obtained in this work are focused on application in modern radar, telecommunication, ultra-wideband, optical, acoustic, and "intelligent" systems for detecting and transmitting data.
Keywords: Persymmetric cyclic quasi-orthogonal matrices, discrete code sequences, correlation function.

INTRODUCTION

At present, the field of application of discrete code sequences (DCS) with given correlation and spectral characteristics has significantly expanded from individual tasks of radar, sonar and navigation, to the use of such signals in communication: in addressing, information transmission, synchronization, coding, etc. ; using them in neural networks at the training stages; when creating medical equipment of high resolution and accuracy; in computing systems, automation and telemechanics systems for protection against unauthorized access, ensuring high noise immunity, cryptographic resistance, electromagnetic compatibility, etc. [1-10].

At the moment, the theory of synthesis of sequences with given correlation and spectral characteristics is sufficiently developed, but far from being completed. This fact is noted in [11], where a classification of DCS is given, and methods for synthesizing DCS with given correlation and spectral characteristics known at the time of writing are systematized.

For a long time, the main content of research on this topic has been focused on clarifying the properties of known DCS, expanding the power of known coding rules and areas of application of DCS. This indicates the need to search for new methods for the synthesis of such sequences.

Recently, in the field of searching for DCS with given correlation characteristics, there has been interest in the search and study of extremal matrices. Such matrices, for example, are orthogonal and quasi-orthogonal matrices of symmetric and block-symmetric structures [12-14], and matrices of the maximum of the determinant [15-17]. An example is the Barker codes used in the IEEE 802.11 set of standards. The analysis showed that although they were calculated independently of the matrix theory, they are fragments of the rows of the matrix of the maximum of the determinant calculated by G. Barba [18].

The development of the theory of quasi-orthogonal matrices and new practical results open up the possibility of revising methods for diagnosing noise-immune codes, developing new algorithms for processing signals and images.

In this paper, the task is to study the correlation characteristics of DCS based on rows of quasi-orthogonal matrices for comparative analysis and the possibility of using structures based on them with the alphabet (1, -b) [12] - sequences of maximum length, such as sequences formed on the basis of quadratic residues and Jacobi symbols [19] i.e. to move away from the classical approach, when the alphabet of the code structure is integer and symmetric.

SEARCH FOR NEW CODE SEQUENCES

In [19, 20], the most convenient strategies for computing cyclic quasi-orthogonal matrices were identified, based on sequences of maximum length - m sequences, Legendre sequences and Jacobi sequences. This paper proposes a complementary strategy based on the Raghavarao sequences.

Strategy 1. Calculation of the first row of a matrix based on Legendre symbols for lengths N = 3, 7, 11, 19, 23, etc. In this case, the Legendre sequence is characterized by the fact that the number of negative and positive elements differs by one.

Strategy 2. Calculation of the first row of the matrix based on Jacobi symbols, for lengths N = 3, 15, 35, 143, etc. In this Jacobi sequence is characterized by the fact that a double prime of the form N = p (p + 2), where p is a prime number.

Strategy 3. Calculation of the first row of a matrix based on m-sequences and its modified forms for lengths N = 3, 7, 15, 31, 63, 127, etc. In this case, the modified m-sequences differ in that the alphabet of the sequence is asymmetric, as in the classical case.

Strategy 4. Calculation of the first row of the matrix based on the sum of squares of adjacent natural numbers [21]. For example, for lengths N = 5, 13, 25, 41, 61, 85, 113, etc., where $5=1^2+2^2$, $13=2^2+3^2$, $25=3^2+4^2$, $41=4^2+5^2$ $61=5^2+6^2$, etc. In this case, the number of negative elements in a line corresponds to a smaller square in the sum, respectively, a larger one. Cyclic matrices of Raghavarao correspond to this strategy.

After the strategies are determined, it is required to search for the code sequences with the best correlation characteristics.

At the same time, the modification of the indicated code constructions with the alphabet (+1, –b) is considered in this study as a difference from the existing approach with a symmetric alphabet (+1, –1).

To do this, in accordance with strategies 1-4, each of the original sequences (Legendre, Jacobi, m-sequences and Raghavarao) is modified by replacing negative, or zero in the case of an m-sequence, elements with –b. After that, the following procedure is performed:

- a square matrix is formed, consisting of (+1, –b) by shifting the modified sequence one position to the right for each new row of the desired cyclic matrix;
- the resulting matrix is multiplied by the transposed itself;
- matrix elements that do not lie on the main diagonal after the multiplication operation will contain an expression with an unknown value b;
- the resulting expression is equated to zero and the value of the element b is selected, which is characteristic of quasi-orthogonal matrices [12-14].

The block diagram of the algorithm for obtaining modified code sequences is shown in figure 1.

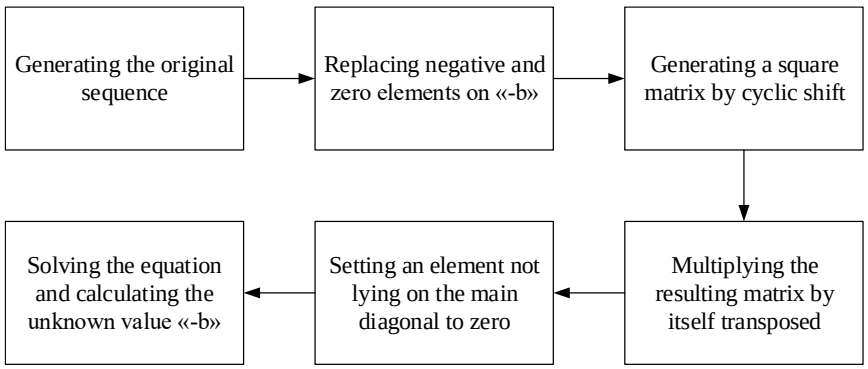

Figure 1 - The procedure for generating a code sequence

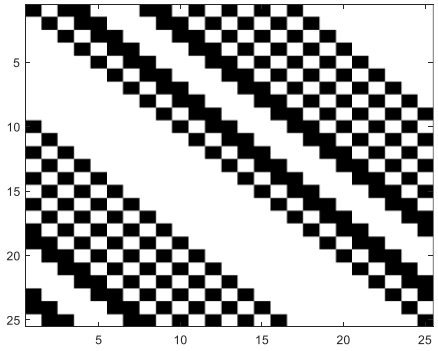

Figure 2 - Portrait of a cyclic quasi-orthogonal matrix based on a Raghavarao sequence of length 25

The result is a square matrix, an example of which is shown in figure 2, where the white square corresponds to the value «+1», and the black one corresponds to «-b».

COMPARATIVE ANALYSIS OF CORRELATION CHARACTERISTICS OF THE OBTAINED CODE SEQUENCES

The most important characteristic of DCS for solving the problems listed in the introduction is the correlation function (CF). In practical applications, the CF of the code sequence should have a maximum center peak and a minimum level of side lobes. To analyze the code sequences, a comparative analysis of the periodic CF and the aperiodic CF should be carried out. In this case, for the CF-th one should identify those that have the maximum level of the main peak of the CF and the minimum level of side lobes [22, 23].

Comparative analysis based on computational experiments for modified sequences of maximum length obtained from matrices:

- Mersenn type (strategy 1),
- formed on the basis of Jacobi symbols (strategy 2),
- formed on the basis of modified m-sequences (strategy 3),
- formed on the basis of Raghavararo sequence (strategy 4), for correlation characteristics - aperiodic autocorrelation function (ACF) and periodic autocorrelation function (PACF).

The essence of the experiment is as follows. From the initial sequence obtained for each of the strategies described above, a square matrix with elements (+1; -1) was formed by cyclic shift. In this matrix, we searched for the best in terms of the minimum of the maximum of the side lobe normalized to unity of the autocorrelation function of the matrix row, as shown in Figure 3, where the autocorrelation function of the first row is shown in red, and the autocorrelation function of the found row with the lowest level of the side lobe is shown in blue. Hereinafter, it should be stipulated that N will denote the order of the matrix.

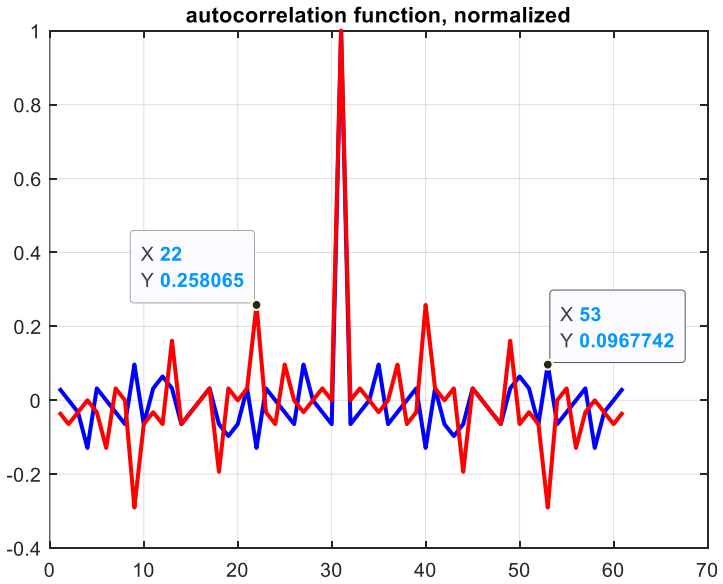

Figure 3 - Normalized ACF of the first row of the matrix for N = 31 formed on the basis of strategy 1 (red) and the row with the lowest sidelobe level (blue)

After this procedure, the matrix with the values (1, –1) was replaced by a quasi-orthogonal one according to the algorithm shown in Figure 1. The resulting matrix with the values of the elements (1, –b) was also subjected to the procedure for finding a row with a minimum of the maximum of the side lobe of the ACF. Then the best rows of the matrix (1, –1) and matrix (1, –b) were compared for the value of the ACF sidelobe level, as shown in Figure 4.

Next, with the same order N = 31, we analyze the periodic autocorrelation functions of sequences with elements (1, –1) and (1, –b) to make sure that the background of negative side lobes is uniform. The result is shown in Figure 5.

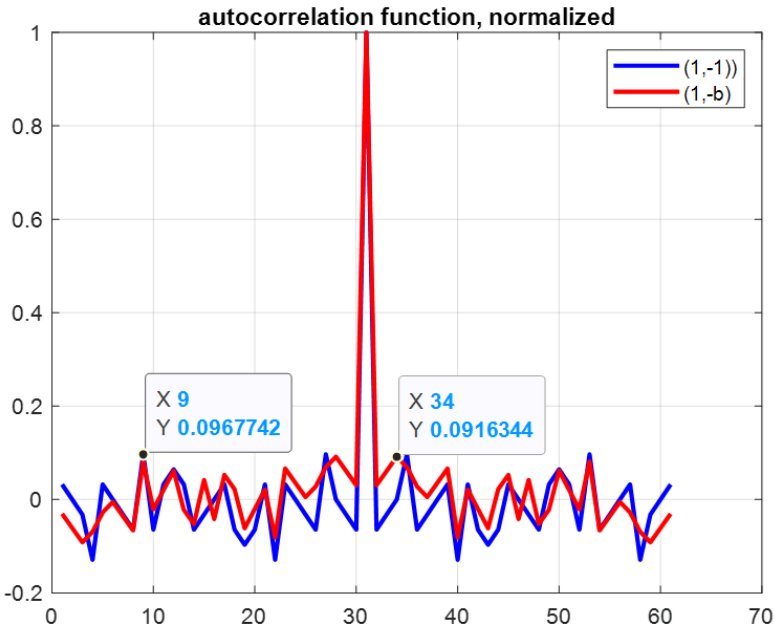

Figure 4 - ACF of the sequences based on strategy 1 with elements (1, –1) and (1, –b) for the best by the criterion of the minimum of the maximum of the side lobe of the autocorrelation function for N = 31

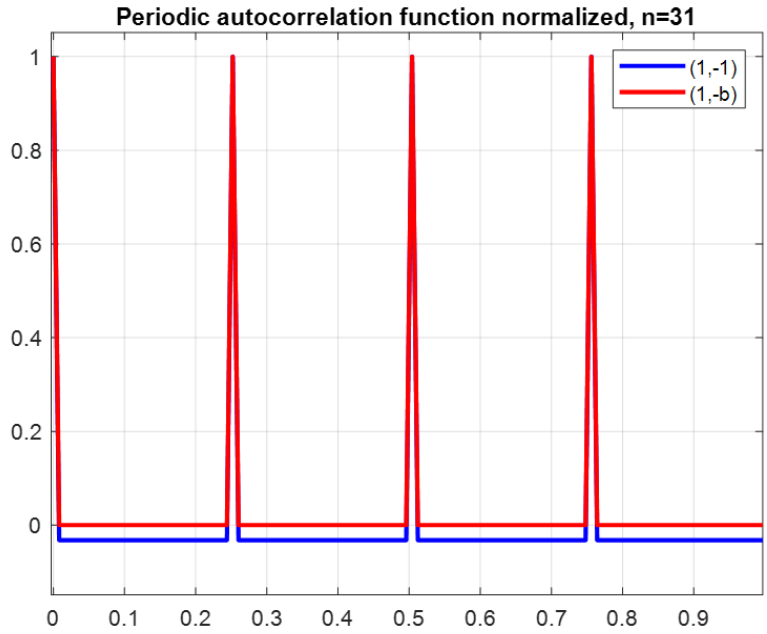

Figure 5 - PAKF codes obtained on the basis of strategy 1 for N = 31

Consider another example of improving the autocorrelation function of the original code structure. Take a row of the Raghavarao matrix (strategy 4) of order 13, and calculate its ACF, then modify the original sequence by a known procedure and obtain a sequence of the form (1, –b). We also calculate the ACF for the resulting sequence. The results are shown in Figure 6.

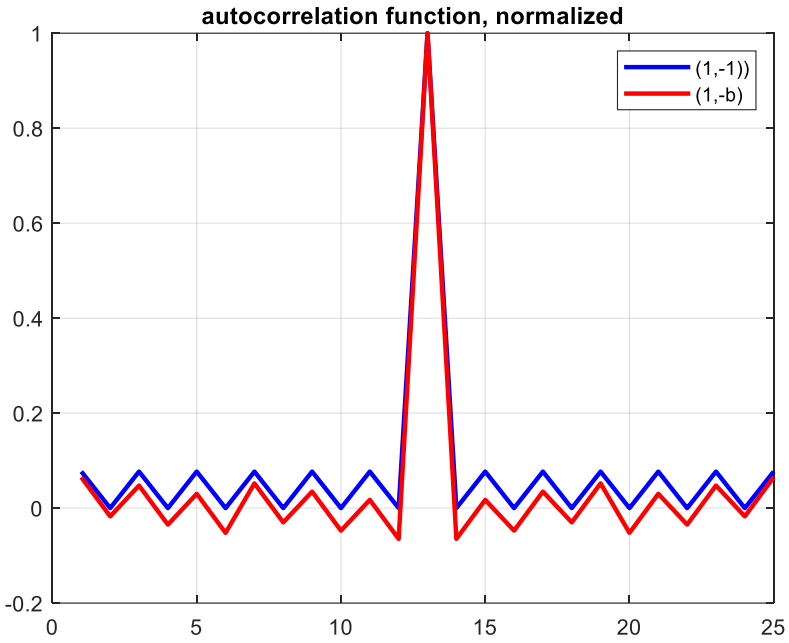

Figure 6 - ACF of the best according to the criterion of the minimum of the maximum of the side lobe of the autocorrelation function of the Raghavarao matrices of order N = 13 with elements (1, –1) and (1, –b)

In the case of PACF for strategy 4 with N = 13, an interesting result was obtained, shown in Figure 7, the values of the side lobes are lower in the case of the modified Raghavarao sequence than in the classical representation.

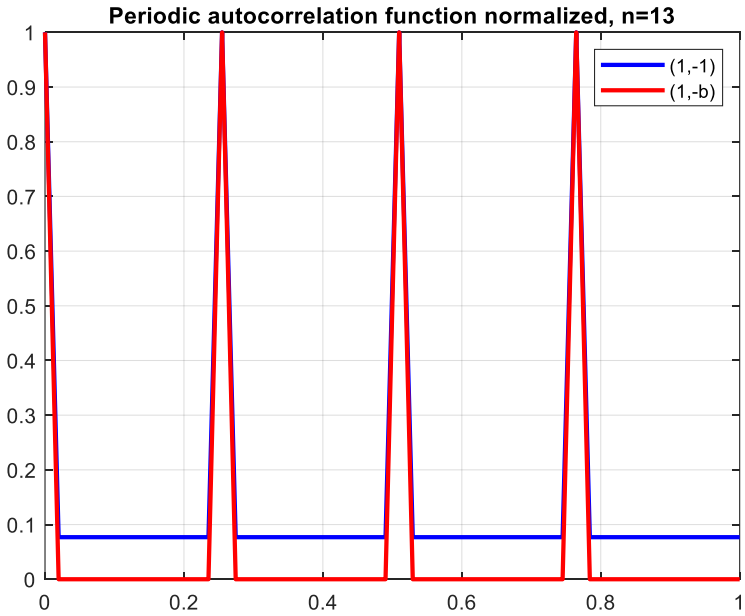

Figure 7 - Periodic autocorrelation function of the Raghavarao code sequence, order N = 13

Table 1 summarizes the ACF sidelobe level values obtained for the matrices for each of the four strategies. Some missing values in Table 1 are explained by the existence of these matrices in this order. This is rather an advantage of these strategies, rather than a disadvantage, since it allows you to implement a larger number of code sequences.

The obtained values show the feasibility of the proposed approach based on replacing the symmetric alphabet from (1, –1) to the asymmetric (1, –b).

Table 1

Maximum ACF sidelobe level

Order		15	31		143	511
Strategy 1	(1,–1)	0.1333	0.0968		0.3936	0.4012
	(1,–b)	0.2091	0.0916		0.3996	0.4216
Order		15		35	143	
Strategy 2	(1,–1)	0.1333		0.0857	0.0699	
	(1,–b)	0.1389		0.1067	0.0686	
Order		15	31			511
Strategy 3	(1,–1)	0.1333	0.0968			0.391
	(1,–b)	0.1100	0.1086			0.381
Order		13	25	41		
Strategy 4	(1,–1)	0.0769	0.280	0.1220		
	(1,–b)	0.0648	0.3316	0.1241		

CONCLUSION

The paper discusses the mechanisms for the formation of discrete code sequences based on persymmetric cyclic quasi-orthogonal matrices of four types. Comparative analysis of the results of computer simulation of the use of widely known and modified code sequences shows the advantage of the latter. At the same time, for the sequences considered in the work, an analysis was carried out from the correlation properties.

The result of the study shows that the codes obtained on the basis of persymmetric quasi-orthogonal circulants provide greater noise immunity of signals in radio channels, as well as an increase in the probability of their correct detection against the background of external interference.

The results obtained in this work show that the described approach is promising and make it possible to conclude that it is advisable to use it in modern distributed radar, telecommunication, ultra-wideband, optical, acoustic, and “intelligent” systems for detecting and transmitting data.

ACKNOWLEDGMENTS

Research on software imple- mentations of persimetric cyclic quasi-orthogonal matrices of Raghavarao, as well as analysis of their correlation characteristics was carried out with the financial support of the Russian Foundation for Basic Research within the framework of scientific project № 19-29-06029

The study on the search for new modified code sequences was prepared with the financial support of the Ministry of Science and Higher Education of the Russian Federation, subsidy of FSRF – 2020–0004 “Scientific foundations for building architectures and communication systems of onboard information and computing complexes of a new generation for aviation, space systems and unmanned vehicles”

REFERENCES

D. Jansson, Mathematical modeling of the human smooth pursuit system, Ph.D. thesis, Uppsala University, Division of Systems and Control, Automatic control, 2014.

1. D. Jansson, Mathematical modeling of the humansmooth pursuit system, Ph.D. thesis, Uppsala University, Division of Systems and Control, Automatic control, 2014.

2. M. G. Wattimena, V. A. Nenashev, A. A. Sentsov and A. P. Shepeta, "On-Board Unlimited Aircraft Complex of Environmental Monitoring," 2018 Wave Electronics and its Application in Information and Telecommunication Systems (WECONF), St. Petersburg, 2018, pp. 1-5.

3. Nenashev V. A., Kryachko A. F., Shepeta A. P., Burylev D. A. Features of information processing in the onboard two-position small-sized radar based on UAVs, SPIE Future Sensing Technologies, Tokyo, Japan, 2019, pp. 111970X-1-111970X-7.

4. Kapranova E.A., Nenashev V.A., Sergeev A.M., Burylev D.A., Nenashev S.A. Distributed matrix methods of compression, masking and noise-resistant image encoding in a high-speed network of information exchange, information processing and aggregation, SPIE Future Sensing Technologies, Tokyo, Japan, 2019, pp. 111970T-1-111970T-7.

5. Sergeev M.B., Sentsov A.A., Grigoriev E.K., Nenashev S.A. Simulation model of the radar environment of an intelligent control system for distributed radar facilities. Modeling, Optimization and Information Technology. 2020;8(3). DOI: 10.26102/2310-6018/2020.30.3.038 (In Russ).

6. Kapranova E A, Nenashev V A and Sergeev M B, Compression and coding of images for satellite systems of Earth remote sensing based on quasi-orthogonal matrices // Proc. of SPIE, Image and Signal Processing for Remote Sensing XXIV. Berlin, Germany. 2018. Vol. 10789. PP. 1078923-1 - 1078923-6; doi: 10.1117/12.2324249

7. Sergeev A.M., Nenashev V.A., Vostrikov A.A., Shepeta A.P. and Kurtyanik D.V., Discovering and analyzing binary codes based on monocyclic quasi-orthogonal matrices //Smart Innovation, Systems and Technologies. 2019. T. 143. C. 113-123

8. Nenashev V.A., Vasiliev I.A., Sergeev A.M. Modeling of complex code-modulated signals for modern systems of detection and transmission of information // Scientific session of the SUAI: collection of articles. report: at 3 pm Part II. Technical science. - SPb.: GUAP, April 8-17, 2019. pp. 413-417.

9. Nenashev V.A. Investigation of the influence of industrial noise on the compression characteristics of phase-shift keyed signals in primary radars / V. A. Nenashev, V. A. Sinitsyn, S. A. Strakhov // Innovative technologies and special-purpose technical means: tr. IX general Russian. scientific-practical Conf.: in 2 volumes. Baltic State Technical University "Voenmekh" D.F. Ustinova. 2017. pp. 351–355.

10. Wang R. Introduction to Orthogonal Transforms with Applications in Data Processing and Analysis. Cambridge University Press. 2010. 504 p.

11. Gantmaher, V.E. Noise-like signals / V.E. Gantmaher, N.E. Bystrov, D.V. Chebotarev // Analysis, synthesis, processing. – Saint-Petersburg: Science and technology, 2005. – 400 p. (in Russian)

12. Balonin N., Sergeev M. Quasi-Orthogonal Local Maximum Determinant Matrices // Applied Mathematical Sciences. 2015. T. 9. № 8. C. 285-293. DOI: 10.12988/ams.2015.4111000

13. Sergeev A. M., Blaunstein N. S. Orthogonal matrices of symmetric structures for image processing tasks // Information and Control Systems. 2017. № 6(91). C. 2–8. doi: 10.15217/issn1684-8853.2017.6.2

14. Sergeev A. M., Vostrikov A. A. Special matrices: calculation and application. SPb: Polytechnic, 2018. 112 p.

15. Balonin N. A., Sergeev M. B., Vostrikov A. A. Conjecture of maximum determinant matrices with orders equal to prime Fermat numbers // Information and Control Systems. 2020. № 2. P. 2–7. doi:10.31799/1684-8853-2020-2-2-7

16. Neubauer M. G., Radcliffe A. J. The maximum determinant of ± 1 matrices // Linear Algebra and its Applications. 1997. T. 257. № 1–3. P. 289–306.

17. Popescu O., Rose Ch., Popescu D. Maximizing the determinant for a special class of block-partitioned matrices // Mathematical Problems in Engineering. 2004. № 1. P. 49–61.

18. Barba G. Intorno al Teorema di Hadamard sui Determinanti a Valore Massimo // Giorn. Mat. Battaglini. 1933. Vol. 71. P. 70–86.

19. Grigoriev E.K. Methods of generation and analysis of strategies for calculating cyclic quais orthogonal matrices // Bulletin of the UNESCO department «Distance education in engineering» of the SUAI: Collection of the papers. St. Petersburg, Issue 4. – SPb.: SUAI, 2020. p. 73-77.

20. Nenashev V.A., Grigoriev E.K., Sergeev A.M., Samohina E.V. Strategies for calculating persymmetric cyclic quasi-orthogonal matrices as bases of codes // Electrosvyaz. 2020. №10. P. 58-61

21. Raghavarao, D. Some optimum weighing designs // Ann. Math. Statist. 1959. Vol. 30. P. 295–303.

22. A. P. Shepeta, A. M. Makhlin, V. A. Nenashev and A. F. Kryachko, «Performance of UWB Signal Detecting Circuits» 2018 Wave Electronics and its Application in Information and Telecommunication Systems (WECONF), St. Petersburg, 2018, pp. 1-4.

23. Makhlin A.M., Nenashev V.A., Shepeta A.P, «Comparative characteristics of quasi-optimal digital detectors of ultra-wideband signals» 2018 Wave Electronics and its Application in Information and Telecommunication Systems (WECONF), St. Petersburg, 2018, pp. 257-254. (In Russ).

STATISTICAL EQUIVALENTS OF THE TUKKA AND HUBER MODELS

Maria Ivanova

St. Petersburg State University of Aerospace Instrumentation, SUAI
St. Petersburg, Russia
E-mail: ivanovamariya_94@mail.ru

Abstract
The paper presents the results of a study of the statistical equivalents of input signals of complex systems using the composite distributions of Tukka and Huber to assess the robustness of automation systems, built on the basis of histograms of distributions with given percentages of clogging. For Tukky's model, unimodal normal distributions with the same mean and different variances were chosen; for the Huber model, the distributions of the Weibull family were taken, which differ in the means, which leads to the polymodality of the composite Weibull distribution. The histograms of the corresponding composite distributions obtained by the methods of simulation modeling of the input signals of the systems on the computer are given.
Keywords — complex system, automation, input signal, statistical equivalent, histogram, modeling algorithm, normal distribution, Weibull distribution, Tukki's model, Huber's model, robustness.

INTRODUCTION

The design of complex automation systems also implies the need to study the stability of these systems when the assumptions made in their synthesis change regarding the statistical characteristics of the input signals of these systems. In this case, it is desirable to use real records of input signals as test signals, the statistical characteristics of which were, as a rule, in a simplified form, used as mathematical models in determining the algorithm for processing input signals. Such simplifications are almost always present, since a rigorous analytical synthesis can be carried out only with known functional relationships with respect to the probabilistic characteristics of input actions. It is virtually impossible to select the exact characteristics of the input signals, which is why, after the synthesis of the processing algorithm, the problem arises of investigating the robustness (stability) of the system to deviations of the statistical characteristics of real signals from the characteristics of the signals used in the synthesis.

It is, of course, possible to investigate the robust properties of the system using more complex models of input signals, in particular, using models with "weighted" distribution tails, but it is better to use real recordings of signals, which must be at the disposal of the designer, otherwise the synthesis of the system will be based only on theoretical assumptions that may not be met in practice. The problem here is that there may be few such records, in particular, when designing processing algorithms based on the use of artificial intelligence, they are always lacking. Therefore, the method of using statistical equivalents of input signals replicating different implementations of input streams that are statistically indistinguishable from the actually observed data is one of the main directions of overcoming the "lack" of data.

When using statistical equivalents, in contrast to traditional classical methods for approximating the statistical characteristics of input signals, using, for example, goodness-of-fit criteria, the developer "does not know" the statistical characteristics of the simulated input streams, but knows that these streams have exactly the same statistical characteristics as in reality. recorded input signals, and, therefore, do not contradict these experimental recordings. This explains the practical value of using statistical equivalents when analyzing the performance of designed systems on a computer, since, in this case, a machine experiment is as close as possible to a real experimental study of the system.

ALGORITHMS FOR GENERATING STATISTICAL EQUIVALENTS USING DISTRIBUTION HISTOGRAMS

In [1], two algorithms for the implementation of generators of statistical equivalents of input streams, using histograms of distributions of input signals of complex systems being designed, are considered. We will use these algorithms to study the possibilities of generating input streams, when the approximation of the statistical characteristics of input signals from experimental data is difficult or even impossible. Such situations arise, in particular, when it is necessary to use composite distributions to approximate the input flows, since it is practically impossible to "pick" both the distributions themselves and the corresponding weight coefficients

in such cases. In this case, we will consider the two most probable, in our opinion, cases - Tukki's model and Huber's model.

As an algorithm that generates a signal flow that is statistically equivalent (in terms of the histogram) to the real flow, we will take the algorithm presented in [2,3]. Let's briefly present this algorithm.

Let the domain of definition of the histogram $\mathbf{a}_x = \lfloor a_0, a_n \rfloor$ of the original sample **X**, according to which the histogram $h_\xi(x)$ is constructed, be represented by the union of *n* subsets

$$\mathbf{a}_x = \left[a_0, a_n\right] = \left[\left[a_0, a_1\right) \cup \left[a_1, a_2\right) \cup \ldots \cup \left[a_{n-1}, a_n\right]\right], \quad a_i - a_{i-1} = 2\Delta,\ i = 1,2,\ldots n, \tag{1}$$

Vector $\mathbf{b}_y = (b_1, b_2, \ldots b_n)^{\mathrm{T}}$ is a vector whose elements b_i are proportional to the empirical frequencies of the random variable ξ hitting the intervals $[a_i - a_{i-1}),\ i = 1,2,\ldots n-1$, and $[a_n - a_{n-1}]$, respectively, fig. 1.

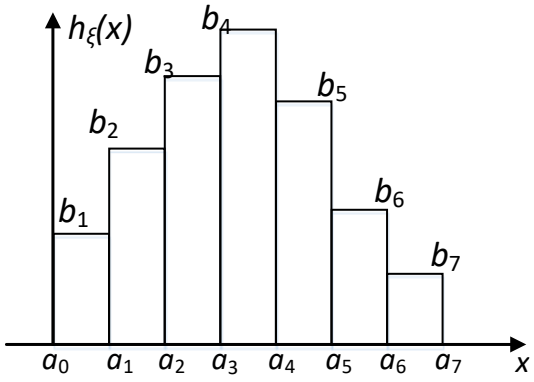

*Fig.1.Histogram $h_\xi(x)$ of the original sample **X**, n = 7.*

Scale along the (0Y) axis in fig. 1 is chosen so that the area of the histogram S_h is equal to 1, that is, so that the equality

$$S_h = b_1(a_1 - a_0) + b_2(a_2 - a_1) + \ldots + b_n(a_n - a_{n-1}) = \sum_{i=1}^{n} b_i(a_i - a_{i-1}) = 2\Delta\sum_{i=1}^{n} b_i = 1, \tag{2}$$

since only in this case, with an increase in the sample size and an increase in n, the histogram $h_\xi(x)$ converges to the true distribution density $f_\xi(x)$ of the sample **X**.

Using the given histogram $h_\xi(x)$, integrating, we construct an empirical distribution function $F_\xi(x)$ of the sample **X** corresponding to the histogram $h_\xi(x)$. This function is piecewise linear

$$F_\xi(x) = \int_{\mathrm{X}^{(0)}}^{x} f_\xi(x') \cdot dx' = \begin{cases} 0,\ x < \mathrm{X}^{(0)}, \\ \mathrm{Y}^{(m-1)} + \dfrac{\mathrm{Y}^{(m)} - \mathrm{Y}^{(m-1)}}{\mathrm{X}^{(m)} - \mathrm{X}^{(m-1)}}\left(x - \mathrm{X}^{(m-1)}\right), x \in \left[\mathrm{X}^{(m-1)}, \mathrm{X}^{(m)}\right), \\ 1,\ x \geq \mathrm{X}^{(M)},\ m = 0,1,...M, \end{cases} \tag{3}$$

where $Y^{(m)} = F_\xi\left(X^{(m)}\right) = \sum_{j=1}^{m} p_j$ is the value of the function at the break points. The $F_\xi(x)$ function is shown in fig. 2.

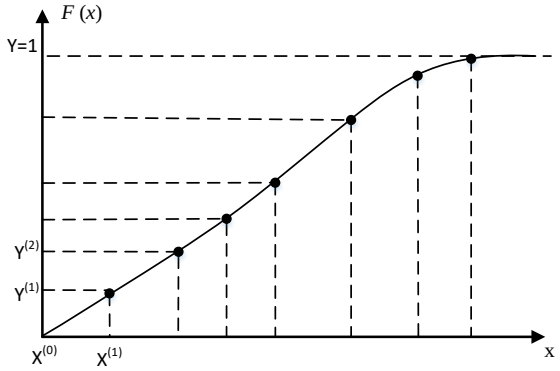

*Fig. 2. The empirical function of the sample **X**, built on the histogram* $h_{\xi}(x)$.

Using the sequence r_i, i=1,2,…k…, uniformly distributed in the interval [0,1) pseudo-random numbers, we obtain a pseudo-random sequence of numbers R_i, i=1,2,…k…, the distribution function of which is equal to $F_{\xi}(x)$

$$R_i = F^{-1}(r_i) = \mathrm{X}^{(m-1)} + \frac{\mathrm{X}^{(m)} - \mathrm{X}^{(m-1)}}{\mathrm{Y}^{(m)} - \mathrm{Y}^{(m-1)}}\left(r_i - \mathrm{Y}^{(m-1)}\right), \tag{4}$$

This sequence of numbers with $k \to \infty$ and fixed n and partitions of the set $\mathbf{a}_x = \lfloor a_{0,} a_n \rfloor$ has a histogram that completely coincides with the original histogram $h_{\xi}(x)$. Thus, the sequence R_i, i=1,2,…k…, is the statistical equivalent of the original sample **X**.

It should be noted that we do not approximate the distribution of the sample **X** with any known distribution and, even in general, we do not need to know what kind of distribution the original sample belongs to, but at the same time, generating the sequence R_i, we repeat the real experiment, that is, we replicate various implementations of the original sequences observed in practice, which do not contradict empirical data.

This approach is convenient in practice, especially in cases where it is virtually impossible to find theoretical distributions. This mainly applies to all distributions that are composite distributions, special cases of which are the Tukki and Huber distribution models, which are used quite often in the analysis of the robustness of algorithms for processing input signals of complex systems. Below we consider examples of using this approach to the synthesis of statistical equivalents using the example of the Tukki and Huber distributions.

GENERATION OF STATISTICAL EQUIVALENTS OF THE TUKKI MODEL DISTRIBUTIONS

As a first example, let us consider the application of the proposed method for generating statistical equivalents to the Tukki model used to study the robust properties of input signal processing algorithms in the case of noise with “weighted” distribution tails. Traditionally, we will use two normal distributions with the same means, but with different variances.

In our example, it does not matter what absolute values are specified for the distribution parameters, only the relationships between the distribution parameters are important. So, let the basic distribution of the normal random variable ξ_1 with density $f_{\xi_1}\left(x / m_1, \sigma_1^2\right)$, where m_1 and σ_1^2 the mathematical expectation and variance of the distribution, and the contaminating distribution of the normal random variable ξ_2 with density $f_{\xi_2}\left(x / m_2, \sigma_2^2\right)$, where m_2 and σ_2^2 the mathematical expectation and variance of the distribution, respectively, be given,

$$f_{\xi_1}\left(x / m_1, \sigma_1^2\right) = \frac{1}{\sqrt{2\pi}\sigma_1} \exp\left(-\frac{\left(x - m_1\right)^2}{2\sigma_1^2}\right), \tag{5}$$

$$f_{\xi_2}\left(x/m_2,\sigma_2^2\right)=\frac{1}{\sqrt{2\pi}\sigma_2}\exp\left(-\frac{\left(x-m_2\right)^2}{2\sigma_2^2}\right). \tag{6}$$

Let the clogging factor be γ. For the traditional Tukki model, we can put m_1=m_2=0, $\sigma_1=1$ and $\sigma_2=3\sigma_1=3$, the clogging factor γ is set equal to $\gamma=0.3$. Then the composite Tukki distribution for the random variable ξ_3, which is a mixture of the distributions of the random variables ξ_1 and ξ_2, can be written in the form

$$\begin{aligned} f_{\xi_3}\left(x/m_3,\sigma_3^2\right)&=\left(1-\gamma\right)f_{\xi_1}\left(x/m_1,\sigma_1^2\right)+\gamma f_{\xi_2}\left(x/m_2,\sigma_2^2\right)=\left(1-\gamma\right)\frac{1}{\sqrt{2\pi}\sigma_1}\exp\left(-\frac{\left(x-m_1\right)^2}{2\sigma_1^2}\right)+\\ &+\gamma\frac{1}{\sqrt{2\pi}\sigma_2}\exp\left(-\frac{\left(x-m_2\right)^2}{2\sigma_2^2}\right)=\frac{1}{\sqrt{2\pi}}\left(0.7\exp\left(-\frac{x^2}{2}\right)+0.1\exp\left(-\frac{x^2}{18}\right)\right), \end{aligned} \tag{7}$$

where m_3 and σ_3^2 the mathematical expectation and variance of the distribution of the random variable ξ_3

In fig. 3 shows the graphs of the functions $f_{\xi_1}\left(x/m_1,\sigma_1^2\right)$, $f_{\xi_2}\left(x/m_2,\sigma_2^2\right)$ and their additive mixture $f_{\xi_3}\left(x/m_3,\sigma_3^2\right)$

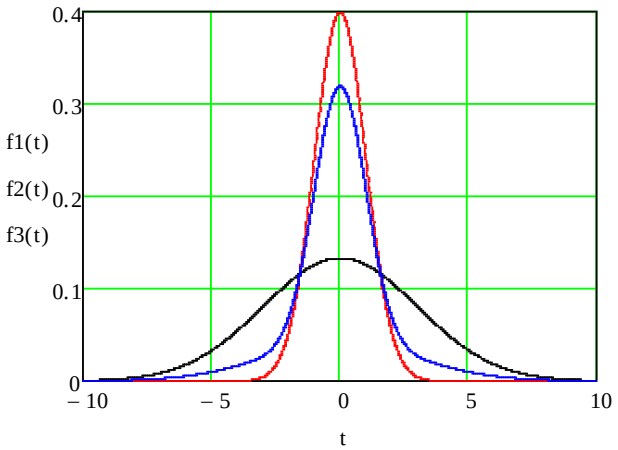

Fig. 3

In fig. 4 shows a histogram constructed when generating random numbers distributed over the function $f_{\xi_3}\left(x/m_3,\sigma_3^2\right)$

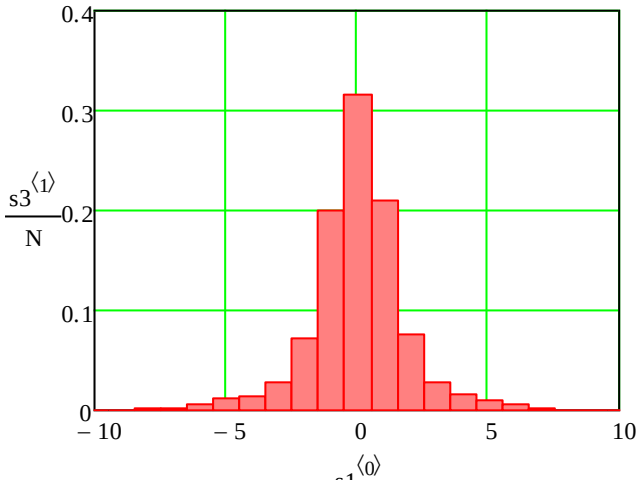

Fig. 4. Histogram plotted on the basis of the additive mixture $f_{\xi_3}\left(x/m_3,\sigma_3^2\right)$

In fig. 5 shows a histogram constructed when generating random numbers distributed over the function $f_{\xi_3}\left(x / m_3, \sigma_3^2\right)$ histogram for N = 1000.

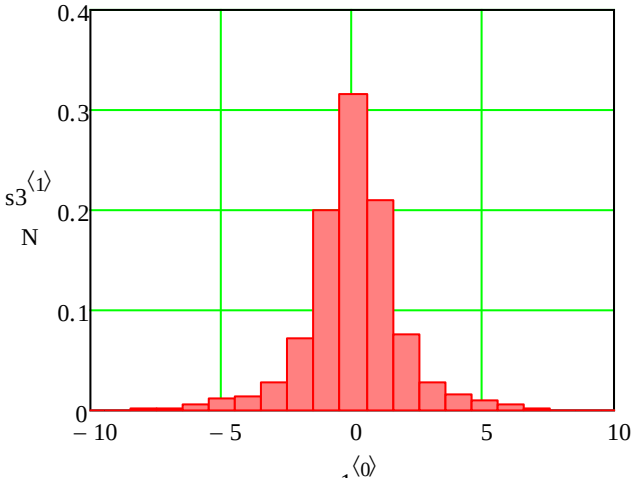

Fig. 5. The histogram, built when generating random numbers distributed over the histogram of the function $f_{\xi_3}\left(x / m_3, \sigma_3^2\right)$

In fig. 6 shows a histogram constructed when generating random numbers distributed over the function histogram for N = 10000.

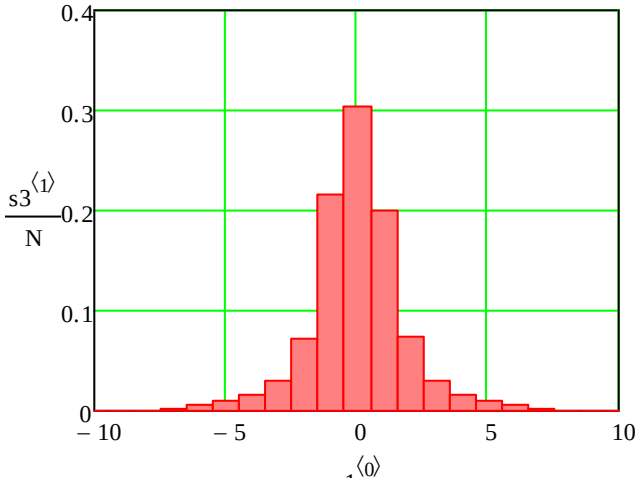

Fig. 6. The histogram, built when generating random numbers distributed over the histogram of the function $f_{\xi_3}\left(x / m_3, \sigma_3^2\right)$ *for N = 10000.*

It can be seen from the graphs that the histograms obtained during the generation of sequences according to expression (7), fig. 4, and according to the histogram shown in fig. 4, fig. 5 and fig. 6 almost coincide. This is not only a visual coincidence, but a real one, since the histograms shown in fig. 5 and fig. 6 by construction converge to the histogram shown in fig. 4.

GENERATION OF STATISTICAL EQUIVALENTS OF DISTRIBUTIONS OF THE HUBER MODEL

As a second example, consider the application of the proposed method for generating statistical equivalents to the Huber model, which is also used to study the robust properties of input signal processing algorithms in the case of noise with “weighted” distribution tails. We will use two distributions of non-negative definite random variables, for which we will take log-normal distributions with different means and variances, and such that the composite distribution turns out to be bimodal. This choice is due to the fact that it is practically

impossible to "select" theoretical distributions in the case of the observed polymodal distribution for the synthesis of the simulation algorithm, and the proposed method of the statistical equivalent easily copes with this task, since it does not require the selection of distributions and estimation of their parameters.

Let the basic distribution of a log-normal random variable ξ_1 with density $f_{\xi_1}\left(x/\bar{x}_1,\sigma_1^2\right)$

$$f_{\xi_1}\left(x/\bar{x}_1,\sigma_1^2\right)=\frac{1}{\sqrt{2\pi}\cdot x\cdot\sigma_1}\cdot\cdot\exp\left(-\frac{\left(\ln x-\ln\bar{x}_1\right)^2}{2\sigma_1^2}\right),\ x\geq 0, \tag{8}$$

where $\bar{x}_1$ and σ_1^2 are distribution parameters associated with the mathematical expectation m_1 and the variance of the distribution D_1 by the relations

$$m_1=\bar{x}_1\ \exp\left(\frac{\sigma_1^2}{2}\right), \tag{9}$$

$$D_1=\bar{x}_1^2\exp\left(\sigma_1^2\right)\left(\exp\left(\sigma_1^2\right)-1\right). \tag{10}$$

The clogging distribution of the random variable ξ_2 is also logarithmically normal $f_{\xi_2}\left(x/\bar{x}_2,\sigma_2^2\right)$ with parameters $\bar{x}_2$ and σ_2^2. The mathematical expectation and variance of the distribution ξ_2 are determined by similar expressions.

With a clogging factor equal to γ, the composite distribution of the Huber model is written in a form similar to expression (7)

$$f_{\xi_3}\left(x/\bar{x}_3,\sigma_3^2\right)=(1-\gamma)\,f_{\xi_1}\left(x/\bar{x}_1,\sigma_1^2\right)+\gamma f_{\xi_2}\left(x/\bar{x}_2,\sigma_2^2\right)=$$
$$=(1-\gamma)\frac{1}{\sqrt{2\pi}\sigma_1 x}\exp\left(-\frac{\left(\ln x-\ln\bar{x}_1\right)^2}{2\sigma_1^2}\right)++\gamma\frac{1}{\sqrt{2\pi}\sigma_2 x}\exp\left(-\frac{\left(\ln x-\ln\bar{x}_2\right)^2}{2\sigma_2^2}\right) \tag{11}$$

Below is the composite Huber distribution for the parameters $\bar{x}_1=1$, $\bar{x}_2=4.5$, $\sigma_1^2=1$, $\sigma_2^2=0.04$ and $\gamma=0.3$, which was used for the corresponding calculations

$$f_{\xi_3}\left(x/\bar{x}_3,\sigma_3^2\right)=0.7\,f_{\xi_1}\left(x/1,1\right)+0.3\,f_{\xi_2}\left(x/4.5,0.04\right)=\frac{0.7}{\sqrt{2\pi}x}\exp\left(-\frac{\left(\ln x_1\right)^2}{2}\right)+\frac{15}{\sqrt{2\pi}x}\exp\left(-\frac{\left(\ln x-1.5\right)^2}{0.08}\right) \tag{12}$$

In fig. 7 shows the graphs of functions $f_{\xi_1}\left(x/\bar{x}_1,\sigma_1^2\right)$, $f_{\xi_2}\left(x/\bar{x}_2,\sigma_2^2\right)$ and their additive mixture $f_{\xi_3}\left(x/\bar{x}_3,\sigma_3^2\right)$

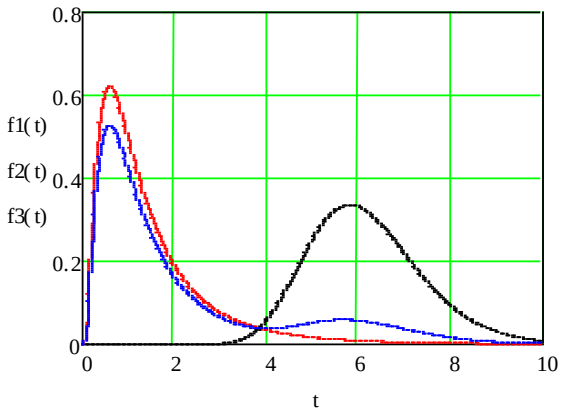

Fig.7. Histogram plotted on the basis of the additive mixture $f_{\xi_3}\left(x/\bar{x}_3,\sigma_3^2\right)$

In fig. 8 shows a histogram constructed when generating random numbers distributed over functions $f_{\xi_3}\left(x/\bar{x}_3,\sigma_3^2\right)$

In fig. 9 shows a histogram constructed when generating random numbers distributed over the histogram of the function $f_{\xi_3}\left(x/\bar{x}_3,\sigma_3^2\right)$ for N = 1000.

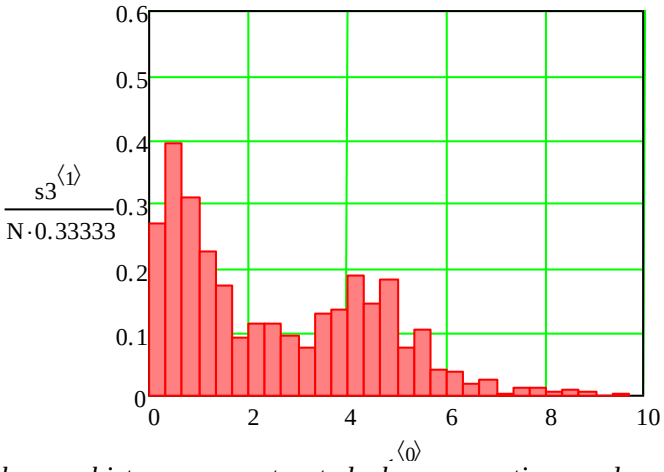

In fig. 9 shows a histogram constructed when generating random numbers distributed over the histogram of the function for N = 1000.

In fig. 10 shows a histogram constructed when generating random numbers distributed over the histogram of the function for N = 10000.

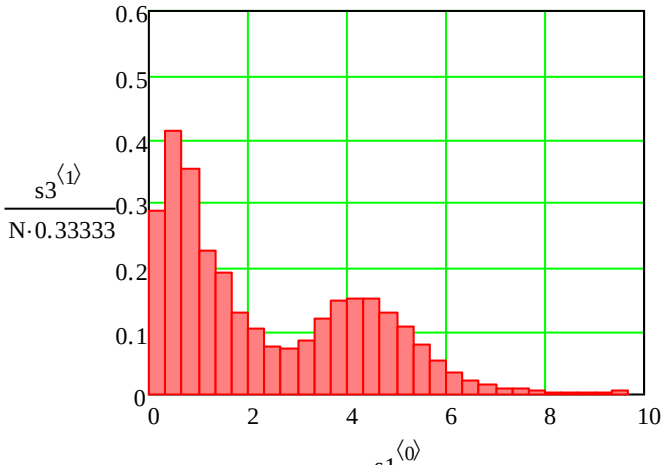

Fig.10. Histogram, built when generating random numbers distributed over the histogram of the function $f_{\xi_3}\left(x/\bar{x}_3,\sigma_3^2\right)$

It can be seen from the graphs above that the histograms of the Huber model obtained during the generation of sequences according to expression (11), fig. 8, and according to the histogram shown in fig. 8, fig. 9 and fig. 10, as well as for the Tukky model, practically coincide, since, by construction, they converge to the histogram shown in fig. 8.

FINDINGS

The paper presents calculations for a simple but quite effective algorithm for modeling input signals of information processing systems, using empirical data on the statistical characteristics of input streams. The algorithm allows you to generate input streams that are statistical equivalents of input signals of complex systems, that is, it actually allows you to replicate records of realizations of input signals obtained in real conditions. It should be noted that in this case, the researcher does not need to approximate the statistical characteristics of the records of real signals, since the algorithm will automatically take into account these

characteristics even in such complex cases when there are “weighted” distribution tails, as in the Tukki model, or the distributions of real signals are polymodal, as in the model. Huber.

REFERENCES

1. Maurits V.G. A mathematical model of the echoes of the sea surface observed by airborne aircraft locators./ V.G. Maurits, M.A.Klimova, M.S. Ivanova// In the collection: Scientific session of SUAI. Collection of reports. In 3 parts. 2018. P.351-357.

2. Shakhov, V.V. Review and comparative analysis of libraries of generators of pseudo-random numbers / V.V. Shakhov // Problems of Informatics. –2010. – No 2. –C. 66-74.

3. Isakov V.I., Modeling location signals. reflected from the edge of the land-sea/ D.A. Shepeta., V.I. Isakov // Information management systems. 2017. No5 (90). P. 89-94.

STUDY OF THE OPTICAL RADIATION SPECTRUM OF THE COMBUSTION OF GASEOUS HYDROCARBON FUEL USING THE OCEAN OPTICS SPECTRAL DEVICE

Veniamin Kitaev

Saint Petersburg State University of Aerospace Instrumentation
Saint-Petersburg, Russia
E-mail: veniamin.kitaev@gmail.com

Annotation
In this paper, the dependence of the change in the propane combustion process on the change in the ratio of the supplied gas-air mixture is considered when using the spectroscopic method of research using the Ocean Optics spectral instrument.

Introduction

Air pollution is becoming more and more relevant topic in the field of ecology every year. Many cities in the world suffer from high levels of harmful substances in the air, which adversely affects the environment and the body of animals, including humans.

The control of the combustion process in modern thermal power plants consists of complex interconnected systems of instruments and control programs that monitor such parameters as consumption, temperature, fuel and oxidizer (air) pressure; temperature and pressure inside the combustion chamber; composition and concentration of combustible gases, oxidation products (CO2 and H2O) and oxidation by-products (CO, C2 and CH4) in the chamber, as well as composition and concentration of flue gases. A large number of devices, various sensors and monitoring equipment, which have their inertia and, at other times, insufficient sensitivity, inevitably lead to an increase in the response time of the necessary control units under already changed controlled conditions, which cannot allow achieving the required efficiency indicators of the installation and reducing harmful emissions into the atmosphere [1].

The combustion process of gaseous hydrocarbon fuel, the main part of which is methane (CH4) from 76 to 98%, consists in its chemical combination with oxygen and proceeds in the form of a branched chain reaction with a large release of heat. In this case, the air-gas ratio in the mixture entering the flame front is of great importance. In this case, the appearance of the flame and, consequently, its spectrum change depending on the air-gas ratio in the mixture, pressure and air flow rate [2].

The combustion process is characterized by a number of informational parameters, including spectroscopic ones. In this work, to solve the problems of monitoring the combustion of gaseous hydrocarbon fuel, it is proposed to use the methods of applied optical spectroscopy. The control device is a spectral-selective device that examines optical radiation as a signal carrying spectroscopic information about the combustion process and can supplement, improve and optimize flame control on the objects used (replace most of the control and measuring equipment located on the object). The proposed device performs spectral measurements in specified areas of the optical range using a set of narrow-band interference optical filters tuned to specific wavelengths.

Description of the laboratory setup

The study of the combustion process is carried out on two different types of burners with the same gas pressure (3.5 kPa): gas-air with compressed air (Figure 1) and Teklu type (Figure 2). The fundamental difference between them lies in the system and the principle of air supply. The compressed air supplied from the compressor is adjusted using a reducer on the compressor (lowering the outlet pressure from the compressor to 10-15 psi), valves and manometers (then rotameters and more accurate manometers will be installed in the system). The air supply in a Teklu burner is regulated according to the principle of rotation of the adjusting disc under the combustion chamber, but during the operation of this equipment it is impossible to determine the air flow.

The Ocean Optics USB2000 + spectral instrument is used as a measuring device. The spectrometer combines an ADC with a frequency of 2 MHz, programmable electronics, a linear CCD detector with 2048 ele-

ments and a high-speed USB 2.0 interface. This combination of components provides high speed and resolution up to 0.035 nm (FWHM). When connected to a USB 2.0 port, the full spectrum is transferred to the computer memory every millisecond (1000 full spectra per second). The USB2000 + is suitable for chemical, biochemical and other applications where fast reaction control is required. The detector of the spectrometer is sensitive in the range 200–1100 nm.

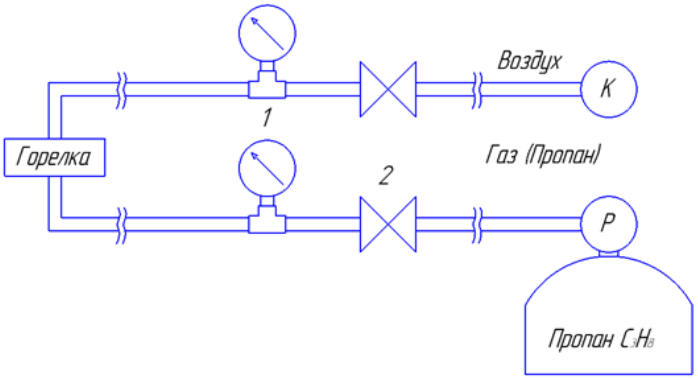

Figure 1. Diagram of the gas and compressed air supply control system for the model, where: 1 - pressure gauge; 2 - gas valve; K - compressor; P - gas reducer.

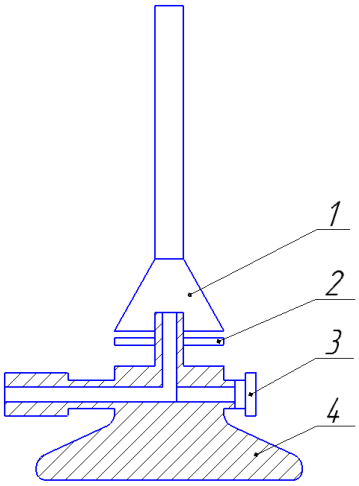

Figure 2. Scheme of a Teklu burner, where: 1 - tube; 2 - air supply control disk; 3 - screw for adjusting the gas supply; 4 - stand

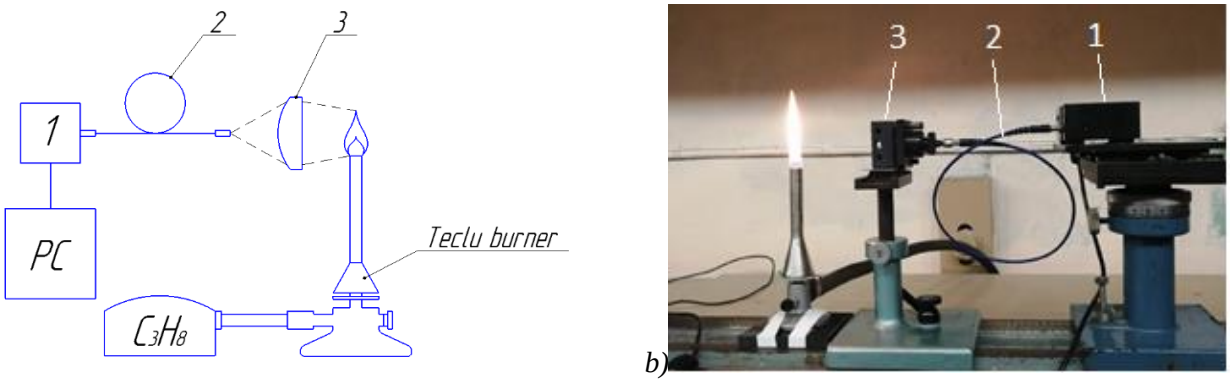

a) *b)*

a - scheme of the stand for the study of the combustion process; b - photo of the stand

Figure 3. Schematic of the laboratory model, where: 1 - Ocean Optics USB2000 + spectrometer; 2 - Fiber optic cable; 3 - Collecting lens. Photo of the experiment

Results of the experiment performed using a gas-air burner and a spectral instrument Ocean Optics

This experiment was divided into three parts: igniting pure propane without air supply (creating an orange - red flame), a slight supply of air (appearance of a blue flame with an orange front) and creating an excess air condition (transparent flame with a green - blue front).

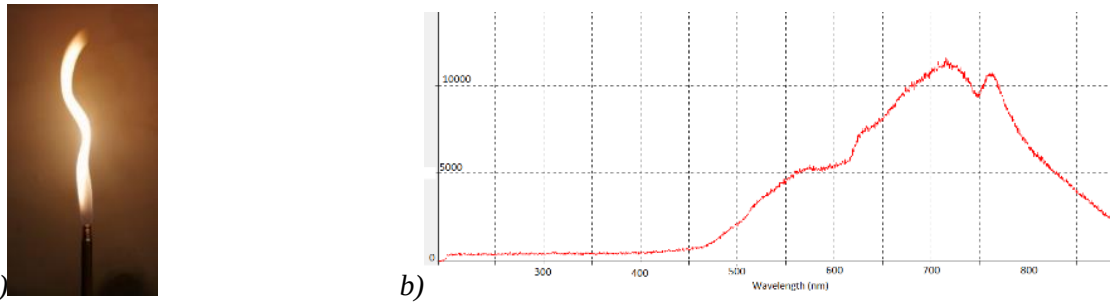

a) - photograph of the flame of a two-component burner; b) - spectrogram

Figure 4. The emission spectrum arising from the combustion of propane without the supply of an oxidizer.

When the air supply is shut off, we get a bright glowing flame, the spectrum of which is mainly continuous in nature, which is caused by the thermal radiation of coal particles.

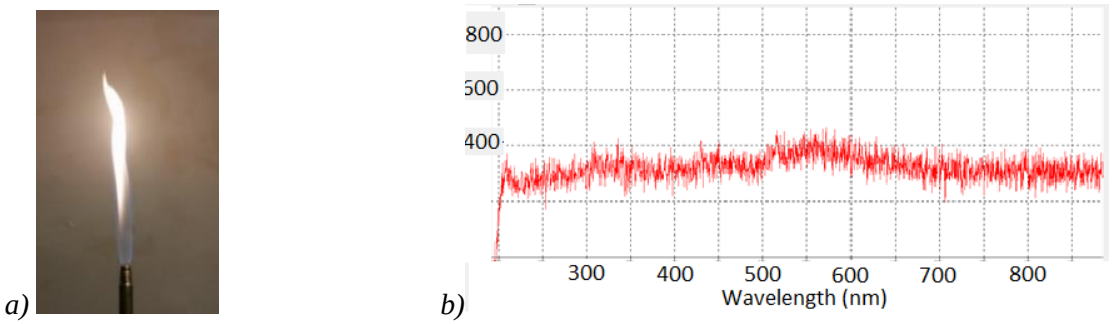

a) - photograph of the flame of a two-component burner; b) – spectrogram

Figure 5. The emission spectrum arising from the combustion of propane with an insignificant air supply.

With a small supply of oxidizer (air), a bright yellow flame becomes much less bright, transparent blue-violet, called non-luminous.

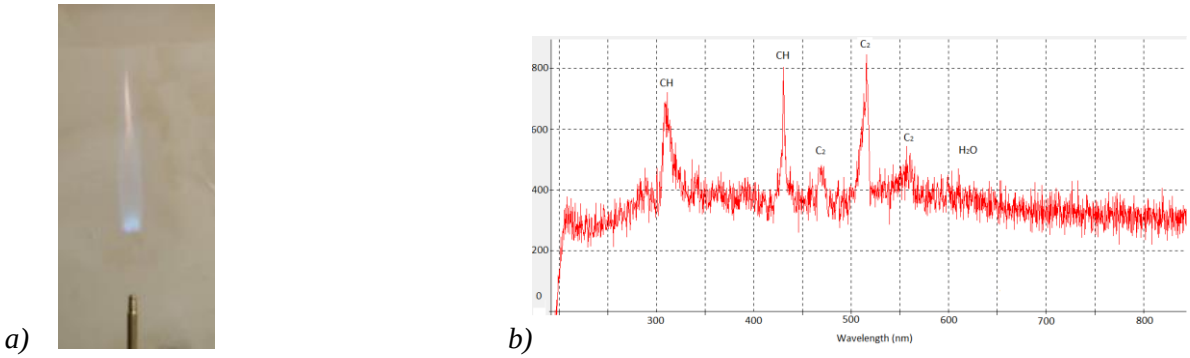

a) - photograph of the flame of a two-component burner; b) - spectrogram

Figure 6. The emission spectrum arising from the combustion of propane with excess air supply.

The increase in air supply divides the flame into two cones: the inner one is bright blue - green; and the outer is much more intense, blue-violet.

Results of the experiment using the Teklu burner and the Ocean Optics spectral instrument

Three experiments were performed for this burner: propane combustion with a tight disk (air supply shut off), normal combustion, and excess air during combustion.

a) 

b) 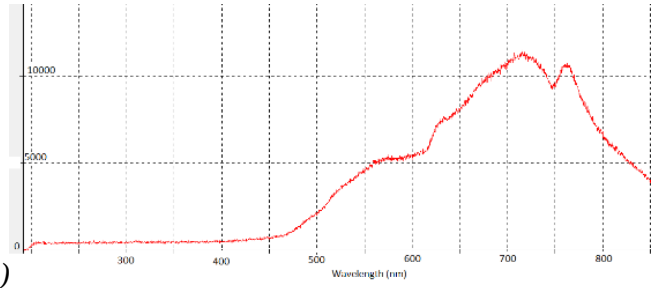

a) - photograph of the flame of a Teklu burner; b) - spectrogram

Figure 7. The emission spectrum arising from the combustion of propane in the Teklu burner with the closed air supply to the combustion chamber

a) 

b) 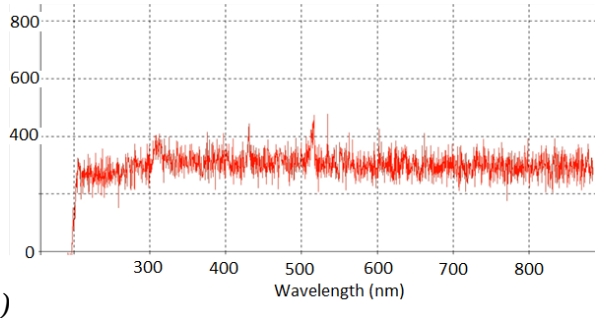

a) - photograph of the flame of a Teklu burner; b) – spectrogram

Figure 8. The emission spectrum arising from the combustion of propane in the Teklu burner with a minimum supply of air to the combustion chamber

a) 

b) 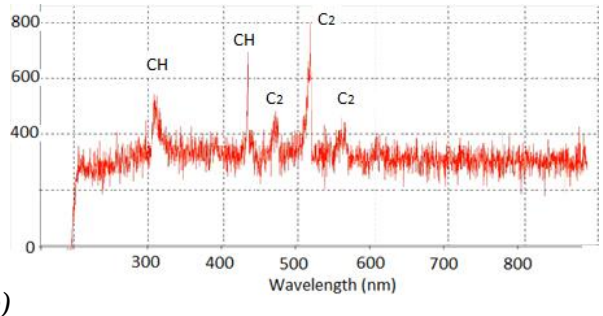

a) - photograph of the flame of a Teklu burner; b) – spectrogram

Figure 9. The emission spectrum arising from the combustion of propane in the Teklu burner on the verge of flame blowou

When studying a Bunsen flame, you can immediately notice that the appearance of the flame, and therefore its spectral characteristics, change depending on the speed and volume of the supplied air, which in the case of using a Teklu burner is determined by the air gap between the chamber and the adjusting screw, and when using a two-component the burner is determined by the outlet pressure from the compressor and by turning the adjusting screw on the model.

The most intense systems in the spectra of tribes are systems of bands of such radicals as OH (wavelength λ: 308-320, 326, 342 and 349 nm), CH (wavelength λ: 310-320, 431 - 438 nm), C2 (wavelength wavelength λ: 467 - 472, 513 - 516, 559 - 564 nm). In the visible wavelength range, three main groups of bands are observed: CH (431 - 438 nm), C2 (467 - 472, 513 - 516, 559 - 564 nm) and water molecules at wavelengths 591 and from 616 to 625 nm. The luminescence of CH (431 - 438 nm) and C2 (467 - 472, 513 - 517 nm) are most pronounced when the composition of the gas-air mixture changes, namely, an increase in the supplied volume of air relative to the gas. In the ultraviolet part of the spectrum, the OH band is most clearly visible in the range from 306 to 320 nm and a not very intense system consisting of a large number of bands (301 - 358 nm) [3].

Conclusion

In this work, the dependence of the change in the propane combustion process on the change in the ratio of the supplied gas-air mixture was investigated when using the spectroscopic research method. As part of the study, a stand was developed with a burner, with a fuel and air supply system. Experiments were carried out for three combustion modes for two burners. The emission spectra resulting from the combustion of gaseous hydrocarbons were obtained using the Ocean Optics USB2000 + spectral instrument. The dependences of the change in the emission spectra on the change in the gas-air ratio are obtained. The obtained spectra were studied and the substances related to each spectrum were determined.

This work was financially supported by the Russian Foundation for Basic Research (RFBR), project No. 20-07-00648.

REFERENCES

1. Novikov O.N., Okatiev A.N. Shkarovsky A.L. Automatic control of the quality of fuel combustion is thekey to energy saving and energy-ecological safety of the enterprise. URL: http://www.kb-agava.ru/avtomaticheskoe_upravlenie_kachestvom_szhiganiya_topliva (accessed 03.02.2020).

2. A. Marjanovic, M. Krstic, Z. Durovic, and B. Kovacevic, “Control of Thermal Power Plant Combustion Distribution Using Extremum Seeking,” IEEE Transactions on Control Systems Technology, vol. 25(5), pp.1670-1682, 2017

3. Gaydon, G., [Spectroscopy and Combustion Theory], Chapman and Hall, London, 191 (1942).

AUTOMATION OF ECO-MONITORING PROCESSES IN THE URBAN ENVIRONMENT FOR ASSESSING AND PREDICTING ITS CHANGE

Lydia Klimochkina

St. Petersburg State University of Aerospace Instrumentation
E-mail: B1T2K3@yandex.ru

Annotation
The impact on the environment of human economic activity is increasing every year, which leads to significant disturbances in the balance between nature, anthropogenic load and degradation of environmental conditions. The growth of urbanization, the emergence of industrial facilities - all this leads to environmental pollution and its degradation.

The ecological assessment of the territory contains data from all types of monitoring. It should be especially emphasized that taking into account self-organization processes is necessary to ensure safety. Therefore, the creation of an integrated intelligent automated system for environmental monitoring, management of technological processes of coal enrichment and management of environmental and economic decisions based on the principles of systemic and integrated approaches and methods of mathematical modeling and identification, statistical information processing, database and knowledge management systems, methods of modern management theory (including those with fuzzy logic) and computer technologies. It is necessary that the developed systems meet all the basic principles, requirements and standards for creating environmental and economic monitoring systems (EMS) and management and be applicable to similar enterprises when creating local and regional EMS. For continuous monitoring, I use equipment capable of accumulating and processing statistical data. one. The quality of environmental monitoring largely determines the effectiveness of control actions aimed at ensuring the required state of environmental safety. The information obtained within the framework of environmental monitoring - eco-information - must meet the following basic requirements: reliability and objectivity, scientific validity, representativeness, comparability, reliability, transparency and openness, focus on priorities, compliance with regulatory and legislative documents.

In most regions of Russia, various structures (environmental, sanitary and epidemiological, hydrometeorological) carry out regular or periodic quality control of environmental components. The process of assessing in the environmental monitoring system is the comparison of the actual (formed at the moment) environmental situation with the models of the normal environmental situation for the territory under consideration.

Both in Russia and abroad, the solution to the problem of implementing highly effective environmental monitoring is in the following areas: development and implementation of the latest equipment and metrological support; development of remote control and observation methods, including aerospace; development of modern methods and models for assessing and forecasting the level of pollution of the natural sphere from man-made objects.

In the Russian Federation, environmental monitoring, its development and software are handled by the Unified State System of Environmental Monitoring (EGSEM), created in 1993. EGSEM is guided by the territorial-departmental principle of building systems. State environmental monitoring is understood as a comprehensive observation of the state of the environment, including the components of the natural environment, natural ecological systems, the processes occurring in them, phenomena, assessment and forecast of changes in the state of the environment.

With all this, it is very important to note that in the modern economy, the problem of environmental protection in the technogenic regions of the country is acquiring paramount (global) significance. Over the years, various departments have created a huge amount of valuable information about the state of the environment. For example, in the CIS, there are more than 1,500 stations and control posts monitoring air pollution (in approximately 500 cities and towns), pollution of inland water bodies - about 4,000, sea pollution - more than 2,000 control posts, etc. However, the aggravation of the environmental and radiation situation has led to an urgent need for further strengthening and a qualitatively new approach to the creation of a system of environmental monitoring, control and making informed management decisions aimed at improving and stabilizing the environmental situation as a whole.

Figure 1. An example of a monitoring complex

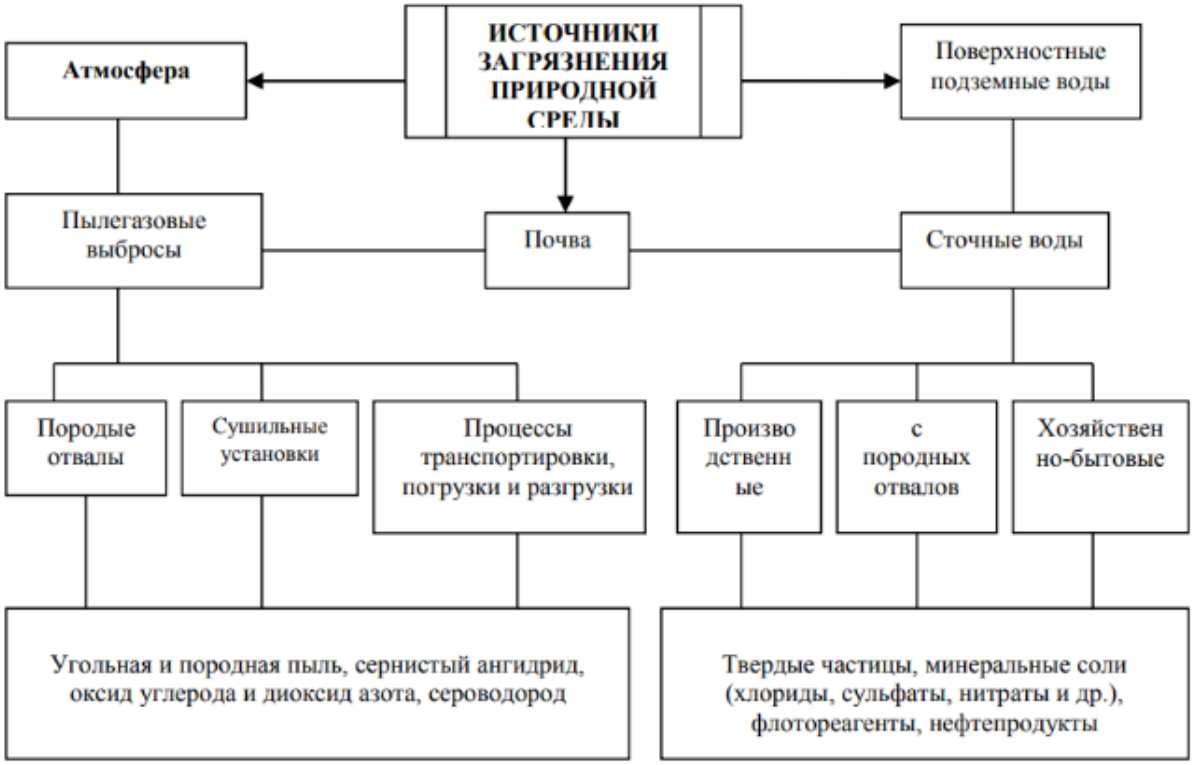

Figure 2. Sources of pollution

To carry out, based on environmental monitoring data, a qualitative and / or quantitative assessment of trends in changes in the state of the environment that occurs under the impact of man-made sources, characteristics called environmental criteria or indicators are used in all industrial countries of the world.

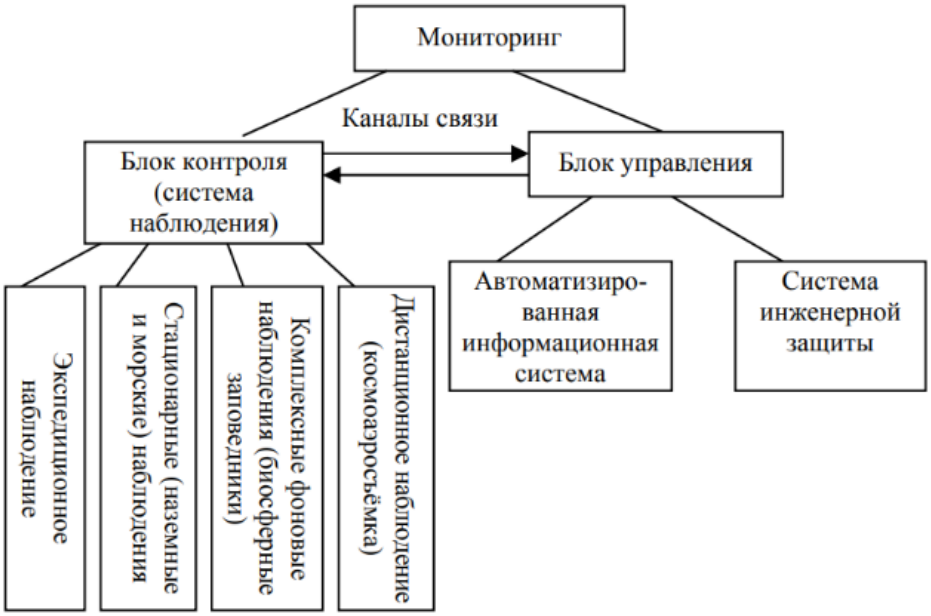

Figure 3. Structural monitoring scheme

Figure 3 - Scheme of characteristics of the type of impact of man-made sources on the environment of settlements

When choosing the technical and technological characteristics of production and transport facilities as parameters for environmental monitoring, it is necessary to take into account that their negative impact on the environment corresponds to a certain nature, level and sustainability.

It should be especially noted that when modeling and organizing the functioning of an automated environmental monitoring system in a specific territory, it is rational to rank technogenic objects as sources of environmental pollution and to single out specialized subsystems for monitoring directly in the zone of influence of those objects (their totality) that are most significant from the point of view in terms of environmental damage.

The quality standards for the components of the natural environment may vary for territories (or premises) of various types. So, for example, the urban area is subdivided into the following zones: residential (residential), public and business, production (industrial), sanitary protection, engineering and transport infrastructure, recreational, special purpose (cemeteries, dumps) and military facilities. The environmental quality standards

in the Russian Federation are the maximum permissible concentrations (MPC) of chemical compounds in the components of the natural environment, the maximum permissible levels (MPL) and the maximum permissible doses of physical impact, the maximum permissible waste disposal, etc.

The basis of the organizational structure of environmental monitoring is an automated information system (AIS), which is created on the basis of computer tools. The tasks of AIS monitoring are: storage and search of regime information about the state of the environment; purposeful continuous processing and evaluation of information; implementation of permanent forecasts of development and the state of the environment; solving optimization problems for environmental management. It follows from this that the very structure of AIS monitoring, which consists of four interconnected main blocks. The first block of the AIS is an automated information retrieval system (AIPS).

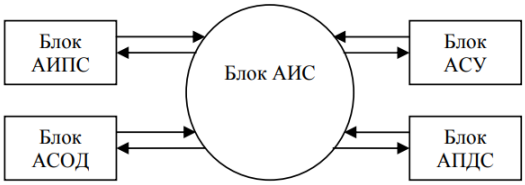

Figure 4. Structure of AIS monitoring

The second block of AIS is the automated data processing system (ASOD). The third block of AIS is an automated predictive and diagnostic system (APDS). The fourth block is an automated control system (ACS). The main issue in the organization of AIS is its information, technical and mathematical support. All blocks of the automated system for monitoring the environmental situation must meet the requirements of adaptability and mobility to current changes in the monitoring / management facility and the external environment.

The main functions of the eco-monitoring system, which, in turn, should be a component of the overall intelligent territory management system:

- automated collection of information on the quality indicators of the components of the natural environment that have an impact on the health and life of the population of the considered territory

- automated collection of information about the parameters characterizing the state of man-made objects; the power of the emission of pollutants into the natural environment, etc.), which determine not only the economic characteristics of the region, but also the result of the formation of the ecological situation in the given territory;

- automated collection of information about the parameters of external influence; subset of natural and climatic parameters; a subset of parameters related to regulations and their changes, etc.);

- preliminary processing of data and their transfer through information communication channels to interested parties (decision-makers, specialized environmental structures, the population, the media, etc.). These four functions are traditional from the point of view of organizing the work of the environmental monitoring system.

Conclusion

It should be noted that monitoring systems are developed differently for different components of the natural environment. The most advanced systems in this area are air control and monitoring systems, despite the fact that the concept of environmental and analytical control currently in force in Russia (Federal Service of the Russian Federation for Hydrometeorology and Environmental Monitoring) is outdated.

In view of what follows the need to update this system.

List of used literature:

1. E.G. Yazikov, A. Yu. Shatilov. Geoecological monitoring. Textbook for universities.- Tomsk, 2003.- 336 p. Quality management of additive products / A. V. Chabanenko // RIA: Journal: “Standards and Quality”. 2018. No. 2. S. 90-94.

2. Interstate standard GOST 24.104-85: “Unified system of standards for automated control systems. Automated control systems. General requirements". Moscow, STARDARTINFORM, 2009

3. "Organization of monitoring and control over the ecology of the environment." Poluyanov V.P. Bulletin of BSTU im. V.G. Shukhov, 2009, No. 4.

4. Volkodaeva M.V. Volkodaeva M.V., Kiselev A.V. On the development of the system of environmental monitoring of atmospheric air quality // Notes of the Mining Institute. 2017.Vol. 227, p. 589-596. DOI: 10.25515 / PMI.2017.5.589

MATHEMATICAL MODELING OF THERMAL PROCESSES OCCURRING DURING THE OPERATION OF AN LED LIGHT SOURCE

Vladimir Kuzmenko

Saint-Petersburg State University of Aerospace Instrumentation,
Saint-Petersburg, Russia
E-mail: mr.konnny@gmail.com

Abstract.
In the established by industry standards and implemented in practice methods for controlling LED lighting devices, most often the only controlled thermal parameter is the junction-case thermal resistance, which determines the amount of overheating of the active region of the crystals relative to the case temperature with a power dissipation of 1 W. In order to improve the reliability of rejection of devices with heat sink defects, mathematical modeling of heat and mass transfer of individual layers of the LED lamp structure was performed.

INTRODUCTION

Currently, there are many articles and studies devoted to the construction of mathematical models that describe or clarify the processes of heating and heat transfer of LED light sources of various designs and capacities. However, it is very difficult to convey the entire complete picture of the ongoing process by a mathematical model due to the need to make various kinds of assumptions and approximations for the process under study.

There are a large number of thermal models based on the idea of thermal resistances of LED crystals and its substrate; however, these studies often do not take into account the fact of the closed space of the LED [1, 2, 3].

In the control methods established by industry standards and implemented in practice, most often the only controlled thermal parameter of the SOP is the junction-case thermal resistance, which determines the amount of overheating of the active region of the crystals relative to the case temperature with a power dissipation of 1 W [4, 5].

In order to increase the reliability of rejection of devices with heat sink defects, active development of methods and means for measuring the thermal resistance of individual layers of the semiconductor device structure, including SOP, is underway. When implementing these methods, it is usually customary to solve the problem by identifying the parameters of thermal equivalent circuits, for which an integral measurement of the thermal characteristics of devices is necessary.

When setting the problem, we will take into account the following assumptions taken in mathematical modeling:

1) When a current flow through the p-n junction in the crystal, energy is released in the form of radiation, as a result of which the elements of the system are heated.

2) Due to the reflector, the radiation into the base is insignificant, as a result of which it can be neglected. Thus, the formation of emitting fluxes of LED crystals, which are coated with a phosphor, occurs. As a result of thermal conductivity, the substrate and the crystal coated with the phosphor are heated.

3) Over time, the degree of heating of the entire LED increases, which over time leads to degradation of the luminous flux and failure of the LED.

It is assumed that the crystal is covered with a homogeneous medium - a phosphor with constant thermophysical characteristics. This assumption is typical for building this kind of thermal models.

For the investigated mathematical model of a LED household lamp in the SolidWorks software environment, a three-dimensional model of a physical analogue lamp was built, which was tested earlier [6]. The figure shows a model of the LED lamp under study, taking into account the real dimensions, electrical and thermal characteristics of the physical analogue. The model was built in the SolidWorks environment and is shown in Figure 1.

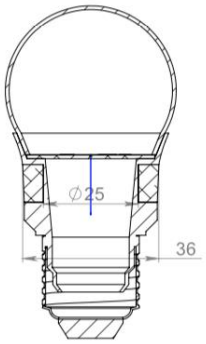

Fig. 1 *Model of the LED lamp, taking into account the actual dimensions*

The figure shows that the main role in the complexity of the problem is played by the configuration of the light source and the presence of a spherical closed space. The shape of the reflector, the crystal band gap and the change in these factors with increasing temperature also play an important role.

SIMULATION

According to the Joule-Lenz law, the amount of heat released by the crystal matrix when an electric current flow through the crystal can be determined by the following expression [7]:

$$Q = I^2 Rt$$

where Q is the amount of heat generated by the flow of electric current through the crystal, J; I - current strength, A; R - electrical resistance, Ohm; t - time, s.

To describe the formulated physical conditions of the problem in combination with the processes of heat and mass transfer, a heat and mass transfer medium is considered in the form of a "LED substrate - a crystal coated with a phosphor".

The energy equation for heat and mass transfer for the substrate (0 <R <R2; 0 <Z <Z1):

$$\rho_1 C_1 \frac{\partial T_1}{\partial t} = \lambda_1 \left(\frac{\partial^2 T_1}{\partial r^2} + \frac{1}{r}\frac{\partial T_1}{\partial r} + \frac{\partial^2 T_1}{\partial z^2} \right).$$

The energy equation for heat and mass transfer for a crystal (0 <R <R1; Z1 <Z <Z2):

$$\rho_2 C_2 \frac{\partial T_2}{\partial t} = \lambda_2 \left(\frac{\partial^2 T_2}{\partial r^2} + \frac{1}{r}\frac{\partial T_2}{\partial r} + \frac{\partial^2 T_2}{\partial z^2} \right) + \frac{Q}{V_{кр} t}.$$

As mentioned above, the thermal model was built in the SolidWorks environment. The geometry of the computational domain consists of a polycarbonate body and a transparent light-scattering shade, a silicon carbide printed circuit board, a driver, and 6 LED matrices fixed on the PCB.

As you know, according to the functionality of the program, specifying temperatures only at the border can be irrational, due to the adoption of temperatures with a zero value for all other locations. When specifying temperatures for the boundary only, you may first need to create and solve a thermal study to calculate temperatures at all nodes. Similar to the iterations described above, Solidworks Simulation performs a finite volume calculation. In this add-on, it becomes possible to simulate air flow, while the convection coefficients are calculated independently by the program.

Calculations are also possible through finite element analysis, which is a digital method for analyzing technical structures. The process begins with the creation of a geometric model. The program then divides the model into small pieces of simple shape (elements) connected at common points (nodes). Finite element analysis programs view a model as a network of discrete interconnected elements. The finite element method (FEM) predicts the behavior of a model by comparing information from all the elements that make up the model.

An important step in conducting computer modeling is the correct mesh definition, the program can use an automatic mesh creator to generate constructions based on the global element size, tolerance and local control characteristics of the mesh.

The program determines the element size for the model, taking into account its volume, surface area and other geometric characteristics. The size of the mesh (number of nodes and elements) to create depends on the geometry and dimensions of the model, mesh tolerance, mesh control options, and contact characteristics. In the early stages of structural analysis, where approximate results may be appropriate, you can set a larger element size for a faster solution. For a more accurate solution, a smaller element size may be required.

Meshing yields 3-D tetrahedral solids, 2-D triangular shell features, and 1-D beam features. The mesh consists of elements of the same type, unless the type of the combined mesh is specified. Contact is usually the source of non-linearity. Although nonlinear studies are commonly used to solve contact problems, the program allows you to use static studies to solve contact problems with small or large displacements.

The window for setting the parameters of thermal modeling looks like this (Figure 2). It is important here not to mix up the coordinates and not get negative Y-component values in the gravity section.

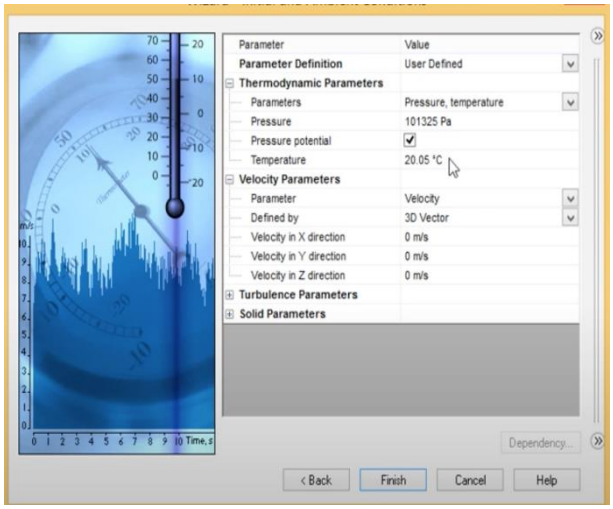

Fig. 2 *Basic parameters input window*

The thermal conductivity was set equal to 1 W / m / K. These values of thermal conductivity are an order of magnitude lower than the values of thermal conductivity of materials traditionally used for the manufacture of radiators in electronic devices (the thermal conductivity of the aluminum layer on the reverse side of the printed circuit board was set to be about 200 W / m / K). The boundary condition for the heat flux was set under the LED module, the total value of the heat flux was 3.5 W, which corresponds to 6.5 W for the entire lamp. At the open boundaries, soft boundary conditions were set with a temperature of 25 ° C. Figure 3 shows the thermal simulation of the LED light bulb under test.

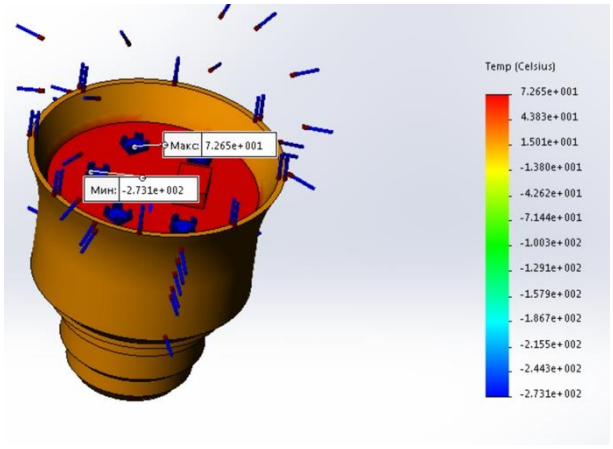

Fig. 3 *Thermal simulation of the LED lamp*

The simulation results show that the main heat is transferred directly from the semiconductor crystal to its metal substrate (lamp body) due to the heat conduction mechanism. Only 5% of the heat is emitted as thermal (infrared) radiation. Satisfactory agreement is observed between the experimental and calculated temperature dependences. The similarity between the experimental and calculated temperature values is satisfactory, and the error is associated with the inability to accurately determine the geometric and thermophysical characteristics of the structure of real LEDs, as well as the measurement error.

CONCLUSION

The model was tested by comparing the calculated and experimental dependences of the thermal resistance of the structure of the LED lighting device [6].

The experimental sample described in the previous section was used to measure the parameters of thermal models of the SOP.

As a result of the work, the efficiency of heat dissipation in plastic cases of LED lamps was evaluated. Based on this thermal model, one can judge the dependence of the maximum temperature at the places where the LEDs are mounted on the printed circuit board of the lamp on the thermal conductivity of the housing material or the radiator, if the latter is present.

Based on the data obtained, it can be concluded that the thermal conductivity of the housing elements of the lamp under study is insufficient and the required increase in the thermal conductivity of the housing materials.

Also, these results show that the main obstacle in ensuring the thermal regime of the LED lamp is the forced elongation of the structure, due to the need to mount the driver inside the SOP. This is a determining factor in the choice of the shape of the case and its base, which leads to high thermal resistances between the far ends of the fins, imitating some kind of radiator (if any) and the place where the LEDs are mounted, as well as the place where the lamp is mounted in the base, where, due to the high According to statistics, accelerated aging of the insulation of the supply wires is observed.

REFERENCES

1. Ivukin I.N., Bougrov V.E., Kovsh A.R., . Odnoblyudov M.A, Shalkovskiy A.G., Romanov A.E.Heat transfer simulation and retrofit LED lamp plastic heat sink material optimization. MPM e-journal No 2, Vol. 17, 2013. p.178-182.

2. Grigor'yeva S.V., Baklanov A.V., Yakovlev A.N. Matematicheskoye modelirovaniye teplomassaperenosa v sisteme teplootvoda dlya vysokoy moshchnosti // Vestnik Karagandinskogo universiteta. Seriya Fizika. – 2015. – №4(80). S. 31-38.

3. Gurin S.YU., Gritsenko B.P., Akimov B.V., Lukash V.S. Issledovaniye vliyaniya konstruktsii svetodiodnogo svetil'nika na yego teplovyye polya // Izvestiya VUZov. Fizika. – 2013. – T.56. – No 12/2. – S. 11-16.

4. LED lamps with base without built-in control device. Part 2. Operational requirements. Development of GOST R. Direct application of project 34 / A / 1353 / NP (2009-06) IEC 62663-2.

5. Light sources are electric. Methods for measuring light and electrical parameters. (Instead of GOST 17616-82 on the territory of the Russian Federation).

6. Kuzmenko V.P., Solyoniy S.V., Shishlakov V.F., Kvas E.S., Solenaya O. Ya. Research tests of LED light sources / Izv. universities. Instrumentation. 2019.Vol. 62, No. 7, pp. 1-10.

7. Bayneva I.I., Baynev V.V. Software model for evaluating the efficiency and reliability of LED light sources and devices // Semiconductor lighting technology. - 2011.– No3.– S. 40-42.

REVIEW OF SMART GRID

Nikita Miroshnichenko, Anastasia Raskopina, Mikhail Sinkin

Saint-Petersburg State University of Aerospace Instrumentation,
Saint-Petersburg, Russia
E-mail: Nikitos_mir.1997@mail.ru, raskopina.nastia@yandex.ru, aweekw@gmail.com

Abstract
The current state of electric power equipment is in a critical degree of wear and tear, and requires energy-efficient solutions and the development of renewable energy sources. Therefore, technologies of intelligent power supply networks are actively developing and developing. Such systems are aimed at increasing operational efficiency, increasing network throughput, optimizing and load sharing in the network, which reduces the need for new substations and transmission lines. However, the introduction of modern technologies is faced with problems of technical integration into the existing infrastructure and requires modeling and simulation. The combination of traditional networks, intelligent systems, renewable energy sources requires the integration of modern information technologies, which need to be tested and analyzed before being introduced into the real electricity network in order to avoid risks in terms of time and the possibility of integration.
Keywords: *SMART GRID, electricity, energy efficiency, renewable energy.*

INTRODUCTION

Smart Grid – a generic term for the use of computer intelligence and networking opportunities in a simple electrical distribution system. Smart grid is a two-way exchange in which electricity can be exchanged in both directions – between utilities and consumers. This growing network of communications, automation, computers and control is helping to make the network more efficient, reliable, secure and green [1].

Energy companies are faced with the need to implement new operating and maintenance standards to continually improve the balance between supply reliability and cost. Due to the huge amount of equipment that requires constant routine maintenance and repair, a key task in the energy sector is the management of equipment maintenance and repairs. Consolidation of information about the state of equipment in a single control system and the ability to provide it to various consumers in the field allows you to reduce downtime for repairs, reduce the cost of spare parts and materials, optimize logistics and workload [2].

The state of power grids in Russia is approaching a critical degree of wear and tear. The reserve of efficiency and strength of energy systems is practically exhausted. To date, approximately 60-70% of the fixed assets of the power grid complex have long been used up. In the context of a sharp increase in the volume of energy consumption, dispatching offices do not always cope with emerging situations, which leads to corresponding consequences and losses for energy companies.

Modern loads on the power system require a quick and most accurate analysis of the state of the operating system to localize problems, or prevent them by predicting loads on individual segments of the system. In this regard, energy grids are increasingly demanding augmentation with new digital intelligent solutions that can help fulfill the tasks of collecting and analyzing large amounts of data.

Another challenge that smart grids can solve is the integration of power plants based on renewable energy sources. One of its key steps in the fight against climate change is the decarbonization of energy.

An effective way towards decarbonization is the development of green energy, that is, solar, wind and hydroelectric power plants. However, the generation of electricity by these stations is very dependent on weather conditions, and taking into account the fact that the number of such stations is measured in hundreds and thousands, only a computer using Smart Grid data and automation will be able to cope with such a volume of information. The computer will be able to quickly respond to almost any change or deviation and provide uninterrupted power supply to consumers of electricity [3].

Key features and benefits of Smart Grid:

1) Leads to lower costs
2) Easy management of changes in production and consumption.
3) By sending information in real time and managing the network remotely, the risk of power outages and incidents is reduced.
4) All different energy sources can be integrated into the grid, Smart grid will eliminate the need for thermal power plants and allow more widespread use of renewable energy sources

MICROGRID

Microgrid is a local power system, which implies the creation of its own power grid structures in a certain territory, capable of operating autonomously. This system has its own sources of energy generation, and will take on the challenge of meeting consumer demand at the maximum peak.

Microgrids are basically no different from large power grids; they generate and deliver electricity to consumers on their own, only they do it locally. The main difference of Microgrid is that it is installed in remote places where it is impossible to enter large power grids.

The advantage of Microgrid is that in the event of an emergency, the Smart system will automatically switch between energy sources and continue to operate due to its own energy generation. Microgrid uses distributed generation from solar panels and wind turbines as an energy source, as well as energy stored in high-capacity batteries. Distributed generation ensures that in the event of a failure of one or even more power sources, the system will continue to function stably due to its distributed architecture. [4]

POWER SUPPLY FAULTS

Over the past 50 years, electrical grids have not kept pace with today's challenges. Today, the power grid has some structural defects such as:

1) High demand for uninterrupted power supply, which cannot be satisfied.
2) Digital controlled devices that can change the nature of the electrical load and result in electricity consumption are incompatible with the power system.
3) Security threats posed by energy suppliers.
4) Intermittent supply of alternative energy sources makes it much more difficult to maintain stable power.

Most of the outages are due to the slow response of devices on the network. Production always exceeds demand. The main goal of manufacturers is to minimize the negative impact on the power grid and maximize consumer savings Lack of investment in infrastructure and the growing demand for high-quality digital-level electricity have pushed the electrical infrastructure to the limit [5].

The existing system is outdated and makes it difficult to integrate new technologies. This led to problems with the reliability of electricity and huge losses for the industry.

INDUSTRIAL POINT OF VIEW

The smart grid is designed to integrate advanced grid technologies into electrical grids to make them smarter. The design and implementation of a new communications infrastructure for the network are two important research areas. It is expected that smart grid will affect all areas of the current grid system, from generation to transmission and distribution.

Utilities are wary of using untested technology in critical infrastructure. But the Smart Grid will be able to solve a large number of existing problems.

A smart grid will be able to:

1) Provide better quality electricity which will save money.
2) Provide more bandwidth, which will reduce energy costs.
3) Provide wider penetration of sources of intermittent power generation.
4) Protect against cyber threats.
5) React instantly to systemic problems to avoid power outages

For all this, manufacturers have developed smart mechanisms and energy consumption tactics, which include: smart meters, dynamic pricing, smart thermostats, etc. [6].

RENEWABLE ENERGY SOURCES

The share of renewable energy production in the global demand for electricity is constantly increasing. The most commonly used renewable energy sources are water energy, solar energy and wind energy. Thanks to the use of smart grids, the benefits of renewable energy sources are significantly increased due to the fact that they are integrated into the power supply system at a higher level.

WATER ENERGY

Hydropower is widely used all over the world. Hydroelectric power plants are usually classified according to their capacity, such as large scale, small and micro hydropower systems. Generation methods also differ depending on the availability of water sources and the required capacity, which include conventional water dams, pumped storage technology and runoff from river power plants.

Hydropower is based on the gravitational force of moving water. The potential energy of the falling water is converted into mechanical energy by Hydel turbines, which drive alternators to generate electricity. Hydel power plants operate at high efficiency due to lower energy losses during the conversion process. [7].

SOLAR ENERGY

Solar energy can be harnessed through thermal electricity, solar photovoltaics (PV), which is classified based on the mechanism of capturing solar radiation and converting it into electrical energy.

The advantages of this type of energy are that there is no geographic limitation, flexible scale and inexhaustibility, but there are also significant disadvantages - the high cost of installing photovoltaic installations, power losses in the switching mechanisms of the converter, and researchers constantly turn to these problems in order to overcome them [7].

WIND ENERGY

Wind energy is considered one of the most used because of its renewability and environmental friendliness. Despite the lack of harmful effects and affordable price, there are also certain disadvantages such as uncertainty of availability, uncontrolled power output, etc. Due to its randomness and stochastic behavior, probability-based modeling techniques and their optimal distribution are required.

Kinetic energy is generated by a wind turbine connected to the rotor blades. Then the energy is converted into mechanical energy. And only, passing through the generator for conversion, it is converted into electrical one. The power available from a wind turbine at a specific location usually depends on the wind speed, tower height, and turbine speed characteristics [7].

PROBLEMS OF INTEGRATION OF RENEWABLE ENERGY SOURCES INTO ELECRICAL NETWORKS

There are two different categories of problems in the integration of renewable energy in SGs:

1) Technical problems
2) Problems of an economic, political and regulatory nature [8].

TECHNICAL PROBLEMS

With a higher penetration of RE generation, two dominant technical problems can be distinguished:

1) managing variability and uncertainty during the continuous balancing of the system. Because Variable RES sources are more uncertain and more variable than traditional generators.

2) balancing supply and demand in situations of shortage and excess of generation: the need of system operators to balance supply and demand in situations of high renewable energy production and low demand or low renewable energy production and high demand. Problems associated with high peak loads during periods of low renewable energy production variable selected to compensate for spare capacity or demand response actions [8].

ECONOMIC, POLITICAL AND REGULATORY ISSUES

In addition to technical problems, institutional problems also arise with the increase in the proportion of RE variables. In a broad sense, they refer to the unique economics of RE variables that pose a variety of policy and regulatory challenges. Two specific problems are identified here:

1. Capital-intensive network upgrades

Grid upgrades may be required to harness wind and solar power. Minimizing the cost of upgrades while ensuring system reliability results in a greater return on investment in renewable energy [8].

2. Uncertain project costs and cash flows [8].

Smart grid solutions are associated with two specific problems that have historically negatively impacted the economics of RES projects: the costs of grid modernization shared among the developers of RES projects, and the reduction in energy consumption when the full production of RES cannot be easily integrated into the grid. the project is even more at odds with expectations.

As upgrades become costly or downsizing increases, the investment landscape for RE variables becomes more uncertain and may slow down overall rollout.

Where policies and subsidies shield project investors from these risks - for example, to further improve the investment environment for renewables - the costs and risks can be socialized. Investment in smart grids can also play an important role in reducing these costs and risks.

ENERGY STORAGE

Balancing volatile renewable loads through management strategies is the primary challenge for smart grids. The “balancing action” of the SG can be simplified by conserving less energy on the grid. It is worth noting that in a real SG scheme, all design parameters must be taken into account, ranging from the supply and demand procedures of buildings to the dynamic load of power lines depending on wind speed and temperature [9].

There is a significant difference between power storage and energy storage, and it is strategic in many applications. The use of energy storage is part of demand management, while energy storage is involved in feedback speed, frequency control and rotation reserve. Some engineering applications use energy storage technologies such as compressed air, batteries, hydraulic accumulators, supercapacitors, and flywheels. [10].

Electronic springs have been developed that have been shown to be effective in reducing greenhouse gas emissions through the significant participation of renewable energy sources, contributing to the harmonization of electricity demand and supply [11].

A predictive control method by Torres and Bordons was developed for microgrids based on renewable sources, supplemented by a hybrid energy storage system [12]. The goals of the optimization method were to minimize the dire conditions that occur in each storage system, in addition to maximizing economic profit while taking into account multiple system constraints.

Lisana and others have proposed a comprehensive and innovative view of predictable and flexible energy management in a building, taking into account the use of smart grids, optimal expected utilization, financial and environmental state of affairs, smart regulation and the use of high-density latent heat storage [13].

MODELING

AVERAGE MODEL OF GRID-CONNECTED PHOTOVOLTAIC ARRAY

Consider the example of an average model of grid-connected photovoltaic array. Photovoltaic (grid) array with a power of 100 kW, connected to a 25 kV network through a DC-to-DC step-up converter and a three-phase three-level VSC.

This model contains the following main components:

1) Photovoltaic array, which provides a maximum power of 100 kW under solar illumination of 100 W / m^2.
2) DC / DC boost converter (orange blocks)
3) 3-level 3-phase VSC (blue blocks).
4) Three-phase communication transformer 100 kVA, 260 V / 25 kV.
5) Utility network

A 100 kW photovoltaic battery consists of 66 chains of 5 series-connected 305.2 W modules connected in parallel: Manufacturer specifications per module:

$$66 \cdot 5 \cdot 305.2W = 100,7kW$$

1) Number of cells connected in series: 96
2) Open circuit voltage: Voc = 64.2 V
3) Short-circuit current: Isc = 5.96 A
4) Voltage and current at maximum power: Vmp = 54.7 V, Imp = 5.58 A

The PV array unit has two inputs that allow changing solar radiation (input 1 in W / m ^ 2) and temperature (input 2 ° C). The illumination and temperature profiles are determined by the Signal Builder block, which is connected to the PV array inputs.

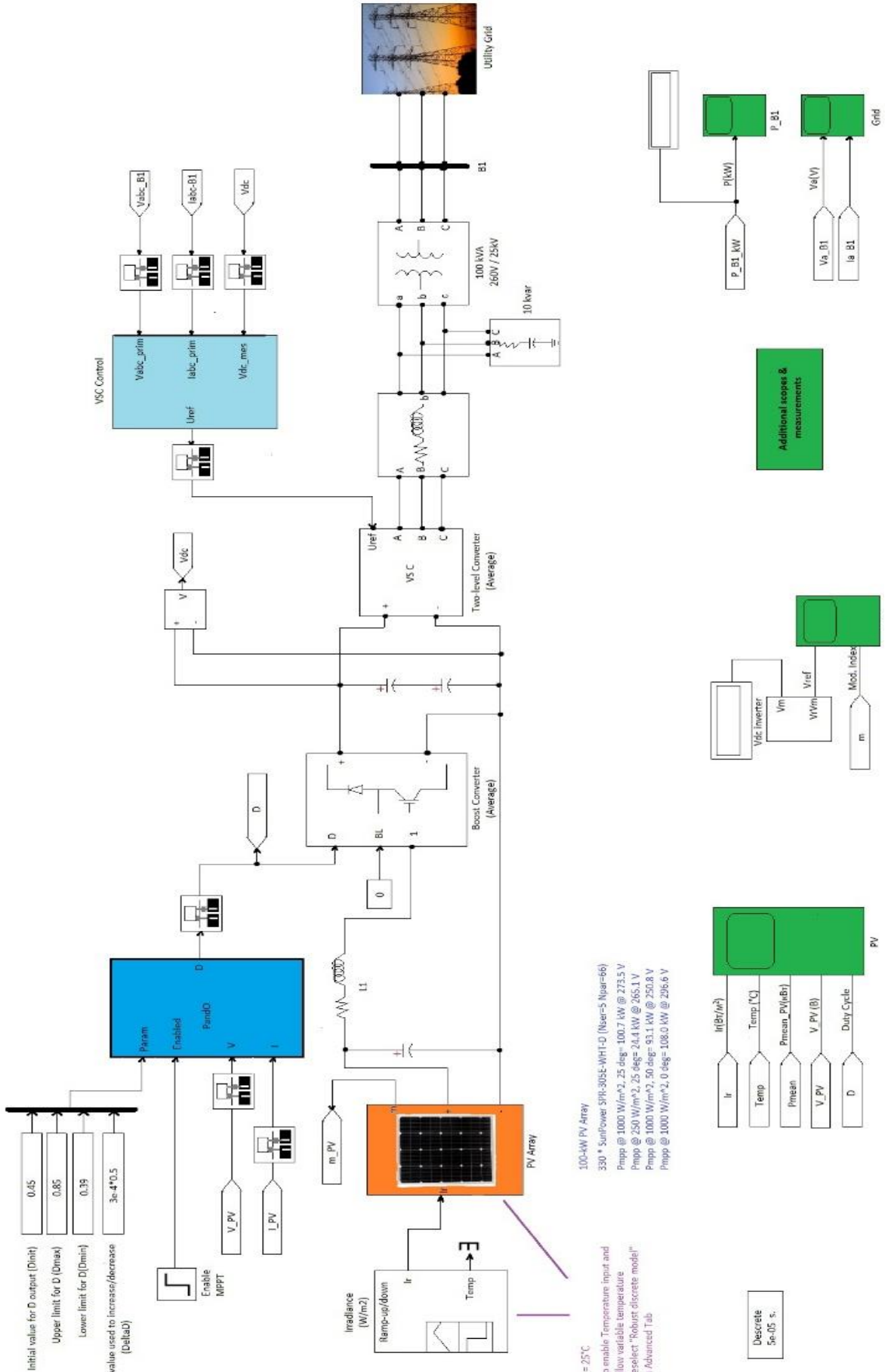

Fig. 1 - On-grid photovoltaic grid with a capacity of 100 kW

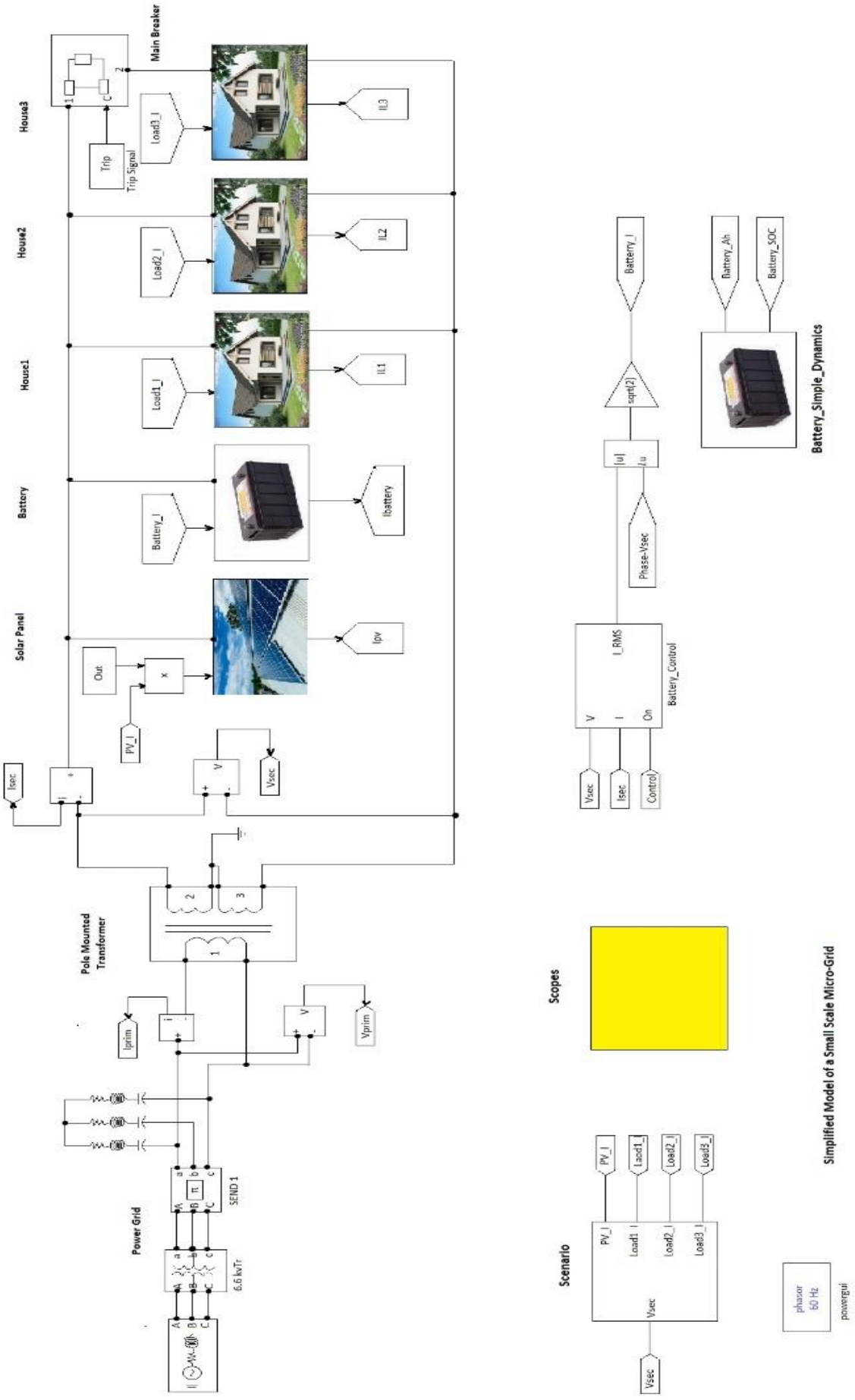

Fig. 2 - Simplified model of a small-scale microgrid

Simulation starts with standard test conditions: (25 ° C, 1000 W / m^2):

From t = 0 seconds to t = 0.3 seconds, the duty cycle of the boost converter is fixed (D = 0.5 as shown in the photovoltaic panel). The resulting PV voltage is:

$$V = (1 - D) \cdot V_{dc} = (1 - 0.5) \cdot 500 = 250V$$

The output power of the photovoltaic array is 96 kW, then the indicated maximum power at an illumination of 1000 W / m^2 is 100.7 kW.

At t = 0.3 seconds MPPT is on. This regulator begins to regulate the voltage of the photovoltaic panel, varying the duty cycle to extract maximum power. The maximum power (100.7 kW) is achieved with a duty cycle of D = 0.453.

From t = 0.3 seconds to t = 0.5 seconds, the PV array operates under standard test conditions (25 ° C, 1000 W / m^2). Duty cycle D ranges from 0.450 to 0.459. PV module voltage = 273.5 V

$$N_{ser} \cdot V_{mp} = 5 \cdot 54.7 = 273.5V$$

and average power = 100.7 kW.

From t = 0.5 seconds to t = 1 second, the brightness of solar radiation decreases from 1000 W / m ^ 2 to 250 W / m^2. The MPPT controller type monitors the maximum power only under constant illumination.

From t = 1 second to t = 1.5 seconds, when the irradiance remains constant at 250 W / m^2, the duty cycle D varies from 0.466 to 0.474. The corresponding photovoltaic voltage and power are V_PV = 265 V and Pmean = 24.4 kW.

From t = 1.5 seconds to t = 6 seconds, solar radiation is restored to 1000 W / m^2, and then the temperature changes from 0 ° C to 50 ° C. The maximum PV output power (107.5 kW) is achieved at minimum temperature (0 ° C).

SIMPLIFIED MODEL OF A SMALL-SCALE MICROGRID

This example shows a simplified small-scale microgrid model running for 24 hours.

Microgrid is a single-phase AC network. The energy source is the electrical grid, solar power generation system and battery.

The battery pack is controlled by the battery controller. This battery absorbs excess power when there is excess energy in the microgrid and provides additional power if there is not enough power in the microgrid. Three ordinary houses consume energy, maximum 2.5 kW.

The microarray is connected to the power grid through a transformer installed on the rack, which reduces the voltage from 6.6 kV to 200 V.

Solar energy and battery are DC power sources that are converted to single phase AC. The management assumes that the microarray is not entirely dependent on the power supplied from the grid and the power supplied from the production and storage of solar energy.

The battery provides insufficient current when the power of the microgrid is insufficient and absorbs excess current from the microgrid when its power exceeds the electrical load.

When there is a lack of power in the microgrid, the system provides insufficient power. When there is excess power in the microgrid, that power is returned to the power system.

CONCLUSION

There are obstacles to the implementation of smart energy in Russia, primarily the complexity of the system itself. A delicate approach to the requirements and needs of the consumer is required, which forces to take into account the individual characteristics of all elements of the network. At the same time, implementation is complicated by the lack of uniform standards and norms that have not yet taken shape. The process is also not facilitated by the large number of regulators and procedures required to obtain certificates and permits. Technical problems still remain unresolved, such as the lack of affordable reliable and efficient energy storage devices or the security and protection of private information transmitted within the network.

A significant result of the introduction of smart energy technologies will be an overall reduction in the fuel costs of power plants. The transition to an innovative development option will be accompanied by a significant decrease in the number of commissioned power plants, as well as the network facilities dependent on them for generating capacity. The introduction of intelligent power supply networks can significantly reduce capital costs and maintenance costs, as well as extend the life of equipment due to the efficient use of the equipment resource.

At the moment, the main direction of global energy development is the transition to the widespread use of renewable energy sources (RES). This is especially important in the face of climate change, low air quality, especially in large cities with local air pollution.

REFERENCES

1. Powerelectronicsnews: The Smart Grid: What's "the grid" and how is it "smart?" URL: https://www.powerelectronicsnews.com/the-smart-grid-whats-the-grid-and-how-is-it-smart/ (accessed 12.12.2020)

2. Tadviser: Smart Grid, URL: https://clck.ru/S264K (accessed 12.12.2020)

3. Nv: Что такое Smart Grid? URL: https://nv.ua/ukraine/so-skorostyu-sveta/chto-takoe-smart-grid-50055452.html (accessed 12.12.2020)

4. neosun: Что такое микрогрид URL: https://neosun.com/ru/chto-takoe-mikrogrid/ (accessed 12.12.2020)

5. Guillaume Guérard, Soufian Ben Amor and Alain Bui, "Survey on smart grid modelling", in Int. J. Systems, Control and Communications, Vol. 4, No. 4, 2012

6. Gao, J., Xiao, Y., Liu, J., Liang, W. and Chen, C.L. (2012) 'A survey of communication/networking in smart grids', Future Generation Computer Systems, Vol. 28, No. 2, pp.391–404.

7. Researchgate: INTEGRATION OF RENEWABLE ENERGY SOURCES IN SMART GRID: A REVIEW, URL: https://www.researchgate.net/publication/315669268_INTEGRATION_OF_RENEWABLE_ENERGY_SOURCES_IN_SMART_GRID_A_REVIEW (accessed 12.12.2020)

8. NREL:The Role of Smart Grid in Integrating Renewable Energy, URL:https://www.nrel.gov/docs/fy15osti/63919.pdf (accessed 12.12.2020)

9. Roberts, B.P.; Sandberg, C. The role of energy storage in development of smart grids. Proc. IEEE 2011, 99, 1139–1144.

10.Bjelovuk, G.; Nourai, A. Community Energy Storage (CES) and the Smart Grid. Presented at the ESA Presentation, May 2009. Available online: www.aeptechcentral.com/ces.

11.Lee, C.K.; Hui, S.Y.R. Reduction of energy storage requirements in future smart grid using electric springs. IEEE Trans. Smart Grid 2013, 4, 1282–1288.

12.Garcia-Torres, F.; Bordons, C. Optimal Economical Schedule of Hydrogen-Based Microgrids with Hybrid Storage Using Model Predictive Control. IEEE Trans. Ind. Electron. 2015, 62, 5195–5207.

13.Lizana, J.; Friedrich, D.; Renaldi, R.; Chacartegui, R. Energy flexible building through smart demand-side management and latent heat storage. Appl. Energy 2018, 230, 471–485.

DEVELOPMENT OF A FAULT TOLERANCE COMPLEX FOR ADDITIVE EQUIPMENT AS AN ELEMENT OF AN INFORMATION SYSTEM

Maria Rassykhaeva

Saint-Petersburg State University of Aerospace Instrumentation,
Saint-Petersburg, Russia
E-mail: mitschiru@gmail.com

Annotation
Information systems, being an integral part of modern technical systems, are complex hardware and software complexes. Many of them, as part of automated control systems (CS), carry out the function of controlling technological processes in real time. Structural and functional reliability and safety of IS have a decisive influence on the efficiency of functioning of automated control systems. Hence, it is obvious that for the stable and error-free operation of the CS it is necessary to ensure the reliability of information systems. The tasks of building reliable information systems are complex - they cover both structural and functional reliability. Structural reliability is the reliability of objects (elements, systems). Thus, functional reliability means the reliability of the provision of services: execution of processes, processing, transmission, collection of information, management of subordinate objects. Only a combination of ways to improve both one and the other components of reliability gives a tangible effect. This effect can be expressed in a significant increase in the reliability of the system and at the same time in saving the amount of additional resources, one of such systems is the additive installation figure 1.

Fault tolerance systems (FSS) are an integral part of information systems (IS) and are formed during their design from the provided redundant hardware and software. All systems for providing fault tolerance (FSS) IS for the organization of the architecture of these systems can be divided into the following three groups:

- closed type;
- open type;
- mixed type.

Figure 1. An example of an additive

To a certain extent, the disadvantages inherent in closed and open COOs are eliminated in a mixed COO. The state graph of these systems is shown in Fig. 2. In state 0, the information system is in preparation for operation. Malfunctions are prevented by creating comfortable operation of hardware and programs, and preliminary localization of malfunctions is carried out by solving control problems, monitoring the functioning of the IC, diagnostic testing of programs and equipment.

Figure 2 graph of ensuring fault tolerance in the production process.

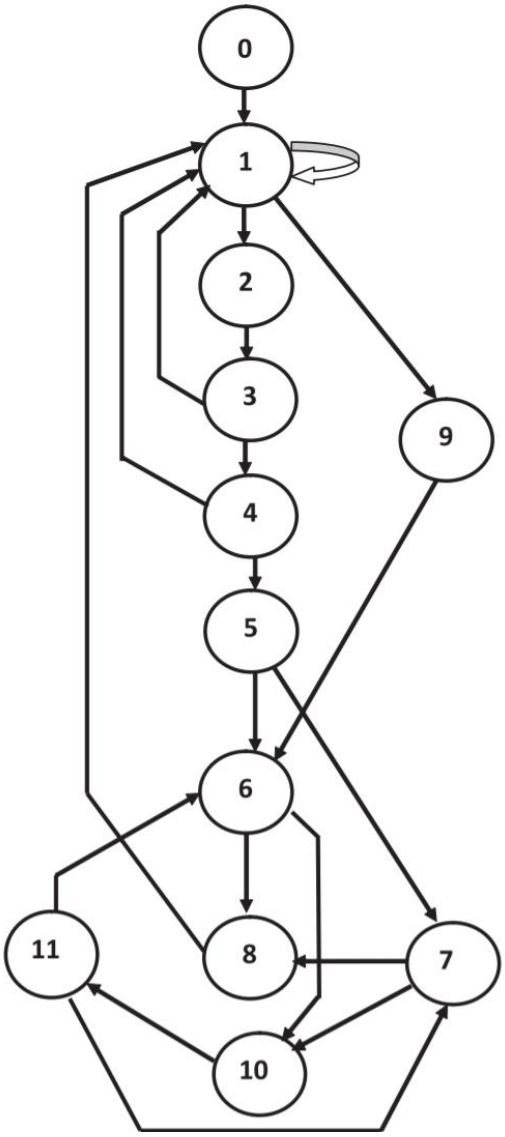

Figure 2. Count states of the information system's resilience system:
0 - preparation mode for IS operation; 1 - the state of normal functioning, fault-tolerant operation of the IS;2 - detection of the fact of a malfunction;3 - localization of the detected malfunction;4 - identification of failures or failures, failure analysis;5 - detection of the location of the failed element;6 - IS reconfiguration using redundant modules;7 - IS reconfiguration based on gradual degradation of the system;8 - complete restoration of the computing process;9 - masking of faults;10 - repair status of a failed system element;11 - reintegration of the repaired system element

Fault tolerance of IS in additive manufacturing is important when printing a part due to possible failure and shape changes.

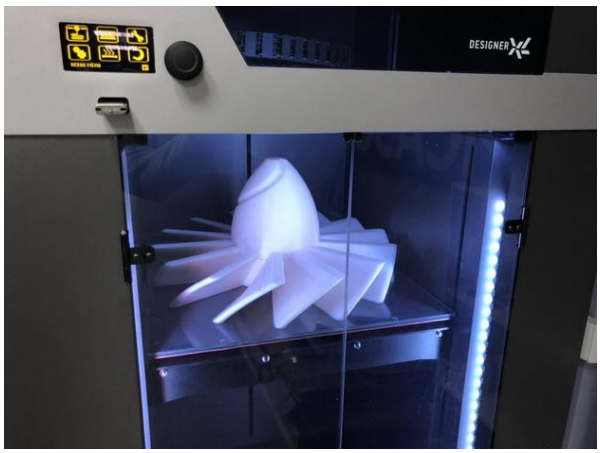

Figure 3. Printing the product on additive installation

With any reconfiguration option, there will be a transition to the 8 state of complete restoration of the computing process with a further transition 8-1, followed by a transition to state 10: repair of the failed module. Reintegration of a repaired module (or replaced with a serviceable one) is performed with priority of system state 7 over state 6. This fault tolerance system is the basis for building an adaptive fault tolerance (active protection) system.

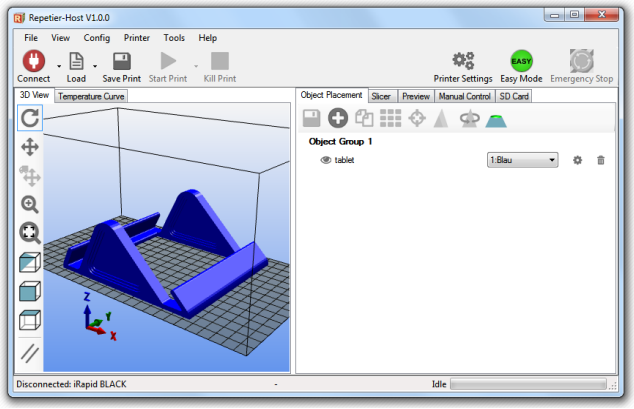

Figure 4. Layered fusion information system window

The use of additional funds that are redundant in relation to the minimum necessary funds to perform the provided functions applicable to ensure the reliability of an object is understood as redundancy.

Structural redundancy in information systems is created using additional hardware.

- there are fundamental differences between the content of safety and reliability of systems - if unreliability leads to unacceptable levels of availability, technical use, reliability and cost of maintenance, then insufficient safety leads to accidents and loss of life;

- there are contradictions between the goals of ensuring the reliability and functional safety of systems, the elimination of which is possible on the basis of a compromise; the requirements for reliability and functional safety must be balanced among themselves;

- in facilities posing an increased hazard, in potentially hazardous and critical systems, priorities are given to safety tasks, and the required reliability levels should be set considering cost constraints after meeting safety requirements.

Structural redundancy is classified according to the following criteria:

• by the degree of coverage of the object and its constituent elements by the reserve. On this basis, a distinction is made between general and separate redundancy. General Reservation: Reservation in which the object as a whole is reserved. Split reservation: reservation in which individual elements of an object or their groups are backed up.

• according to the purpose of the elements of the object in performing the required function. On this basis, the main and backup elements are distinguished. Basic element: an element of an object necessary to perform the required functions without using 96 Reliable fault-tolerant information systems of the reserve. Back-up

element: an element designed to perform the functions of a main element in the event of a failure or replacement.

• by the degree of attraction of the elements of the object to perform the required function. On this basis, they are distinguished: -reservation by replacement,

-reservation m of n,

-mixed reservation,

-permanent reservation,

- majority reservation.

• by the uniformity of the characteristics of the reliability of the elements of the object. On this basis, the same and different types of elements of the object are distinguished. Completely similar objects with identical hardware and software and identical reliability characteristics have become widespread.

• according to the degree of maintainability, recoverable and non-recoverable redundant objects are distinguished. We are talking about the possibility of restoration in the process of functioning of the object. It is usually believed that redundancy with restoration is a redundancy in which the restoration of failed main or backup elements of an object is technically possible without disrupting its operability and is provided for by the operational documentation. If recovery in stationary information systems is possible, then the efficiency of redundancy increases dramatically.

Conclusion

Reducing the frequency of dangerous failures is also possible as a result of building an effective system for protecting the communication channel with additive equipment. However, the costs of increasing the efficiency of communication with the installation are far from always commensurate with the damage from dangerous failures that can lead to equipment breakdown.

The list of literature used:

1. Ensuring the quality of additive production through the layer synthesis control system / A.V. Chabanenko, E.G. Semenov, V.O. Smirnov, A.O. Smirnov, N.N. Rozhkov // Radio electronics issues. 2018. №10. S. 75-79.

2. Management of the quality of additive products / A.V. Chabanenko // RIA: Magazine.: "Standards and quality." 2018. №2. S. 90-94.

3. Procedures of conversion of the 3D model into the executable stl file for layered synthesis Chabanenko A.V., Kurlov V.V. In the collection: MODELING AND SITUATIONAL MANAGEMENT FOR THE FORECAST SYSTEM. A collection of reports from the First All-Russian Scientific Conference. St. Petersburg, 2020. S. 190-192.

4. Managing the quality of 3D printing by modeling the component base of the additive installation Chabanenko A.V. In the collection: Selected scientific works of the eighteenth International Scientific and Practical Conference "Quality Management." THE WORLD WORK 18th International Scientific and Practical Conference. 2019. S. 362-368.

5. Creation of hull elements of the rea at the installation of layered synthesis of materials within the framework of the project work of students of GUAP Chabanenko A.V. In the collection: XXIII International Bios Forum and Youth Bios-Olympics 2018. Proceedings. 2019. s. 133-137.

AUTOMATIC SPEECH RECOGNITION WITH SPEAKER DIARIZATION AND NAMED ENTITY DETECTION

Nikolay Reutov

Saint-Petersburg State University of Aerospace Instrumentation, Saint-Petersburg, Russia
E-mail: nicolre239@gmail.com

Introduction

The widespread use of audio and video communication technologies opens opportunities for automating business processes. The use of modern technologies in the field of business has become even more relevant recently, because of pandemic and the mass transition of company employees to remote work.

In this paper, we review a software system designed for automatic logging of meetings. This system, based on the audio recording of the meeting, creates a summary of it, highlighting the main theses and main information (dates, decisions taken, assigning tasks to employees, etc.).

System fundamentals

The operation of the system consists of several stages:

1) Collecting information
2) Speech diarization
3) Speech recognition
4) Named entities recognition in produced text
5) Results representation

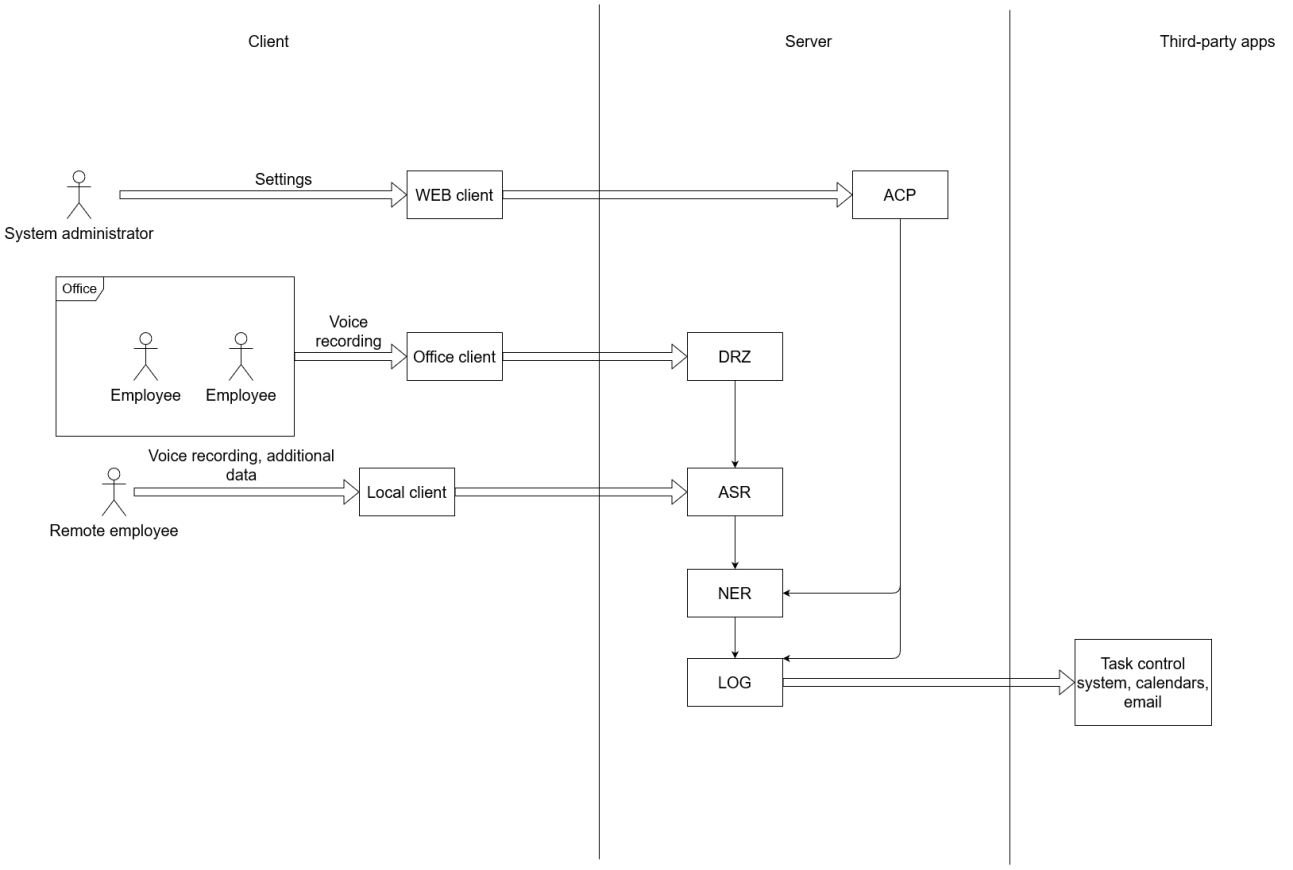

Figure 1– software system scheme

Below we will discuss each stage in more detail.

The meeting can be attended by several employees who are present in the same office, as well as employees who connect remotely. At the stage of collecting information, the client part of the software system makes an audio recording of the meeting, using the microphones of the participants. For participants who connect remotely, the resulting recording represents the speech of each employee individually and, therefore, does not need to be diarized. The recordings received at the office are a compilation of the voices of several participants, and for such recordings, speech recognition stage is preceded by diarization. Also, using client part of system, users provide information about the number and composition of participants (last names, initials, positions, etc.).

After receiving the records, additional information is attached to them, for example, the need for diarization is noted, information about the participants is added. After that, the records are sent to the server for further processing.

This stage also includes configuring the system using the administrator panel (the ACP – Administrator Control Panel module in Figure 1). By setting up the system, we mean specifying the entities that the system needs to highlight in the recognized text, the duration of data storage on the server, methods for results representation, and so on.

The diarization task consists in the division of the input audio stream into segments, according to the personality of the speaker. So, the program should divide the input single audio track into several segments equal to the number of people speaking on the audio recording, according to their voices.

The diarization problem is complex. For example, it includes tasks such as:

- Voice activity recognition
- Voice pattern recognition
- Number of speakers definition
- Voice overlap handling

It is important to note, that in the system, diarization is performed only for audio recordings, that were marked as multi-voice at the previous stage. To simplify the task, the user provides information about the number of speakers on the record via the client. The detection of voice activity in this software system is not necessary, since diarization is performed for the complete audio recording. Thus, the diarization task in this system consists of two subtasks: the recognition of voice patterns and voice overlap handling.

Voice pattern recognition is an extremely important task, which consists in determining the speech characteristics of each of the speakers on the audio recording and then using these features to assign sections of the audio recording with the participation of the same speaker to the same segment.

Voice overlap handling – is the task of selecting one or more voice tracks from an audio recording and determining the speaker for each of them in the case of simultaneous sounding of several voices.

An important point is the fact that for a multi-voice audio recording, diarization is performed before speech recognition (the DRZ and ASR modules in Figure 1, respectively). This approach allows to perform speech recognition based on the context of different speakers, which improves the quality of recognition. An example of contextual recognition is shown in Figure 2 below.

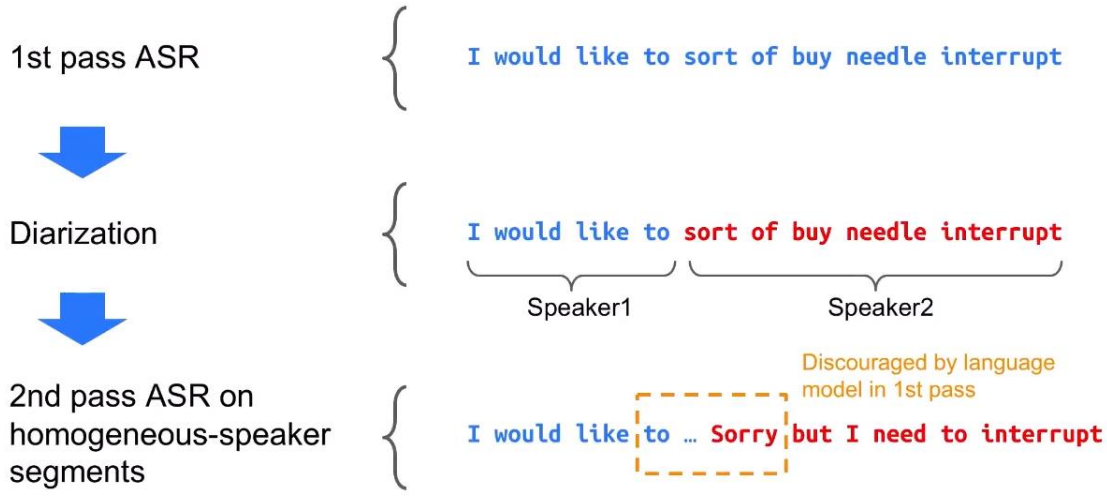

Figure 2 – automatic speech recognition improvement, using speaker change context

Automatic speech recognition task (ASR) in this case consists in determining the text, that sounds on each of the audio recordings, comparing the audio recording with the speaker, arranging all the recognized segments by time and generating a general transcript of the meeting from them. At this stage, to improve the quality of recognition, it is also necessary to use a language model trained on the transcripts of meetings. Using such model will help to identify the typical and most common phrases, which will allow to conduct contextual analysis of speech during its recognition.

Named Entity Recognition task (NER) consists in searching of objects in unstructured text and classifying them into predefined categories. In the case of this software system, the NER task is required to analyze the meeting text. For example, to highlight dates, employee names, assign tasks, and so on, Entity recognition occurs according to the settings set in the ACP by the administrator responsible for the meeting.

Results representation is a process of transferring of the final information about the meeting to its participants (LOG module in Figure 1). This task can be solved by sending emails, making appointments via Google Calendar or Outlook, or creating tasks in JIRA. These actions are performed automatically, based on the meeting information received from the NER, and based on the settings set via the ACP.

System implementation

When developing a system, you should pay attention to the fact that, despite using the same conceptual scheme, the implementation will differ depending on the language for which the system is being created. Since each language has a large number of phonetic and linguistic features, and even several dialects of the same language can differ extremely much, some models and approaches show better results for some languages than for others. Therefore, when developing the system, it is necessary to pay close attention to the choice of optimal language models, speech recognition models, and diarization models.

The easiest way to implement is to build system, working with English language, because of its relative linguistic and phonetic simplicity, as well as the large number of studies on these topic, conducted by American scientists. As a result of these factors, there is a wide range of models for these task that show impressive results. For example, in Shafev et al. [1] recurrent neural networks are used to solve the problem of diarization and speech recognition. Moreover, these tasks are solved together, which allows to improve the quality of recognition. However, using this approach to implement a system, working with russian speech does not guarantee even a repeat of success, neither improvement of result, due to the difference in the structure of the languages.

In addition to the problem with language differences, there is also a problem with training models for any languages other than English. The problem is that training neural networks requires training samples of very large volumes [2]. In this case, the situation is complicated by the fact that the training sample is "marked data" - not just a set of audio recordings, but also additional information about them: strict transcripts of sounding phrases, labels for changing the speaker, etc. At the same time, the minimum size of the training sample is about 800 hours of audio material.

In the case of English, training samples are available in the public domain in a fairly large amount. For the Russian language, of course, there are also training samples provided, for example, by the VoxForge or Mozilla Common Voice projects, but their volumes are clearly not enough for training (about 20 hours). That is why, in this case the work on generating training samples was done before training DeepSpeech neural network [3].

DeepSpeech neural network training

Since the training sample represents a huge amount of data, an automatic system was created to generate it. This system used the autosubtitering system of the YouTube service, audiobooks and their original text. With the help of this system, about 500 hours of training material were created.

After generating the training sample, a language model was also created. To generate it, the KenLM utility was used [4]. The language model was generated on a corpus of 2.6 billion phrases obtained by processing more than 80 thousand books. From this corpus, the utility allocated 500 thousand of the most common words, and then created a language model on 5-grams.

After generating the training sample and the language model, the neural network was trained. To evaluate the final result, the WER (Word Error Rating) metric was used, calculated using the following formula:

$$WER = \frac{I + D + S}{N} \quad (1)$$

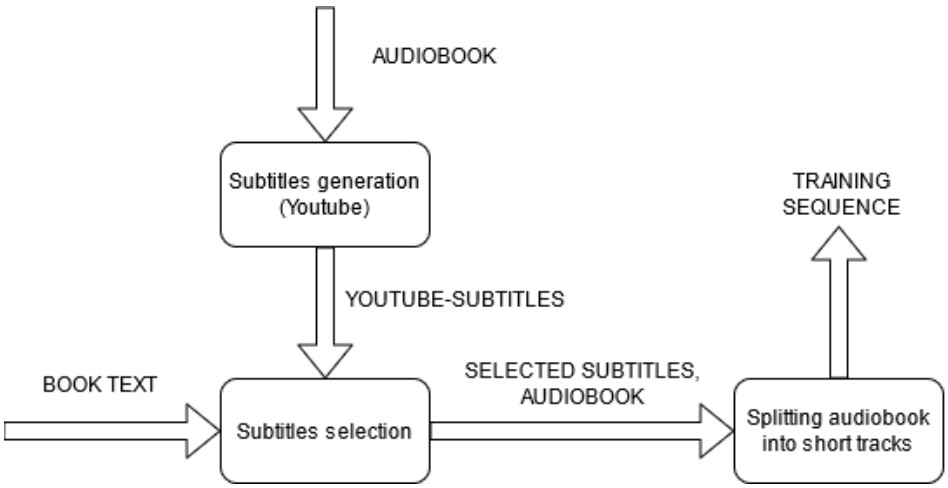

Figure 3 – training set generation scheme

Here ***I*** is the number of words added to the string, ***D*** is the number of words removed from the source string, ***S*** is the number of words replaced, and ***N*** is the number of words in the source string.

It should be noted that metric depends on the set on which the testing is performed, so the testing was made on three sets:

- nativetest – a test set, generated from the same dataset as the training sample, according to the principles described by Ng et al. in the article [5].
- cleantest – a test set, generated from the VoxForge project dataset. It is characterized by high purity and quality of recording. Approximate duration – 20 hours.
- noisytest – a test set, generated from the Common Voice project dataset. It is characterized by low purity of the recording, a large number of artifacts, and unclear diction of the speakers. Approximate duration- 20 hours.

After training and testing the neural network, the following results were obtained:

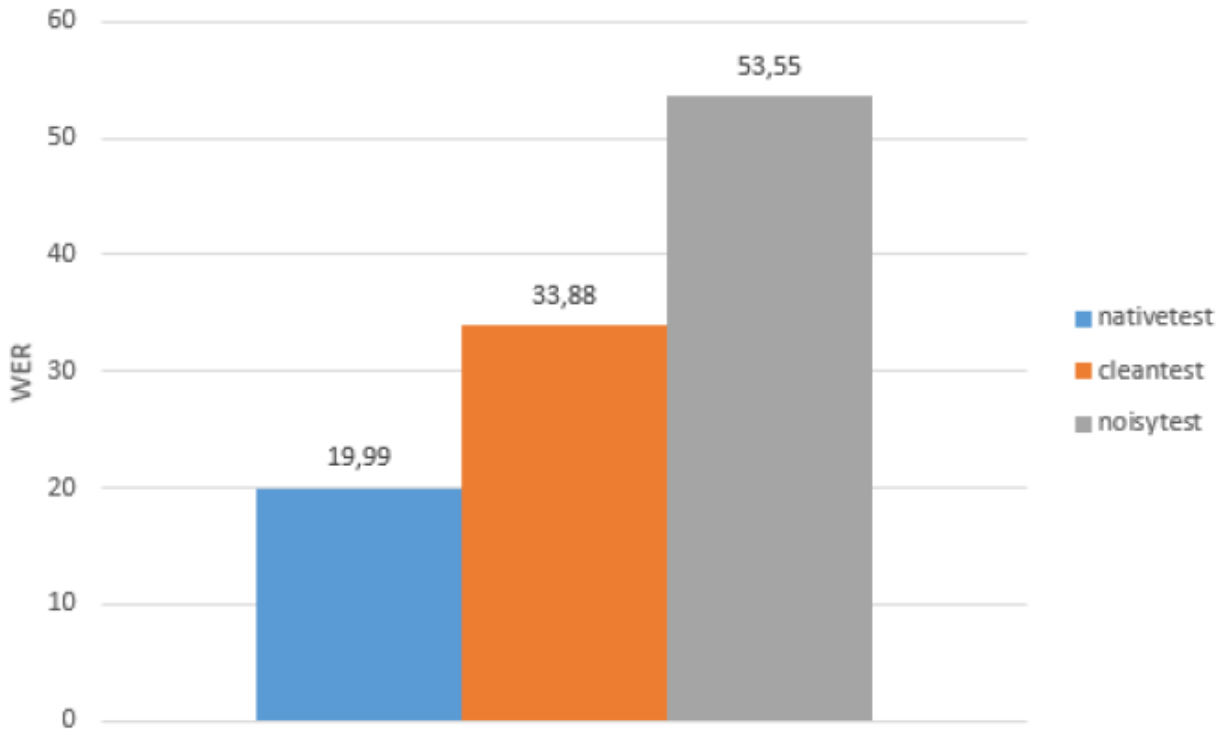

Figure 4 – WER metric for three test sets

The relatively high error rate is explained by the following disadvantages of the training sample:

1) Excessive “purity” of the training sample. Since audiobooks were used to generate the training sample, there is an extremely small amount of noise on these recordings. Also, the people who record them, are professional speakers, which means that these audio recordings have high clarity of diction. This disadvantage is especially noticeable when testing on the noisytest set – the error rate increases dramatically due to poor recording conditions.

2) Insufficient voice diversity. The sample was created by splitting audiobooks into short segments. At the same time, the number of audiobooks from which the sample was created does not exceed 20. Thus, the training sample has an extremely small voice diversity, which may explain the deterioration of the result on the cleantest set.

3) Small training sample size. The recommended sample size for training this neural network is about 1000 hours.

Data augmentation technologies can be used to eliminate these problems. These technologies allow to add noise to "pure" speech, change the tempo and tone of speech [6], simulate echoes [7, 8], and so on. Actual methods for expanding audio data are described by Park et al. in the work [9].

Conclusion

To create the system, described in this article, it is necessary to carefully select models for performing the tasks of diarization, speech recognition, and named entity search. The following models will be selected for working with the Russian language:

- ASR – DeepSpeech. The approach, described by the authors of the neural network in [3], is based on the phonetic objects of the language, which greatly simplifies the training of this model for other languages. Also, there is a training sample for this model, which needs to be finalized.
- Diarization - an interesting project is “LIUM Diarization”, which combines mixed Gaussian models and i-vectors [10, 11]
- NER – NLTK library for Python [12]

References

1. Shafey L. E., Soltau H., Shafran I. Joint speech recognition and speaker diarization via sequence transduction //arXiv preprint arXiv:1907.05337. – 2019.

2. Deep Learning. Nature. 2015. № 521. P. 436–444. Doi: 10.1038/nature14539.

3. Hannun A. et al. Deep speech: Scaling up end-to-end speech recognition //arXiv preprint arXiv:1412.5567. – 2014.

4. KenLM Language Model Toolkit / K. Heafield // Kenneth Heafield Informatics Forum 4.21. 2013 URL: https://kheafield.com/code/kenlm/

5. Splitting into train, dev and test sets. Best practices to split your dataset into train, dev and test sets / A. Ng, K. Katanforoosh // CS230 Deep Learning Stanford // 2020 URL: https://cs230.stanford.edu/blog/split/:

6. Ko T. et al. Audio augmentation for speech recognition //Sixteenth Annual Conference of the International Speech Communication Association. – 2015.

7. Kim C. et al. Generation of large-scale simulated utterances in virtual rooms to train deep-neural networks for far-field speech recognition in Google Home. – 2017.

8. Ko T. et al. A study on data augmentation of reverberant speech for robust speech recognition //2017 IEEE International Conference on Acoustics, Speech and Signal Processing (ICASSP). – IEEE, 2017. – С. 5220-5224.

9. Park D. S. et al. Specaugment: A simple data augmentation method for automatic speech recognition //arXiv preprint arXiv:1904.08779. – 2019.

10. Verma P., Das P. K. i-Vectors in speech processing applications: a survey //International Journal of Speech Technology. – 2015. – Т. 18. – №. 4. – С. 529-546.

11. Rouvier M. et al. An open-source state-of-the-art toolbox for broadcast news diarization. – 2013.

12. Natural Language Toolkit - NLTK 3.5 Documentation // 2020 URL: https://www.nltk.org/

A PROPOSAL OF HOME SECURITY SYSTEM

Giuseppe Antonio Romano
Davide Pio Micciché

Kore University of Enna - Italy
giuseppeantonio.romano@unikorestudent.it
davidepio.micciche@unikorestudent.it

Abstract
This paper shows a proposal for a modular, smart home, security system. The whole system is based on a centralized core, acting as a central processing unit and different modules, or devices, connected to it.
Each module sends its data to the central unit that raises a corresponding alarm state. For the sake of this paper, three modules only were implemented: two different types of sensors and a manual key override.

INTRODUCTION

The proposed system falls in one of the most interesting topics of last years: home automation. It was designed with the proposal to minimize the work needed to install it thanks to the massive use of wireless communication between modules and the central unit. The used technology is the 802.15.4 ZIGBEE structured as in a star topology network. Section II will describe the architecture algorithms used. Section III presents the simulation of a scenario assisted by the presence of images. Section IV shows graphs and tables of the simulation results. In section V conclusions will be discussed.

THE PROPOSED APPROACH

The proposed architecture was modeled using wireless and wired technologies in combination. The wireless network n.1 is based on the 802.15.4 (ZigBee) resulting in a star type topology with three nodes (For this simulation. More modules can be connected).

- One motion sensor that detects movements in the room. Its control function reads the input values, encapsulates them in a "movim_signal" type packet which stores the data detected by the sensor and the instant in time in which those were detected, then sends them to node #3 (gateway). It is powered by a battery. It belongs to network n.1 of which is node n.1.

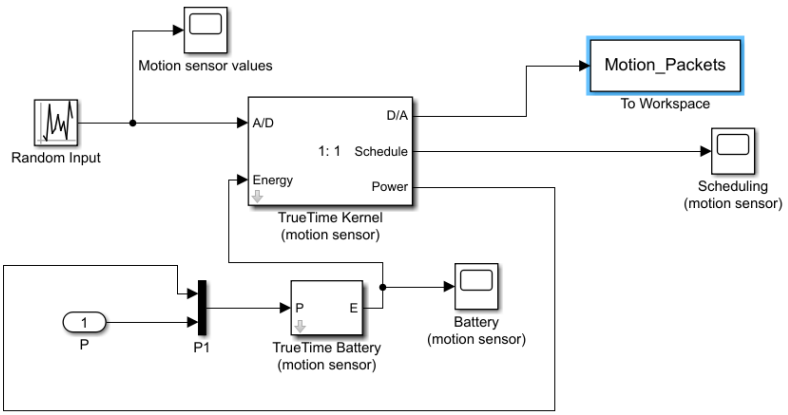

Figure 1: Motion sensor structure

- Door-opening sensor: Detects the opening of a door and stores how long it has been open. It sends the detected data to the gateway. Powered by a battery. It belongs to network n.1 of which is node #2.

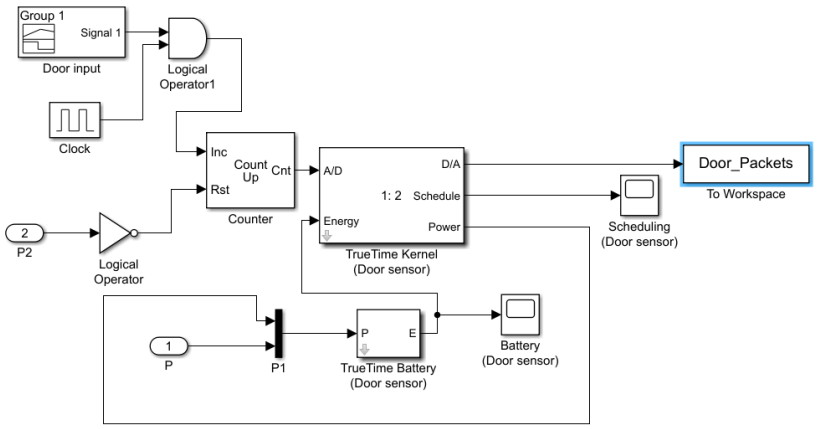

Figure 2: Door-opening sensor structure.

- Gateway: Transmits the incoming data received from network n.1 (Sensors) and sends them to network n.2 (Controller & Control unit). Battery-powered. It belongs to network n.1 of which is node #3 and to network n.2 of which is node #2.

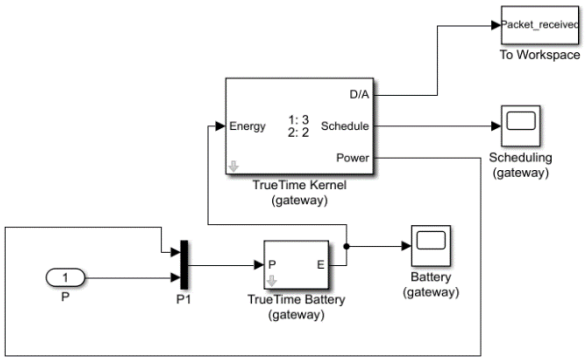

Figure 3: Gateway structure.

The wired network n.2 is based on the CMSA/CD (Ethernet) resulting in a ring topology composed of 3 nodes. (The gateway was analyzed above).

- Controller: Receives the values detected by the sensors from the gateway and processes them using a Fuzzy logic that will decree the alarm level and send it back to the controller input to allow it to be sent to the control unit. It does not need a battery to function. It belongs to network n.2 of which is node n.1.

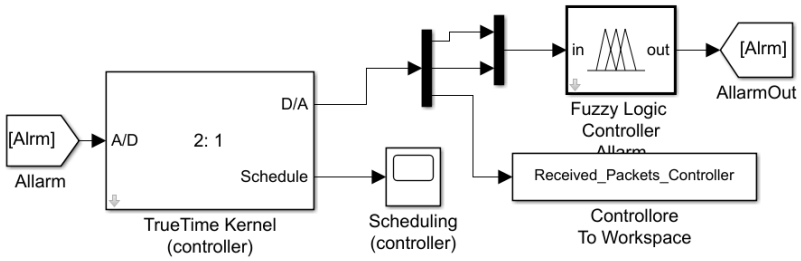

Figure 4: Controller structure.

- Control unit: Receives from the controller the values detected by the sensors and the alarm level generated. It also receives the key insertion signal from an MBSD. Use a function to decide what actions need to take based on sensor values and alarm level. The hypothesized cases depend on the alarm level: Low, Medium,

or High. The actions taken in this POC are automatic door closing, automatic emergency call, and activation of an acoustic alarm.

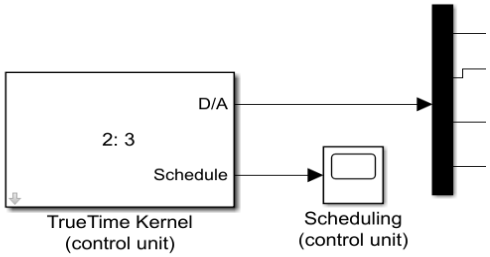

Figure 5: Controller structure.

Fuzzy logic function analysis: Two inputs and one output. Detected movements and door opening time will be used as input while alarm level will be the output. The detected movements range from 0 to 3 in the low case, from 2 to 9 in the medium case, and from 8 to 10 in the high case. The opening time (in seconds) ranges from 0 (door closed) to 25 in the low case, from 20 to 50 in the medium case, and from 45 to 80 in the high case. The alarm level ranges from 0 to 4.6 in the low case, from 4 to 7 in the medium case, and from 6.4 to 10 in the high case.

The nine control rules that were used:

- With low movement and low doors, the alarm level will be low.
- With low movement and medium doors, the alarm level will be low.
- With low movement and high doors, the alarm level will be medium.
- Medium movement and low doors the alarm level will be low.
- Medium movement and medium doors the alarm level will be medium.
- With medium movement and high doors, the alarm level will be high.
- With high movement and low doors, the alarm level will be medium.
- With high movement and medium doors, the alarm level will be high.
- With high movement and high doors, the alarm level will be high.

MBSD function analysis: Two states, on and off. When the interaction of the disarm key is detected, it switches from off to on, temporarily deactivating the alarm.

It then waits for 1 second (chosen for the simulation to affect only one instant of time) and returns to the off state.

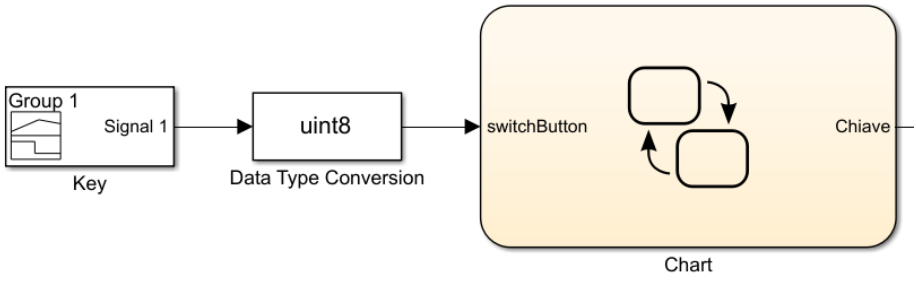

Figure 6: MBSD structure.

SCENARIO

The simulated environment implements three parameters.

- Movements detected by the “Motion sensor”: Generated randomly. Indicate the number of detections from a single sensor during a whole instant of time. In this POC the maximum detections/second have been set to 10.
- Door open signal: Indicates how many seconds the door stayed in the open state. A logic AND between the signal and a clock with a period of 1 allows a rising edge counter to advance for all the instants of time in

which the signal stays 1, resetting it when the control unit detects an alarm signal and closes the door. The counter indicates the time elapsed between opening and closing the door.

- Key insertion signal: Simulates the insertion of the disarm key. Passes through an MBSD used as a switch.

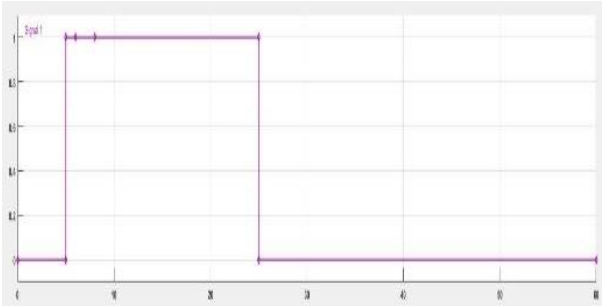

Figure 7: Door opening signal.

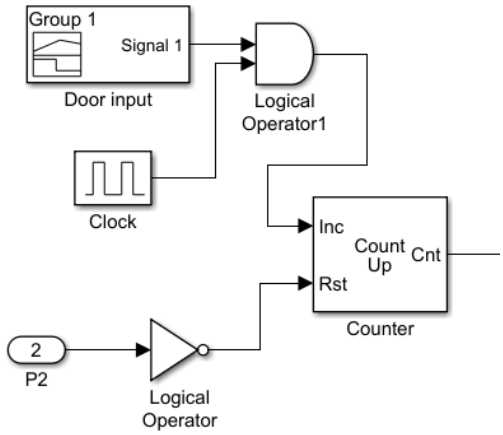

Figure 8: Door elapsed time circuit.

PERFORMANCE EVALUATION

The motion sensors function stores the number of packets sent. The same function applies to the door-opening sensor. The Gateway can read how many packets are received from the sensors checking their content and sends them to the controller. This function also stores the delay between the moment one packet is sent by the sensor and its reception time and the number of packets sent and received. The controller function stores the propagation time of a message between sensors and the controller itself.

```
t= 0.33109 CONTROLLER: no value received
t= 0.33115 Control Unit: Received -> M:3.0912D:1A:2.3766
Delay = 0.15104
t= 0.40104 GATEWAY: door sensor value received ->1
t= 0.40109 CONTROLLER: door sensor value received ->1
Delay = 0.12104
t= 0.47104 GATEWAY: motion sensor value received ->3.0912
Delay = 0.47109

t= 58.2911 CONTROLLER: motion sensor value received ->3.3205
t= 58.2912 Control Unit: Received -> M:3.3205D:1A:2.4637
Delay = 1.311
t= 58.361 GATEWAY: door sensor value received ->1
t= 58.3611 CONTROLLER: door sensor value received ->1
Delay = 1.381
t= 58.431 GATEWAY: motion sensor value received ->3.3205
Delay = 58.4311
```

Figure 9: Obtained results.

CONCLUSIONS

The project has great development potential thanks to both the versatility of the technology used and the various types of modules that can be created. It can be used as a starting point for the home smart security market and in the implementation of a warehouse smart alarm system.

REFERENCES

1. P. K. Madupu and B. Karthikeyan, "Automatic Service Request System for Security in Smart Home Using IoT," 2018 Second International Conference on Electronics, Communication and Aerospace Technology (ICECA), Coimbatore, India, 2018, pp. 1413-1418, doi: 10.1109/ICECA.2018.8474684.
2. K. Sohrabi, J. Gao, V. Ailawadhi, G.J. Pottie. “Protocols for self-organization of a wireless sensor network”, Year: 2002, IEEE Personal Communications.
3. Dan Henriksson, Anton Cervin, Karl-Erik Årzén. “TrueTime: Real-time Control System Simulation with MATLAB/Simulink”, Year: 2003

LIBRARY DEVELOPMENT FOR ANALYTICAL SIGNAL SIMULATION

Maxim Rusanov

Saint-Petersburg State University of Aerospace Instrumentation,
Saint-Petersburg, Russia
E-mail: hatrue.max@gmail.com

Annotation
This paper presents a software implementation of the analytical signal model in Python 3.6.9. The article describes the mathematical model of the signal under investigation: the structure of the analytical signal; Hilbert transform and its basic properties; signal parameters description:
• Amplitude
• Power
• Frequency
The block diagram of the implemented algorithms, the program code and an example of signal simulation.

INTRODUCTION

An analytical signal (complex signal) is a mathematical representation of an analog signal in the form of a complex analytical function of time used in signal processing theory. The usual, real signal x is in this case the real part of the analytic representation *s(t)*. The theory of analytical signals is a developed direction in the theory of control systems.

As a rule, ready-made models of the studied phenomenon are used to solve applied problems. In particular, if the solution of the problem is performed in any programming language, then ready-made libraries of functions and methods are used. This speeds up the development of a software solution and allows you to concentrate on solving the problem, bypassing the technical implementation of

the subject. The layer of abstraction is also increased, allowing for a more flexible approach to the solution.

Therefore, when approaching the problem of modeling the analytical signal, such a method was chosen. Based on the already built mathematical models, an interface (library of functions) was developed for modeling the signal and its parameters. In connection with the often encountered problem of signal noise, the function of smoothing signals (including parameters) was also developed, implemented by the "simple moving average" method.

MATHEMATICAL MODEL

The formal definition of a complex signal is as follows:

$$s(t) = u(t) + iv(t), \tag{1}$$

where *u(t)* is a real signal with a Fourier image; v (t) - conjugate signal by Hilbert transform method.

In this case, the conjugate signal is related to the real part using the Hilbert transform as follows:

$$v(t) = \frac{1}{\pi} \int_{-\infty}^{\infty} \frac{u(\tau)}{t-\tau} d\tau \equiv H\left[u(t)\right]. \tag{2}$$

We list the most important properties of the Hilbert transform:

1. $\left|H(i\omega)\right| = \left|sgn(\omega)\right| = \begin{cases} 1, & \omega \neq 0 \\ 0, & \omega = 0 \end{cases}$,

where sgn(x) – sign function. (3)

2. $$H\left[H\left[u(t)\right]\right] = -u(t) \;\rightarrow\; H^{-1} = -H\,. \tag{4}$$

Formula (3) gives an idea of the amplitude-frequency characteristic of the Hilbert transform, (4) the formula shows how the inverse transformation is represented, that is, the return to the original signal.

In addition to the listed properties, it is also very important that the Hilbert transform is expressed through the Fourier transform. This fact plays a major role in the software implementation of the analytical signal model.

Let $U(i\omega) = F[u(t)]$ be the Fourier image of the real signal. Since the Fourier image $s(t)$ is:

$$S(i\omega) = (1 + sgn\,\omega)U(i\omega) = 2U(i\omega),\ \omega > 0. \tag{5}$$

Then you can calculate $v(t)$ complement by the formula:

$$v(t) = Im\{F^{-1}\left[2U(i\omega)\right]\},, \tag{6}$$

where $Im(z)$ is the imaginary part of z; F^{-1} - Inverse Fourier Transform.

Based on the complex signal model, it is also possible to give definitions of the main parameters of the signal, its amplitude $a(t)$ or power $c(t)$:

$$a(t) = \sqrt{u^2(t) + v^2(t)},\quad a^2(t) \equiv c(t) = u^2(t) + v^2(t), \tag{7}$$

and phases:

$$\varphi(t) = \tan^{-1}\left(\frac{v(t)}{u(t)}\right) = \cos^{-1}\left(\frac{u(t)}{a(t)}\right) = \sin^{-1}\left(\frac{v(t)}{a(t)}\right), \tag{8}$$

and also frequencies:

$$\omega(t) = \frac{u(t)\dot{v}(t) - \dot{u}(t)v(t)}{u^2(t) + v^2(t)} \equiv \frac{d}{dt}\varphi(t). \tag{9}$$

In this implementation of the signal model, the present smoothing method works according to the following principle. A certain area is taken before and after a certain point and, taking into account the numerical values of the measurements included in this area, we calculate the average value. Formally, this can be described as follows.

Let there be a sample of N points $\{f1, f2, \ldots, fN\}$. Then, to find the average in the vicinity of the selected point i, we take the arithmetic mean of M previous and subsequent points, including the point i itself. Then the new values of the points, let g_i, will be calculated by the formula:

$$g_i = \sum_{j=-M}^{M} \frac{f_{i+j}}{2M+1} \tag{10}$$

PROGRAM DESCRIPTION

When developing a complex signal model in Python 3.6.9, the following functions were implemented, covering the construction of the conjugate signal by Hilbert transform method, the construction of an analytical signal, the calculation of the main signal parameters, as well as noise smoothing.

The work is carried out as follows: the library file is included in the program header; code is written using the functions described below; below is the code that displays the received data; launched through the OS command line; the user receives an image (graph) of the simulated signal. The library interface consists of the following functions:

• *hilbert (signal)* - the function takes an array of signal values, returns an array representing the values of the Hilbert transform.

• *ort_signal (signal)* - the function takes as a parameter an array of values of a valid signal and returns an array representing the values of the conjugate signal.

• *analitic_signal (signal)* - takes an array of signal values, returns an array of complex analytical signal values.

• *amp (signal)* - takes an array of analytical signal values, returns the amplitude of the analytical signal.

• *cap (signal)* - takes an array of analytical signal values, returns the analytical signal power.

• *frq (signal, dx)* - takes an array of analytical signal values (signal) and a signal sampling step (dx), returns the frequency of the analytical signal.

• *smoothing (signal, M)* - smooths the input signal using the moving averaging method, takes an array of values of the actual signal (signal) and the degree of smoothing (M), returns a smoothed signal.

ALGORITHMIC DESCRIPTION

In this part of the work, the block diagrams of the above described functions are given with comments, with the exception of the functions amp (signal) and cap (signal), the implementation of which is trivial.

1.*hilbert ()*:

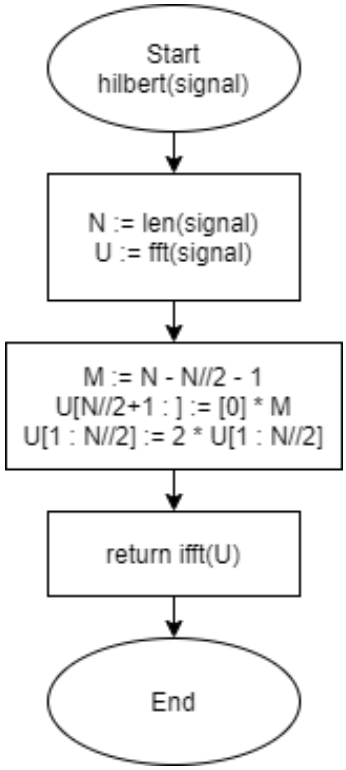

Fig 1. Block diagram of the Hilbert transform function

The *Start* block indicates the beginning of the program and contains the name of the function, as well as the accepted parameters. Further, in the description of subsequent functions, commenting is carried out starting from the second block. The second block: *N* - a variable containing the length (*len ()*) of the sample of signal values; *U* is the direct Fourier transform (*fft ()*) of the input signal. Third block: *M* - sample center. The next two lines calculate the Fourier image of the analytical signal, where, according to the theory, at negative frequencies ω the image is equal to zero, and at positive frequencies it is equal to the doubled value of the image of the real signal. Fourth block: Returns the inverse Fourier transform of a complex-valued signal. End of the algorithm.

The second block: *h* - an array of values of the signal converted according to Hilbert; *ort_signal* is an empty array for storing the values of the coupled signal. The third block: the loop of variable *i* passing from 0 to the end of the array, in the body of the loop, the imaginary part of the *h* array is assigned to the *ort_signal* array. Fourth block: the function returns the array *ort_signal*. End of the algorithm.

The second block: *analitic_signal* - an array for storing the final value; *h* and *ort_signal* have the same meaning as in the previous algorithm. The third block: *Loop 1* - performs the same functions as in the previous algorithm. The fourth block: *Loop 2* - loop of variable *i* passing from 0 to the end of the array, complex values are assigned to the *analitic_signal* array in the loop body, where the real part is the input signal, and the imaginary part is the conjugate signal. Fifth block: the function returns an array *analitic_signal*. End of the algorithm.

2.*ort_signal ()*:

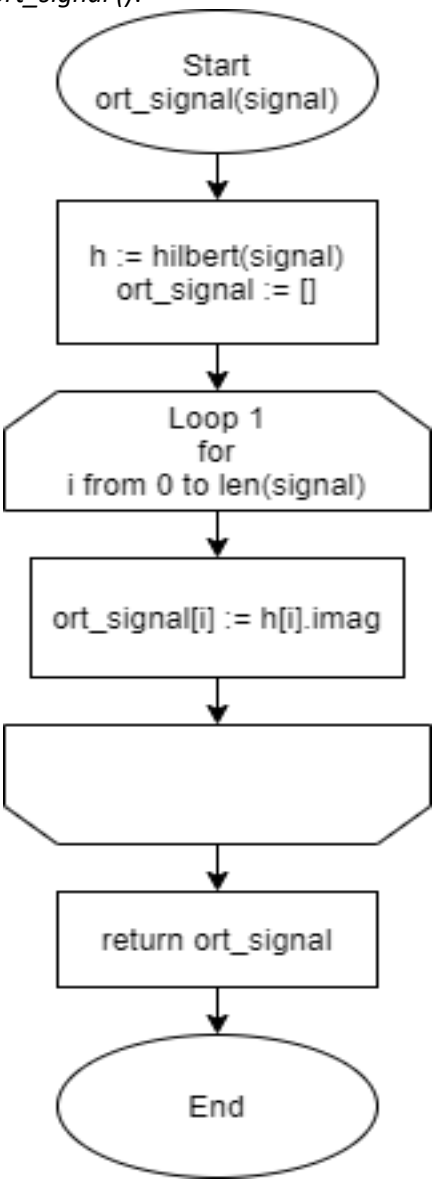

Fig 2. Block diagram of the orthogonal signal function

2.*analitic_signal ()*:

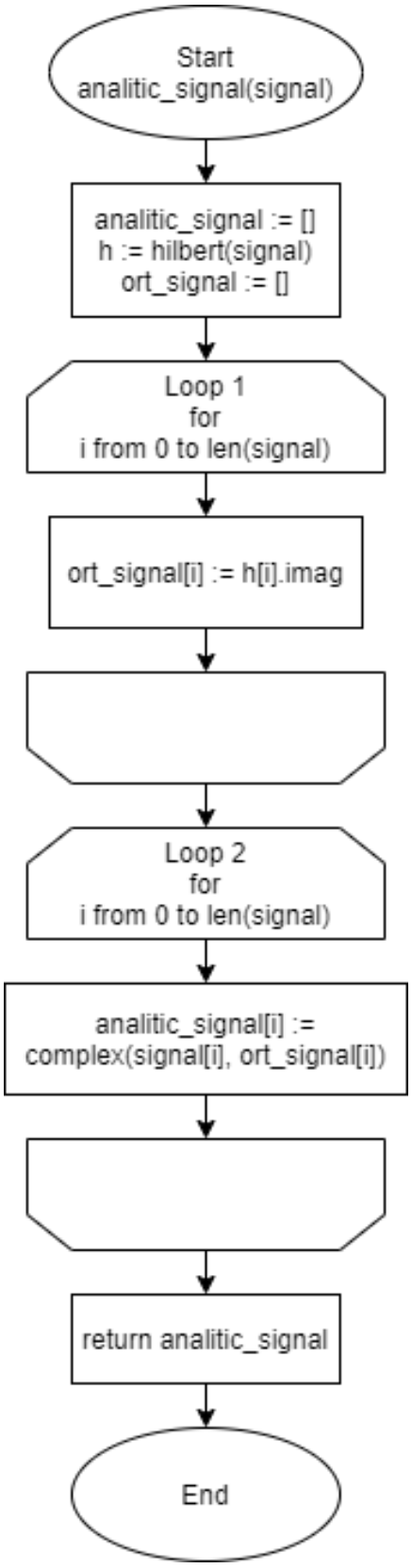

Fig 3. Block diagram of the analytical signal function

3.smoothing ():

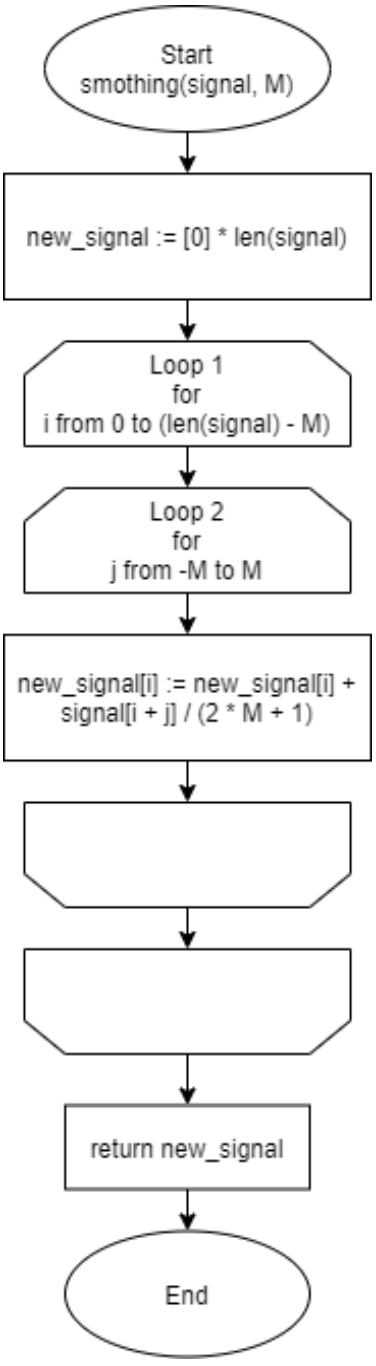

Fig 4. Block diagram of the function that implements signal smoothing

5.frq ():

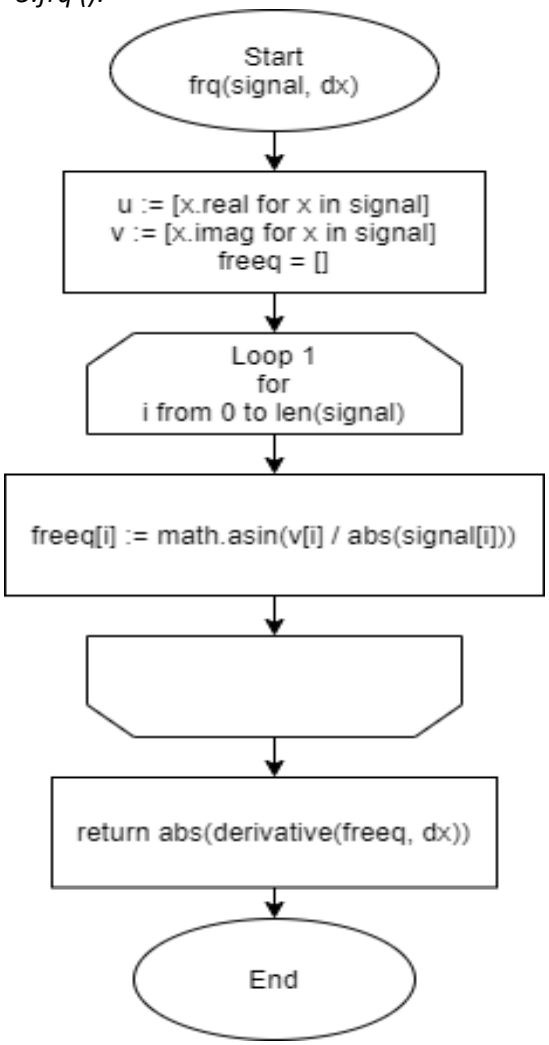

Fig 5. Block diagram of the analytical signal frequency function

Second block: *new_signal* - an array for storing the final value. The third block: *Loop 1* - loop of the variable *i*, passing from 0 to the end of the array, except for the last *M* points. *Loop 1* contains a nested loop, *Loop 2*, which calculates new averages of the signal using the "simple moving average" method. Fourth block: the function returns the new_signal array. End of the algorithm.

Second block: *u* - array of real values of the analytical signal; *v* - array of the imaginary part of the analytical signal; *freeq* is a variable for storing the total frequency values. The third block: *Loop 1* - the loop of variable *i* passing from 0 to the end of the signal sample. In the body of the loop, the phase values of the signal are calculated using the formula (8) with the arcsine. Fourth block: the function returns the time derivative of the phase, that is, the frequency value. End of the algorithm.

Full program code:

```
import matplotlib.pyplot as plt
import numpy as np
import math as m
from scipy.fftpack import *


def hilbert_1(signal):
    N = len(signal)
    U = fft(signal)
    M = N - N//2 – 1

    U[N//2+1:] = [0] * M
    U[1:N//2] = 2 * U[1:N//2]
    v = ifft(U)

    return v

def derivative(f, dx):
    df = []
    df.append(((f[1] - f[0]) / dx)

    for i in range(1, len(f)):
        df.append(((f[i] - f[i - 1]) / dx)

    return df


def ort_signal(signal):
    h = hilbert_1(signal)
    ort_signal = []

    for i in range(0, len(signal)):
        ort_signal.append(h[i].imag)

    return ort_signal


def analitic_signal(signal):
    analitic_signal = []
    h = hilbert_1(signal)
    ort_signal = []

    for i in range(0, len(signal)):
        ort_signal.append(h[i].imag)
    for i in range(0, len(signal)):
        analitic_signal.append(complex(signal[i], ort_signal[i]))

    return analitic_signal


def smoothing(signal, K):
    new_signal = [0] * len(signal)

    for i in range(K, len(signal) - K):
        for j in range(-K, K):
            new_signal[i] += signal[i + j] / (2*K + 1)
```

```
    return new_signal


def amp(signal):
    return np.abs(signal)


def cap(signal):
    return np.abs(signal) * np.abs(signal)


def frq(signal, dx):
    u = [x.real for x in signal]
    v = [x.imag for x in signal]
    freeq = []

    for i in range(0, len(signal)):
        freeq.append(m.asin(v[i] / np.abs(signal[i])))

    return np.abs(derivative(freeq, dx))
```

EXAMPLE OF SIGNAL CONSTRUCTION

As an example of the program operation, the following code was written to simulate the conjugate signal for the *sin(x)* function. As a result, we have the following code:

```
from signal_model import *

d = 10
discr = 0.0008
l = int(d / discr)

axis = [(x * discr) for x in range(0, l)]
signal = [m.sin(x) for x in axis]

ort_signal = ort_signal(signal)
analitic_signal = analitic_signal(signal)

plt.axis([0, d, -2.5, 2.5])

plt.plot(axis, signal)
plt.plot(axis, ort_signal, color = 'red')

plt.plot(axis, amp(analitic_signal))
plt.plot(axis, cap(analitic_signal))
plt.plot(axis, smoothing( frq(analitic_signal, discr), 50), color = 'grey')

plt.show()
```

The result of the program can be seen in the following figures:

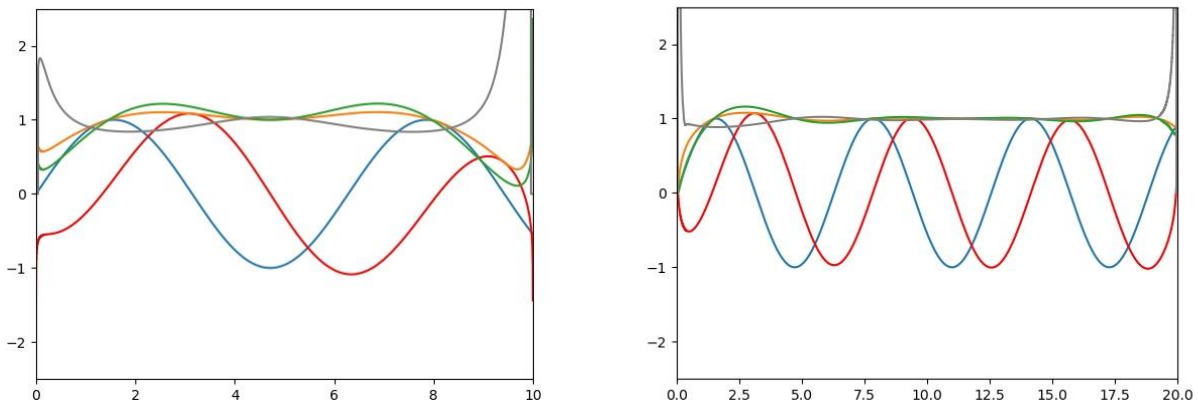

Figure 6 - 7. The result of the program. Blue - input valid signal; Red - conjugate signal by Hilbert transform method; Orange - amplitude; Green - power; Gray – frequency.

In particular, as mentioned earlier, sometimes when the signal is noisy, it becomes necessary to smooth it, which is demonstrated below:

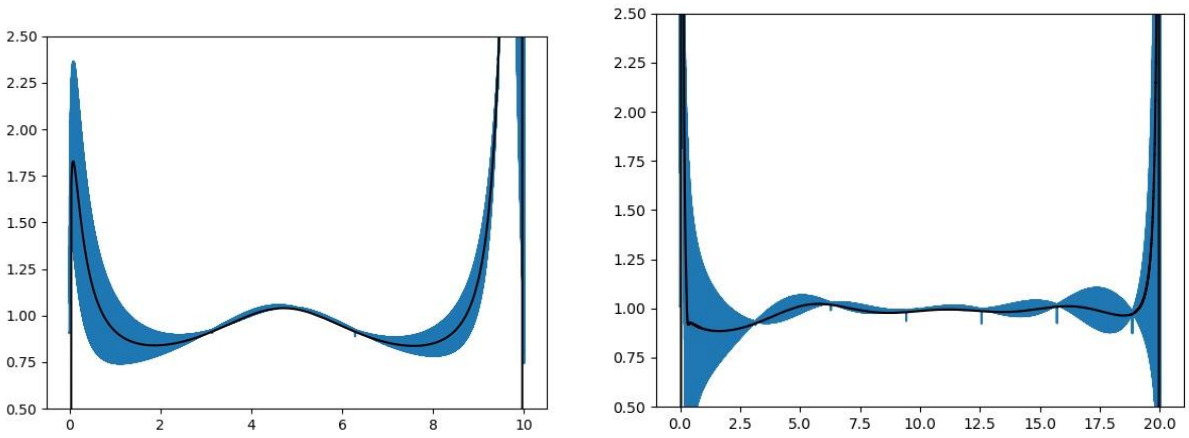

Fig. 8 - 9. An example of the smoothing function. Blue - noisy signal; Black - anti-aliased.

REFERENCES

[1] https://ru.dsplib.org/content/hilbert/hilbert.html

[2] Faleev SP Calculation and modeling of signal processing devices of control systems. Tutorial. / Leningrad Order of Lenin Electrotechnical Institute named after V.I.Ulyanov (Lenin)

[3] Sato Yukio. Digital signal processing. / Yukio Sato: trans. with jap. Selina T. G. M.: Dodeka-XXI, 2010 .-- 176 p. : ill. - Add. Titus. l. jap. - ISBN 978-5-94120-251-5.

DEVELOPMENT OF A MODEL OF A PRODUCTION CELL OF ADDITIVE TECHNOLOGIES USING A ROBOTIC ARM

Daria Shchukina

Saint-Petersburg State University of Aerospace Instrumentation, Saint-Petersburg, Russia
E-mail:shchukinad@icloud.com

Annotation
The article presents the basic model of an updated production cell with a high degree of automation. It includes design solutions for the location of 3D printers with a centralized module for automated control of the operation of 3D printers with a high degree of mechanization in the form of a robotic arm.

Today, the presence of production cells among domestic enterprises is in demand. The main problems in traditional industries are: the human factor, diagnostic time, equipment maintenance, a high percentage of defects in manufactured products, due to the low qualification of personnel, imperfect quality control processes of machining processes, molding and casting processes, as well as high work rates, due to the dynamically developing demands of the market sector.

The unattainability of a sufficient level of automation in traditional industries is due to the presence of the human factor, which entails a number of time costs, such as: unnecessary movement, excessive processing of products, the presence of inconsistencies, the elimination of defects, overspending of resources for the process. The solution to this problem area is the conceptual development of a layer-by-layer synthesis system with remote control, which allows for automated quality control of the manufactured product by using X-ray technologies based on the principle of an X-ray separator.

Today, all manufacturing enterprises are experiencing uncertainty in both stable and rhythmic market demands. For the sustainability and implementation of the management of continuous monitoring of the process, as well as the possibility of reducing the time spent on transportation and storage of finished products, it is advisable to implement a mass production system with a control center in another city (country).

The structure is based on a square arrangement of 3D printers connected by a robot manipulator, as well as a conveyor belt (Fig. 1). This system covers the product life cycle from receiving a digital model to the control point to the processing process and iteration of this process.

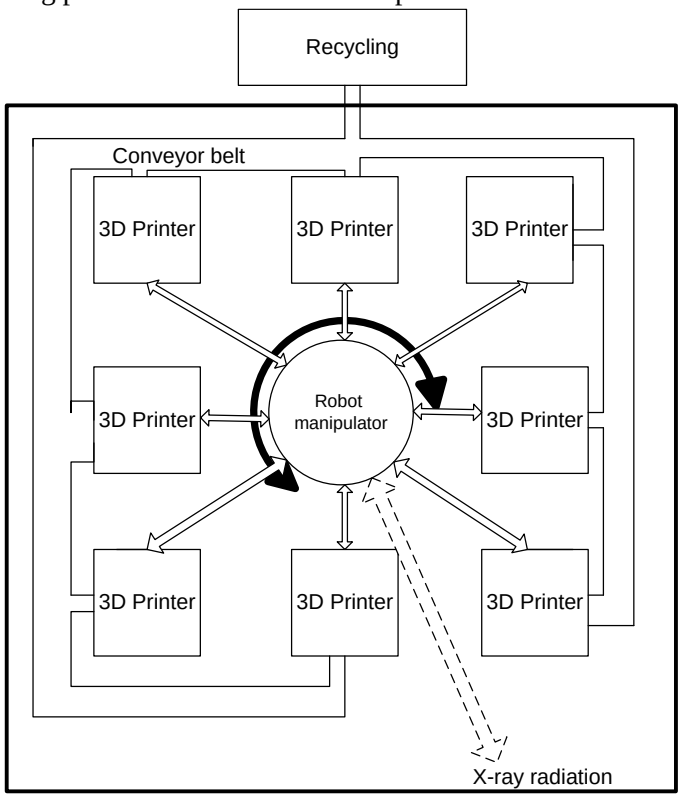

Figure 1-Block diagram of a layer-by-layer synthesis system with remote control.

The principle of operation of the system is a cyclic and waste-free process of additive manufacturing with remote control and the exclusion of the human factor. The remote control gives the command to print the product and loads the data on the permissible errors. The robot manipulator starts the printing process on 3D printers located around the manipulator. During the printing process, there is constant monitoring by X-ray radiation and, if a discrepancy between the pre-set parameters of the product is detected, the printing process is stopped, to move the defective part to recycling, by using a conveyor belt.

The advantage of this system is that there are no workplaces with operators replaced by workstations, according to the principle of unification. A robot manipulator with a high degree of mechanization was installed to control the quality of the process of the additive plants of the production line. The main task of the robot manipulator is the process of continuous monitoring of the quality level of the filamented product in the process of layer-by-layer synthesis.

Conclusion

The main advantage of the developed concept is the reduction of all losses in the production process associated with the human factor and equipment maintenance. The innovation of the developed system is to cover the full life cycle of the production cell, which implements all stages of the process of layer-by-layer synthesis, and the possibility of processing defective products.

Therefore, the proposed conceptual solution is the basis for the implementation of an automated technological line of the full life cycle, with the exception of the development of the technical specification for the creation of the first experimental part of the filamented product.

Literature

1. GOST 26228-90. Production systems are flexible. Terms and definitions, nomenclature of indicators
2. Shchukina D. S., Development of an automated system of layered synthesis with application of robotics. / Proceedings of the UNESCO Department of GUAP "Remote Engineering Education" / Collection of articles, Issue 5, 2020, 118-120 p.
3. Shchukina D. S. "Development of an automated system of layer-by-layer synthesis with the use of robotics", / "Modeling and situational quality management of complex systems" / Collection of reports Youth section, 2020, 76-78 p.
4. Shchukina D. S. "Development of an automated system of layer-by-layer synthesis with the use of robotics", / International Forum "Metrological support of innovative technologies" / Collection of works 2020g., 108-109 p.
5. Shchukina D. S. "The system of layer-by-layer synthesis with the use of a robot manipulator" / 19 scientific and practical conferences "Quality management" / Selected scientific works, 2020, 308-313 p.
6. Shchukina D. S. " Creating a 3D model of an object for subsequent physical construction by FDM technology.", / "The future of strong Russia in high technologies" / Collection of theses of works of participants of the section "Technology" of the Open Youth scientific and practical Conference, 2019, 21-22 p.
7. X-ray seed separator based on the method of shooting with direct image magnification / / [Electronic resource] / / URL: https://www.natural-sciences.ru/ru/article/view?Id=36558 (Accessed 05.02.2021)
8. Nazarevich, S. A. Integration of search methods for engineering solutions through the use of synthesis of combinatorics and heuristic methods / S. A. Nazarevich, E. G. Semenova / / Formation of a modern information society. Problems, prospects, innovative approaches: Materials of the International Forum. St. Petersburg: Publishing house: GUAP. 2010. - p. 105-109
9. Nazarevich, S. A. Sovershenstvovanie svyazi sistemy purveyor - innovatsionnoe predprinimatel'stvo (Improvement of relations of the supplier-innovative enterprise system) / / Quality management in educational institutions and scientific organizations. Collection of articles. St. Petersburg: Publishing house: Legacy. 2012. - p. 136-139.

RADIO-OPTICAL ANALYSIS OF PRISM SPECTRAL DEVICE

Kseniia Serdiuk

Saint-Petersburg State University of Aerospace Instrumentation
Saint-Petersburg, Russia
E-mail: molegd@mail.ru, kserdiuk@yandex.ru

Abstract
On the basis of radio optics methods, an alternative description of the action of a prism spectral device is proposed, which is based on transformations of an optical signal by an optical coherent Fourier processor. The analyzed optical radiation is introduced into the optical coherent Fourier processor by a dispersing element in the form of a prism. The transmission function of the prism as a transparency and the input-output ratio of the prism spectral device for complex spectra in the form of a linear integral operator, in which the complex instrumental function is determined by the transmission function of the prism, are established
Keywords: spectral measurements; radio-optical approach; diffraction prism spectral device; optical coherent Fourier processor; prism; transparency; transmission function; instrument function.

Introduction

In physics and technology, spectral methods and devices are among the most common, and there are currently no visible reasons that would change this situation. Harmonic spectrum analysis is one of the most important physical and technical measurements. The very widespread use of instruments for analyzing harmonic spectra is due to the importance and variety of information obtained with their help, both in fundamental studies of the structure of matter (astrophysics, radio astronomy, spectroscopy) and in solving applied problems.

The role of harmonic analysis is especially great in spectroscopy, where spectral instruments investigate electromagnetic radiation as a signal sent by matter and carrying a variety of spectroscopic information.

Among the instruments for scientific research, the equipment of harmonic analysis occupies a special place: the technique of spectroscopy has been developing for many years at a very high rate, faster than in other areas of physical experiment and analysis. The result of this development is a number of methods for analyzing harmonic spectra and the widest range of spectral instruments.

The huge role of instrumental harmonic analysis in modern science and technology and the high level of development of spectral instrumentation require a well-developed theory of spectral measurements. Analysis of the modern state of spectrometry has shown that a number of issues in the theory of spectral measurements remain insufficiently developed and require additional research.

Thus, the main task of the theory of spectral measurements is to establish a connection between the spectrum in the mathematical sense and the instrumental spectrum, i.e. registered as a result of spectral measurements [1], in other words, the input-output connection of the spectral device. Within the framework of the theory of optical spectral measurements, a solution to this problem was proposed in [2], where, on the basis of heuristic reasoning, a linear integral operator in the form of a convolution was obtained, which initially describes the measurement of energy spectra. It's the connection between the input and output of the spectral device in the form of a convolution that served as the basis for solving the inverse problem, i.e. reduction to an ideal spectral instrument. The ideology of the work [2] has firmly taken a place in the known manuals on optical spectroscopy techniques [3, 4, 5, 6, 7]. It should be emphasized that article [2] notes a change in resolution within the analyzed wavelength band, which is contrary to the folding operation.

Characteristically, in the mentioned manuals [3, 4, 5, 6, 7] the core of the integral operator, i.e. the instrumental function of the spectral device, is not directly related to the parameters of the dispersing systems of diffraction spectral devices. For lattice spectral devices, the issue of direct connection of the instrumental function with the parameters of the diffraction grating is to a certain extent solved in papers [8, 9, 10, 11]. In this paper, an attempt has been made to solve the issue of connecting a instrumental function with the parameters of a dispersing system for a prism spectral device within the framework of establishing an input-output connection of a spectral device for complex spectra of optical radiation.

Functional scheme of the diffraction spectral device and it's radio-optical interpretation

The general functional scheme of the diffraction prism spectral device [7] is shown in Fig.1, it consists of two parts: the collimating system (A) and the analyzing (resolving) system (B). The collimating system (A) generates the analyzed signal in the form of a uniform plane wave beam. The analyzing system (B) includes a dispersing system (DS), an optical system consisting of two layers of free space and a positive lens between them and a recording device. The recording device performs photodetection and temporal integration of its results and ultimately provides the recipient with spectroscopic information in the form of an energy spectrum.

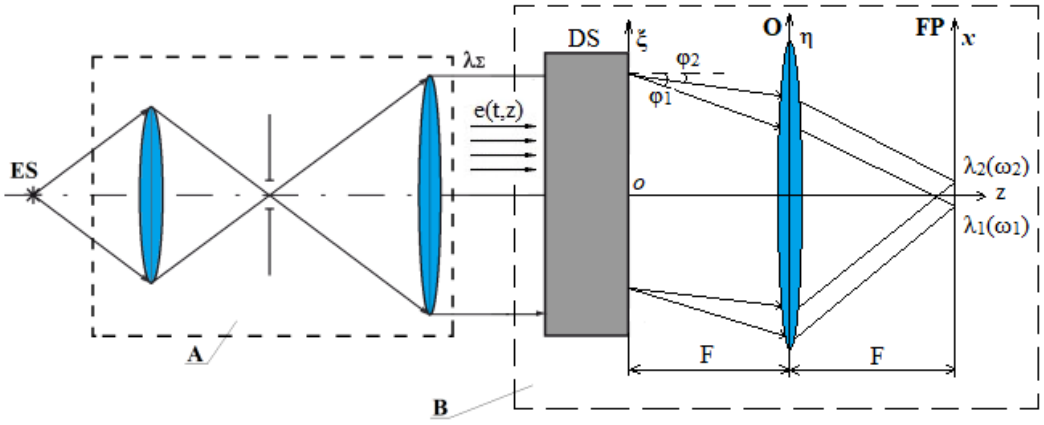

Fig.1. Optical scheme of the diffraction prism spectral device

The dispersing system, as a one-dimensional transparency [12], introduces the analyzed optical radiation into the analyzing system, which includes two layers of free space and an ideal thin positive lens with a focal length F between them. Within the framework of the radio-optical approach [13], it was shown that an optical system including in the following order: a layer of free space with an extension F, an ideal thin positive lens with a focal length F, and a layer of free space with an extension F. When illuminating this optical system with a uniform flat monochromatic light wave, a spatial transformation of the function $f(\xi, z=0)$ is performed in the form [14]:

$$S_s(\omega_x,\omega') = \sqrt{\frac{2\pi c_0 \mathrm{F}}{\omega'}} \cdot \exp(i\pi/4) \cdot \hat{F}[f(\xi, z=0)] = \\ = \sqrt{\frac{2\pi c_0 \mathrm{F}}{\omega'}} \cdot \exp(i\pi/4) \cdot \int_L f(\xi, z=0)\exp(-i\omega_x \xi) d\xi \quad , \tag{1}$$

where $S_s(\omega_x,\omega')$ - spectrum of spatial frequencies; $\hat{F}$ - direct Fourier transform operator; $\omega_x = \dfrac{\omega' x}{c_0 \mathrm{F}}$ - spatial frequency; c_0 - скорость света в вакууме; F - focal length of the ideal thin lens; ω' - angular frequency of uniform flat monochromatic wave incident on dispersing system:

$$e(z,t) = \dot{E}_0 \exp[i(\omega' t - k' z)], \tag{2}$$

where $\dot{E}_0$ - complex amplitude; t - current time; k' - wave number; z - direction of wave motion $e(z,t)$.

Spectrum of spatial frequencies $S_s(\omega_x,\omega')$ is formed in plane (FP) $z = 2\mathrm{F}$ on sensitive surface of photodetector as spatial modulation of space-time signal

$$s(x,t) = \dot{E}_0 \exp(i\omega' t) \cdot S_s(\omega_x,\omega'). \tag{3}$$

In this case, the function $f(\xi, z=0)$ is the result of spatial modulation of a uniform flat monochromatic wave (2) by a dispersing system, which is considered a one-dimensional placard. According to the definition of the transparency transmission function [14], in what follows, we mean

$$f(\xi, z=0) = \mathrm{T}(\xi). \tag{4}$$

Performing the spatial Fourier transform (1) served as a basis to call such a system an optical coherent Fourier processor [15].

prism transmission function

The dispersing system of the prism spectral device is a prism, here it is a straight triangular prism with a base in the form of an isosceles triangle. The cross section of the prism is shown in Fig. 2.

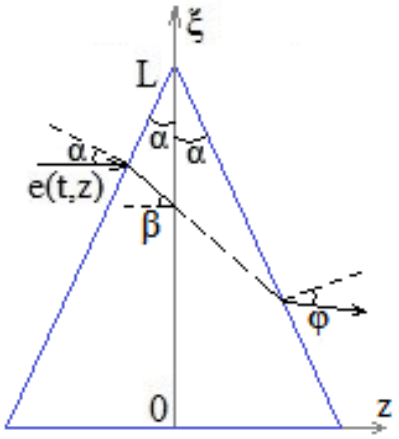

Fig.1. Optical scheme of the dispersive system of a prism spectral device

To establish the transmission function of a prism, the original prism is presented in the form of two partial equal-area right triangular prisms with an initial height and bases in the form of two equal-sized right-angled triangles, as shown in Fig.2. In this case, the transmission function of the transparency in the form of the original prism is given as:

$$\dot{T}(\xi,\omega') = \dot{T}'(\xi,\omega')\cdot T''(\xi,\omega'), \tag{5}$$

where $T'(\xi,\omega')$, $T''(\xi,\omega')$ - transmission functions of partial prisms, respectively.

The main parameters of a prism are the refractive index of the prism material $n(\omega')$, the size of its entrance aperture L, and the angle of the prism α. Further, it is assumed that there are no losses in the prism material, i.e. $n(\omega')$ real function of frequency.

Through these parameters, the transmission functions of partial prisms, as phase banners, are expressed in forms:

$$\dot{T}(\xi,\omega') = \exp\left[-i\omega'\cdot\frac{n(\omega')(L-\xi)\operatorname{tg}\alpha}{c_0}\right]\cos\alpha, \tag{6}$$

$$\dot{T}''(\xi,\omega') = \exp\left[-i\omega'\cdot\frac{n(\omega')(L-\xi)\operatorname{tg}\alpha}{c_0}\right]\cos\beta, \tag{7}$$

Substitution of relations (6) and (7) into expression (5) gives the transmission function of the original prism

$$\dot{T}(\xi,\omega') = \exp\left\{-i\omega'\frac{2(n(\omega')(L-\xi)\operatorname{tg}\alpha}{c_0}\right\}\cdot \cdot\cos\alpha\cos\beta \tag{8}$$

The ratio (8) is suitably presented in the form:

$$\dot{T}(\xi,\omega') = \exp\left[-i\omega\frac{2n'(\omega')L\operatorname{tg}\alpha}{c_0}\right]\cdot \cdot\exp\left[i\omega'\frac{2n(\omega')\xi\operatorname{tg}\alpha}{c_0}\right]\cdot\cos\alpha\cos\beta, \tag{9}$$

where $0 \le \xi \le L$.

Input-output ratio of a prism spectral device for complex spectra

The input-output ratio of a spectral device for complex spectra is given in the form of a linear integral operator [8]:

$$\dot{S}_a(\omega,t) = \int_{\Delta\Omega} \dot{K}(\omega,\omega',t) \cdot \dot{S}_0(\omega') d\omega', \tag{10}$$

where $\dot{S}_a(\omega,t)$ - instrumental complex spectrum; ω - current temporal angular spectral frequency; $\Delta\Omega$ - - the band of the analyzed frequencies; $\dot{K}(\omega,\omega',t)$ - complex instrumental function; $\dot{S}_0(\omega')$ - complex mathematical spectrum of the analyzed optical vibration $e(t)$, i.e.

$$\dot{S}_0(\omega) = \hat{F}[e(t)] = \int_{T_s} e(t)\exp(-i\omega t)dt, \tag{11}$$

where T_s - signal duration $e(t)$.

The apparatus function, according to the definition of the general theory of linear systems, is the response of a linear system to $\delta-$action, the meaning of which is determined by the problem being solved; in the case of measuring a complex spectrum, the $\delta-$action is a spectral function $\delta(\omega-\omega')$. Then the complex instrumental function of the spectral device is given by the expression:

$$\dot{K}(\omega,\omega',t) = \hat{L}[\delta(\omega-\omega')], \tag{12}$$

where $\hat{L}$ - some linear bounded operator, which in general form establishes the transformation of the spectral function (11) when performing spectral measurements and which requires additional interpretation.

A linear operator $\hat{L}$ can be represented in the form of a product of linear bounded operators [11]:

$$\hat{L} = \hat{A}_a \hat{V} \hat{F}^{-1}, \tag{13}$$

where $\hat{F}^{-1}$ - the operator of the inverse Fourier transform, the result of which is the transformation of the spectral function $\delta(\omega-\omega')$ into a harmonic vibration $\exp(i\omega' t)$; the operator $\hat{V}$ converts the harmonic vibration $\exp(i\omega' t)$ into a homogeneous plane monochromatic wave $\exp[i(\omega' t - k' z)]$; the operator $\hat{A}_a$ describes the action of the analyzing system of a spectral instrument on a homogeneous plane monochromatic light wave.

Taking into account expression (13), the complex instrumental function of the spectral device, as a wave analyzer, in the operator room takes the form:

$$\dot{K}(\omega,\omega',t) = \hat{L}[\delta(\omega-\omega')] = \hat{A}_a \hat{V} \hat{F}^{-1}[\delta(\omega-\omega')], \tag{14}$$

where the complex instrumental function $\dot{K}(\omega,\omega',t)$ determines the time-varying complex spectra [11].

According to the above, the complex instrumental function $\dot{K}(\omega,\omega',t)$ is the result of the implementation of the algorithm for the operation of an optical coherent Fourier processor at different frequencies ω' of a homogeneous plane monochromatic light wave, and here

$$\hat{A}_a = \sqrt{\frac{2\pi c_0 \mathrm{F}}{\omega'}} \cdot \exp(i\pi/4)\hat{F}. \tag{15}$$

Then, taking into account relations (1), (3), (4), the complex instrumental function is expressed in the form:

$$\dot{K}(\omega,\omega',t) = \sqrt{\frac{2\pi c_0 \mathrm{F}}{\omega'}} \cdot \exp(i\pi/4) \cdot \exp(i\omega' t) \cdot \cdot \int_0^L T(\xi)\exp(-i\omega_x \xi)d\xi. \tag{16}$$

Substituting a relation (9) in an expression (15) results in an expression:

$$\dot{K}(\omega,\omega',t)=\sqrt{\frac{2\pi c_0\,\mathrm{F}}{\omega'}}\cdot\exp(i\pi/4)\cdot\exp(i\omega' t)\cdot$$
$$\cdot\exp\left[-i\omega'\frac{2n(\omega')L\,\mathrm{tg}\,\alpha}{c_0}\right]\cdot\cos\alpha\cos\beta\cdot \quad . \qquad (17)$$
$$\cdot\int_0^L\exp\left[i\omega'\frac{2n(\omega')\xi\,\mathrm{tg}\,\alpha}{c_0}\right]\cdot\exp(-i\omega_x\xi)d\xi$$
$$..$$

Integration in expression (17) gives:

$$\dot{K}(\omega,\omega',t)=\sqrt{\frac{2\pi c_0\,\mathrm{F}}{\omega'}}\cdot\exp(i\frac{\pi}{4})\cdot\exp(i\omega' t)\cdot$$
$$\cdot\exp\left(i\frac{\omega' xL}{2c_0}\right)\cdot\exp\left[-i\omega'\frac{n(\omega')L\,\mathrm{tg}\,\alpha}{c_0}\right]\cdot \quad . \qquad (18)$$
$$\cdot\frac{\sin\left[\omega'\frac{2n(\omega')\,\mathrm{tg}\,\alpha}{c_0}-\omega_x\right]\cdot\frac{L}{2}}{\omega'\frac{2n(\omega')\,\mathrm{tg}\,\alpha}{c_0}-\omega_x}\cdot\cos\alpha\cos\beta$$

In relation (18), the following part can be distinguished in the form:

$$\dot{H}(\omega')=\sqrt{\frac{2\pi c_0\,\mathrm{F}}{\omega'}}\cdot\cos\alpha\cos\beta\cdot\exp(i\frac{\pi}{4})\cdot$$
$$\cdot\exp\left(i\frac{\omega' xL}{2c_0}\right)\cdot\exp\left[-i\omega'\frac{n(\omega')L\,\mathrm{tg}\,\alpha}{c_0}\right] \qquad (19)$$

and, proceeding from relation (10), to interpret it as a transfer function of some imaginary two-port network, i.e.

$$\dot{H}(\omega')=\left|\dot{H}(\omega')\right|\cdot\exp(i\arg\dot{H}(\omega')\,. \qquad (20)$$

In relation (20), the function

$$\left|\dot{H}(\omega')\right|=\sqrt{\frac{2\pi c_0\,\mathrm{F}}{\omega'}}\cdot\cos\alpha\cos\beta \qquad (21)$$

has the meaning of the amplitude-frequency characteristic, and the function

$$\arg\dot{H}(\omega')=\pi/4+\frac{\omega' xL}{2c_0}-\omega'\frac{n(\omega')L\,\mathrm{tg}\,\alpha}{c_0} \qquad (22)$$

s considered as phase-frequency response.

Imaginary four-pole device with transfer function (20) is introduced into the process of measuring complex spectrum of optical radiation by algorithm of prism spectral device action. This allows the expression (10) to be represented in the form:

$$\dot{S}_a(\omega,t)=\int_{\Delta\Omega}\dot{K}(\omega,\omega',t)\cdot\dot{S}'(\omega')d\omega'\,, \qquad (23)$$

in expression (23)

$$\dot{S}'(\omega')=\dot{H}(\omega')\;\dot{S}_0(\omega') \qquad .(24)$$

The statement of the imaginary four-pole imaginary four-pole allows us to represent the complex hardware function of a prism spectral device in the form of:

$$\dot{K}(\omega,\omega',t)=\frac{\sin\left\lfloor(\omega-\omega')]\frac{T_a}{2}\right\rfloor}{\omega-\omega'}\cdot\exp(i\omega' t)\,. \tag{25}$$

Based on expression (24), the complex instrumental spectrum when measured with a prism spectral device is described by the expression:

$$\dot{S}_a(\omega,t)=\int\limits_{\Delta\Omega}\frac{\sin\left\lfloor(\omega-\omega')]\frac{T_a}{2}\right\rfloor}{\omega-\omega'}\cdot\exp(i\omega' t)\cdot\dot{S}'(\omega')d\omega'\,. \tag{26}$$

The complex instrumental function (25) establishes a time-varying complex spectrum (26) and is a necessary and sufficient condition for measuring the instantaneous complex spectrum of the signal $e(t)$ [11], the definition of which (instantaneous spectrum) was proposed in [16].

In expression (26), the quantity

$$\omega=\omega(x,\omega')=\frac{\omega' x}{2n(\omega')\,\mathrm{F}\,\mathrm{tg}\,\alpha} \tag{27}$$

is the current temporal spectral angular frequency, which is expressed as a non-linear function of the coordinate x, since the refractive index of the prism material $n(\omega')$ is described by a non-linear function. Further, the quantity

$$T_a(\omega')=\frac{n(\omega')L\,\mathrm{tg}\,\alpha}{c_0}\,, \tag{28}$$

having the dimension of time, is interpreted as "analysis time", since it determines the resolution of the prism spectral instrument when measuring the instantaneous spectrum.

When measuring the spectra of optical radiation, i.e. signals of the optical range of electromagnetic phenomena, the recipient of the spectroscopic information is given energy spectra.

When measuring the complex instantaneous spectrum, the energy spectral function is understood as the energy spectrum $G_a(\omega)$ as a result of performing the following operations [11]:

$$G_a(\omega)=\frac{1}{T_R}\int\limits_{T_R}\left|\dot{S}_a(\omega,t)\right|^2 dt\,, \tag{29}$$

where the time integration of the photodetection result is presented.

The integration in expression (29) was performed in [8, 11], as a result, the relation:

$$G_a(\omega)=M\cdot\int\limits_{\Delta\Omega}\frac{\sin^2\left\lfloor(\omega-\omega')\frac{T_a}{2}\right\rfloor}{(\omega-\omega')^2}\cdot G'(\omega')d\omega'\,, \tag{30}$$

where $G'(\omega')=\left|\dot{S}'(\omega')\right|^2$; $M=const$.

Relations (29) and (30) indicate that the phase-frequency distortions of the complex spectrum caused by the function $\arg\dot{H}(\omega')$ do not affect the measurement result of the energy spectrum, while the amplitude-frequency distortions described by the function $\left|\dot{H}(\omega')\right|$ distort the measurement result of the energy spectrum.

Relation (30) is not a usual convolution, since the temporal spectral angular frequency ω is a function ω'; moreover, the quantity T_a is also a function ω' and is not a constant. This is the internal difference between the integral operator (30) and the corresponding integral operator introduced in [2].

CONCLUSION

This paper is a continuation of the application of the radio-optical approach in the theory of diffractive optical spectral devices. Earlier, radio optics methods were used to describe the operation of a grating spectral device [8, 10, 11], which made it possible to give a consistent description of the conversion of the optical radiation spectrum from the input aperture of the spectral device to the issuance of spectroscopic information to the recipient in the form of an energy spectrum. The intermediate result is the statement of the complex spectrum of optical radiation.

In this paper, the use of radio-optical ideas also made it possible to show the processing of the optical radiation spectrum from the entrance aperture of a prism spectral device to obtain an energy spectrum and also to state the complex instrumental spectra in spectroscopic measurements in the optical range with a prism spectral device. Namely, on the basis of these complex spectra, specific errors in the analysis of energy spectra with a prism spectral device were established, undoubtedly, the same distortions are inherent in spectral measurements with grating spectral devices, but these distortions were not established in [8, 10, 11].

It should be emphasized that the noted specific errors in spectral measurements in the optical range can hardly be established within the framework of the existing methodology of optical spectrometry based on the principles of geometric optics.

ACKNOWLEDGMENT

This work was financially supported by the Russian Foundation for Basic Research (RFBR), project № 20-07-00648.

REFERENCES

1. G.S. Gorelik Oscillations and waves / Moscow: Fizmatlit, 2007.

2. S. G. Rautian Real spectral devices / S. G. Rautian // Advances in physical sciences, 1958. T. 66. №. 3. pp. 475-517.

3. V. I. Malyshev Introduction to experimental spectroscopy / Moscow: Nauka, 1979. 480 p.

4. K. I. Tarasov, Spectral devices / K.I. Tarasov, edition 2-nd L .: Machine building, Leningrad Branch, 1977. 367 p.

5. V.V. Lebedeva, Optical spectroscopy technique, 2-d edition, Publishing house of Moscow University, Moscow University, 1992. 352 p.

6. Yu.M. Belyakov, N.K. Pavlycheva, Spectral instruments, Kazan: Izd-vo Kazan. state tech. un-ta, 2007. 203 p.

7. A.N. Zaidel, G.V. Ostrovskaya, Yu.I. Ostrovsky Technique and practice of spectroscopy / Moscow: Nauka, 1978. 392 p.

8. Moskaletz O.D. Classical and quantum approach to power spectrum measurement by diffractional methods. Proc. SPIE // Vol. 3900, P. 297-308. 1999.

9. V.I. Kazakov, O.D. Moskaletz Complex spectra in a diffraction grating spectral device // Radioindustry. - 2016. - № 4. pp. 32-37.

10.Kazakov V.I., Moskaletz O.D. Alternative theory of diffraction grating spectral device and its application for calculation of convolution and correlation of optical pulse signals // Proc. SPIE 10680, Optical Sensing and Detection V, p. 1068025, 2018

11.Kazakov V.I., Kuryleva A.S., Moskaletz D.O., Moskaletz O.D. Instantaneous spectra in spectral and correlation processing of dynamic signal devices of radio and optical ranges and their linear and nonlinear transformations // Proc. SPIE 10680, Optical Sensing and Detection V, p. 1068025, 2018

12.Born M., Wolf E.. *Principles of optics*. Second (revised) edition. PERGAMON PRESS. Oxford-London- New York-Paris-Frankfurt, 1964. 856 p.

13.Zverev, N.S. Stepanov, Foreword of editors, Experimental radiooptics / Moscow: Nauka, 1979, pp. 6-10.

14.Papoulis A. Systems and Transforms with Applications in Optic. McGRAW - HILL BOOK COMPANY. New York - St. Louis - San Francisco - Toronto - London – Sydney, 1968.

15.Kendall Preston, Jr. Coherent optical computers. McGraw-Hill Book Company, 1972. 400 p.

16.Moskaletz OD Dynamic signals and spectral measurements. Successes of modern radio electronics. №2, 2013. pp.152-158.

INVESTIGATION OF PHYTOPLANKTON DYNAMICS IN THE NEVA BAY WITH THE "PREDATOR-PREY WITH FOOD" MODEL

Aleksandra Shchegoleva

Saint Petersburg State University of Aerospace Instrumentation
Saint-Petersburg, Russia
E-mail: aleksandrasheg@yandex.ru

Abstract
The “bloom” of some phytoplankton species (for example, blue-green algae) can threaten the environment. Therefore, it is of interest to build models for predicting such a “bloom”. This model is based on the Lotka-Volterra equations. This paper describes a method for the selection of coefficients according to biomonitoring data for the obtained model, a method that improves the selection of coefficients, and a statistical analysis of the obtained models.
Keywords: Lotka-Volterra equations, predator-prey model, population biology, ecological monitoring.

THE “PREDATOR-PREY WITH FOOD” MODEL

The Lotka-Volterra equations [1, 3] describes interspecific relations of the “predator-prey” type. It is represented by a system of two differential equations (1), where x_1 and x_2 are the population of prey (Cyanophyta, also known as blue-green algae) and predators (Cyclopoida), respectively, $\alpha_1, \alpha_2, \beta_1, \beta_2$ - are the coefficients influencing the change in populations:

$$\begin{cases} \dfrac{dx_1}{dt} = f_1 = \alpha_1 x_1 - \beta_1 x_1 x_2 \\ \dfrac{dx_2}{dt} = f_2 = -\alpha_2 x_2 + \beta_2 x_1 x_2 \end{cases} \quad (1)$$

The system above is solved by the Euler method since it cannot be solved analytically due to its nonlinearity. The paper [2] substantiates why Euler's method is used to solve the system.

In order for the system (1) to be applied to simulate the "bloom", control was designed (2) according to the ADAR method of synergetic control theory. The author of this method is Professor A. A. Kolesnikov [6, 7]. Since the "bloom" is characterized by a significant increase in the Cyanophyta population, the target value x^*, relative to which the control is based, is a certain value of the prey population, many times greater than the initial value of the population, i.e., $x^* = k \cdot x_1(0)$. The paper [2] provides a detailed description of the control design for this system.

$$\begin{cases} \dfrac{dx_1}{dt} = f_1 = \alpha_1(t) x_1 - \beta_1 x_1 x_2 \\ \dfrac{dx_2}{dt} = f_2 = -\alpha_2 x_2 + \beta_2 x_1 x_2 \\ \dfrac{d\alpha_1}{dt} = U(t) \\ U(t) = -\dfrac{\psi^{(1)}}{T_{1\ 3}} + \dfrac{d\varphi}{dt} \\ \psi^{(I)}(t) = \alpha_1(t) - \varphi(x_1(t), x_2(t)) \\ \varphi(x_1, x_2) = \beta_1 x_2 - \dfrac{1}{T_2} + \dfrac{x_1^*}{T_2 x_1} \\ \dfrac{d\varphi(x_1, x_2)}{dt} = -\dfrac{x_1^*}{T_2 x_1^2} f_1 + \beta_1 f_2 \end{cases} \quad (2)$$

COEFFICIENT SELECTION METHOD

Real monitoring data of the water system are represented by two values (populations of Cyanophyta and Cyclopoida) at three points. The first at the beginning of the observation period, the second after 84-85 days and the third at the end of the observation period (after 153-154 days). The data at the beginning of the observation is used as the initial data for the system (2). The numerical solution step is equal to 1 day. To select the coefficients $a_1, a_2, \beta_1, \beta_2$, stations are grouped according to certain criteria. In this paper, they were grouped by territorial proximity.

The monitoring data were taken from the yearbook of the state of the waters of the Neva Bay and the eastern part of the Gulf of Finland according to hydrobiological indicators in 2012 [5]. Figure 1 shows the location of the stations. For calculations, we take stations No. 6, 10 and 11 (highlighted in red).

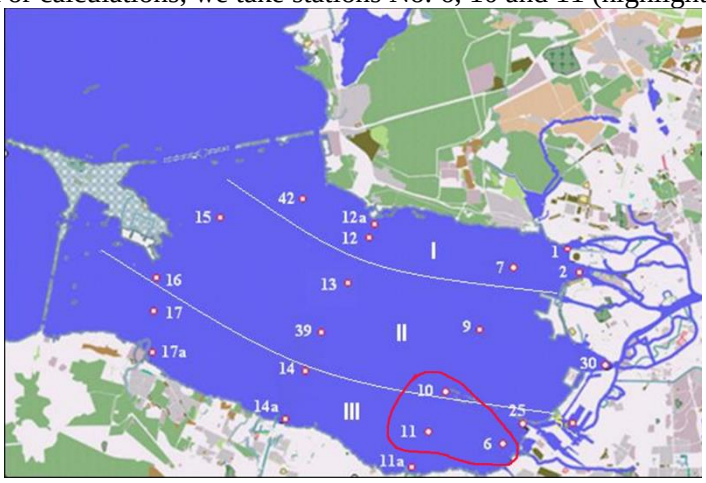

Figure 1. Location of stations in the Neva Bay

First, the coefficients $a_1, a_2, \beta_1, \beta_2$ are selected for the system (1). The selection of the values of the coefficients for the system (2) existing on the time interval T is carried out according to the following criteria:

1. $\forall x_1(t), x_2(t) > 0, t \in [0;T]$
2. $\forall x_1(t), x_2(t) < 10^6, t \in [0;T]$ (stability criterion)

Since a numerical method is used to solve the system, an "error" appears. The "error" value is calculated using the least squares method (LS). As theoretical values, monitoring data from all stations of the group are taken - y_1 for Cyanophyta, y_2 for Cyclopoida. The "error" is calculated using the following formula (3). x_1, x_2 are used as the calculated values. The final set of coefficients will be the set in which the "error" value will be the smallest.

$$\sum_{j=1}^{2}\sum_{i=1}^{n}\left(x_{ji} - y_{ji}\right)^2 \to \min \tag{3}$$

A set of coefficients is obtained for each station. An example of such a selection of coefficients for stations No. 6, 10, 11 is Table 1.

Table 1

Coefficients for stations No. 6, 10, 11

	a_1	a_2	β_1	β_2
Station No. 6	0.12	0.05	0.11	0.02
Station No. 10	0.07	0.07	0.03	0.04
Station No. 11	0.07	0.06	0.02	0.02
Mean value	0.09	0.06	0.05	0.03

For further modeling, these coefficients are averaged. The obtained values will be used in the construction of models based on the system "predator - prey with food" (2) to predict a possible "bloom". Next, you should select the values T_1, T_2 (coefficients affecting the time to reach the goal) for the target value - x^*. They are selected taking into account the following conditions:

1. $T_1, T_2 > h$
2. The goal is considered achieved if the condition - $\left|x_1 - x^*\right| \le 0.01 \cdot x^*$ (goal achievement criterion) is satisfied for a certain interval.

In a system with control (2), coefficient a_1 is a function of food $a_1(t)$; we take its value as the initial value for food $a_1(0) = a_1$. As an example, let us say $x^* = 20 \cdot x_1(0)$. The model built on the basis of the found coefficients and satisfying all the criteria described above is shown in Figure 2.

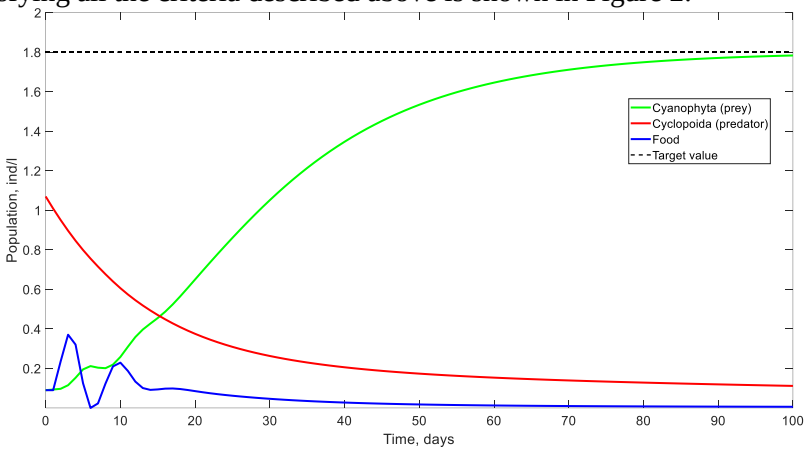

Figure 2. Model with control $\left(a_1(0) = 0.09, a_2 = 0.06, \beta_1 = 0.05, \beta_2 = 0.03, T_1 = 5.4, T_2 = 18\right)$

The next stage of the study is to study the maximum possible value of x^* for the obtained coefficients.

EXPLORING THE MAXIMUM VALUE OF x^*

To find the maximum value of x^*, at which the model meets all the criteria, the models were calculated using constant values of the coefficients $a_1, a_2, \beta_1, \beta_2$. Based on the data obtained, a histogram was built (see Figure 3) of the relative frequency of the value k - the magnification factor to obtain x^*.

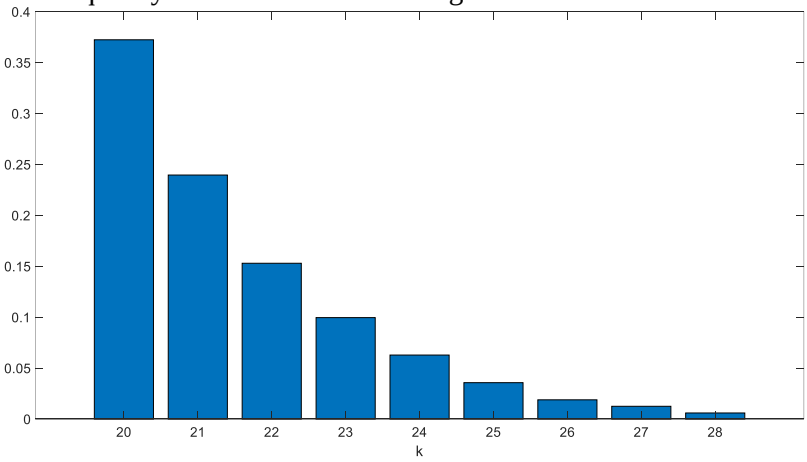

Figure 3. Histogram of values for models with control, built using the coefficients from Table 1

As can be seen from Figure 3, the maximum possible increase for a given set of coefficients is a 28-fold increase ($k_{max} = 28$). This value is acceptable, but not optimal, since in nature, during the "bloom", more significant increases in the prey population can be observed. It is of interest to study ways to increase the target value. The next section describes this method.

APPLICATION OF THE OUTLIER METHOD

As a method that would allow solving the problem of the limited increase in the population of preys, it is proposed to make an artificial outlier at one of the monitoring stations: in the second dimension of the Cyanophyta population, increase its value by n times. Then the data at such a station will look like this: $[y_{11} \quad n \cdot y_{12} \quad y_{13}]$.

The decision to use the outlier was made on the basis of the following observation: at station No. 10, the second dimension of the cyanophyte population is more than 800 times higher than the first dimension. At the same time, the coefficients obtained in groups including 10 stations, in a theoretical study, turned out to be more stable at different target values.

As theoretical research, the values of the second measurement at station No. 6 were increased by 5, 50 and 100 times. Further, the method of selection of coefficients, described earlier, was applied. For stations No. 6, 10 and 11, the following coefficients were obtained (Table 2).

Table 2

Coefficients for stations No. 6, 10, 11 at different values of outliers

	a_1	a_2	β_1	β_2
$n=5$				
Station No. 6	0.11	0.1	0.17	0.04
Station No. 10	0.09	0.1	0.31	0.02
Station No. 11	0.1	0.06	0.07	0.02
Mean value	0.1	0.09	0.18	0.03
$n=50$				
Station No. 6	0.26	0.04	0.35	0.01
Station No. 10	0.08	0.06	0.06	0.02
Station No. 11	0.18	0.04	0.15	0.01
Mean value	0.17	0.05	0.19	0.01
$n=100$				
Station No. 6	0.17	0.05	0.21	0.01
Station No. 10	0.1	0.09	0.37	0.01
Station No. 11	0.4	0.03	0.36	0.01
Mean value	0.22	0.06	0.31	0.01

Figure 4 below shows the results obtained. As can be seen from the figure, the maximum value of k has increased by about 3 times ($k_{\max} > 80$).

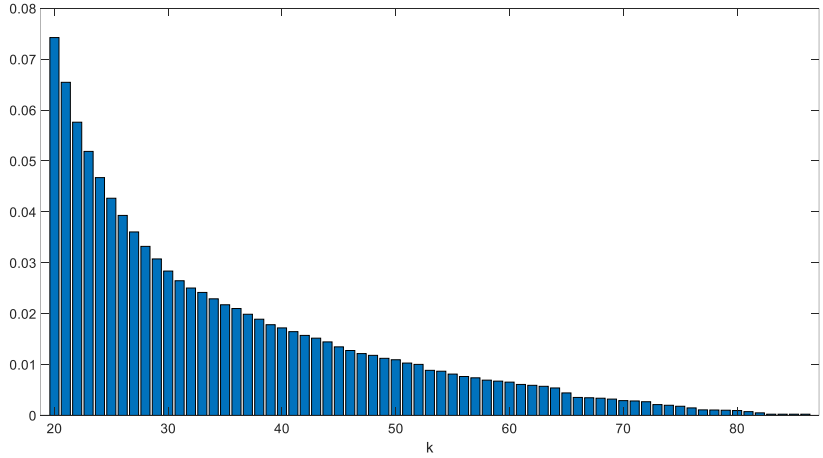

Figure 4. Histogram of values for models with control, built using the coefficients from Table 2

It can be concluded that the use of an artificial outlier at this group of stations made it possible to build stable models with a large value of k for calculating x^*, which makes it possible to simulate various variants

of the “bloom”. The data array obtained during the modeling is allowed to carry out a statistical analysis of the obtained models and compare the models without an outlier and with an outlier by a factor of 100.

STATISTICAL COMPARISON OF OBTAINED MODELS

Let us make a statistical comparison of the models for the group of stations No. 6, 10 and 11, obtained on the basis of the coefficients from Table 1 and Table 2 (outlier by a factor of 100). One of the important parameters for evaluating the model is the time to reach the goal. It is the first value $t_i, i = 1 \ldots N$, for which the goal achievement criterion is met. Let us designate this value as t^*. To determine the possible values of t^*, let us build histograms (see Fig. 5.1, 5.2), allowing you to clearly see this.

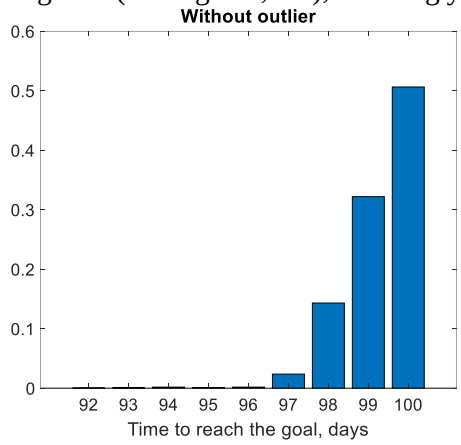

Figure 5.1. Histogram of values t^* for models with control, built using the coefficients from Table 1

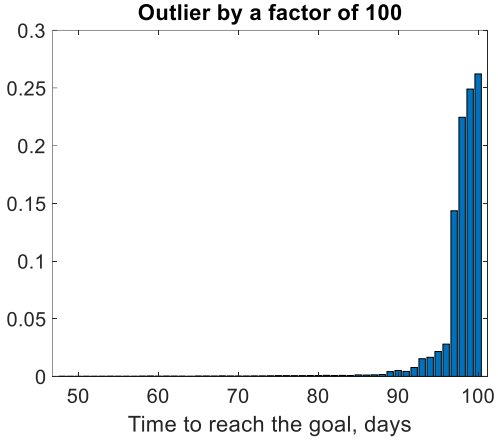

Figure 5.2. Histogram of values t^* for models with control, built using the coefficients from Table 2

As can be seen from Figure 5.1, for a set of coefficients found without an artificial outlier, in more than half of the cases, the time to reach the goal is practically equal to the entire time period, that is, $t^* \approx T$. Considering that the "bloom" most often occurs in August [8], such a time goal is possible and theoretically sound.

Figure 5.2 shows that the artificial ejection allowed increasing the range of values t^* by several times. Although small values of t^* are not as common as longer ones ($t^* > 90$), there are such values, and the resulting models satisfy all the criteria. An example of such a model with “quick” goal achievement ($t^* = 48$) is shown in Figure 6.

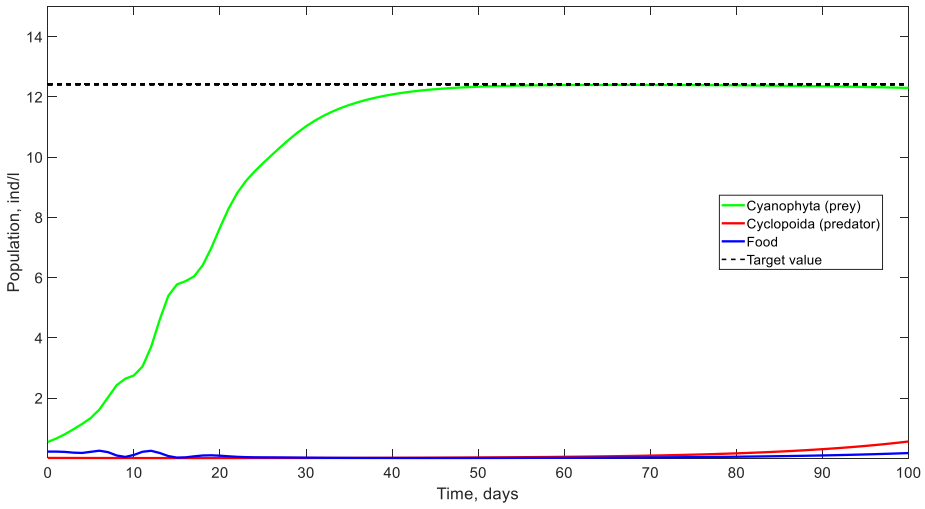

Figure 6. An example of a model with "quick" goal achievement

The next object of research is the establishment of the dependence of the value t^* on k (multiplicity of magnification $x_1(0)$). Figure 7 shows a tendency - with an increase in k , the time to reach the goal increases. This is because a larger difference between the start and target makes the transient response take longer as preys require more food to transition from one state to another.

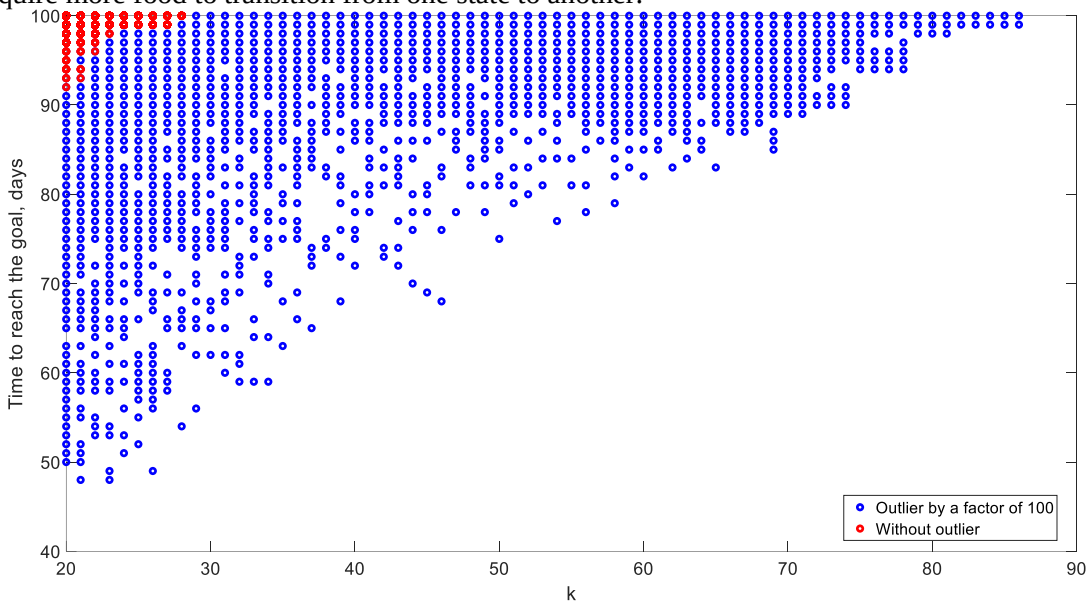

Figure 7. Scatter plot for t^* and k

The last object of research on the time to reach the goal is the study of its dependence on $x_1(0)$ and $x_2(0)$. In Figure 8.1 it can be seen that with an increase in $x_1(0)$, the value of t^* decreases in both sets of the coefficients, i.e. there is an inverse proportionality. However, knowing from Figure 7 that t^* is also influenced by the value of k , we can conclude that with selected $x_1(0)$ and k it is possible to achieve the most optimal value of t^*. Figure 8.2 shows that as $x_2(0)$ increases, the value of t^* decreases in both sets of the coefficients. This is explained by the fact that the more predators, the more preys they can eat and reproduce (since in the "predator-prey" system all the eaten biomass of preys passes into the biomass of predators [4, p. 24]. Accordingly, the more predators, the slower preys multiply.

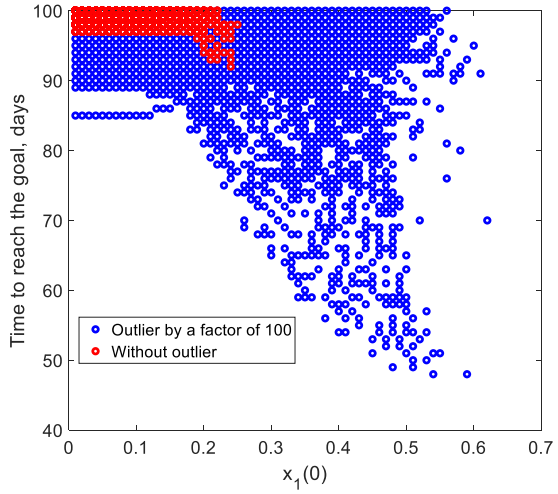

Figure 8.1. Scatter plot for t^* and $x_1(0)$

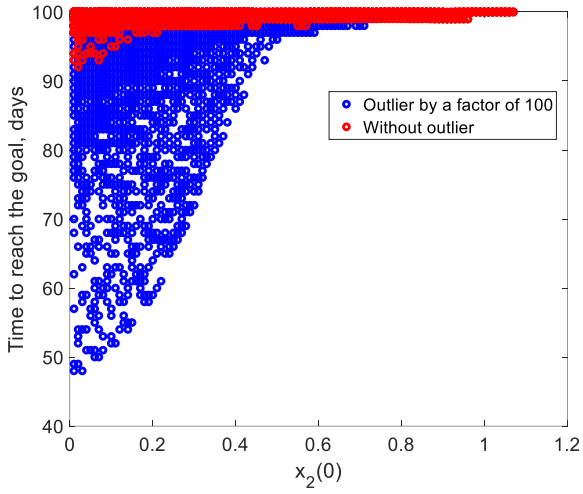

Figure 8.2. Scatter plot for t^* and $x_2(0)$

The next important issue is to establish the ranges of possible values for $x_1(0)$ and $x_2(0)$, since in nature the population of Cyanophyta and Cyclopoida is constantly changing and the model must meet all criteria when changing its initial values. For this, box plots were built (see Fig. 9.1, 9.2).

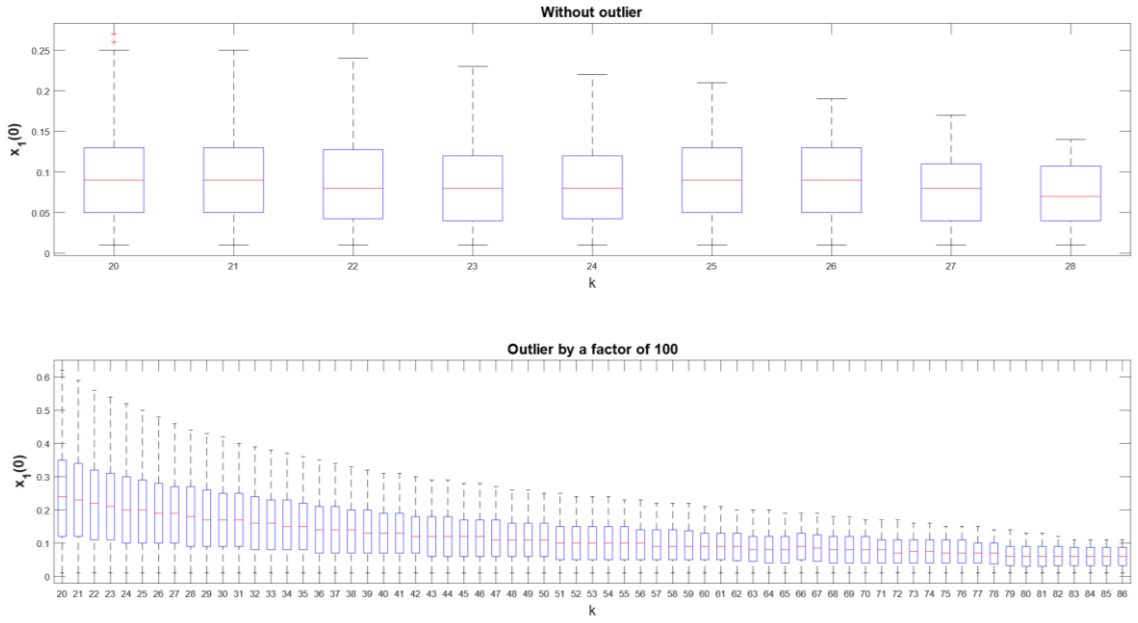

Figure 9.1. Box plot for $x_1(0)$

In Figure 9.1, you can see that as k increases, the upper range of $x_1(0)$ values decrease in both sets of models. This is due to the fact that, as mentioned earlier, the larger k, the longer it will take to reach the t^* target, respectively, the predators have much more food in the form of preys, which affects their reproduction rate. The constant increase in the rate of reproduction of predators leads to an exponential increase in the population of predators. From Figure 9.2, you can see that the upper range of $x_2(0)$ values also decrease with increasing k. This can also be explained by the fact that at higher values, the predator population will grow exponentially. Such models are likely to fail to meet the sustainability criterion. All this indicates an additional restriction on the initial values of the model, which should be taken into account in the simulation.

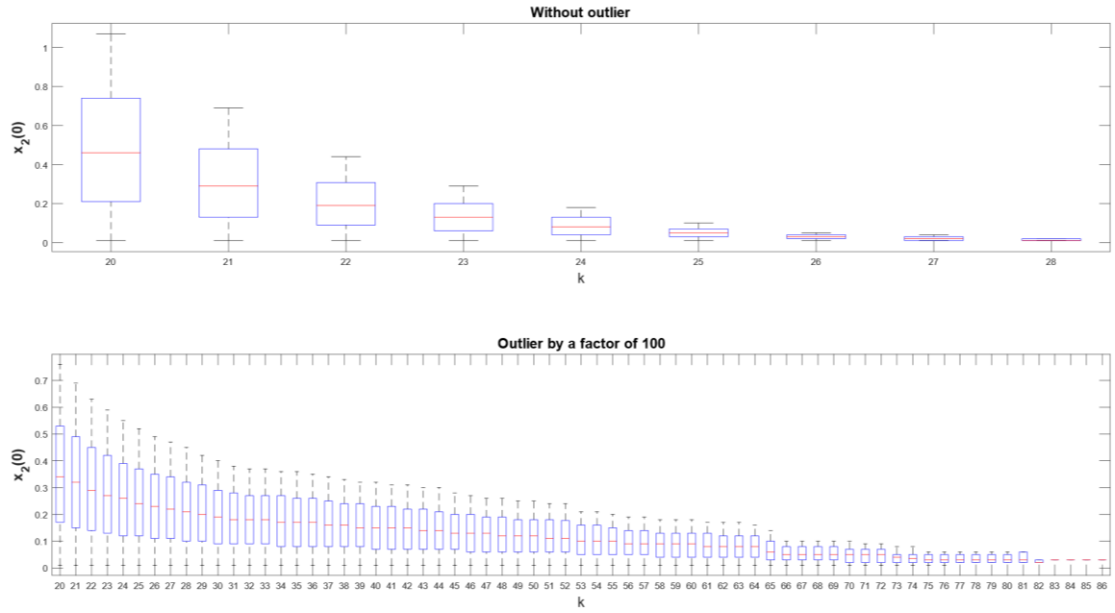

Figure 9.2. Box plot for $x_2(0)$

Summing up the results of a statistical comparison of the two sets of coefficients, we can say that both sets are generally similar in their behavior (decreasing the ranges of values of $x_1(0)$ and $x_2(0)$, decreasing t^* with the growth of $x_1(0)$, increasing t^* with the growth of $x_2(0)$, etc.). The main difference between the two sets is the different range of k values. Some of the behavioral features of the models are explained by the peculiarities of the "predator-prey" system, while others have biological patterns.

CONCLUSION

The paper considers a method for selecting coefficients based on monitoring data, which makes it possible to find sets of coefficients by which it is possible to build stable models described by a system with control (2). The method of artificial outlier is also considered, which allows finding the coefficients at which it is possible to build models with a larger target value. A statistical comparison of the obtained sets of coefficients and models is carried out. Conclusions are drawn about the behavior of the models for different parameters.

REFERENCES

1. Lotka A. J. Contribution to the Theory of Periodic Reaction // The Journal of Physical Chemistry A. 1910. №3. p. 271-274.

2. Shchegoleva A. The mathematical model of the biological system "predator-prey with food" // Bulletin of the UNESCO department "Distance education in engineering" of the SUAI: Collection of the papers. SPb: SUAI, 2020. p. 112-117.

3. Volterra V. Variations and Fluctuations of the Number of Individuals in Animal Species living together // ICES Journal of Marine Science. 1928. №3. p. 3-51.

4. Bazykin A. D. Mathematical biophysics of interacting populations // Nauka, Moscow, 1985. 181 p.

5. Ezhegodnik sostoyaniya vod Nevskoi guby i vostochnoi chasti Finskogo zaliva po gidrobiologicheskim pokazatelyam. T. 2: 2012. - SPb.: FGBU «Sankt-Peterburgskii TSGMS-R», 2013. – 352 c.

6. Kolesnikov A. A. Synergetics and problems in control theory. M: FIZMATLIT, 2004. 504 p.

7. Kolesnikov A. A., Kolesnikov A. A., Kuz'menko A. A. The ADAR Method and Theory of Optimal Control in the Problems of Synthesis of the Nonlinear Control Systems // Avtomatizatsiya, Upravlenie, 2016, vol. 17, no. 10, pp. 657—669.

8. Lavrova O.Yu., Soloviev D.M., Strochkov A.Ya., Shendrick V.D. Sputnikovyi monitoring intensivnogo tsveteniya vodoroslei v Rybinskom vodokhranilishche // Sovremennye problemy distantsionnogo zondirovaniya Zemli iz kosmosa. 2014. №3. p. 54-72

DIAGNOSTIC SYSTEMS BASED ON THE ROBOTIC COMPLEX

Maria Sozdateleva

Saint-Petersburg State University of Aerospace Instrumentation,
Saint-Petersburg, Russia
E-mail: macreatoor@yandex.ru

Abstract. This article discusses a robotic complex that allows you to assess the technical condition of ventilation systems. Methods and means of obtaining data on the state of the ventilation pipeline are described. The parameters under study are: ambient temperature, composition and flow rate of air masses, as well as pressure. The advantages of using a robotic complex regarding existing methods of diagnostics of ventilation systems are presented.

1 INTRODUCTION

Automation is one of the most important factors in increasing productivity and improving working conditions. The methods of work used make it possible to achieve lower costs, not only financial, but also time and human resources, both in mass production conditions, and in individual conditions.

Inspection of engineering systems or assessment of their technical condition is a set of measures carried out to assess their current state and functional capabilities, the compliance of the structure of engineering systems with the existing design and as-built documentation, applicable rules and regulations, as well as the suitability of engineering systems for further operation, modernization or repair [1-3].

The concept of pipeline diagnostics consists in the desire to obtain information about the technical state of the system, including such types as information about the environment and objects of man-made origin, transported fluids and the state of protective systems (external and internal coatings, inhibitor protection, etc.) [4].

Depending on the purpose of the pipeline, the method of its laying, the main negative factors of degradation and the risks associated with its operation, one or several types of information on the technical condition may be prioritized over others.

Ensuring the efficient operation of ventilation systems is one of the main tasks that contribute to improving working conditions, increasing productivity, and minimizing industrial injuries.

The effective operation of systems largely depends on high-quality and timely diagnostics.

Diagnostics of ventilation systems can be carried out for the purpose of prevention, that is, to confirm the compliance or non-compliance of this ventilation system with the current regulatory and technical documents, to detect problems in the system, the purpose of which is to find out the cause of the problem and its subsequent elimination [5].

Today, there are two ways to service ventilation systems: a complete analysis of the structure, or diagnostics is carried out using a device equipped with a camera and an air flow sensor, lowered into the ventilation shaft at a limited distance.

The scope and content of diagnostic measures are regulated by the type of ventilation. There is supply, exhaust, supply and exhaust, duct ventilation systems and others. Supply and exhaust aeration is often used, since such a system must simultaneously supply fresh air and extract exhaust air.

The method of diagnosing the state of ventilation implies the determination of such parameters as: ambient temperature, air flow rate of air masses, as well as humidity and air composition.

The robotic complex is a set of electric drives for moving in all directions of the ventilation pipeline, as well as a set of sensors for the functioning of the data collection algorithm, such as: atmospheric pressure of the environment, air mass flow rate, air quality, temperature.

The use of this robotic complex will make it possible to carry out diagnostic measures eliminating the need to dismantle ventilation systems, which in turn will allow to spend less resources, such as time, finances, man-hours, and will also provide the operator with the opportunity to supervise the diagnostic process remotely, which is significant and a priority factor in systems that are dangerous or difficult to reach for humans [6].

High humidity and high pressure are taken into account when designing the robot and choosing materials. The model was built in the SolidWorks environment and is shown in Figure 1.

2 SIMULATION

Solid modeling begins with an analysis of the outer diameters of the ventilation ducts and the minimum diameter of the robot. The design of the housing takes into account the space for the actuators and the technological openings for the sensors and buttons.

On the sides of the body there are 8 cutouts for retractable drives with wheels for movement. Technological holes for wiring are made inside the crosspiece. The body covers are flat without a conical shape to increase aerodynamic properties.

Since it is necessary to measure the speed of the air flow and its composition, it is impossible to allow the flow to envelop the body with less friction and a drop in speed. The body and covers are made symmetrically so that the operator can install and operate the robot in any position.

The mechanisms for moving the robot inside the ventilation duct are shown in Figure 2, they combine a worm gear used to increase the length of the robot's leg, at the end of which a gear wheel is installed, which has a specific shape to minimize the size and weight of the robot, as well as end sensors. When unfolded, the wheel span reaches 440 mm.

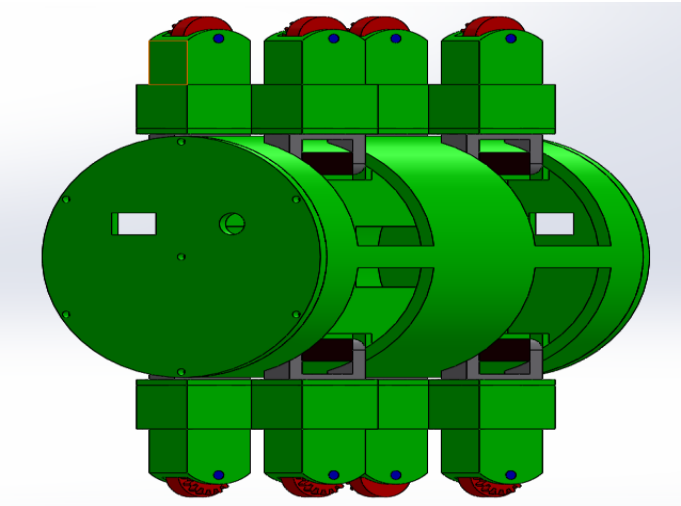

Fig. 1 *General view of the unfolded robot*

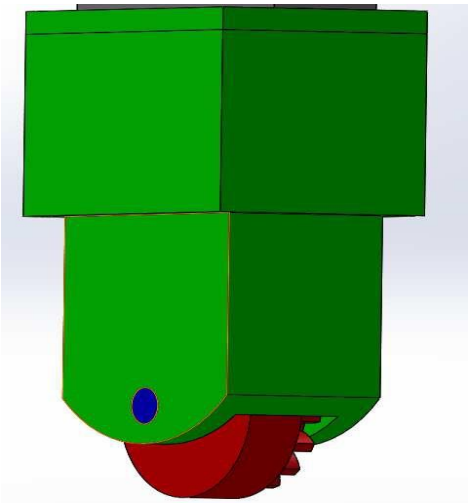

Fig. 2 *Unfolded state of the robot leg.*

The robot deployment process follows the following algorithm [12]:

```
void go () { btca2a.ReadCommand();
if (btca2a.ButtonPressed (BUTTON_L)){
servo.write(180);
DANGER = 1; delay (3000); }
if (btca2a.ButtonPressed
(BUTTON_R)){ servo.write(0);
DANGER = 0; delay (3000); }
If (btca2a.ButtonPressed (BUTTON_A) &&        DANGER=1){
analogWrite(PIN_ IN1, 255);
analogWrite(PIN_ IN3, 255);
digitalWrite(PIN_ENA, 1);
analogWrite(PIN_ IN2, 0);
analogWrite(PIN_ IN4, 0);
digitalWrite(PIN_ENB, 0);}
```

The use of a gearbox makes it possible to supply an engine of lower power and dimensions, since the torque on the shaft will be increased inversely with the decrease in speed. To study aerodynamic properties, the package of add-ons SolidWorks Flow Simulation [7,8] is used.

To study the air flow, its speed, pressure and temperature, additional plugs are created, which reduce the investigated volume and facilitate calculations [11].

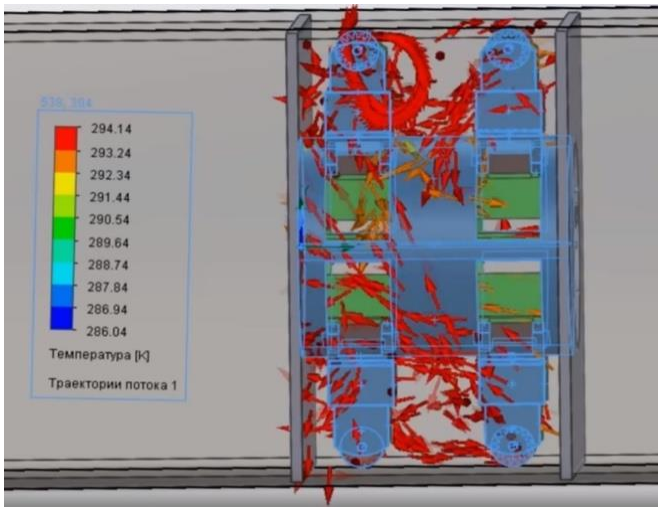

Fig. 3 *Temperature Graph in Flow Simulation.*

According to the study presented in Figure 3, it can be seen that the increase in air temperature is insignificant and at the peak is equal to 2 degrees. The movement of air shows that the maximum temperature rise occurs in the area of the wheels due to the absence of cutouts.

Based on the results of the study [9,10] (Fig. 4), the pressure exerted on the robot does not exceed 160 kPa or 1.6 atmospheric pressure.

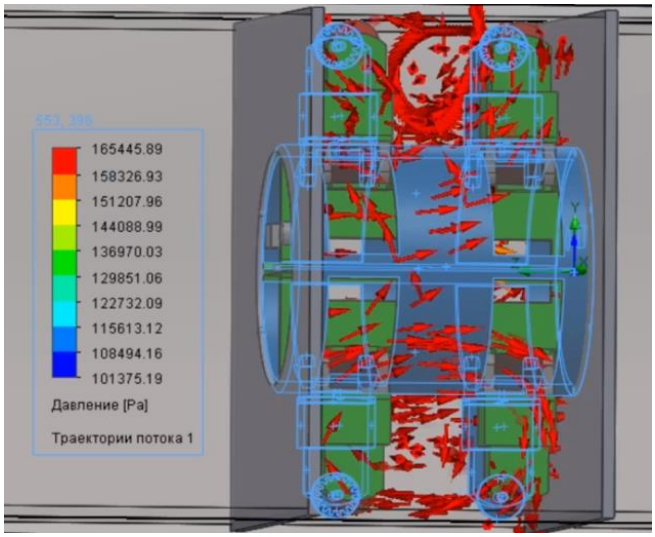

Fig. 4 *Pressure Plot in Flow Simulation*

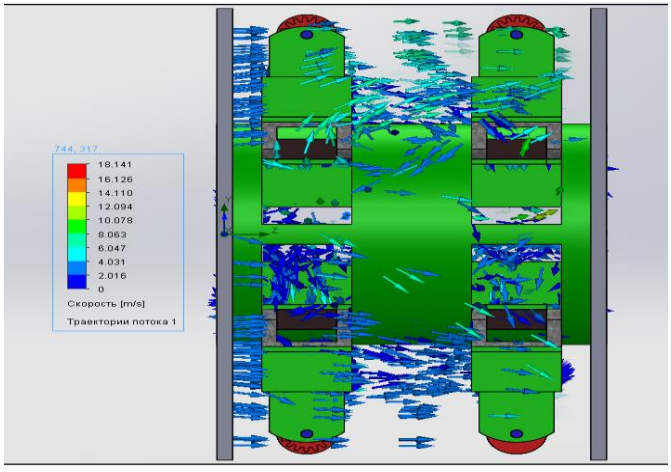

Fig. 5 *Plot of air flow rate in Flow Simulation*

The simulation results presented in Figure 5 showed that the highest speed value falls on the central part of the hull, where there are practically no obstacles and is equal to 4 m / s. Due to the swirl of air inside the case, a force appears that presses it against the upper wall of the ventilation duct.

3 CONCLUSION

Automation of the process of diagnostics of ventilation systems will increase economic efficiency, improve working conditions, the introduction of such a robotic complex will allow collecting more voluminous and accurate data on the technical condition of ventilation systems, as well as minimizing human participation in diagnostic activities.

The gradual introduction of cyber-physical systems into technological production processes already in the current production conditions will allow expanding markets and increasing the competitiveness of various sectors of the economy. Fundamentally new, breakthrough technologies should become instruments for such a transformation. This place will be taken by technologies such as: 3D printing, robotization, the Internet of things, digital platforms.

Combining all these technologies within a single concept allows us to imagine the production of the future: a fully integrated and optimized workflow with significantly increased efficiency, as well as the distance between man and machines in heavy production areas: complete replacement of man with machine labor, replacement of some of the simplest work positions with standard operations by robotic systems capable of independent interaction with each other in real time.

REFERENCES

1. GOST R 53778-2010: Buildings and structures. Inspection rules for monitoring technical condition;
2. SP 255.1325800.2016 - Buildings and structures. Operating rules. Basic provisions;
3. GOST R 58033-2017 - Buildings and structures. Dictionary. Part 1. General terms
4. SNiP 3.05.05-84. Process equipment and process pipelines;
5. SP 336.1325800.2017: Ventilation and air conditioning systems. Operating rules;
6. Berbyuk VE Dynamics and optimization of robotic systems / V.E. Berbyuk. - M .: Naukova Dumka, 2014 .-- 192 p .;
7. SolidWorks. Computer modeling in engineering practice / A.A. Alyamovsky and others - M .: BHV-Petersburg, 2016 - 800 p .;
8. Alyamovsky, Andrey SolidWorks Simulation. How to solve practical problems / Andrey Alyamovsky. - M .: BHV-Petersburg, 2011. - 486 p .;
9. Dudareva, Natalya Self-study guide SolidWorks 2010 / Natalya Dudareva. - M .: BHV-Petersburg, 2010 .-- 215 p .;
10. Ponomarev, Nikolay SolidWorks 2007/2008. Computer modeling in engineering practice / Nikolay Ponomarev. - M .: BHV-Petersburg, 2010 .-- 591 p.; M
11. Solyony, S.V., Solyonaya, O. Ya., Kulikov, D.D. / Theoretical foundations for the development and modeling of individual simple modules and mechatronic systems // teaching aid, SPb .: GUAP. - 2018. - 153 p.
12. Certificate of state registration of the computer program 2020662373 Russian Federation. Robotic complex control program for diagnostics of ventilation systems / Solyoniy, S.V., Sozdateleva, M.E. ; copyright holder Federal State Autonomous Educational Institution of Higher Education "St. Petersburg University of Aerospace Instrumentation" - No. 2020662373; publ. 10/13/21 - 1s.

HARDWARE AND SOFTWARE COMPLEX FOR CARRYING OUT FIELD EXPERIMENTS WITH THE LORAWAN NETWORK

Nikita Stepanov

Saint-Petersburg State University of Aerospace Instrumentation,
B.Morskaya 67, 190000, Saint-Petersburg, Russia
E-mail: Leos29-07@yandex.ru

Abstract
This paper proposes a technique for conducting experiments on a small number of devices to evaluate systems with a large number of devices. A software package for evaluating the functioning of LPWAN (Long Range Wide-Area Networks, LoRaWAN) networks is presented. An example of the operation of this software package in relation to the LoRaWAN network is shown to assess the probability of message delivery from the number of devices to the base station when implementing this technique. And also the conditions for the successful reception of messages in the LoRaWAN network are determined, taking into account the overlap of messages from different terminal devices. This technique can be used to assess the efficiency of other LPWAN networks.

Keywords*:* software, LPWAN, Packet delivery ratio, create model, analysis of experiments, describes the method, LoRa, Queueing Systems.

INTRODUCTION

The key parameter for assessing the efficiency of the system is the probability of successful delivery of packets from the number of end devices to the base station. To estimate this probability, both calculations in simplified models and the results of real experiments can be used. However, real experiments cannot be carried out on a large number of devices. This section describes a technique that allows using a real experiment to evaluate the operation of a real system in a ratio of 4: 1000, i.e. replacing with 4 end devices in the experiment 1000 end devices of a real system.

More details about the scenario are described in the next section. At the same time, using end devices of class A in the unacknowledged mode and an adaptive rate adjustment (ADR) mechanism for the purity of conducting experiments. Then the rationale for using this method to organize the experiment is carried out. The following is a description of the methodology and analysis of message overlaps. The results of experiments are presented. In conclusion, conclusions are drawn from the research carried out.

LORAWAN TECHNOLOGY DESCRIPTION

LoRaWAN network consists of one network server, one or more base stations and end devices. All data sent by the end device goes through the base station to the network server and vice versa. End devices, depending on the state of the radio channel between them, can use one of several quasi-orthogonal spreading factors for communication. Essentially, choosing a quasi-orthogonal spreading factor allows the device to trade airtime (and hence power consumption) for range. End devices usually use an ALOHA-like media access mechanism, randomly choosing one of the supported network channels. In Europe, LoRaWAN networks are typically deployed in the unlicensed industrial, scientific and medical 868 MHz band. It is important to note that unlike many other LPWAN technologies, LoRaWAN networks can be deployed not only by telecom operators (so-called "public" networks), but also by private organizations and individuals (so-called "private" networks).

Rationale for using an approach to organizing an experiment

Let all end devices have the same SF, which is selected in such a way that, in the absence of overlaps, messages are successfully delivered to the base station. In this case, you can use the upper (formula (2)) and lower (formula (1)) bounds for the probability of successful delivery.

$$Pr\{T = t_{mes.}\} = e^{-\lambda N 2t}, \quad (1)$$

where T is the length of the interval in which messages from other end devices did not appear.

$$Pr\{T = t_{mes.}\} = e^{-\lambda N t}. \quad (2)$$

It can be seen from formulas (1) and (2) that the product $tN\lambda$ affects the probability of successful delivery. In real systems, the message transmission interval from one terminal device $T_{r.}$ = 10 minutes can be used. Hence the intensity of message transmission $\lambda_{r.}$ = 1/600. Within the framework of the system under study, real end devices should be $N_{r.}$ = 10000, hence the product $tN\lambda$ is equal to:

$$t_{r.}N_{r.}\lambda_{r.} = 68700, \quad (3)$$

where $t_{r.}$ is the duration of the short burst is $4.12 \cdot 10^{-4}$ s. (10 bytes) [1]

These parameters of a real system meet the characteristics of the base station [2] and end devices.

The experiment should reduce the retransmission time of messages and increase the length of the message. Taking into account the limitations of the configuring firmware and the characteristics of the end devices, the interval between the transmission of messages from one device $T_{e.}$ = 7 s. [1]. From this we obtain the intensity of message transmission $\lambda_{e.}$ = 1/7, the number of end devices $N_{e.}$ = 41. The values of the products $tN\lambda$ for the experimental system and the real system should be approximately equal:

$$T_{\text{e.}}N_{\text{e.}}\lambda_{\text{e.}} \approx t_{r.}N_{r.}\lambda_{r.}, \quad (4)$$

where $t_{e.}$ is the duration of the long burst is $1.18 \cdot 10^{-5}$ s. (64 bytes) [1].

Thus, simulating a large number of message overlaps in a real system, we obtain a ratio of one terminal device in the experimental system to the number of terminal devices in a real system of the order of approximately 4: 1000.

Description of the methodology and analysis of message overlaps

This technique will allow you to determine the conditions for successful reception for a scenario when the signal strength from all end devices is the same, and all end devices use the same SF. They are configured according to the script from the first section. Where the uplink transmission period will be 7 seconds to obtain an intensity similar to that in real systems for a given number of endpoints. However, there is no way to simulate a fixed delay. A large number of end devices will increase the likelihood of overlapping messages in the channel, due to this, the results will be closer to the real system. As part of the experiments, we will assume that all end devices are located in the same radio conditions, since they are located close to each other.

The message overlap analysis was performed in several stages:

1. Obtaining a set of time stamps for each end device. Each timestamp indicates the end of reception of a transmission at the base station from a specific end device.
2. Interpolation of the end time stamps of the transmission of messages that were not received at the base station.
3. Search for each packet for the nearest packet by the time stamp value from the sets of successfully transmitted and interpolated packets.
4. Checking the presence of the fact of intersection by the formula (5). If the difference between the values of the time of receiving the considered packet (T) and the packet closest to it (T_i) is less than the message transmission time (t), then an overlap has occurred.

$$x_i = |T - T_i| < t. \quad (5)$$

5. Determination of the area of overlap by the difference in the values of the time of receiving packets.
6. As a result, one of the counters of a certain area increases. The counter of not received messages is incremented if the packet in question was from the interpolated set. And vice versa, the counter of successfully received messages is increased if a packet from the set received from the base station was considered.

EXPERIMENTAL RESULTS

To test this technique, the following equipment was used: base station RisingHF Type: RHF2S008 [2] and Vega SI-11 - pulse counter [1]. As a result of experiments with the number of end devices on the order of 20, a histogram of the group probability is obtained when only the first packet is transmitted. Figure 1 clearly shows the offset from zero to the right, since in this case the interfering packet was transmitted later.

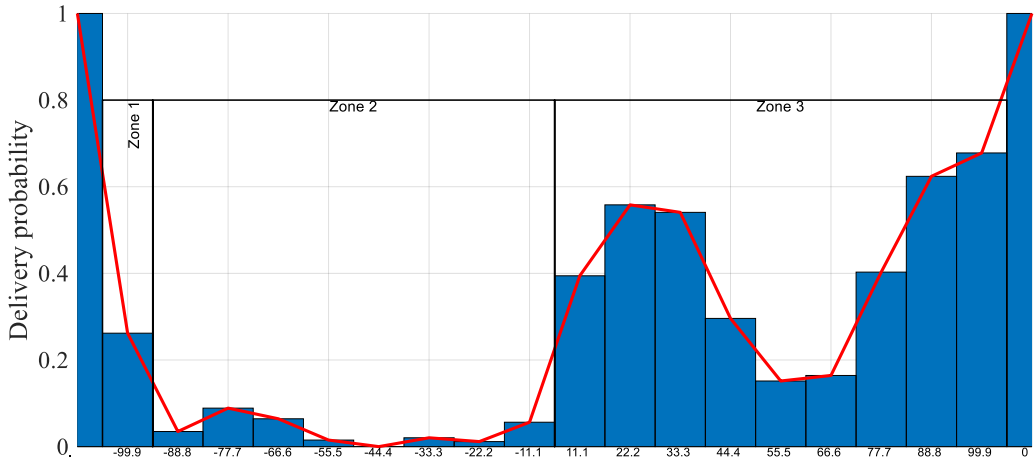

Figure 1. *Probability of successful delivery relative to the overlap site*

The results are close to the results from the following papers [3], [4]. The presence of zone 2 is primarily due to the fact that after the start of packet transmission, the base station becomes inactive to receive new frames. As a result, packets are lost during 8/9 t. In one of the works [5], a similar statement is given.

CONCLUSION

The proposed model will clarify the theoretical formula for the probability of successful message delivery when two packets overlap for more network webs.

In the future, it is planned to continue research to clarify the behavior of the network when overlapping more than two messages. Since the proposed methodology allows us to study the effect of overlapping messages from different end devices on the success of message reception by the base station.

The proposed technique can be generalized to a more general scenario, when the signal strength from different end devices at the base station is different, which leads to the need to use different SF values for different end devices.

REFERENCES

1. Vega Absolute: LoRa Equipment. URL: http://iotvega.com/product/si11 , [Online; accessed 30-March-2020]

2. AuroraEvernet: Equipment LoRa. URL: http://www.auroramobile.ru/product_855.html [Online; accessed 30-March-2020]

3. Haxhibeqiri, J. Lora scalability: A simulation model based on interference measurements / J. Haxhibeqiri, F. Van den Abeele, I. Moerman, J. Hoebeke//Sensors. 2017. T. 17, №. 6, C. 1193.

4. Sørensen R. B. Analysis of LoRaWAN Uplink with Multiple Demodulating Paths and Capture Effect / R. B. Sorensen, N. Razmi, J. J. Nielsen, P. Popovski // ICC 2019-2019 IEEE International Conference on Communications (ICC). IEEE. 2019. C. 1-6.

5. Rahmadhani A. When LoRaWAN Frames Collide / A. Rahmadhani, F. Kuipers // Proceedings of the 12th International Workshop on Wireless Network Testbeds, Experimental Evaluation & Characterization (ACM WiNTECH 2018). 2018. C. 89-97.

SEM IMAGE PROCESSING TO CHARACTERIZE NANOPARTICLE ENSEMBLE

Vitaly Studzinsky

Peter the Great St.-Petersburg Polytechnic University,
St. Petersburg, Russia
E-mail: svm.fl@mail.ru

Abstract
A SEM image processing method to derive properties of an ensemble of nanoparticles on various substrates is presented. This method allows determining the number and size distribution of nanoparticles. Method is based on precise analysis of shades grade and additional tools. Derived distributions allow assessing the impact of different modifications on nanoparticle transformation.

Introduction

The assembly of functional nanomaterials using bottom-up techniques for controlling the patterns of the nanomaterials, is extremely useful in many micro and nanoscale electronic, optical and biological applications. The patterning of nanoparticles, apart from fabrication techniques, relies on the selected substrate and the interaction of nanoparticles with the substrate. One of the popular techniques to form metallic nanoparticles on substrates is via dewetting of metallic thin films, which has gained much attention due to their novel physical and chemical properties [1-4]. The average size and separation of metal nanoislands can be moderately controlled with the initial thickness of a thin metal film [5].

To analyze a structure of nanoparticles on a surface, it is necessary to estimate the size and number of different particles. Scanning electron microscopy (SEM) is widely utilized to study structure and peculiarities in the sub-micro scale. If there are several particles appear in the SEM image, their number and size can be derived manually, but in the case there are a large number of particles, manual counting will take waste of time. On the other hand, counting the number of gold particles and deriving their size distribution are regular enough problems to automate this routine process. Indeed, in some cases it also could be impossible to find separated nanoparticles in the image. In such a case, that for example frequently appear during deposition of thin gold layer on different substrates, sample surface looks like a blanket with some cut gaps. In this case, particle counting cannot be performed due to the absence of the particles themselves. Of the most imterest is a variant of the surface of film in the form of separated islands. Analyzing this kind of islands seems to be the most difficult task among mentioned above, as information on the size distribution of particles is important to study various phenomena related to thin film formation and transformation processes. For example, this way one could investigate the effect of temperature [6] or ion-beam irradiation parameters [7, 8] on thin film dewetting on various substrates. This contribution describes the simple and robust way to analyze properties of nanoparticle distribution appears on various substrates using SEM image analysis.

Methods

Let us consider the way to analyze nanoparticle features as revealed by SEM investigation. For processing, we will use the Image pro plus software package [9]. This package allows some methods to separate and count particles while varying the parameters by which it separates particles from the background and from each other. We will discuss automation technique that allows make meaningful analysis rapidly. As an example, an image taken from a sample on the surface, on which silicon nitride and gold are deposited in layers, after irradiation with a dose of 10^{-14} cm^{-2}, will be processed further.

First let us briefly describe possible features that could appear in the SEM images. Fig. 1 presents typical images obtained from different gold nanoparticles deposited onto the Si surface. Fig. 1 (a), and (b) presents separated large and small particles as bright spots. They are bright due to strong secondary electron emission form gold in compare to silicon substrate. Gold film in the Fig.1 (c) is not fully separated, as it happens in the case of relatively thick deposited layers. Indeed, nanoparticles are not formed in this case, but covered fraction can be a measured parameter. On the other hand, one can distinguish separated islands in the Fig.1 (d), where gold layer is of intermediate thickness.

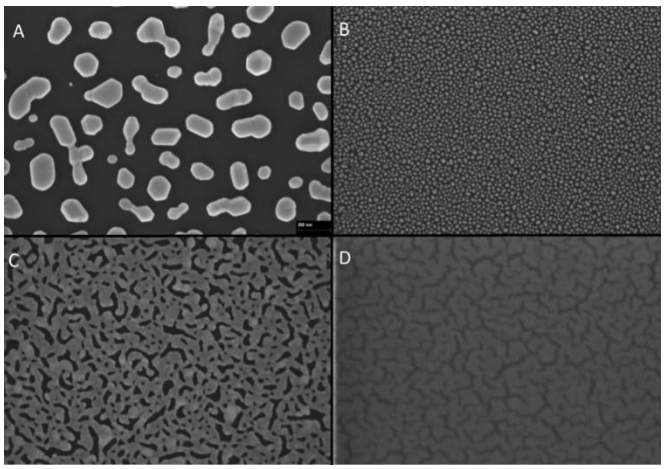

Figure 1. Various types of gold nanoparticles deposited onto the surface of Si.

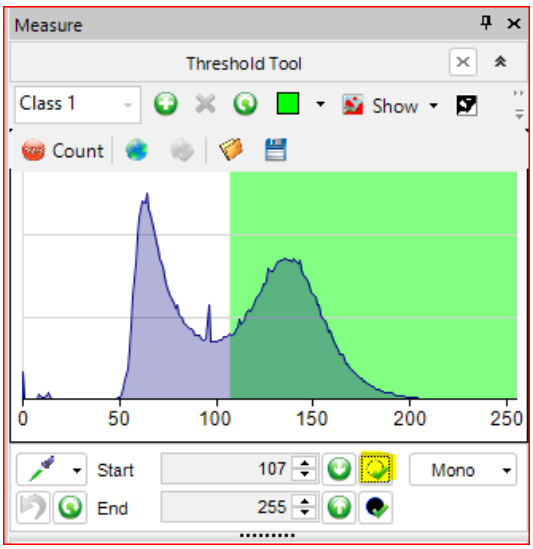

Figure 2.Choice of gray level threshold made to compose the mask and the number of pixels of this shade.

The following is an algorithm derived to select processing parameters. Processing is based on the information that silicon (silicon nitride or other substrate) in the electron microscopy image will looks darker, since it emits much less secondary electrons compare to gold, which will be bright. Therefore, for the nanoparticle analysis, we will choose the counting of white particles (Fig. 2). Figure 2 shows the pixel number distribution vs. their shade within the digital range from 0 to 255. It is seen from the Fig. 2 that pixel distribution is bimodal with one (bright) peak corresponding to areas occupied by nanoparticles, whereas second (dark) comprise pixels reflecting uncoated substrate surface. The problem is how to distinguish the threshold value that corresponds to boundaries of nanoparticles. It is obvious that it is situated in between these peaks. Green area in the Fig.2 denotes the part of distribution that will be masked as particles. The tool shown in the Fig. 2 let user edit boundaries of the pixel color that will correspond to a nanoparticle by choosing corresponding window position and width. After window selection, image will be automatically divided into particles. However, automatic mask application raises various defects. Below we will discuss possible defects and ways to solve them.

For example, there is often a case when particles of the selected brightness are not covered by the mask (fig.3a). This problem can be solved by proper changing the boundaries of the shade of the mask in the monochromatic case (fig. 2).

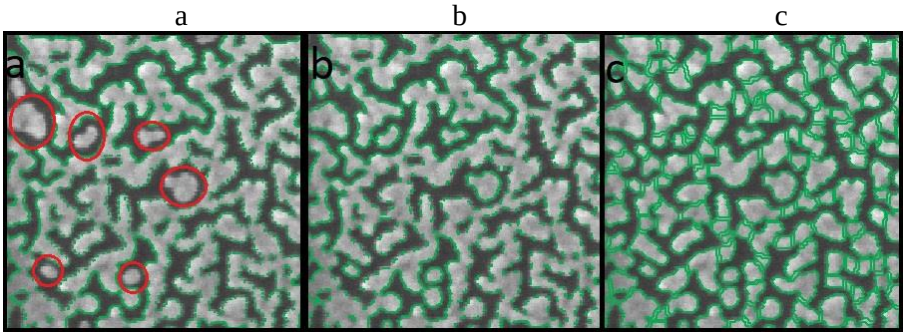

Figure 3. Masks applied onto SEM images for particle number and shape analysis. Mask composed with missing nanoparticles (a), good mask (b), and mask drawing extra-boundaries (c) overestimating number of nanoparticles.

Also, this problem can be caused by a shift in the grain counting boundary (fig. 4). In addition to changing the boundaries, you can see the particle size distribution in this dialog box. This option allows you to exclude large debris or small image ripples from the particle count.

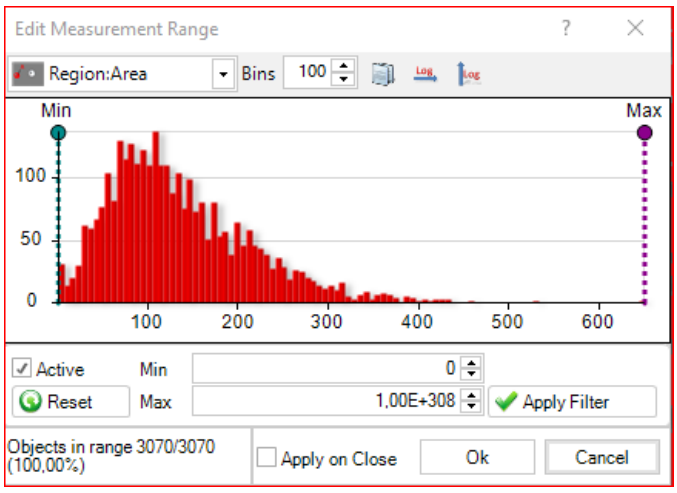

Figure 5.window for setting the size of particles included in the mask.

Problem that is illustrated by the Fig. 3b is associated with the difficulty of determining the boundaries of particles that are not separated from each other at a short distance. To solve this problem, the split tab has a ridge size option that determines the radius of the circle. If this circle does not fit on the edge of the particle, then the program outlines the border, the lower the value of this parameter, the smaller the connection of two particles is enough to recognize them as one particle. In figure 3 b and c, you can look at mask area, but with different values of the ridge size parameter (fig.3b ridge size 1, fig.3c ridge size 50). After selecting all these parameters, this software package allows you to export data in table format about grain size in pixels. After recalculation, this data can be used to build distributions and analyze result.

For further analysis, it is necessary to take into account the size of the image and the size of the individual pixel. Below you can see an example of the finished processing of SEM images of folding samples with a gold film at various temperatures in the atmosphere, figure 6.

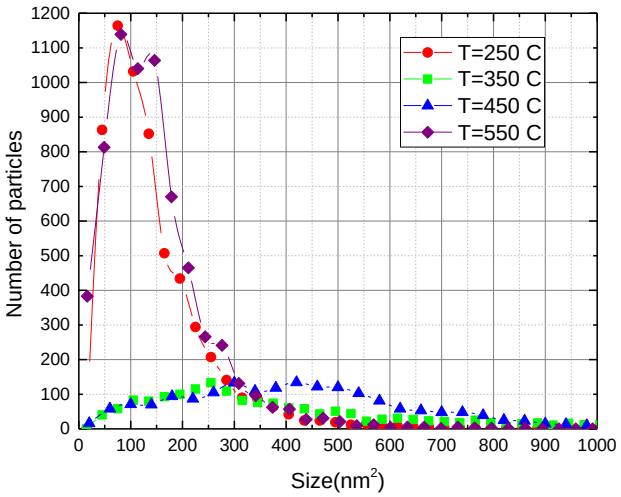

Figure 6.Size distribution of gold particles upon annealing in the atmosphere at different temperatures, the thickness of the gold layer is 1nm.

In addition, this method allows us to notice the difference in the degree of influence of various methods of obtaining nanoparticles from thin films (fig.6, fig.7). In Figure 6, you can see from the distribution that at 250 degrees there are a large number of small nanoparticles. Annealing temperatures up to 350 and 450 degrees lead to a smoother distribution. This is to say that the nanoparticles are assembled into rather large nanoparticles, but the sizes of the particles are different and modes cannot be distinguished. A further increase to 550 results in the return of the distribution of a large number of small nanoparticles.

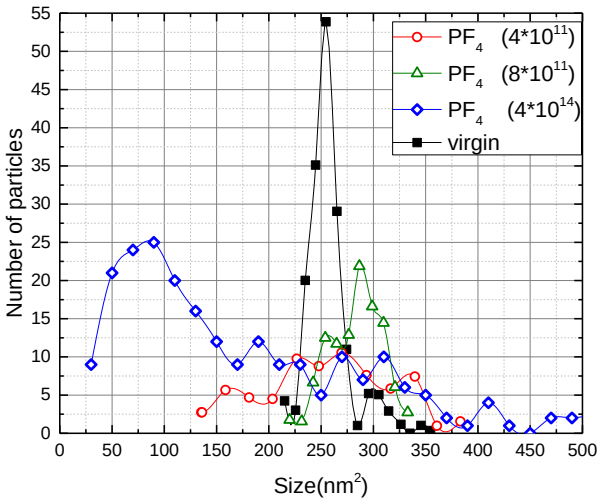

Figure 7. The number of particles of various sizes before (closed black symbols) and after (open colored symbols) irradiation with accelerated PF4 ions to different fluences, as indicated in the legend.

Figure 7 shows graphs of the size distribution of gold nanoparticles on a polymethylmethacrylate substrate before and after irradiation with different doses. It can be seen that the particle distribution has a clear peak before irradiation. The particle distribution is smoothed out after irradiation with a lower dose. By increasing the dose, the distribution will shift to the left, gradually increasing the peak. This suggests that irradiation with PF_4 ions leads to the modification of the initial layer depending on the dose.

Conclusions

In conclusion, the way to process SEM image in order to study ensemble of nanoparticles on various substrates is developed. This processing technique makes it possible to determine the distribution of metal nanoparticles on various types of substrates. The method is based on careful analysis of applied mask parameters with possibility of manual correction. This routine allows to obtain information on the size and number of nanoparticles and to estimate the parameters of their ensemble. The use of this technique makes it possible to study the effect of radiation, temperature, and other parameters on nanoparticle ensemble from thin metal films.

References

1. J. Bischof, D. Scherer, S. Herminghaus, and P. Leiderer, *Phys. Rev. Lett.*, **77**, 1536 (1996).
2. M. Kang, SG.Park, KH.Jeong, *Sci Rep* **5,** 14790 (2015).
3. R. LoSavio, L.Repetto, P.Guida, et. al. Solid State Comm., 240, 41, (2016)
4. Z. Huang, N. Geyer, P. Werner, J. de Boor, U. Gösele, Advanced Materials, **23**, 285, (2011).
5. T. W. H. Oates, H. Sugime, S. Noda, J Phys Chem C. **113**, 4820 (2009).
6. Bespalova P. et al. Gold Nanoparticle Array Formation by Low-Temperature Annealing. In: Velichko E., Vinnichenko M., Kapralova V., Koucheryavy Y. (Eds.) International Youth Conference on Electronics, Telecommunications and Information Technologies. Springer Proceedings in Physics, vol 255. Springer (2021).
7. M. S. Tuzhilkin, P. G. Bespalova, M. V. Mishin, et al., Semiconductors, 54, 137, (2020).
8. V. M. Studzinsky, M. V. Mishin, P. A. Karaseov, K. V. Karabeshkin and U. V. Yurina, *IEEE International Conference on Electrical Engineering and Photonics (EExPolytech)*, St. Petersburg, Russia, 2020, pp. 216, (2020).
9. https://meyerinst.com/library/IP-Brochure.pdf

AN EARLY FIRE DETECTION SYSTEM BASED ON THE ANALYSIS OF SPECKLE PATTERNS IN INTERACTION WITH A THERMAL CONVECTIVE FLOW

Aleksey Tupitsyn

undergraduate student
Saint-Petersburg State University of Aerospace Instrumentation (SUAI),
Saint-Petersburg, Russia
yweazcv@yandex.ru

Annotation
The aim of the work is to increase the efficiency of functioning of safety systems for early detection of fires. A structural diagram of an early fire detection system based on an analysis of spatial characteristics of speckle patterns in interaction with a thermal convective flow is proposed. Experimental studies have been carried out to measure the spatial characteristics of speckle patterns when interacting with a thermal convective flow from a candle flame. Measurement of the spatial characteristics of the beams was performed using a CCD camera and special software for the analysis of optical beams BeamGage.
Keywords: fire detector, heat convective flow, speckle pattern, optical beam, fire.

INTRODUCTION

Currently, domestic and foreign industry produces a wide range of technical means (detectors) for detecting fires. Most often, smoke detectors are used in fire systems, the principle of which is based on the detection of scattered optical radiation on smoke particles in the detector chamber. Unfortunately, the actuation of such fire detectors occurs at the moment when the fire center reaches a serious size.

Meanwhile, it is generally accepted that the earliest signs of the onset of ignition are the appearance of a thermal convective flow and carbon monoxide CO. Thermal convective flow occurs already at the stage of smoldering, therefore it is timely registration makes it possible to detect the beginning of a fire as quickly as possible and prevent serious material damage and, possibly, save human lives.

At the same time, it should be noted that at the moment there are no developed and widely used technical means capable of detecting the presence of a thermal convective flow. One of the promising in this direction is the use of fiber-optic technologies [1,2], which is due to several factors. First, fiber optic sensors are immune to electromagnetic interference. Secondly, the fiber-optic sensors themselves are absolutely explosion-proof, and the processing unit containing live parts can be removed a considerable distance from the monitored object, measured in kilometers. The use of suck systems is especially important at explosive facilities and industries [3]. The paper proposes a system based on a multimode optical fiber, which is capable of responding to changes in the spatial characteristics of optical radiating emerging from the end of the fiber when radiation propagates through a thermal convective flow.

1. STRUCTURAL DIAGRAM OF THE SYSTEM

Thermal convective flow [4] from a glowing object is a random distribution of the density of the medium in the field of action of mass forces, which leads to the movement of the medium and convection. With natural convection of air, gravity and buoyancy force act on its molecules, while in artificial convection of air, it is carried out with the help of a fan. The efficiency of convective heat transfer is determined by the particle velocity, temperature gradient, object surface area, and thermal properties of the environment.

Due to the fact that a random change in the refractive index of air is observed in the space of a convective flow from a glowing object, it should be expected that the laser beam will undergo random changes in spatial characteristics.

In order to detect fluctuations in beam changes, it is proposed to use a beam with a non-uniform distribution of intensity along the profile, so that changes in spatial characteristics are manifested even more strongly. A collimated beam from the end of a multimode optical fiber is suitable for these purposes. It is known that the field at the end of a multimode optical fiber is a speckled structure (speckle pattern) [5], which arises due to the peculiarities of the formation of guided modes in the drawing. An example of such a speckle pattern is shown in Figure 1.

Figure 2 shows a block diagram of a system for detecting a thermal convective flow based on a multimode optical fiber.

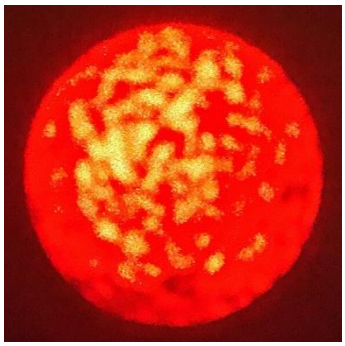

Figure 1 – Speckle pattern at the end of a multimode optical fiber

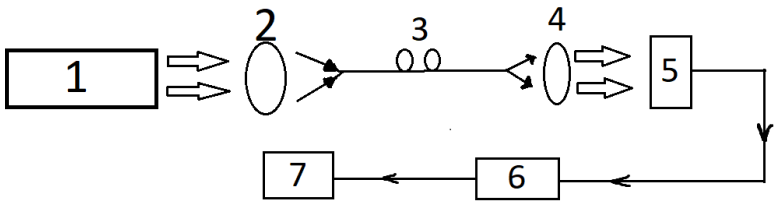

Figure 2 - Block diagram of the system for detecting thermal convective flow

The system includes:
1. Laser;
2. A system for introducing radiation into an optical fiber,
3. Multimode optical fiber;
4. System for the formation of a collimated beam with a speckle pattern;
5. System of registration of spatial characteristics of speckle-picture;
6. Processing unit;
7. Block for issuing an alarm.

The system works as follows. The laser emitter can operate in both continuous and pulsed (to reduce power consumption) mode. The system for inputting radiation into an optical fiber is designed to efficiently input radiation into a multimode optical fiber and reduce energy losses. At the exit from the multimode fiber, a diverging beam is formed within the numerical aperture of the fiber; therefore, the purpose of the collimated beam formation system is to form a weakly divergent laser beam that propagates along the controlled space. The system for recording spatial characteristics is a CCD matrix that allows you to analyze the spatial distribution of the beam in two coordinates. The processing unit is designed to process the signals of the CCD matrix and generate an alarm signal that is displayed to the operator or transmitted to the fire warning system in one form or another.

2. EXPERIMENTAL RESULTS

To confirm the idea of registering changes in the spatial characteristics of speckle patterns when interacting with a thermal convective flow, a full-scale laboratory experiment was carried out. The laboratory layout for experimental research is shown in Figure 3.

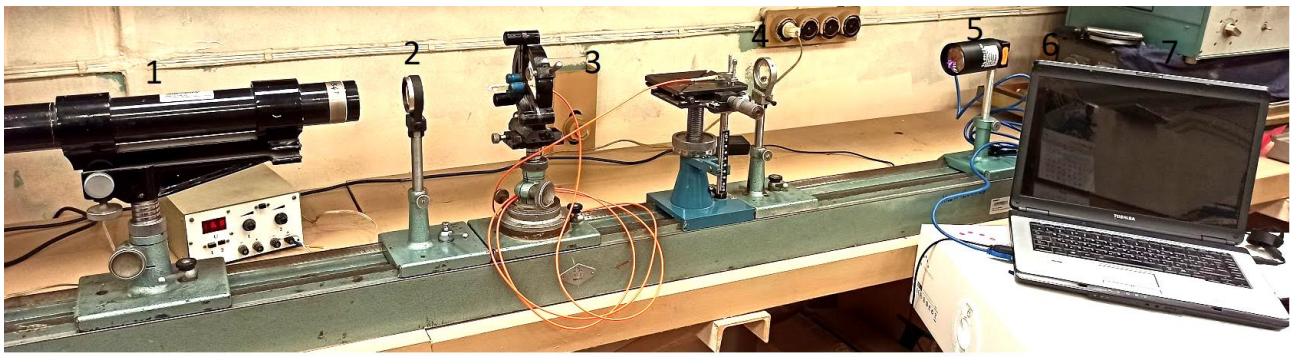

Figure 3 - Laboratory layout of an early fire detection system

1 - Laser LGN-214 with a wavelength of 632 nm;
2 - Collecting lens with a focal length of 110 mm;

3 - Multimode fiber;
4 - 4X Beam Reducer;
5 - Ophir SP928 CCD camera;
6,7 - Personal computer with installed BeamGage software.

An LGN-214 laser with a wavelength of 632 nm was used in the experimental setup. The formed beam from the laser enters a converging lens in order to efficiently introduce radiation into the multimode optical fiber. As a result, a speckle pattern was formed at the exit from the multimode optical fiber. The 4X Beam Reducer is designed to match the beam with the aperture of the Ophir SP928 CCD camera. The CCD camera transmits the acquired data to a PC with BeamGage software installed to analyze the spatial characteristics of the resulting speckle pattern.

The experiment was as follows.

Initially, the spatial characteristics of the speckle pattern were recorded in the absence of a thermal convective flow. For this purpose, speckle painting was registered for 30 seconds. The observation results showed that in the absence of external influences, the speckle pattern changes little. Minor changes in the speckle pattern are due to the instability of the laser source.

Then, a candle flame was placed in the space between the output end of the fiber and the 4X beam reducer to create a thermal convective flow. As a result, a significant tremor of the speckle pattern was observed on the monitor screen, caused by a random change in the refractive index of the air due to the thermal convective flow.

As a result, a jitter of the speckle pattern was observed, as shown in Figure 4.

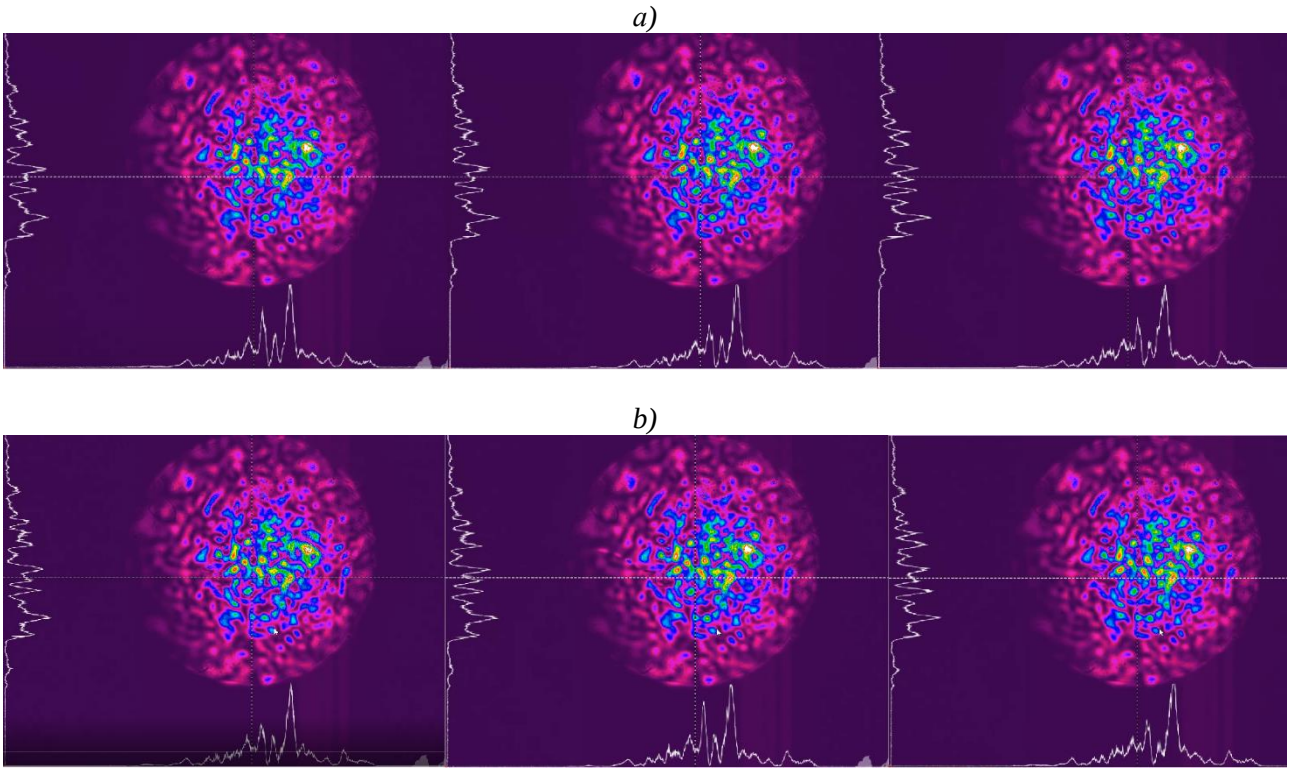

Figure 4 - Speckle patterns in the absence (a) and in the presence of a thermal convective flow (b)

Figure 4 (a) shows the spatial characteristics of the speckle pattern from the laser with an interval of 1 s in the absence of a heat flux. Figure 4 (b) shows the characteristics of the speckle pattern when a candle is lit and a heat convective flow is formed with the same interval.

As can be seen from the experimental results, when a thermal convective flow interacts with a laser beam from the end of a multimode optical fiber, strong measurements of spatial characteristics are observed, which can be recognized as the onset of ignition with appropriate processing of the received signals.

CONCLUSION

In almost any modern production, explosive zones are identified, the possibility of an explosion in which appears in the event of a violation of the technological process, in an accident, etc. Explosive zones include paint and varnish shops, warehouses for explosives, fuels and lubricants, flour and tobacco production. One of the most urgent tasks of fire protection is also the protection of objects with an increased level of radiation and the presence of aggressive chemical environments. The protection of such objects from fires requires the development of new and improved technical means of detecting fires.

The paper considers the issue of the possibility of early detection of fire based on the registration of the thermal convective flow. It is shown that the method of registering changes in the spatial characteristics of speckle patterns upon interaction with a thermal convective flow is effective, which is confirmed by the results of the experiment. A distinctive advantage of the proposed system is its absolute explosion safety, since there are no open current-carrying elements within the controlled space.

REFERENCES

1. Удд, Э. Волоконно-оптические датчики. – М.: Техносфера, 2008. –520 с.

2. Казаков В.И., Москалец О.Д., Пресленев Л.Н. Взрывобезопасный волоконно-оптический пожарный извещатель. Математическая модель чувствительного элемента. // Датчики и системы. – 2015. – №2. – С.19-22.

3. Образцов, С. Особенности применения технических средств охраны во взрывоопасных помещениях. // Технологии защиты. – 2007. – №5.

4. Эккерт Э.Р., Дрейк Р.М., Теория тепло- и массообмена, пер. с англ., М. – Л., 1961. - 680 с.

5. E. E. Dashkevich, R.A. Hansuvarov, V. I. Kazakov, O. D. Moskaletz, A. Yu. Zhdanov . Research of speckle-pictures caused by distribution of optical radiation in a multimode optical fiber and a group of optical fibers. XII International conference for young researchers. Wave electronics and Its Applications in the Information and Telecommunication Systems, St. Petersburg, p.29, 2009.

TAKING INTO ACCOUNT THE GEOMETRIC DIMENSIONS OF GRANULES IN THE SEPARATION PROCESS OF AN AUTOMATED 3D PLASTIC PROCESSING PLANT

Alexandra Vinnichenko

Saint Petersburg State University of Aerospace Instrumentation
E-mail: alex23rain@gmail.com

Abstract
The article presents a technical solution for the development of an automated 3D plastic processing plant, describes the technological aspects of the processes of grinding and dry separation of the automated plant, as well as issues related to the problem of controlling different-dispersed granules.
Keywords: accounting for geometric dimensions, fine granules, separation of 3D plastic, processing of 3D plastic.

3D printing covers an increasingly large segment of both the Russian and global markets. The demand for 3D technologies in industrial enterprises is increasing, it is being put into commercial operation, and companies are actively expanding the range of printed products. The level of 3D printing penetration varies from industry to industry and depends on the advantages that additive technologies bring to the point segments of the market, as well as on the barriers to their operation (Figure 1). [8]

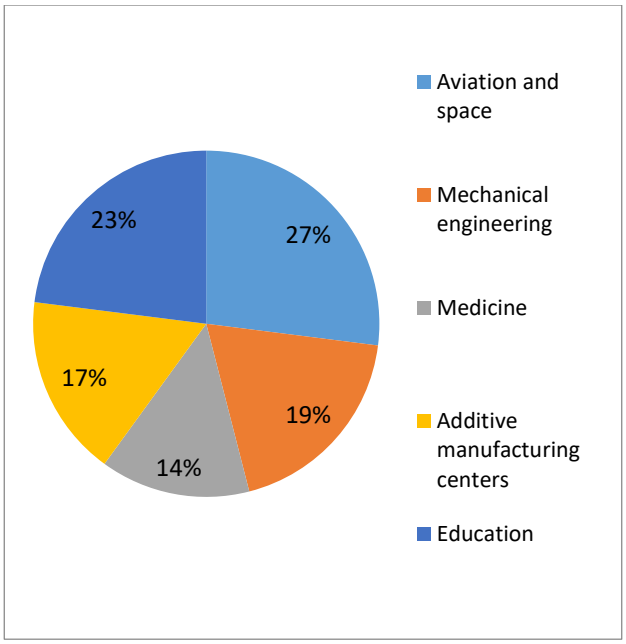

Figure 1-Industry structure of the Russian AP technology market, 2020.

The impetus for a new scientific and technical level of additive manufacturing is possible through the formation of a preventive attitude to the environmental policy in the field of plastic processing for budget and educational organizations and the creation of a pilot product for testing the model of small-scale production. It is also necessary to test the hypothesis of the susceptibility and understanding of the need to process defective 3D parts in order to iteratively use and save the financial budget of educational institutions.

The work was based on the task of learning how to recycle 3D plastic that has worked out its life span, or models with defects and design flaws, in order to reuse it, it must be melted and get the original plastic and be able to sell it again.

Either these are the models that did not work out, they were defective, with some design flaws, or unsuccessful copies. Or there were some staccato lines of materials that need to be overpaid and an object created in a new way, only with a single structure, i.e. the secondary use of plastic [7].

A market analysis was conducted, which showed that additive technologies are in trend and are mainly purchased by budget organizations: universities, schools, colleges. Since these organizations have a constant

mass educational activity, it turns out that when people learn to work with 3 D printers, they often have a large amount of waste, which means that this installation would be useful for them [6].

Table 1-

Market analysis

Organizations	***Total***	***10%***	***5%***
Grammar school	76	7,6	3,8
Lyceums	48	4,8	2,4
Schools	525	52,5	26,2
Cadet School	10	1,0	0,5
Academies	5	2,5	0,25
College	12	1,2	0,6
University	67	6,7	3,35
Radio-electronic industry	85	8,5	4,25
Manufacture of electrical, electronic and optical equipment	139	13,9	6,95
Production of machinery and equipment	85	8,5	4,25
Metallurgical production and production of finished metal products	68	6,8	3,4
Production of vehicles and equipment	48	4,8	2,4
Chemical production	32	3,2	1,6
Textile and clothing manufacturing	22	2,2	1,1
Manufacture of rubber and plastic products	14	1,4	0,7
Scientific research institutes	75	7,5	3,75

The aim of the work is to create a pilot prototype of a recycling plant to meet requests for the secondary use of ABS and PLA plastic (Fig. 2).

The presented technical solution allows you to significantly reduce the consumption of ABS and PLA plastic by not only reusing defective products obtained by disrupting the technological process of additive manufacturing, but also converting unused products that perform the function of exhibition samples and are not used during operation [2].

The grinding process is carried out using a shredder (shredder), due to the small overall dimensions of the installation, therefore, unlike a crusher, the shredder cannot grind the polymer to the desired fraction, since it tears a piece of polymer to large fractions, and therefore after the crushing process, the polymer must be re-crushed [4].

For this reason, the automated 3D plastic recycling plant includes a special separation unit, which has a fraction size ranging from 2-5 mm and [3], therefore, only fine granules of crushed plastic pass through the separation mechanism. In order to re-grind larger pellets, it is necessary to conduct an extraction pipe to the outer part of the unit housing at the level of the separating mechanism. This will allow the large pellets to be moved into the socket for recycling by the shredder using a strong air flow [1].

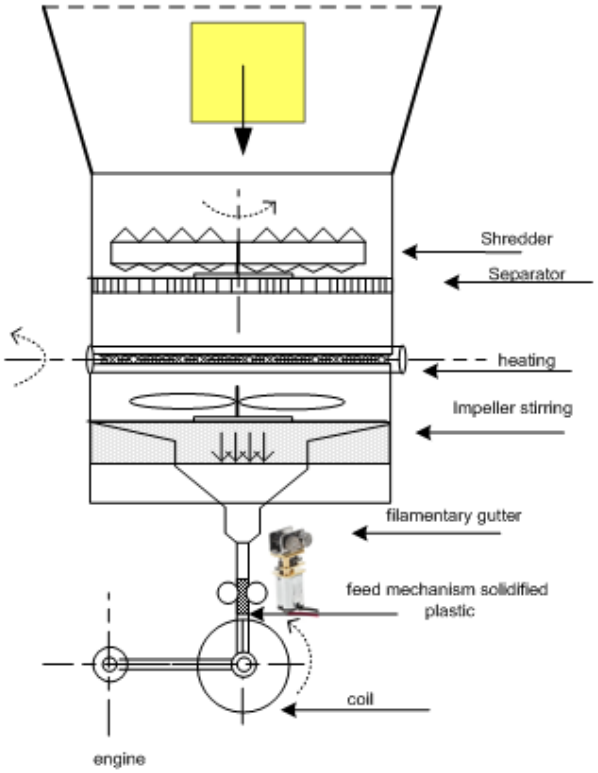

Figure 2-Block diagram of the node operation

The development of a prototype of a processing plant will reduce the costs of budget-funded educational and scientific-technical organizations in educational processes and scientific research processes in the study of the applicability of additive technologies. Such elements are widely used in both small-scale and large-scale production, products and assembly units, which are both homogeneous products and components of assembled products [5, 6].

Reference

1. GOST R 57556-2017. Materials for additive manufacturing processes. Methods of control and testing. Moscow: Standartinform, 2017. 11 p.

2. GOST R 57586-2017. Products obtained by the method of additive manufacturing processes. General requirements. Moscow: Standartinform, 2017. 8 p.

3. GOST 16338-85 Low-pressure polyethylene. Technical conditions (with Change N 1). Moscow: Standartinform, 2005. 35 p.

4. Vinnichenko A.V., Nazarevich S. A., Karpova I. R. Control model of an automated reverse engineering installation // Issues of radio electronics 2020;(4): p. 39-43. [Electronic resource] URL: https://doi.org/10.21778/2218-5453-2020-4-39-43 (accessed: 25.02.2021)

5. Vinnichenko A.V., Nazarevich S. A., Model of interaction of polymer materials processing in 3d technologies / / World science: problems and innovations collection of articles of the XLII International Scientific and Practical Conference. Penza, 2020, p. 73-79

6. Vinnichenko A.V., Nazarevich S. A., Application of the fuzzy logic apparatus for describing the functions of belonging to the parameters of the model installation for processing 3d materials, European scientific conference collection of articles of the XXI international scientific and practical conference. - Penza: ICNS "Science and Education". -2020, p. 27-33.

7. Komarov T. I., A.V. Vinnichenko, A.V. Chabanenko, Introduction of additive technologies in production to ensure quality control// Modeling and situational quality management of complex systems. Collection of reports. Youth Section, 2020, pp. 38-39

8. Vinnichenko A.V., Keplacing reverse engineering in additiv etechnology / Proceedings of the UNESCO Department of the GUAP "Remote Engineering Education" / Collection of articles, Issue 5, 2020. pp. 131-134

MODELING AND INVESTIGATION OF THE COMPRESSION CHARACTERISTICS OF BROADBAND FREQUENCY-MODULATED SIGNALS FOR DATA DETECTION AND TRANSMISSION SYSTEMS

Dmitry Zhdanovich

Saint-Petersburg State University of Aerospace Instrumentation,
Saint-Petersburg, Russia
E-mail: dimon-2255@mail.ru

Abstract
In this paper, we study frequency-modulated signals, namely LFM and LFM signals, their properties, methods of modeling and processing. A comparative analysis of the compression characteristics of LFM and LFM signals obtained during modeling is presented. The expediency of using low frequency signals as the most promising ones is shown.
Keywords: linear frequency modulation signals, nonlinear frequency modulation signals, radar, detection systems.

INTRODUCTION

At present, in the interests of increasing the noise immunity of radar systems and data transmission systems, methods of compression of broadband signals are widely used.

Today, many broadband signals are known that are modulated either in amplitude, or in frequency, or in phase, or simultaneously in several parameters simultaneously. The main broadband signals used in practice are signals with frequency (FM) [1-4] or phase modulation (PM) [5-11].

In fig. 1 shows the varieties of wideband signals, namely FM and PM signals. Frequency modulation of a signal is subdivided into linear frequency modulation (LFM), nonlinear frequency modulation (LFM), as well as discrete-coded signal frequency modulation (DKCHS Costas).

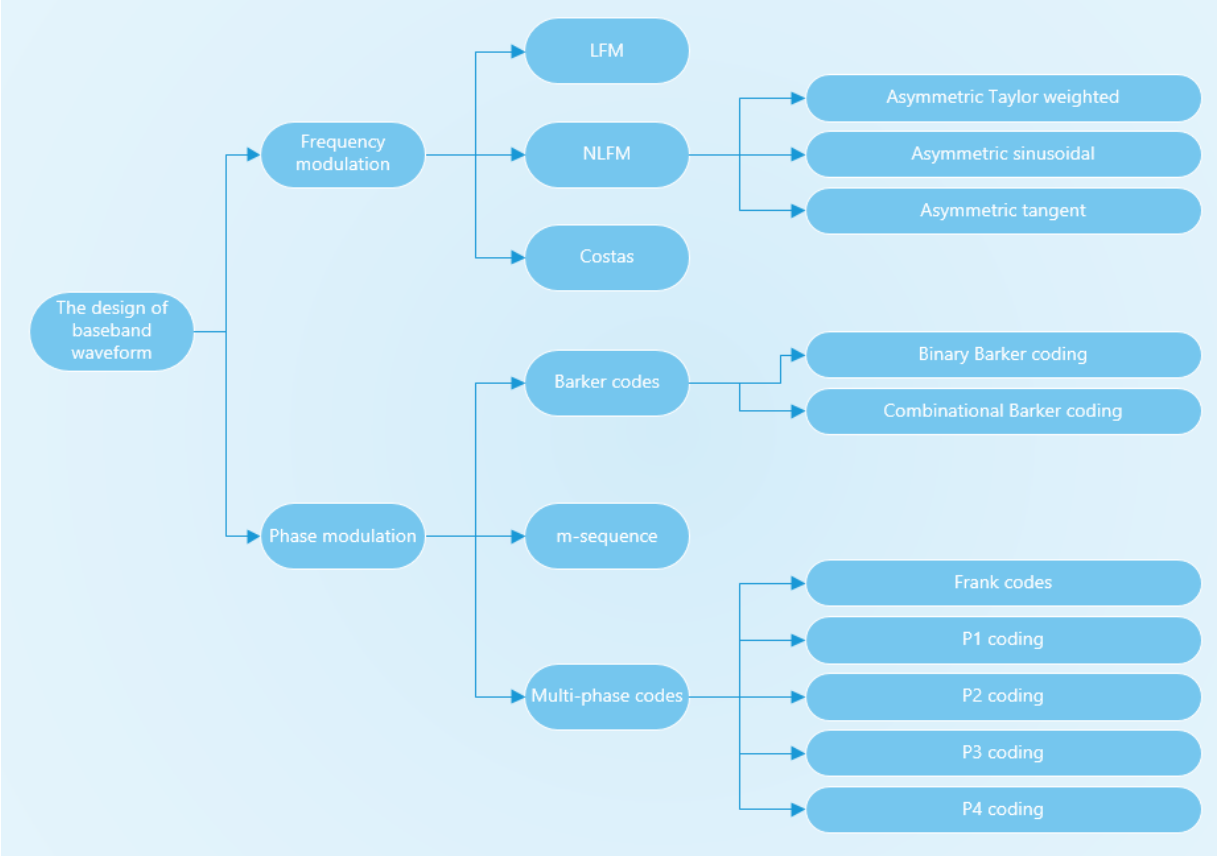

Figure 1 – Types of broadband signals

With regard to phase modulation of a signal, the main codes used are Barker sequences, m-sequences, and polyphase coding. Broadband signals based on Barker codes are subdivided into binary coding and nested Barker code constructs, as well as m-sequences. Multiphase signal coding is based on Frank codes, P1, P2, P3 and P4 codes [11].

Linear and nonlinear FM signals are widely used in radio detection systems for various purposes. The use of FM signals in radar systems allows for joint measurement of the range and speed of objects. A number of Doppler channels are required to use FM signals in a radar. To increase the resolution of object parameters, one can use signals consisting of a number of different FM signals, pulse sequences of FM signals with changing modulation parameters in individual pulses, adaptive FM signals, the parameters of which change depending on the situation, for example, depending on the range. to the goal.

When comparing the compression characteristics of wideband signals, particular attention is paid to the following factors:

1) Doppler frequency offset range;
2) sidelobe level on the time scale;
3) common factors.

In this paper, we investigate in more detail the characteristics of precisely frequency-modulated signals, as they are most often applicable in modern radar detection systems [1-4].

To solve the problem of studying the compression characteristics of broadband frequency-modulated signals, it is necessary to highlight its main characteristics, simulate the FM signals of all types and evaluate their correlation characteristics.

Statement of the problem

The main characteristics of FM signals when solving a specific detection problem [12-14] are the following:

— the ratio of the peak of the autocorrelation function (ACF) to the maximum side lobe in absolute value;
— width of the main lobe of the ACF at the level of -3dB;
— loss in signal-to-noise ratio is minimal;
— low sensitivity to Doppler shifts, to signal shifts relative to the ADC sampling times, to additional noise caused by jitter of the ADC clock signal front, to spectral overlap during analog-to-digital signal conversion.

In this paper, we will consider the algorithms for modeling LFM and NLFM signals, and also consider the methods of their processing in the time and frequency domains [6, 10, 11, 15-17]. Let's carry out a comparative analysis to identify the features of each of them.

LFM and NFM signals

Currently, algorithms and devices for processing signals with frequency modulation are known, in which the frequency changes according to one of two options: LFM or NLFM.

Let's consider each of them in more detail.

a. Linear frequency modulated signals

The linear frequency signal model can be represented by the expression:

$$s(t) = A \cdot \cos(2\pi f_c t + \pi \cdot B / \tau \cdot t^2 + \varphi_0) \quad (1)$$

where A is the signal amplitude, B – is the pulse bandwidth, τ – is the pulse duration and φ_0 – s the initial phase.

The signal model and spectrum of a typical linear frequency modulated pulse are set as follows. The pulse duration is 1 μs and the carrier frequency is 1.25 GHz. Figure 2 shows a chirp pulse with a linearly increasing frequency.

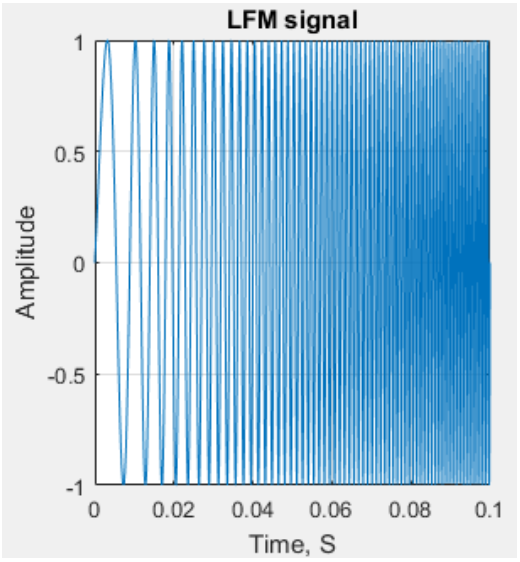

Figure 2 – LFM-signal

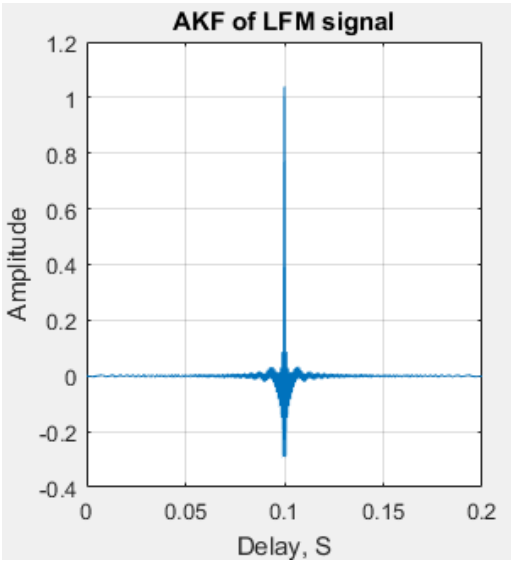

Figure 3 – Compressed – LFM-signal

Such signals are widely used in detection and data transmission systems..

b. Nonlinear frequency modulated signals

However, practice shows that when using radar one has to deal with nonlinear frequency modulation, in which the modulation law can be described by various nonlinear functions.

Non-linear frequency modulated signals have several distinct advantages over chirp signals. They do not need to be weighted in the frequency domain to reduce the side-lobe level over the time scale, since the frequency modulation of the signal must provide the desired spectral shape giving the required time-scale side lobe level after compression. Such formation is carried out by an increase in the slope of frequency modulation at the edges of the pulse and a decrease in its central part.

For a sinusoidal signal, the relationship between time and frequency modulation is expressed as follows:

$$\frac{t}{T} = \frac{f}{B} + \frac{k}{2\pi}\sin(2\pi f / B) \qquad (2)$$

where T is the pulse duration, B is the frequency deviation, k is the sidelobe level control factor over time.

Consider a signal with nonlinear frequency modulation, the change of which in time is subject to a sinusoidal law (Fig. 4).

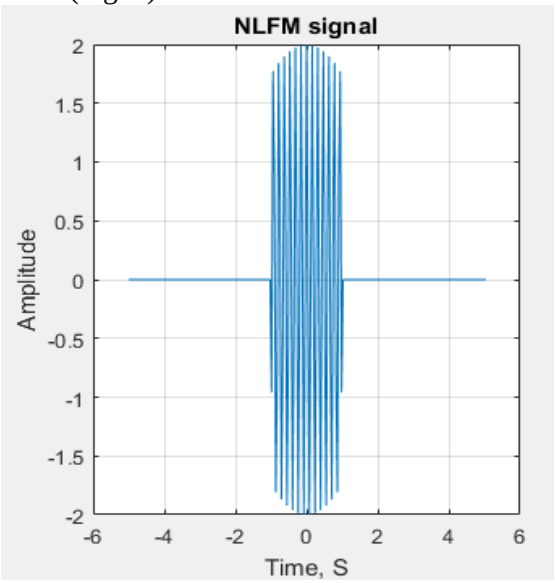

Figure 4 – NLFM-signal

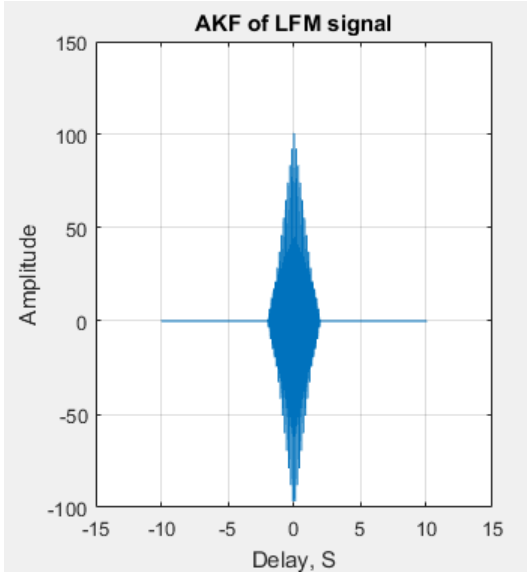

Figure 5 – Compressed – NLFM-signal

Comparative analysis of experimental results

As a result of modeling two types of FM signals, they were compared for evaluating the characteristics of the compression of the signals presented in Figures 2 and 4. In this case, the compression process of the modulated FM signal can be carried out in the time and frequency domain as follows (Fig. 6).

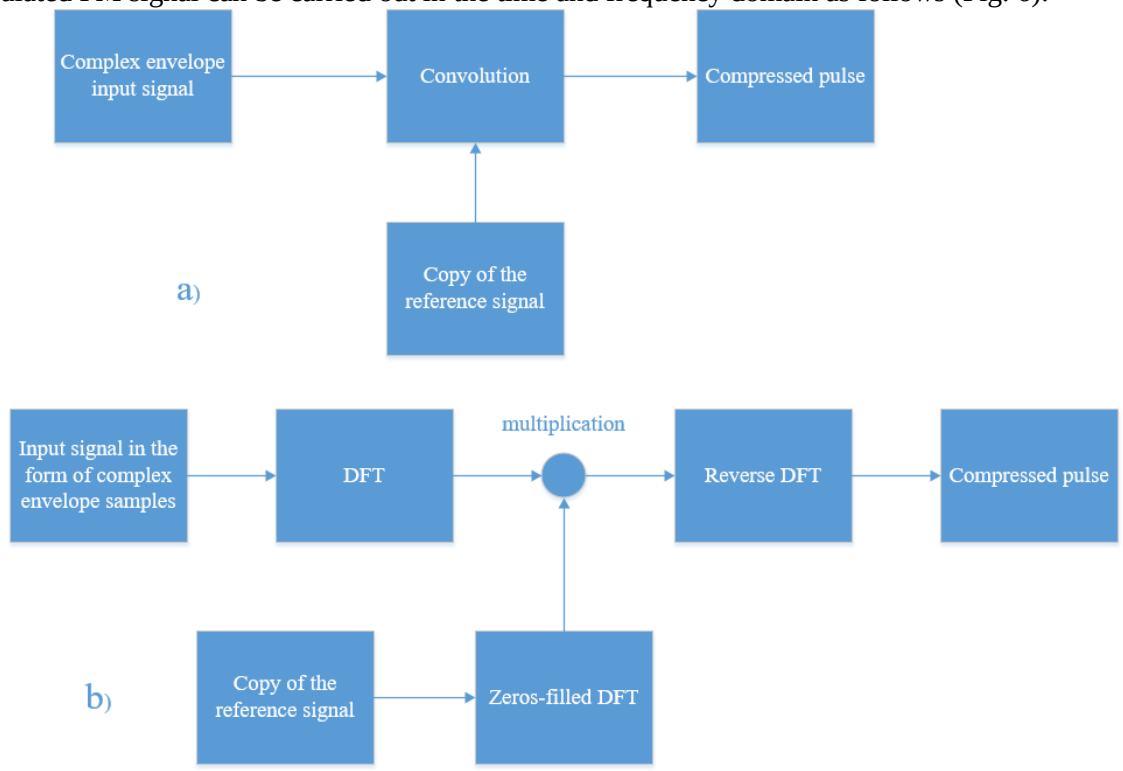

Figure 6 - a-digital pulse compression processor in the time domain; b-digital pulse compression processor in the frequency domain; DFT-discrete Fourier transform

The pulse compression procedure in the time domain is a linear convolution operation between the modulated pulse received by the receiver and its copy.

Linear convolution in the time domain is equivalent to multiplication in the frequency domain. In this case, it is advisable to use the fast Fourier transform to increase the speed of the computation process.

Step 1. Calculate the spectrum of the modulated signal transmitted over the communication channel and its copy by applying the Fourier transform operation to them.

Step 2. The operation (multiplicative, complex) multiplication between the spectra calculated at the first step is performed.

Step 3. The pulse is compressed by applying the inverse Fourier transform to the result of the multiplication of the spectra at step 2.

The result of the compression of the FM signal is shown in Figures 3, 5, in which it is clearly possible to distinguish against the background of noise a narrow pulse obtained after the compression algorithm.

Table 1 shows the results of a comparative analysis of the compression characteristics of LFM and NLFM pulses, on the basis of which it can be concluded that the latter are superior..

Table 1

Comparative analysis of the compression characteristics of chirp and low frequency pulses

Modulation type	Target radial speed (m / s)	Maximum side-lobe level over time (dB)	Average side-lobe level over time (dB)	Filter Mismatch Loss (dB)
LFM	+- 300	-13.32	-36.59	0.024
NLFM	+- 300	-26.07	-47.99	0.038

Thus, using the FM signal compression algorithm, it is possible to separate the transmitted information between the receiver and transmitter from noise..

CONCLUSION

As a result of the work done, the LFM and LFM signals were studied, the patterns of their various parameters from time to time, when simulating the signals. The advantages of LFM signals in signal transmission were also identified, due to the clear difference between the useful signal and the noise after filtering the signal.

REFERENCES

1. Verba V. S., Tatarsky B. G. Radar systems for aerospace monitoring of the Earth's surface and airspace. 2014. No. 1. pp. 304-324.

2. N. Levanon, “Stepped-frequency pulse-train radar signal”, IEE Proc – Radar Sonar Navigation, vol. 149, No. 6, December 2002.

3. Verba V. S., Radar reference guide. In 2 parts. 2014. p. 394-434

4. N. Levanon, E. Mozeson, Radar signals, New York: IEEE Press, John Wiley and Sons Inc., 2004, pp. 106 – 109.

5. Nenashev V.A., Vasiliev I.A., Sergeev A.M. Modeling of complex code-modulated signals for modern systems for detecting and transmitting information // Scientific session of the SUAI: collection of articles. report: at 3 pm Part II. Technical science. - SPb .: GUAP, April 8-17, 2019 .-- P. 413-417.

6. V.A. Nenashev, V.A. Sinitsyn, S.A. Strakhov Investigation of the influence of industrial noise on the compression characteristics of phase-shift keyed signals in primary radars // Innovative technologies and special-purpose technical means: Tr. IX all-Russia. scientific-practical Conf .: in 2 volumes. Baltic State Technical University "Voenmekh" D.F. Ustinova. 2017. pp. 351–355.

7. Sergeev M.B., Nenashev V.A., Sergeev A.M. Nested code constructions BARKER - MERSENNA - RAGHAVARAO // Information and control systems. 2019. No. 3 (100). S. 71-81.

8. Sergeev A., Nenashev V., Vostrikov A., Shepeta A., Kurtyanik D. Discovering and analyzing binary codes based on monocyclic quasi-orthogonal matrices // Smart Innovation, Systems and Technologies. 2019. Vol. 143. pp. 113-123.

9. Nenashev V.A., Sergeev A.M., Kapranova E.A. Research and analysis of autocorrelation functions of code sequences formed on the basis of monocyclic quasi-orthogonal matrices // Information and Control Systems. 2018. No. 4 (95). S. 9-14.

10. Shepeta A.P., Nenashev V.A., Yudin I.A., Kaplin A.Yu. Modeling the method of compression of the FM signal under the influence of active interference for solving problems of noise immunity. Certificate of registration of the computer program RU 2016618938, 08/10/2016. Application No. 2016616140 dated June 14, 2016.

11. V. A. Nenashev, A. A. Sentsov, A. M. Sergeev, M. S. Ivanova. Signal-code constructions. Analysis, processing and modeling: textbook. allowance. - SPb .: GUAP, 2020 .-- 59 p.

12. A. P. Shepeta, A. M. Makhlin, V. A. Nenashev and A. F. Kryachko, "Performance of UWB Signal Detecting Circuits," 2018 Wave Electronics and its Application in Information and Telecommunication Systems (WECONF), St. Petersburg, 2018, pp. 1-4.

13. Makhlin A.M., Nenashev V.A., Shepeta A.P. Comparative characteristics of quasi-optimal digital detectors of ultra-wideband signals // In the collection: Wave electronics and its application in information and telecommunication systems. XXI international youth conference. 2018.S. 257-264.

14. Shepeta A.P., Nenashev V.A., Isakov V.I., Sentsov A.A. Ultra-wideband signals in location measuring devices of generation and processing: textbook. allowance. - SPb .: GUAP, 2020 .-- 56 p.

15. launshtein N. Sh., Sergeev M.B., Shepeta A.P. Applied aspects of electrodynamics. SPb .: Agraf +, 2016.272 p..

16. Blaunstein N.S., Sergeev M.B., Nenashev V.A. Impact of built-up terrain on operational parameters of signals in land-satellite communication links. Information and Control Systems . 2018. № 1 (92). C. 74-84.

17. Podoplekin Yu. F., Shepeta DA, Nenashev VA Modeling of input signals of onboard radar, caused by reflections of the sounding signal from the underlying surfaces of the earth and the sea // Morskoy Vestnik. 2016. No. 4 (60). P. 69–71.

CONTENST

The scientific edition

ИЗВЕСТИЯ КАФЕДРЫ UNESCO ГУАП «ДИСТАНЦИОННОЕ ИНЖЕНЕРНОЕ ОБРАЗОВАНИЕ»

Сборник статей

Выпуск 6

BULLETIN OF THE UNESCO DEPARTMENT “DISTANCE EDUCATION IN ENGINEERING” OF THE SUAI

Collection of the papers

Issue 6

ISBN: 978-5-8088-1571-1

Computer imposition

Papers are publish in author’s edition

Подписано в печать 15.04.2021. Формат 60x84 1\8.
Усл. печ. л. 18,8. Тираж 150 экз. Заказ № 100.

Редакционно-издательский центр ГУАП
190000, Санкт-Петербург, Б. Морская ул., 67
Department of operative polygraphy SUAI
190000, St. Petersburg, st. B. Morskaya, 67